FATE OF FUEL NITROGEN DURING

PULVERIZED COAL COMBUSTION

by

YIH-HONG SONG

B.S., National Taiwan University
(1970)

M.S.Ch.E., University of Massachusetts
(1974)

SUBMITTED IN PARTIAL FULFILLMENT
OF THE REQUIREMENTS FOR THE
DEGREE OF

DOCTOR OF SCIENCE

at the

MASSACHUSETTS INSTITUTE OF TECHNOLOGY

April 1978

Signature of Author...
Department of Chemical Engineering, April 1978

Certified by...
Adel F. Sarofim, Thesis Supervisor

Certified by...
Janos M. Beér, Thesis Supervisor

Accepted by...
Glenn C. Williams, Chairman
Departmental Committee on Graduate Theses

FATE OF FUEL NITROGEN DURING

PULVERIZED COAL COMBUSTION

by

YIH·HONG SONG

FATE OF FUEL NITROGEN DURING

PULVERIZED COAL COMBUSTION

by

YIH-HONG SONG

ABSTRACT

The objectives of this investigation were to determine the effects of temperature and fuel/oxygen equivalence ratio on the overall conversion of coal-nitrogen to NO_x and to elucidate the roles played by the oxidation of char-nitrogen and the nitric oxide/char reaction on the NO_x emissions. Experiments were carried out in a laboratory muffle tube furnace under conditions pertinent to pulverized coal combustors.

Data on the overall conversion of coal-nitrogen to NO_x were obtained at 1250 K and 1750 K for a residence time of one second. The conversion of coal-nitrogen to NO_x decreased monotonically with increasing fuel/oxygen equivalence ratio and decreased slightly with increasing temperature. Oxidation experiments were also carried out on char in order to identify the individual contributions to NO_x emissions of volatile and char. The char used was prepared by the pyrolysis of coal at the temperature and residence time corresponding to those of oxidation experiments. The conversion to NO_x of char-nitrogen was lower than the corresponding value for coal-nitrogen while the char-nitrogen followed a trend similar to that of coal-nitrogen. It was found that volatilized nitrogen compounds accounted for a major fraction of NO_x produced from coal-nitrogen especially at high temperatures and low fuel/oxygen equivalence ratios. The results suggest that in order to favor a low NO_x emission from pulverized coal combustors it is optimal to operate the first stage of a stage combustor at high temperature and fuel-rich condition and then complete the combustion of residual char at latter stages under low temperature and fuel-lean condition.

Kinetic parameters of oxidation of char and char-nitrogen were determined at temperatures of 1250, 1500 and 1750 K and oxygen partial pressures of 0.2 and 0.4 atm for residence times varying from about

100 to 500 milliseconds. The char used was produced by pyrolyzing lignite particles at 1750 K for a residence time of one second. The results showed that the overall char burnout process was controlled primarily by internal pore diffusion. The reaction order with respect to oxygen was found to be 0.98 and the intrinsic rate constant per unit B.E.T. surface area was given by

$$k_B = 2.8 \times 10^3 \cdot \exp(-22,100/RT) \quad \frac{cm}{sec} \left[\frac{g\text{-moles}}{cm^3}\right]^{0.02}$$

The time-resolved variations of nitrogen to carbon ratio of char samples were obtained. No selectivity between nitrogen and carbon loss was observed during oxidation but char-nitrogen was found to undergo pyrolysis in parallel with oxidation. The oxidation rate of char-nitrogen was given by the product of the char oxidation rate and the mole ratio of nitrogen to carbon in the char. The pyrolysis rate of char-nitrogen was correlated by a first order kinetics and the rate constant was given by

$$k_{py} = 5.8 \times 10^3 \cdot \exp(-29,100/RT) \quad sec^{-1}$$

The results indicated that the pyrolysis rate and oxidation rate of fuel-nitrogen were additive and separable during pulverized coal combustion.

The kinetic studies of char/NO_x reaction were carried out at temperatures of 1250, 1500 and 1750 K for a residence time of one second. The reaction was found to be first order with respect to NO_x. The intrinsic rate constant per unit B.E.T. surface area was given by

$$k = 5.0 \times 10^{-5} \cdot \exp(-32,700/RT) \quad \frac{moles}{(sec)(m^2)(ppm)}$$

The reduction of NO_x was strongly dependent upon the temperature level and the char availability. The results showed that a significant fraction of NO_x could be reduced by the contact with char under pulverized coal combustion conditions.

Thesis Supervisors: Adel F. Sarofim
                     Professor of Chemical Engineering

                     Janos M. Beér
                     Professor of Chemical Engineering

Department of Chemical Engineering
Massachusetts Institute of Technology
Cambridge, Massachusetts 02139

April 10, 1978

Professor George C. Newton
Secretary of the Faculty
Massachusetts Institute of Technology
Cambridge, Massachusetts 02139

Dear Professor Newton:

In accordance with the regulations of the faculty, I herewith submit a thesis, entitled "Fate of Fuel Nitrogen During Pulverized Coal Combustion," in partial fulfillment of the requirements for the degrees of Doctor of Science in Chemical Engineering at the Massachusetts Institute of Technology.

Respectfully submitted,

Yih Hong Song

ACKNOWLEDGEMENTS

thanked for reading the manuscript and for his useful comments.

Thanks are extended to Mr. Stanley R. Mitchell for preparing the superb figures in this thesis; to Ms. Deborah A. Lauricella for the excellent typing; and to Misses Beverly A. Andreasen and Patty A. Rich for the secretarial help throughout the course of this study.

This research was funded by EPA under grant numbers R803242 and R805552.

Finally, I am deeply indebted to my wife, Leila, who spent countless nights in the lab to help me on the experiments and held a job in the daytime to support the family. She has also made the past three years a time of great happiness for me. Without her encouragement and moral support this could not have been possible.

TO

MY FAMILY

TABLE OF CONTENTS

TABLE OF CONTENTS (cont.)

TABLE OF CONTENTS (cont.)

TABLE OF CONTENTS (cont.)

TABLE OF CONTENTS (cont.)

TABLE OF CONTENTS (cont.)

TABLE OF CONTENTS (cont.)

LIST OF FIGURES

LIST OF FIGURES (cont.)

LIST OF FIGURES (cont.)

LIST OF FIGURES (cont.)

LIST OF FIGURES (cont.)

LIST OF FIGURES (cont.)

LIST OF TABLES

LIST OF TABLES (cont.)

LIST OF TABLES (cont.)

CHAPTER 1

SUMMARY

1.1 Introduction

Nitrogen occurs in coal, ranging from 0.5% to 2.0% by weight, bound primarily in heterocyclic rings (Beet, 1940). During combustion part of this nitrogen is oxidized to nitric oxide, and without the development of improved control technology this source of NO_x emissions will become unacceptably large (Mason et al., 1977). It is desirable to examine the behavior of the coal-nitrogen during combustion.

In the initial stages of coal combustion, the coal-nitrogen is partially released in volatiles and partially retained in char. Previous studies at M.I.T. (Pohl, 1976; Pohl and Sarofim, 1976) have shown that under the conditions in pulverized coal flames the split of the nitrogen between volatiles and char is kinetically controlled, with higher temperatures and higher residence times in the pyrolysis zone favoring the conversion of coal-nitrogen to volatile-nitrogen. The volatile products are initially in the forms of heavy tars and hydrocarbon (Solomon, 1977; Blair et al., 1977) but these subsequently decompose to yield mostly HCN and NH_3. The times for the secondary pyrolysis are short, estimated to be less than a millisecond at flame temperatures based on studies of model nitrogen compounds (Axworthy, 1975). The volatile-nitrogen will be oxidized either in partially premixed or diffusion flames or heterogeneously with the char when ignition occurs at the coal particle surface prior to complete devolatilization. (The processes of volatiles evolution and particle ignition have been studied by Howard and Essenhigh

(1967a, 1967b)). Some insight on the conversion of gas phase volatile-nitrogen to NO_x can be gained from studies of oxidation of fuel nitrogen compounds to NO_x in premixed and diffusion flames (Fenimore, 1972; De Soete, 1973, 1975; Sarofim et al., 1975; Martin et al., 1972; Bartok et al., 1972; Flagan et al., 1974). These studies indicate that the fractional conversion of fuel nitrogen to NO_x in gaseous flames is insensitive to the chemical form of the nitrogen, decreases with increasing fuel nitrogen concentration, and decreases with increasing fuel/air ratio. Some information on the detailed mechanism leading from the fuel nitrogen to NO_x has been obtained (Haynes et al., 1975) but the kinetics are not sufficiently well known to completely model the fuel nitrogen conversion to NO_x in complex system.

The nitrogen retained by the char is partially converted to NO_x during oxidation. Limited data are available on the efficiency with which char-nitrogen is converted to NO_x but little is known on the kinetics of oxidations of char-nitrogen.

Another factor of unknown importance is the reduction of NO_x to N_2 by char. Such reaction has been shown (Pereira, 1975; Gibbs, Pereira and Beér, 1976) to appreciably reduce the emissions of NO_x from fluidized bed coal combustors but little is known about the significance of this reaction in pulverized coal flames.

The processes that influence the conversion of the coal-nitrogen to NO_x are summarized in Figure 1.1. The two paths to NO_x can be seen to be by way of intermediate volatile-nitrogen compounds or char-nitrogen. The objective in the current thesis is to determine the effects of temperature and fuel/oxygen equivalence ratio on the conversion of
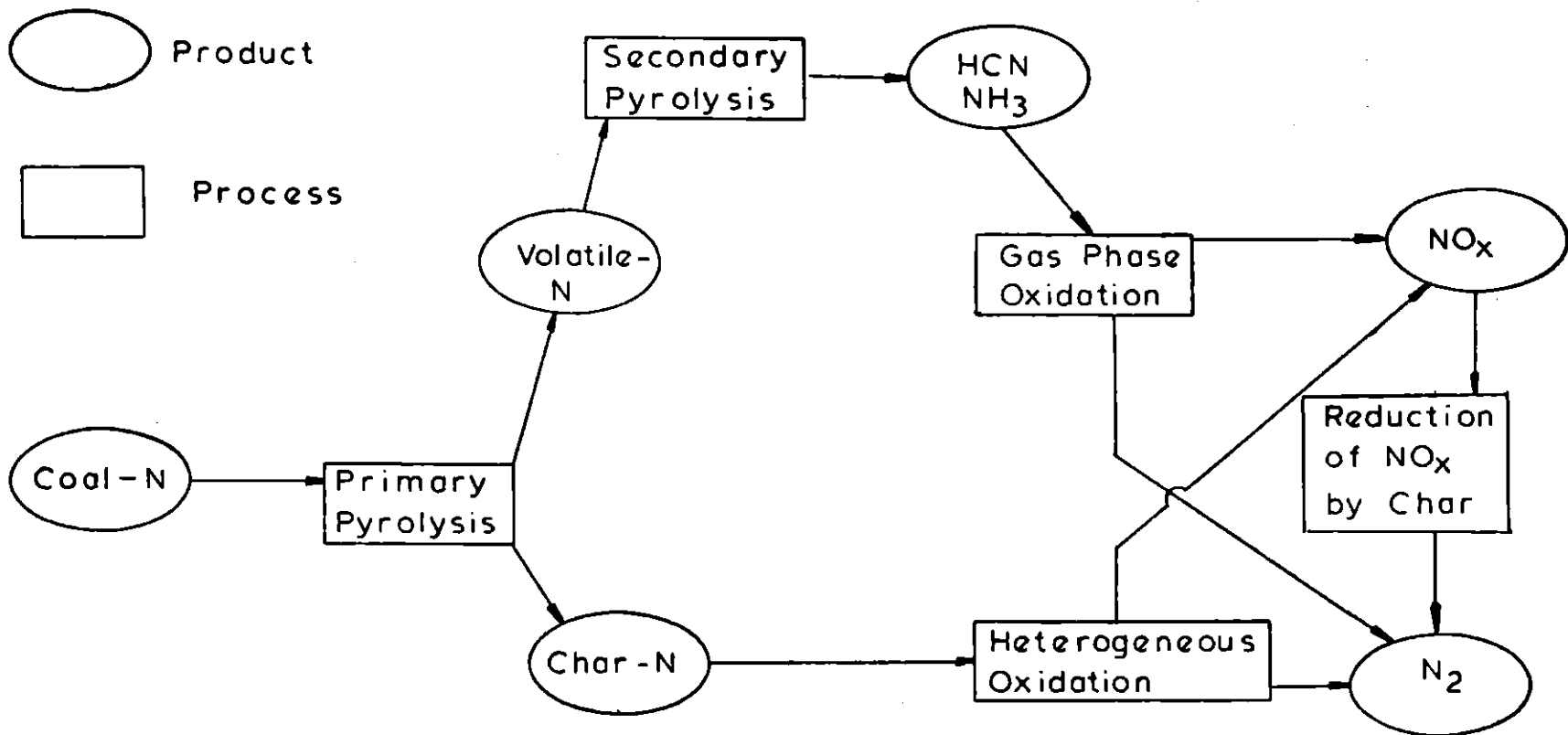
Figure 1.1

Schematic of Processes Occuring During the Formation of Nitric Oxide from Coal Nitrogen.

coal-nitrogen to NO_x by both the homogeneous and heterogeneous paths. In addition, kinetic data were obtained on the oxidation of char-nitrogen and the Char/NO_x reactions which are necessary inputs for a complete NO_x emissions model of pulverized coal flames. It is hoped that the data obtained in the present study would provide quantitative guidelines for the designer in planning NO_x control strategies for pulverized coal combustors.

1.2 Experimental Apparatus and Procedures

The experiments were conducted in an Astro Model 1000 A electrically heated furnace with an alumina muffle tube. The main gas was preheated and fed to the working section of the furnace through a honeycomb straightener. The coal/char particles were fed along the axis in a small carrier gas stream. The furnace was operated in two modes. When studying the effects of temperature and fuel/oxygen equivalence ratio on overall fuel nitrogen conversion the products were withdrawn, after passage through a water-cooled section, from the bottom of the furnace (see Figure 1.2). Residence time in the hot zone simulated those in a proto-type industrial furnace (i.e., approximately one second). When obtaining data on char oxidation kinetics samples were withdrawn through a water-cooled collector probe positioned at varying distances from the char injector (see Figure 1.3). The particles were quenched by injecting gas at the probe tip in an amount sufficient to reduce the mixed cup temperature to about 300 C.

In the studies of overall fuel nitrogen conversion, the air mixture was simulated by 21% oxygen in helium. The main gas flow rate was varied
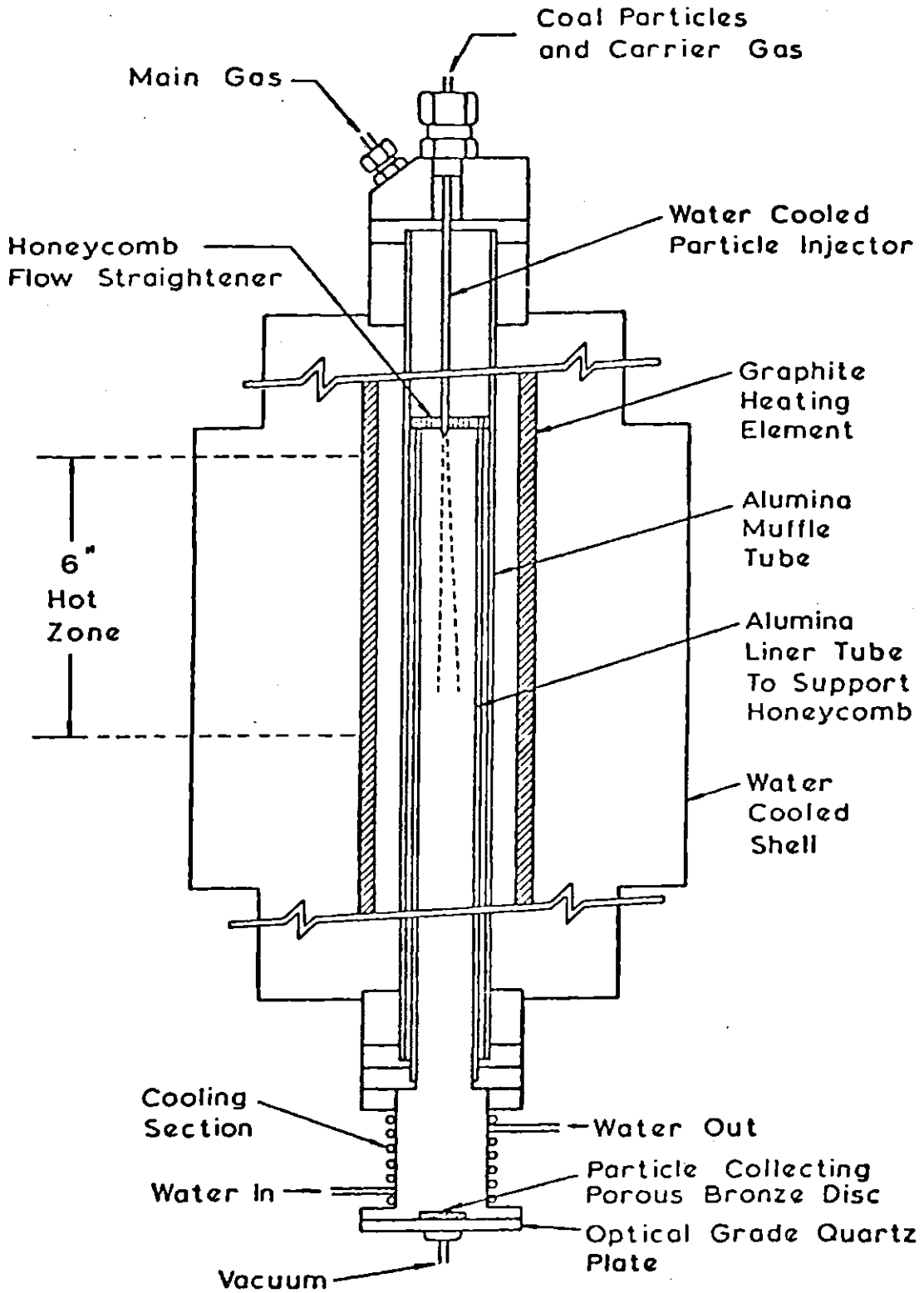
Figure 1.2

Furnace with Bronze Disc Collector
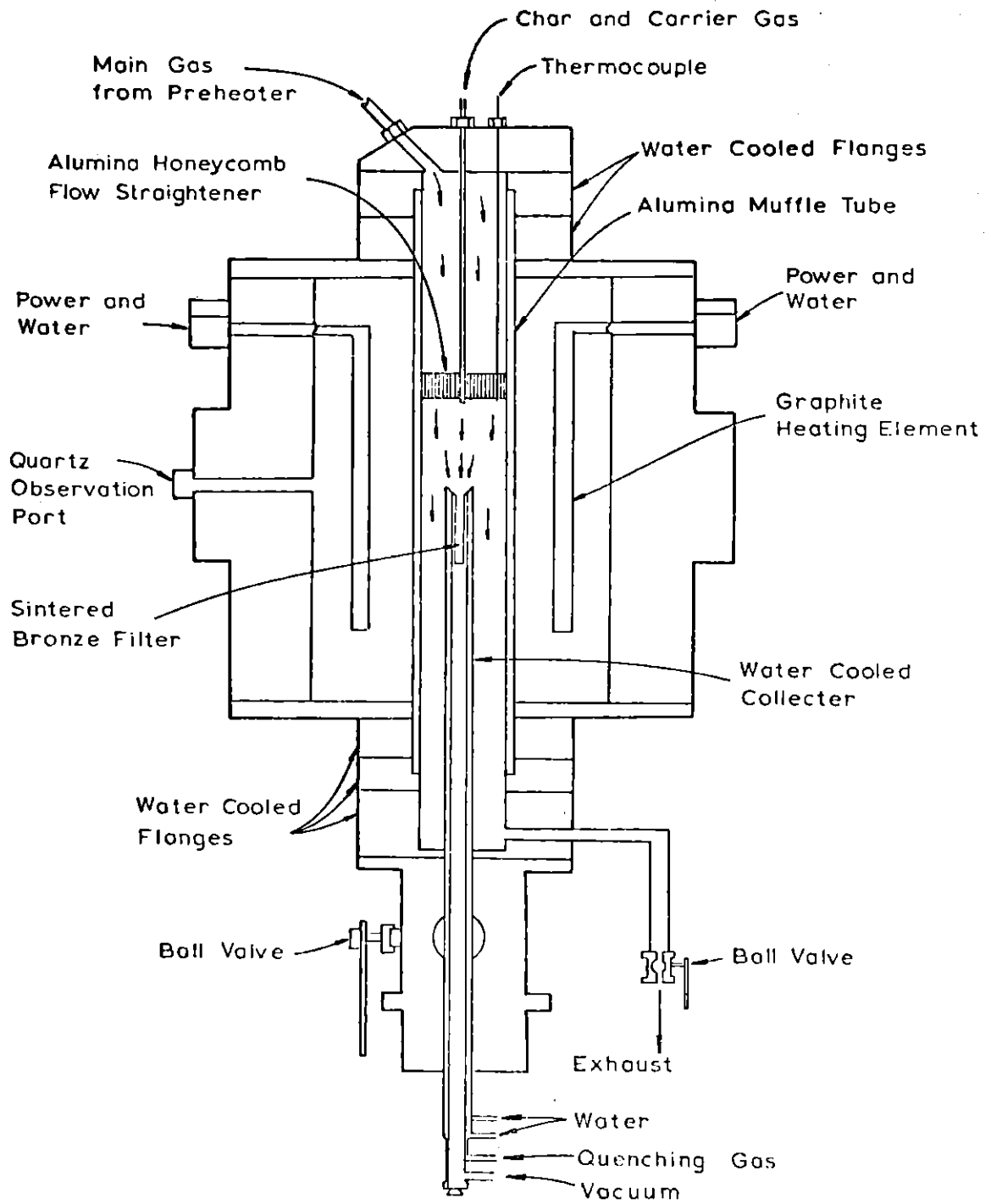
Figure 1.3

Furnace with Collector Probe

between 1 1/min and 3 1/min from run to run in order to obtain different overall fuel/oxygen equivalence ratios. The product gases were withdrawn continuously from the bottom of the furnace for gas phase analyses.

In the kinetic studies of char oxidation, the oxidant stream of oxygen in helium (P_{O_2} = 0.2 or 0.4 atm) was supplied to the furnace at a sufficiently fast rate (i.e., 6 1/min) to prevent significant depletion of the oxygen during reaction.

The kinetic studies of Char/NO_x reaction were carried out using the entire furnace length. Certified gas of NO_x in helium or argon was used as the main gas and the flow rate was typically set at 3 1/min. The NO_x concentration in the off-gas from the furnace was continuously monitored throughout the run.

The coal particles used in the overall fuel nitrogen conversion stuides had a nominal size of 38 to 44 microns. The char used in both kinetic studies of Char/O_2 and Char/NO_x reaction was produced by pyrolyzing lignite coal particles at a furnace temperature of 1750 K for a residence time of one second. The char produced was then size-graded for further experiments. The char was designated "1750 K lignite char". The proximate and ultimate compositions of the coals and chars used are summarized in Table 1.1. The physical characterizations which include the specific B.E.T. surface area, pore volume, average pore diameter and bulk density of the 1750 K lignite char are presented in Table 1.2.

TABLE 1.1

CHEMICAL PROPERTIES OF COALS AND CHARS

Type	Specification	VM	Proximate Analysis A.R. Wt% H_2O	Ash	C	H	Ultimate Analysis A.R. Wt% N	S	0 (by Diff.)
Montana Lignite-A	Savage	36.20	13.60	7.80	54.50	4.96	0.88	0.84	17.42
Montana Sub-Bituminous	Powder River Region	35.16	21.23	9.34	53.26	3.35	0.87	0.78	11.17
1250 K Lignite Char		NM*	4.20	12.08	66.94	2.09	1.02	0.56	13.11
1750 K Lignite Char**		NM	2.02	18.03	76.42	0.69	0.55	1.06	1.23
1750 K Litnite Char***		NM	2.10	19.00	76.11	0.36	0.58	1.11	0.74

*NM = Not Measured

**Used in parametric studies

***Used in Char/O_2 and Char/NO_x kinetic studies

-32-

TABLE 1.2

PHYSICAL PROPERTIES OF 1750 K LIGNITE CHAR

Type	Average Particle Diameter μ	B.E.T. Surface Area m^2/g	Pore Volume cm^3/g	Average Pore Diameter $\overset{\circ}{A}$	Bulk Density g/cm^3
1750 LC-1*	30	110.0	0.160	57.7	1.71
1750 LC-3*	30	121.6	0.157	51.6	1.71
1750 LC-4**	30	175.0	0.184	42.2	1.64

*Used in Char/O_2 kinetic studies

**Used in Char/NO_x kinetic studies

1.3 Results and Discussion

1.3.1 Conversion of Coal-Nitrogen to Nitric Oxide

The percentages of the nitrogen in a Montana lignite that are converted to NO_x for a hot zone residence time of one second as a function of fuel/oxygen equivalence ratio are shown in Figures 1.4 and 1.5 for furnace temperatures of 1250 K and 1750 K, respectively. Also shown at the top of the figures are the total solid weight loss (on a dry-ash-free basis) and, in the middle, the fraction of the original coal nitrogen retained by any unburned char. Oxidation experiments were also carried out on the char in order to identify the individual contribution of char-nitrogen and volatile-nitrogen to the total NO_x emission. The char used in the oxidation studies was prepared by pyrolyzing the coal at the temperature and residence time corresponding to those of the oxidation experiments. Results of char-nitrogen conversions at 1250 K and 1750 K are presented in Figures 1.6 and 1.7. As can be seen from Figures 1.4 to 1.7, the conversion to NO_x of char-nitrogen was lower than the corresponding value for coal-nitrogen while both coal- and char-nitrogen conversion to NO_x were found to decrease monotonically with increasing fuel/oxygen equivalence ratios. In both cases of coal and char oxidations, the percentages of solid weight loss decreased and the percentages of the nitrogen retained in the unburned char increased as the fuel/oxygen equivalence ratio increased. The effect of temperature on fuel nitrogen oxidation was small. In order to better evaluate the effect of tempera-ture on the conversion of coal-nitrogen to NO_x, a series of experiments were conducted in which the fuel/oxygen ratios were fixed and the furnace temperature was varied. The data in Figure 1.8 were obtained for a
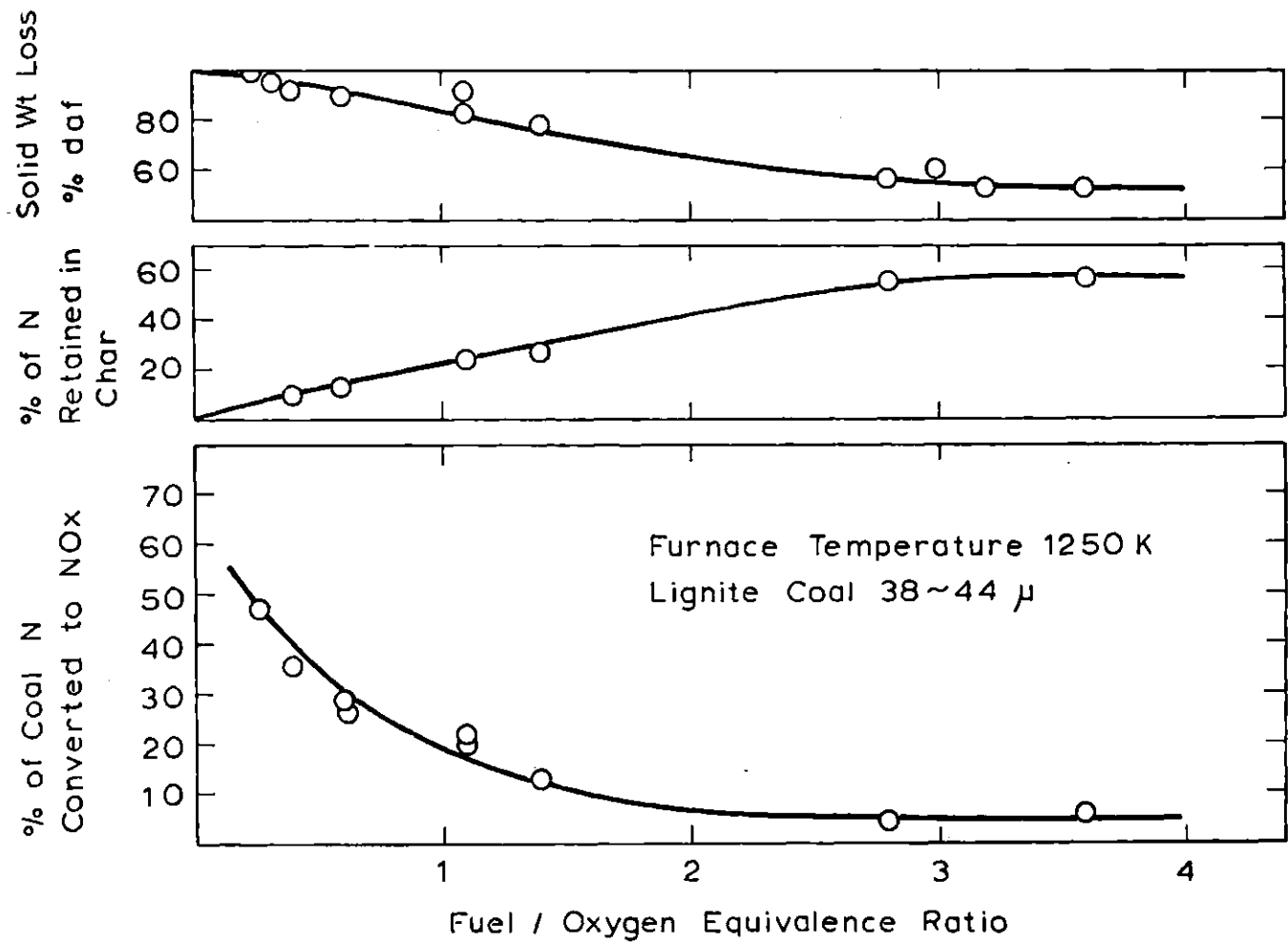
Figure 1.4

Fate of Coal Nitrogen During Oxidation: Conversion to Nitric Oxide (Bottom); Retention by Unburned Char

(Middle); and Combustion Efficiency (Top). Montana Lignite at 1250 K.

Fuel / Oxygen Equivalence Ratio
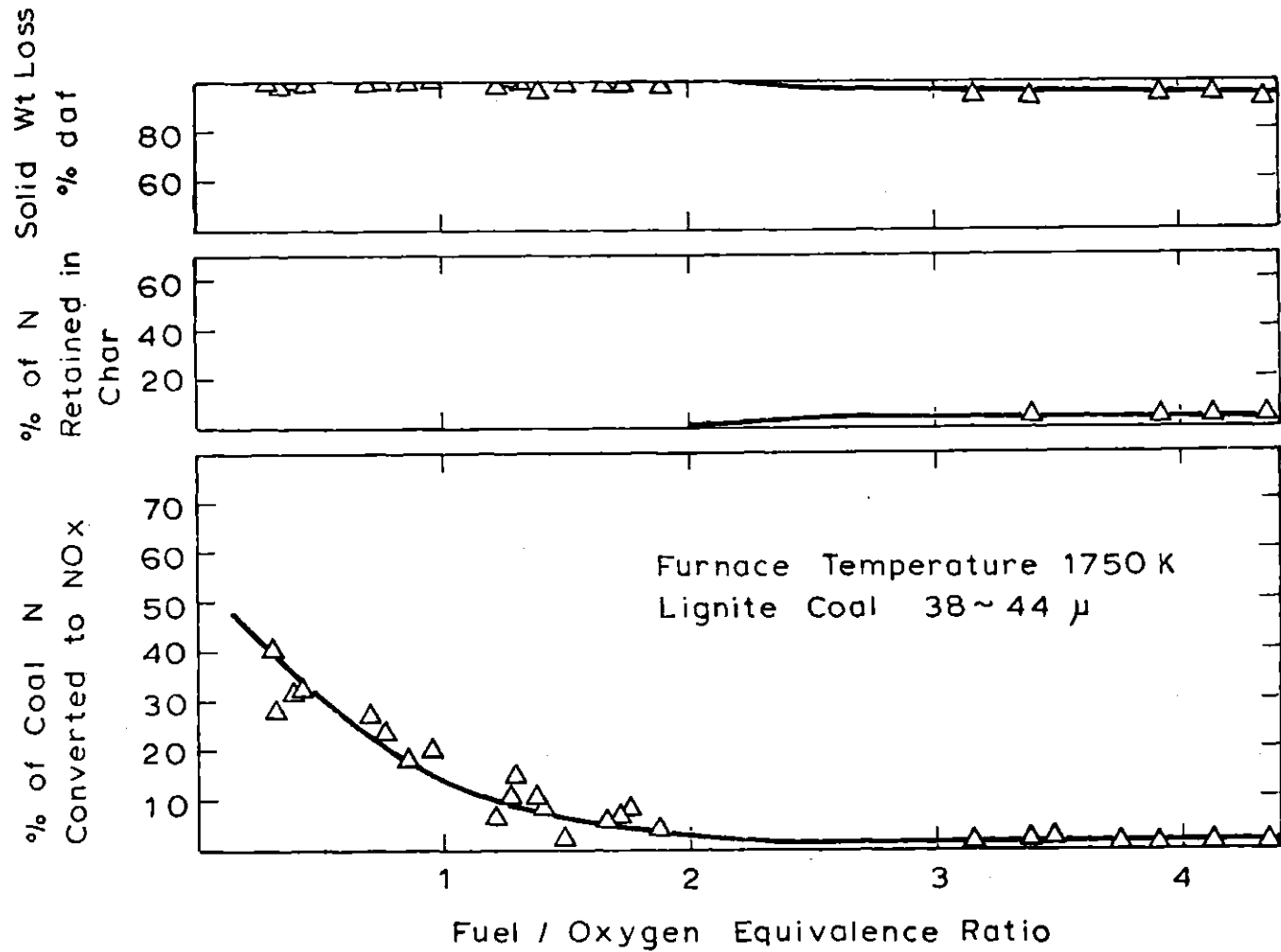
Figure 1.5

Fate of Coal Nitrogen During Oxidation: Conversion to Nitric Oxide (Bottom); Retention by Unburned Char (Middle); and Combustion Efficiency (Top). Montana Lignite at 1750 K.
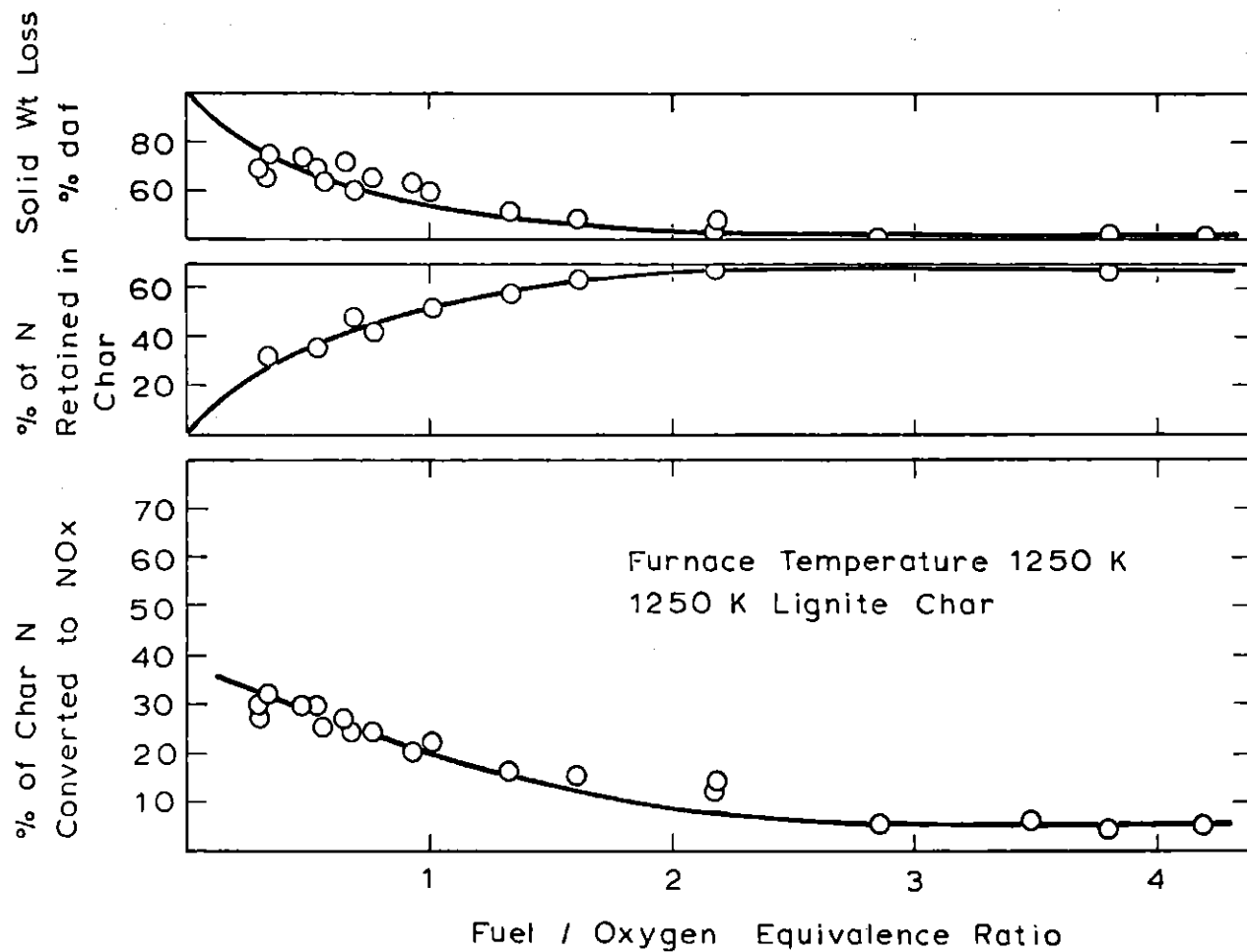
Figure 1.6

Fate of Char Nitrogen During Oxidation: Conversion to Nitric Oxide (Bottom); Retention by Unburned Char

(Middle); and Combustion Efficiency (Top). Char from Montana Lignite

Pyrolyzed and Oxidized at 1250 K.
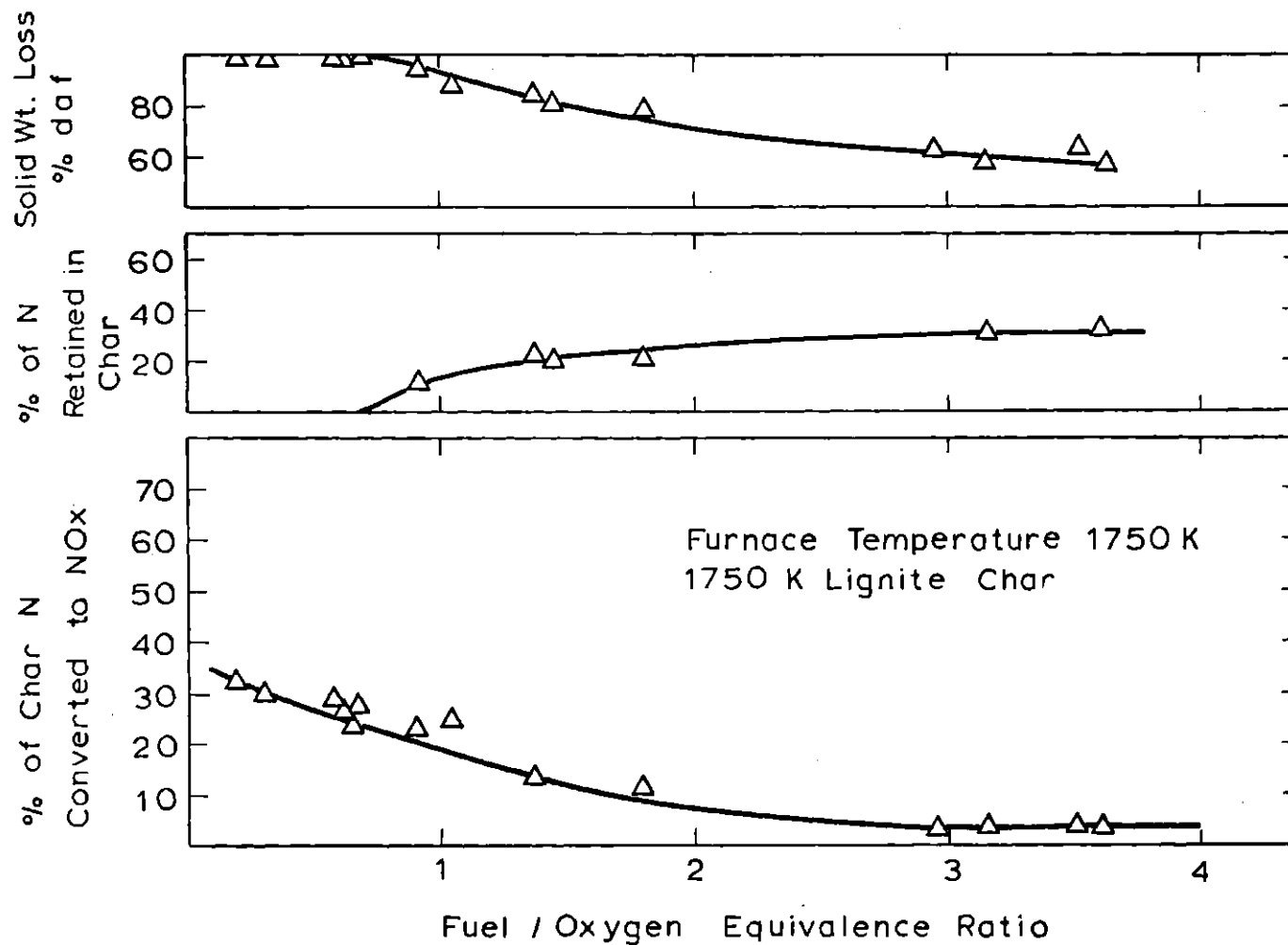
Figure 1.7

Fate of Char Nitrogen During Oxidation: Conversion to Nitric Oxide (Bottom): Retention by Unburned Char

(Middle); and Combustion Efficiency (Top). Char from Montana Lignite Pyrolyzed and Oxidized at 1750 K.
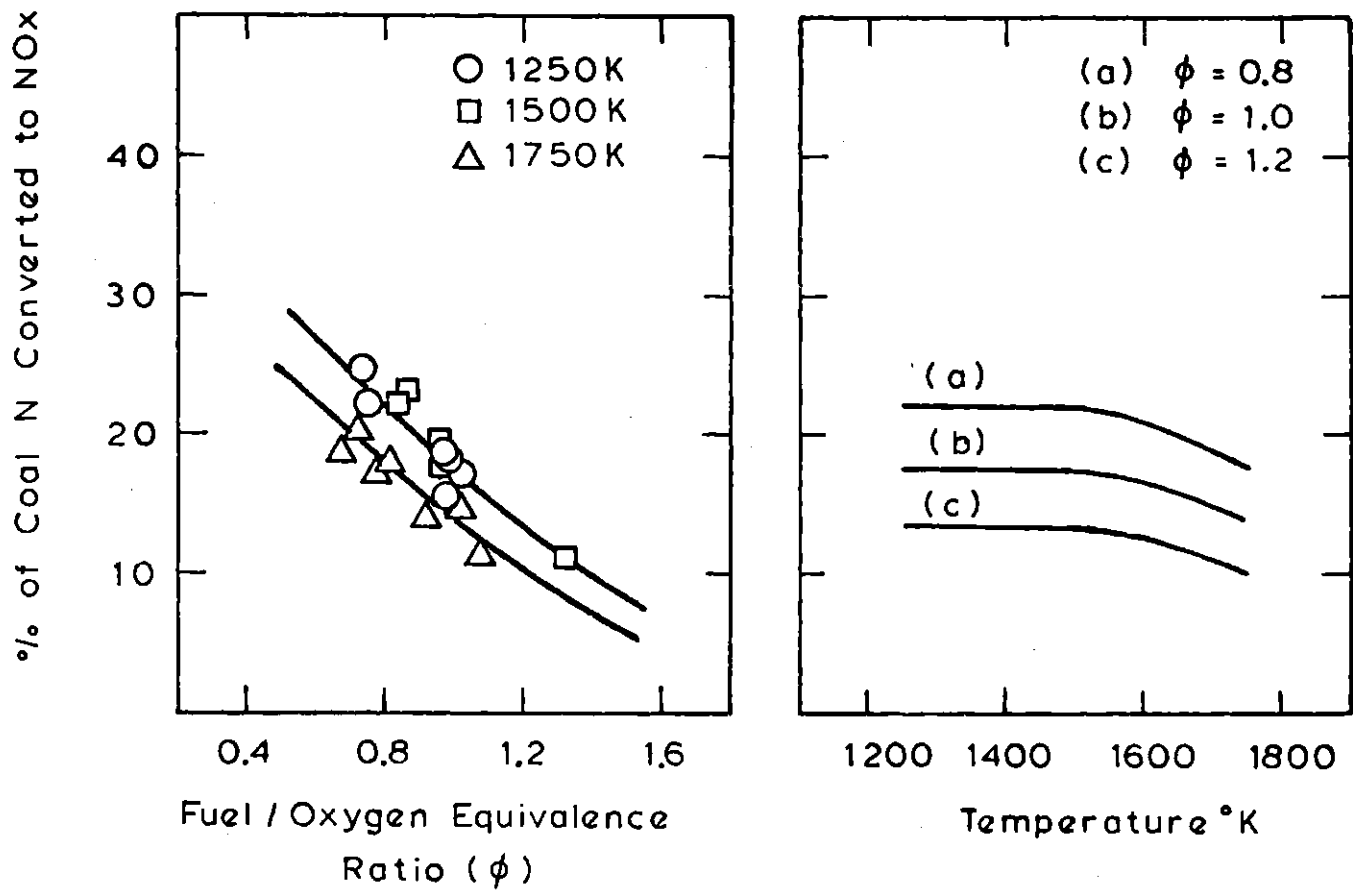
Figure 1.8

Effects of Temperature and Fuel/Oxygen Equivalence Ratio on Conversion of Coal Nitrogen to

Nitric Oxide. Montana Sub-bituminous Coal.

Montana sub-bituminous coal in this manner. The NO_x yields were
essentially the same at 1250 K and 1500 K while they decreased by about
20 to 25 percent as the temperature was increased from 1500 to 1750 K.
This is consistent with results shown in Figures 1.4 and 1.5. Comparison
of the data in Figure 1.8 with those in Figures 1.4 and 1.5 show very
little difference even though different coals are involved. This is
consistent with the findings of Pershing (1976) and results obtained
by Pohl (1976), both of whom reported that the conversion efficiency of
coal-nitrogen to NO_x at a particular temperature and fuel/oxygen
equivalence ratio was approximately independent of coal type.

A simplified scheme that represents the fate of the fuel nitrogen
during combustion of coal has been suggested previously (Pohl, 1976;
Pohl and Sarofim, 1976 and Song, Beér and Sarofim, 1977), and is
summarized below:

By a first order approximation which assumes that the volatile-nitrogen conversion to NO_x and char-nitrogen conversion to NO_x are independent, the overall conversion, η^*, of coal-nitrogen to NO_x is then given by:

$$\eta^* \quad = \quad \alpha\eta_1 \quad + \quad (1 - \alpha)\gamma\eta_2 \qquad\qquad (1.1)$$

overall   volatile   char
conversion   contribution   contribution
to NO_x

where

α = fraction of the coal-nitrogen that is released as volatiles

$1 - \alpha$ = fraction of the coal-nitrogen that is retained in the char

γ = fraction of the char-nitrogen that is consumed

$\gamma\eta_2$ = fraction of the char-nitrogen that is converted to NO_x

η_1 = fraction of the volatile-nitrogen that is converted to NO_x

η^* = overall conversion of coal-nitrogen to NO_x

The values of $(1 - \alpha)$ have been found to be 0.75 at a temperature of 1250 K and 0.27 at 1750 K. The values of η^* were reported as functions of fuel/oxygen equivalence ratio in Figures 1.4 and 1.5 for 1250 K and 1750 K, respectively, and the values of $\gamma\eta_2$ in Figures 1.6 and 1.7. The values of η_1, the efficiency of conversion to NO_x of the volatile-nitrogen and $\dfrac{\alpha\eta_1}{\eta^*}$, the percentage of the total NO_x contributed by volatile-nitrogen have been derived from the above information for temperatures of 1750 K and 1250 K and are reported in Figure 1.9. The efficiency of conversion to NO_x of volatile-nitrogen and the percentage of the total NO_x contributed by the volatile-nitrogen were found to decrease monotonically
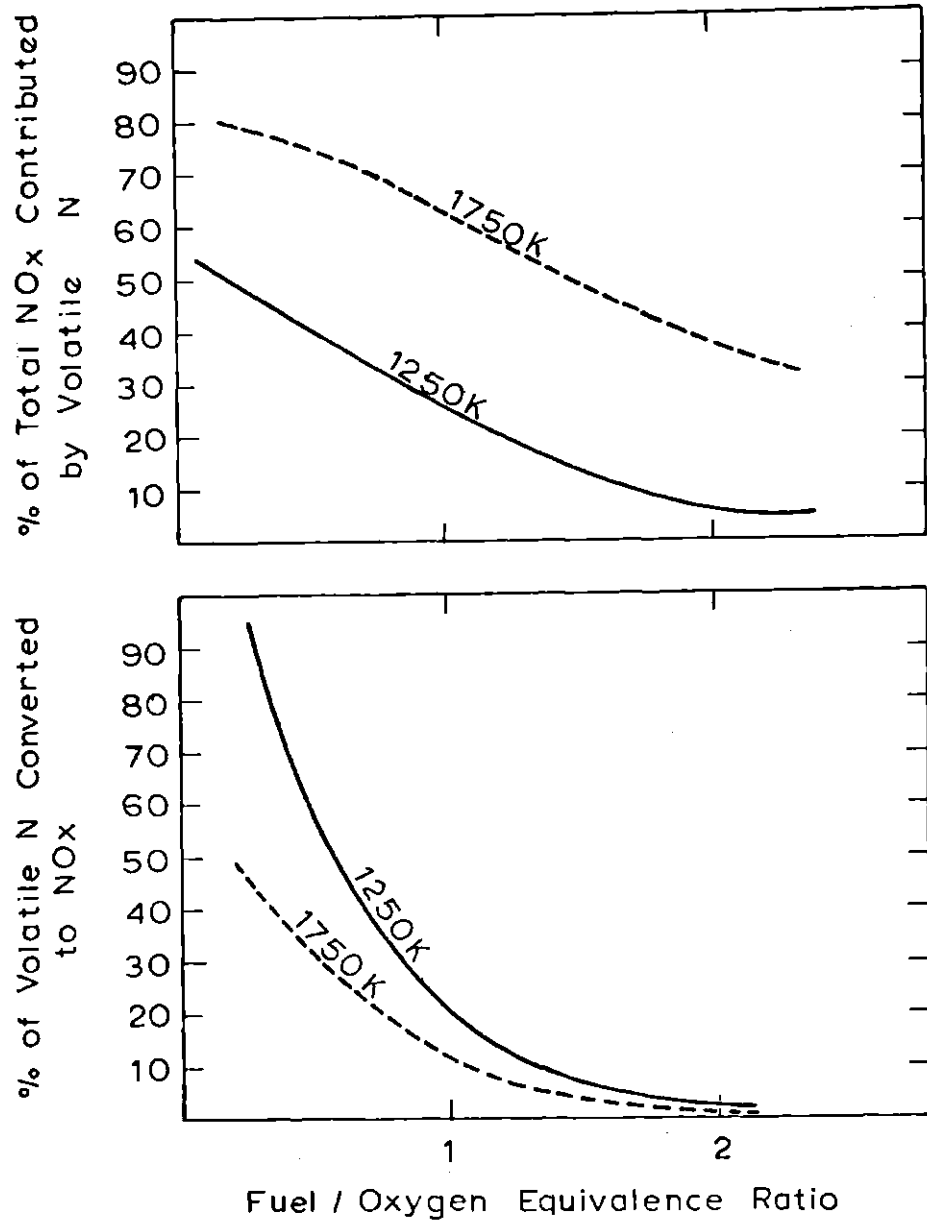
Figure 1.9

Fate of Volatile Nitrogen During Oxidation: Total Nitric Oxide Contributed by Volatiles (Top); Conversion Efficiency of Volatiles to Nitric Oxide (Bottom).

with increasing fuel-oxygen equivalence ratios. As expected, the contribution to NO_x by the volatiles increased with temperatures. The conversion to NO_x of the volatile-nitrogen, however, decreased with increasing temperature. These two effects tend to compensate and partially explain the small dependence on temperature of the conversion to NO_x of coal-nitrogen. In this study, a small net decrease was observed. In an independent study, Pershing (1976) has found practically no effect of temperature on the conversion of coal-nitrogen to NO_x.

It is of interest to note here that the present results of volatile combustion are in good agreement with the generalizations derived from studies on idealized laboratory flame systems (Fenimore, 1972; Sarofim, Williams, Modell and Slater, 1975; etc.). The present study showed that the volatile-nitrogen conversion efficiency decreased with increases in fuel/oxygen equivalence ratio. This result is in general agreement with those reported in flame studies. We have also demonstrated that the volatile-nitrogen conversion to NO_x decreased as the temperature increased. This is because the volatile phase has a higher volatile-nitrogen concentration at higher temperature for any given fuel/oxygen equivalence ratio, and this in turn results in a lower conversion to NO_x which is consistent with flame studies that show that the conversion of fuel-nitrogen to NO_x decreases with increases in concentration of fuel nitrogen.

The interactions between the devolatilization and oxidation steps in pulverized coal combustion complicate the development of NO_x control strategy. For any given temperature, the conversion efficiency to NO_x by volatile-nitrogen is usually higher than the conversion efficiency by char-nitrogen. This is very distinctly demonstrated especially at

fuel lean conditions. With increasing temperature, the extent of coal-nitrogen devolatilization increases but the conversion of the volatile-nitrogen to NO_x decreases. These two effects tend to compensate each other and partially lead to the small dependence on temperature of the total coal-nitrogen conversion to NO_x. Although the results from this study revealed that the total NO_x yields were decreased by about 20% as the furnace temperature was increased from 1500 to 1750 K, it is evident that the combustion modification by changing temperature alone does not have a very significant effect on the total NO_x emissions.

The conversion of fuel-bound nitrogen is most strongly dependent upon oxygen availability. The results above have shown that the conversion efficiencies to NO_x of both volatile-nitrogen and char-nitrogen decreased very significantly with increasing fuel/oxygen equivalence ratio. This suggests that the reduction of NO_x emissions from pulverized coal combustors can be best accomplished by varying the fuel/oxygen equivalence ratio and temperature at different stages of the combustion process. It is optimal to operate the first stage of a combustor at high temperature and fuel-rich conditions to favor the completion of the devolatilization. The residual char with little nitrogen content (the nitrogen content of residual char depends on the extent of nitrogen-devolatilization at first stage) is then transported to the second stage of the combustor to complete the combustion at relatively fuel lean conditions and low temperature. In this manner, a stage pulverized coal combustor will significantly reduce the NO_x emissions while maintaining a high combustion efficiency.

1.3.2 Oxidation of Char-Nitrogen

The above results have provided a general guidance on control strategies. In order to implement such strategies detailed information on the rate controlling kinetic steps is needed. One rate controlling step is the oxidation of the char, as a result of which nitrogen in char may persist beyond the fuel rich first stage of a staged combustor and be oxidized with a higher efficiency of conversion to NO_x in the lean second stage. In order to design the second stage to achieve acceptable levels of char burnout data are needed on the kinetics of char-nitrogen oxidation. Of particular interest is any selectivity that oxygen may show in attacking carbon and nitrogen atoms in a char particle.

Oxidation experiments were carried out on a 1750 K lignite char at temperatures of 1250 K, 1500 K, and 1750 K and oxygen partial pressures of 0.2 atm and 0.4 atm. The time-resolved char retentions are presented in Figure 1.10. In this semi-logarithmic plot, the char retention appeared to level off after the retention became less than about 55%, indicating the decrease of reactivity of char with the extent of burnout.

Selected char samples were further analyzed to determine both the physcial characteristics and chemical compositions. Figure 1.11 shows the behaviors of the normalized specific B.E.T. surface area and the normalized average pore diameter. (They were normalized against the initial properties of the original char.) Up to approximately 45% char burnout, the specific B.E.T. surface area increased and the average pore diameter decreased, implying the opening-up of small pores in the initial stages of char oxidation. In the latter stages, the char burned both externally and internally until, at an advanced stage, it fragmented as
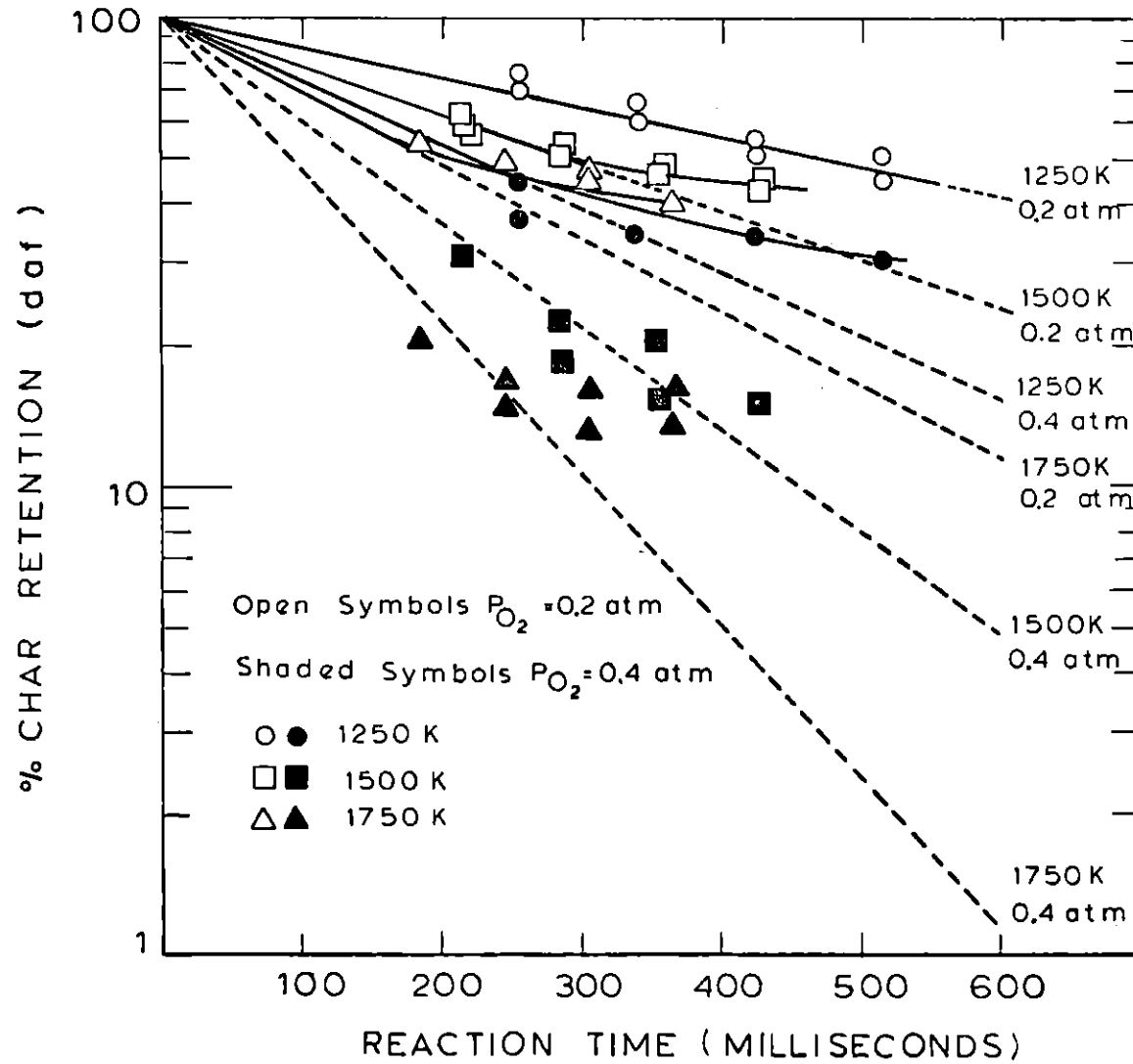
Figure 1.10

Retention of Char as Function of Reaction Time During Oxidation.
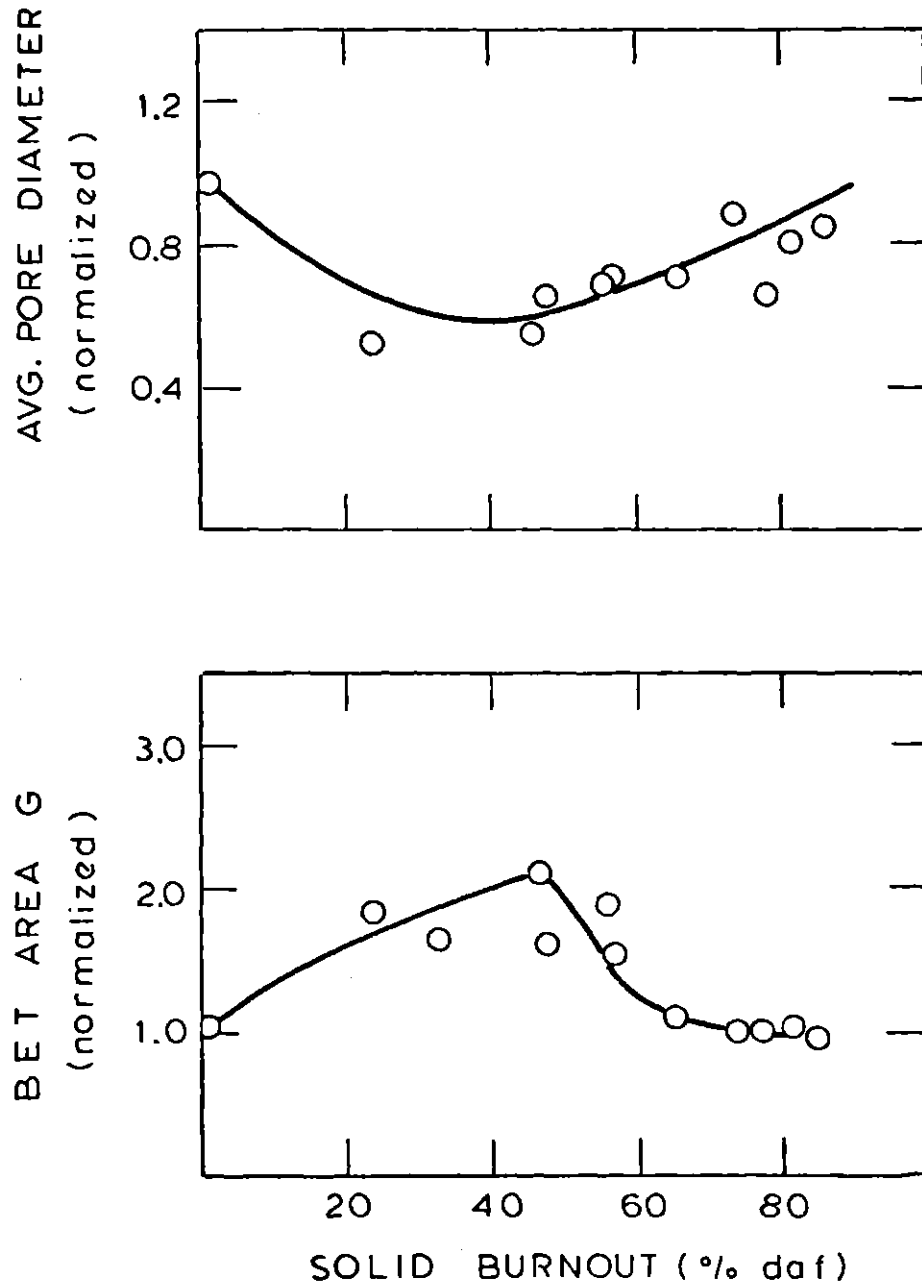
Figure 1.11

Average Pore Diameter and Specific B.E.T. Surface Area as Functions of Solid

Burnout During Char Oxidation

has been observed previously (Anson, Moles and Street, 1971). This is corroborated by the present results showing decreasing specific B.E.T. surface area and increasing average pore diameter in the latter half of the burnout process, which can be interpreted in terms of the destruction of the micropores.

The variation of nitrogen to carbon ratio is reported in Figure 1.12. The plot of the logarithm of nitrogen-to-carbon ratio versus reaction time yields a straight line. The nitrogen to carbon ratio was found to decrease with temperature but to be insensitive to oxygen partial pressure during char burnout.

The initial rates of char oxidation were calculated by determining the initial slopes in Figure 1.10. The derivation of the apparent kinetics for char oxidation requires the knowledge of particle temperatures (T_p) and surface oxygen concentrations. Values of T_p were calculated from the steady-state heat balance which assumed that the primary product at the surface was CO (Ayling and Smith, 1972, Field et al., 1967). The estimated surface temperatures were found to be higher than the surrounding gas temperatures by about 10 to 40 K. The surface oxygen concentrations were estimated by taking into account the external gas phase diffusion. Finally, the apparent kinetics was obtained based on the above information. The apparent reaction order with respect to oxygen was found to be 0.99. The intial apparent rate constant per unit external surface area was found to be

$$k_E = 5.0 \times 10^3 \cdot \exp\ (-11,200/RT)\ \frac{cm}{sec}\ \left(\frac{g\text{-moles}}{cm^3}\right)^{0.01} \tag{1.2}$$
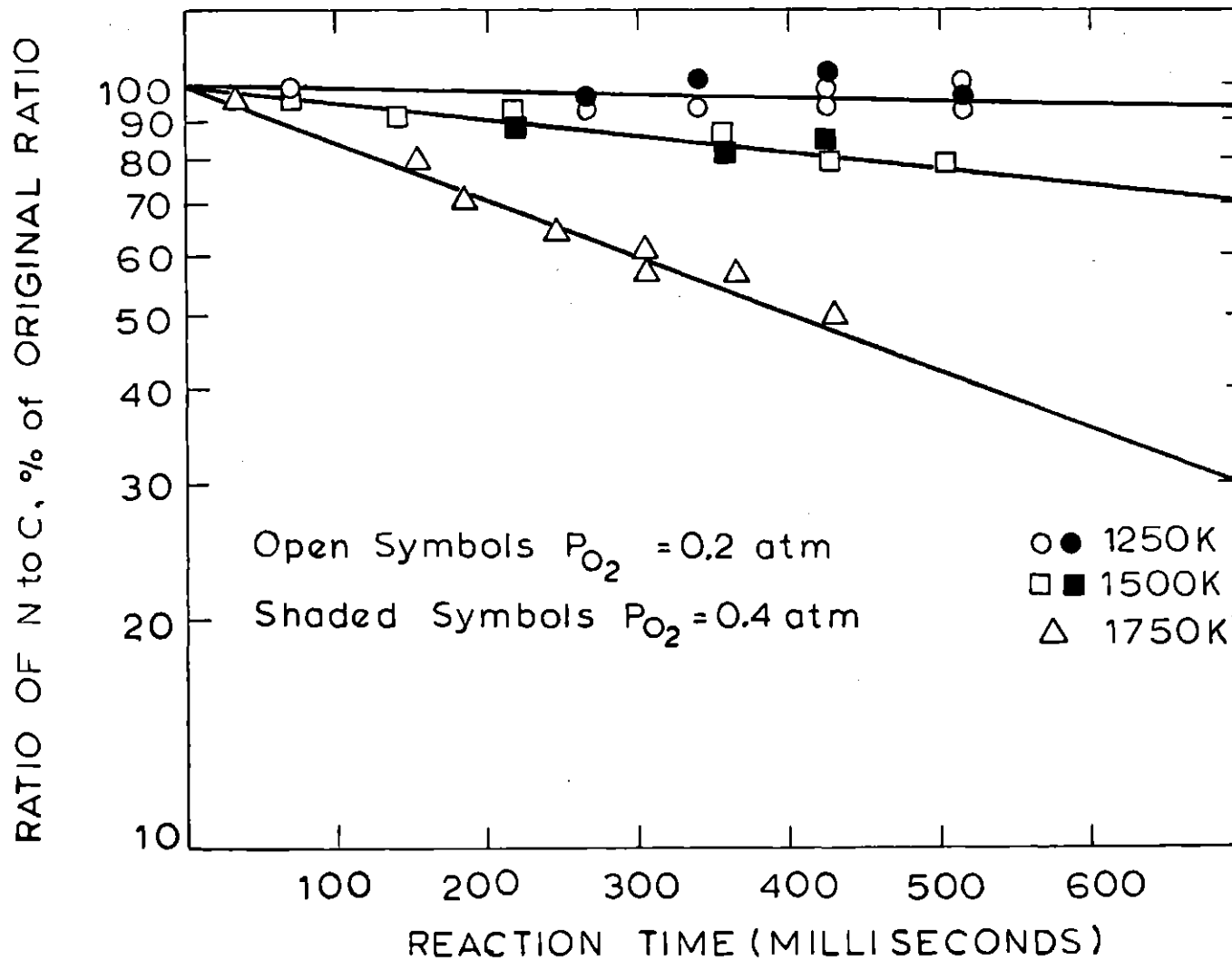
Figure 1.12

Ratio of Nitrogen to Carbon as Function of Reaction Time During Char Oxidation.

This is shown in Figure 1.13.

The internal pore diffusion (Mulcahy and Smith, 1969) has to be taken into account in order to distinguish the intrinsic reaction kinetics from the apparent kinetics. For simplicity, a porous char with a flat-plate geometry was assumed for the mathematical analysis. The reaction order with respect to oxygen was found to be 0.98 and the intrinsic rate constant per unit B.E.T. surface area was found to be

$$k_B = 2.8 \times 10^3 \cdot \exp\ (-22,100/RT)\ \frac{cm}{sec}\ \left[\frac{g\text{-moles}}{cm^3}\right]^{0.02} \qquad (1.3)$$

This is shown in Figure 1.14.

The intrinsic activation energy found in the present study appears slightly low (see Smith, 1971a, 1971b; Smith and Tyler, 1972, 1974; Field et al., 1967; Mandel, 1977), nevertheless, the absolute overall reaction rates are comparable to those reported by Smith and Tyler (1974) for a pulverized brown coal char over a wide range of temperatures.

It has been pointed out earlier that the reactivity of the char changed during the oxidation process. This is shown in Figure 1.15. The reactivity of the char remained constant in the early stage of the burnout process and dropped dramatically in the late stage. This behavior was successfully explained by a pore-mouth poisoning model (Wheeler, 1951, 1955) which has proved to be physically consistent with the combustion process. The details of the pore-mouth poisoning model are not included in this digest but may be found in the text of the thesis.

In regard to the behavior of the char-nitrogen, the nitrogen to carbon ratio was found to decrease with temperature but to be insensitive
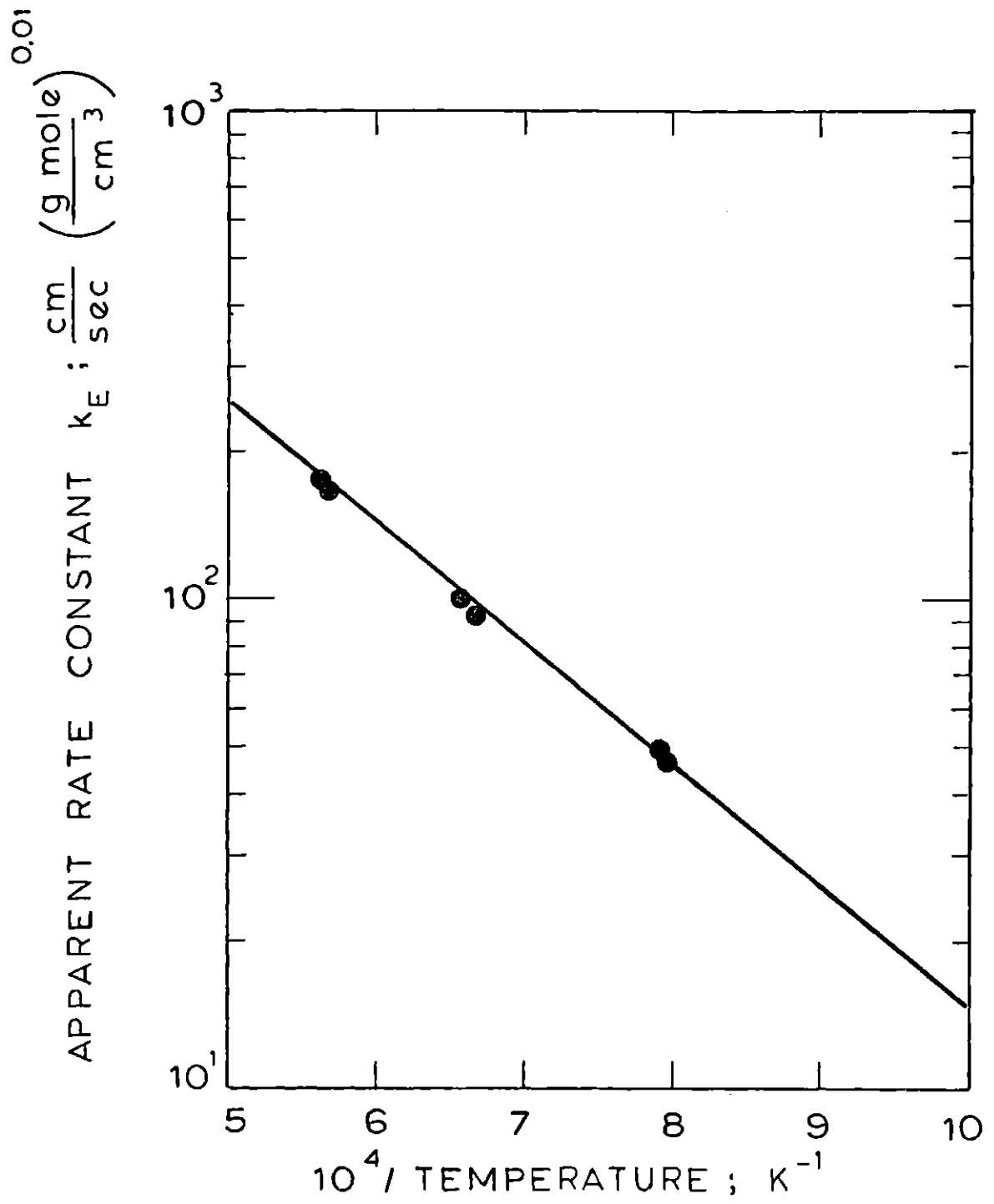
Figure 1.13

Arrhenius Plot of Apparent Rate Constant for Char Oxidation
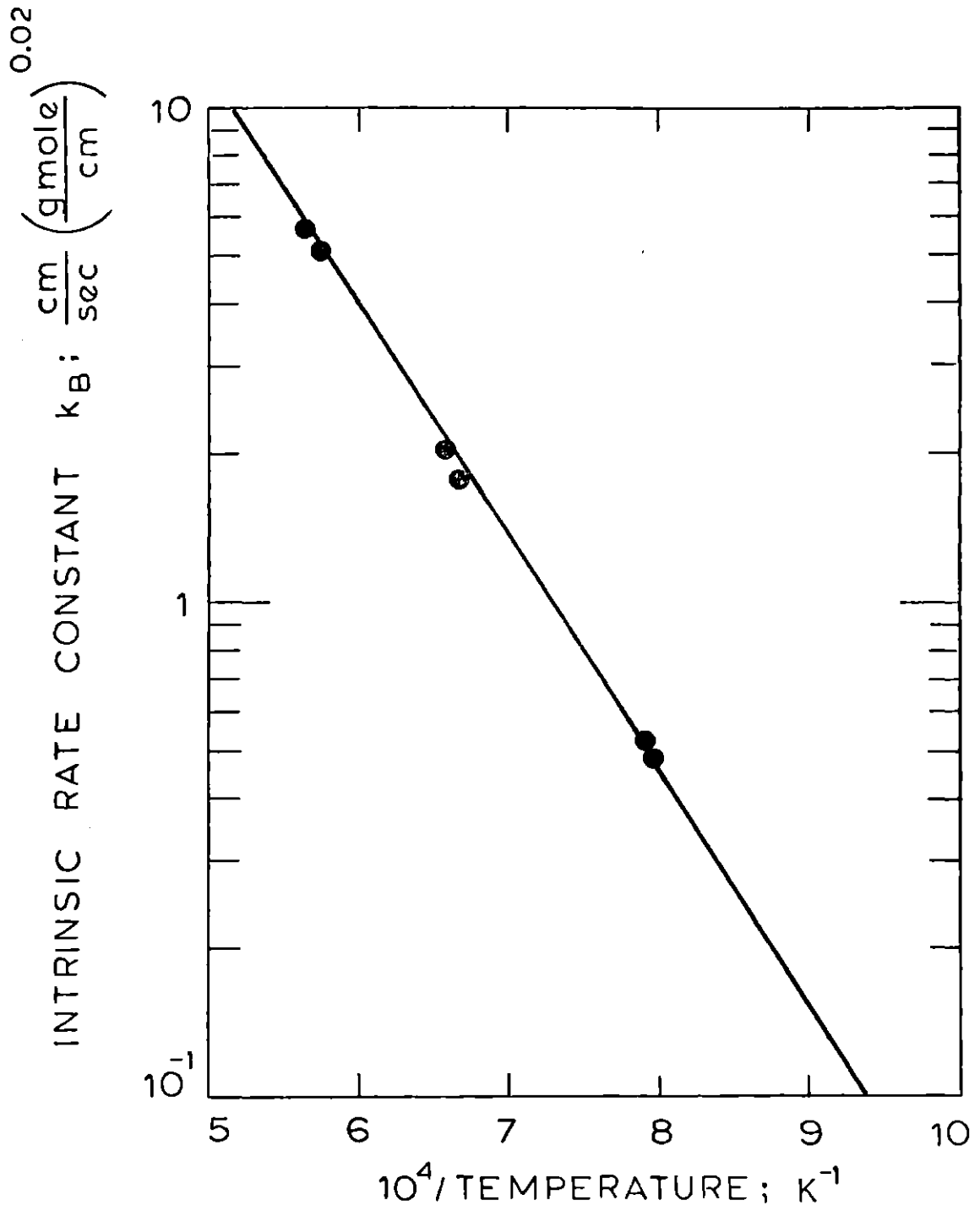
Figure 1.14

Arrhenius Plot of Intrinsic Rate Constant for Char Oxidation
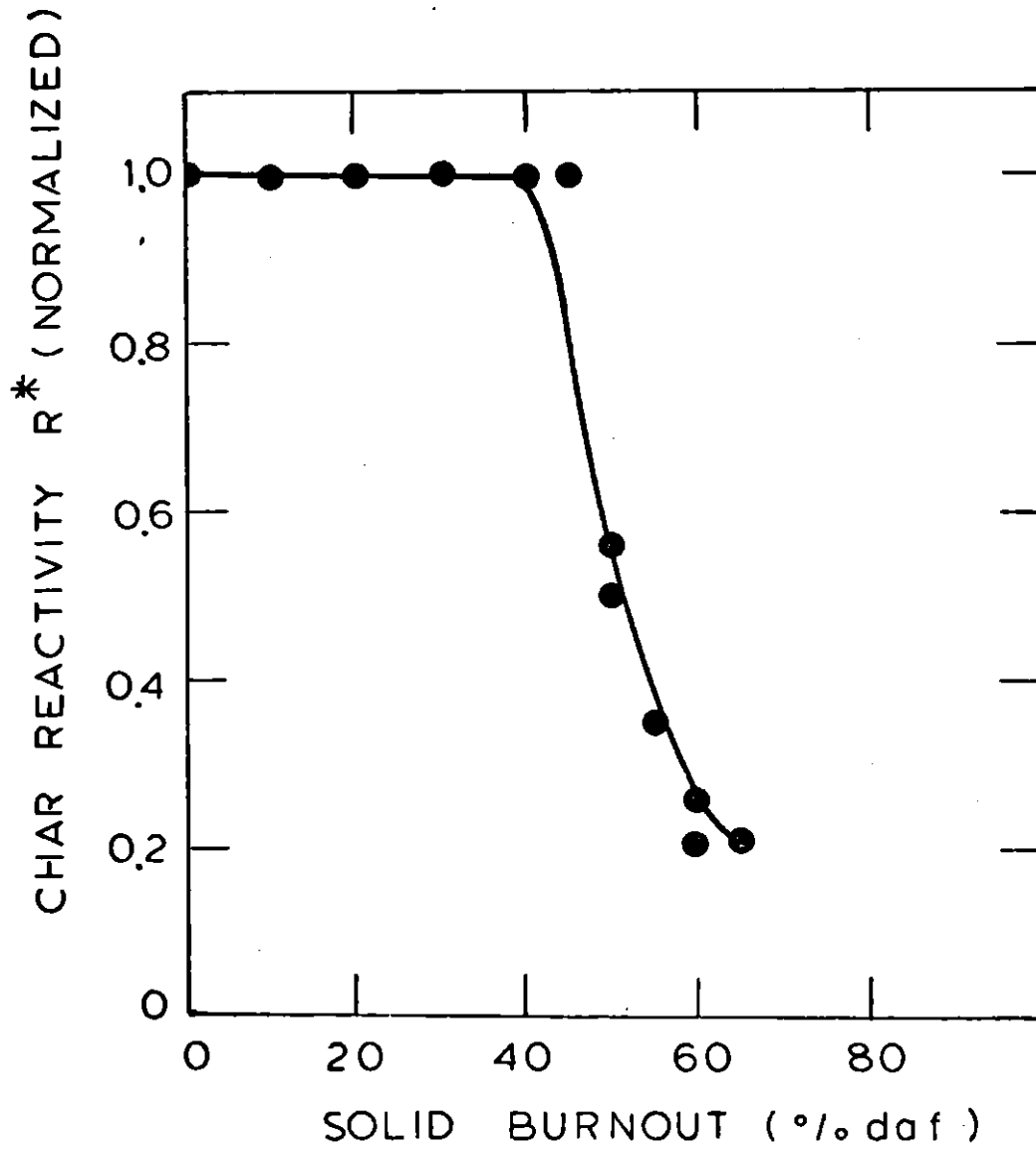
Figure 1.15

Char Reactivity as Function of Solid Burnout During Oxidation

to oxygen partial pressure during char burnout. It has been previously shown (Pohl, 1976) that during coal pyrolysis, the carbon loss reached an asymptotic value within a time of 100 milliseconds at 1750 K, the temperature used to produce the char in this study, but that nitrogen release continued for longer times. The rationalization of these results was that while carbon is present in relatively stable compounds in the char, no comparable stabilized nitrogen structures are formed; consequently, char-nitrogen continues to be released until it is completely eliminated from char. Therefore, when a char particle is oxidized, nitrogen loss will be due to both devolatilization and oxidation, but the carbon loss will be exclusively due to oxidation.

Since the pyrolysis loss and oxidation loss of char-nitrogen are additive, the consumption rate of char-nitrogen can be written as

$$
\left\{ \begin{array}{l} \text{total consumption-rate} \\ \text{of char-nitrogen} \end{array} \right\} = \left\{ \begin{array}{l} \text{consumption-rate of} \\ \text{char-nitrogen due to} \\ \text{pyrolysis} \end{array} \right\} +
$$

$$(1.4)$$

$$
\left\{ \begin{array}{l} \text{consumption-rate of} \\ \text{char-nitrogen due} \\ \text{to oxidation} \end{array} \right\}
$$

or in symbols

$$
\frac{dN}{dt} = \left(\frac{\partial N}{\partial t}\right)_{pyrolysis} + \left(\frac{\partial N}{\partial t}\right)_{oxidation} \tag{1.5}
$$

Assuming the fuel-nitrogen is uniformly distributed throughout the char, the oxidation rate of the nitrogen should therefore equal the product of

the instant oxidation rate of the carbon and the mole ratio of the fuel nitrogen to carbon in the char in that instant (Wendt and Schulze, 1976). We have

$$\left(\frac{\partial N}{\partial t}\right)_{oxidation} = \left(\frac{\partial C}{\partial t}\right)_{oxidation} \cdot \left(\frac{N}{C}\right) \tag{1.6}$$

The carbon loss during combustion is exclusively due to oxidation, i.e.,

$$\frac{dC}{dt} = \left(\frac{dC}{dt}\right)_{oxidation} = \left(\frac{\partial C}{\partial t}\right)_{oxidation} \tag{1.7}$$

Combining Equation (1.5), (1.6) and (1.7), gives

$$\frac{dN}{dt} = \left(\frac{\partial N}{\partial t}\right)_{pyrolysis} + \left(\frac{dC}{dt}\right) \cdot \left(\frac{N}{C}\right) \tag{1.8}$$

A first-order fuel-nitrogen pyrolysis kinetics (Pohl, 1976) gives

$$\left(\frac{\partial N}{\partial t}\right)_{pyrolysis} = -k_{py} \cdot N \tag{1.9}$$

Substituting Equation (1.9) into equation (1.8) yields

$$\frac{dN}{dt} = -k_{py} \cdot N + \left(\frac{N}{C}\right) \cdot \left(\frac{dC}{dt}\right) \tag{1.10}$$

The carbon oxidation rate, $\frac{dC}{dt}$, can be obtained directly from the rate of char-oxidation described previously. The char-nitrogen pyrolysis

rate constant, k_{py} can be obtained from the time dependence of nitrogen to carbon ratio. The slope of the lines in Figure 1.12 yields d ln(N/C)/dt. This may be equated to k_{py} as follows.

$$\frac{d}{dt}\left(\frac{N}{C}\right) = \frac{1}{C}\left(\frac{dN}{dt} - \left(\frac{N}{C}\right)\cdot\left(\frac{dC}{dt}\right)\right) \tag{1.11}$$

Multiplying both sides by C and rearranging the terms, we obtain

$$\frac{dN}{dt} = C\,\frac{d}{dt}\left(\frac{N}{C}\right) + \left(\frac{N}{C}\right)\cdot\left(\frac{dC}{dt}\right) \tag{1.12}$$

Comparing Equation (1.10) and (1.12), gives

$$C\,\frac{d}{dt}\left(\frac{N}{C}\right) = -k_{py}\cdot N \tag{1.13}$$

Upon rearrangement, we have

$$\frac{1}{(N/C)}\,\frac{d}{dt}\,(N/C) = -k_{py} \tag{1.14}$$

or

$$\frac{d}{dt}\left(\ln\left(\frac{N}{C}\right)\right) = -k_{py} \tag{1.15}$$

Figure 1.16 shows the Arrhenius-type correlation for k_{py} and gives the following expression:
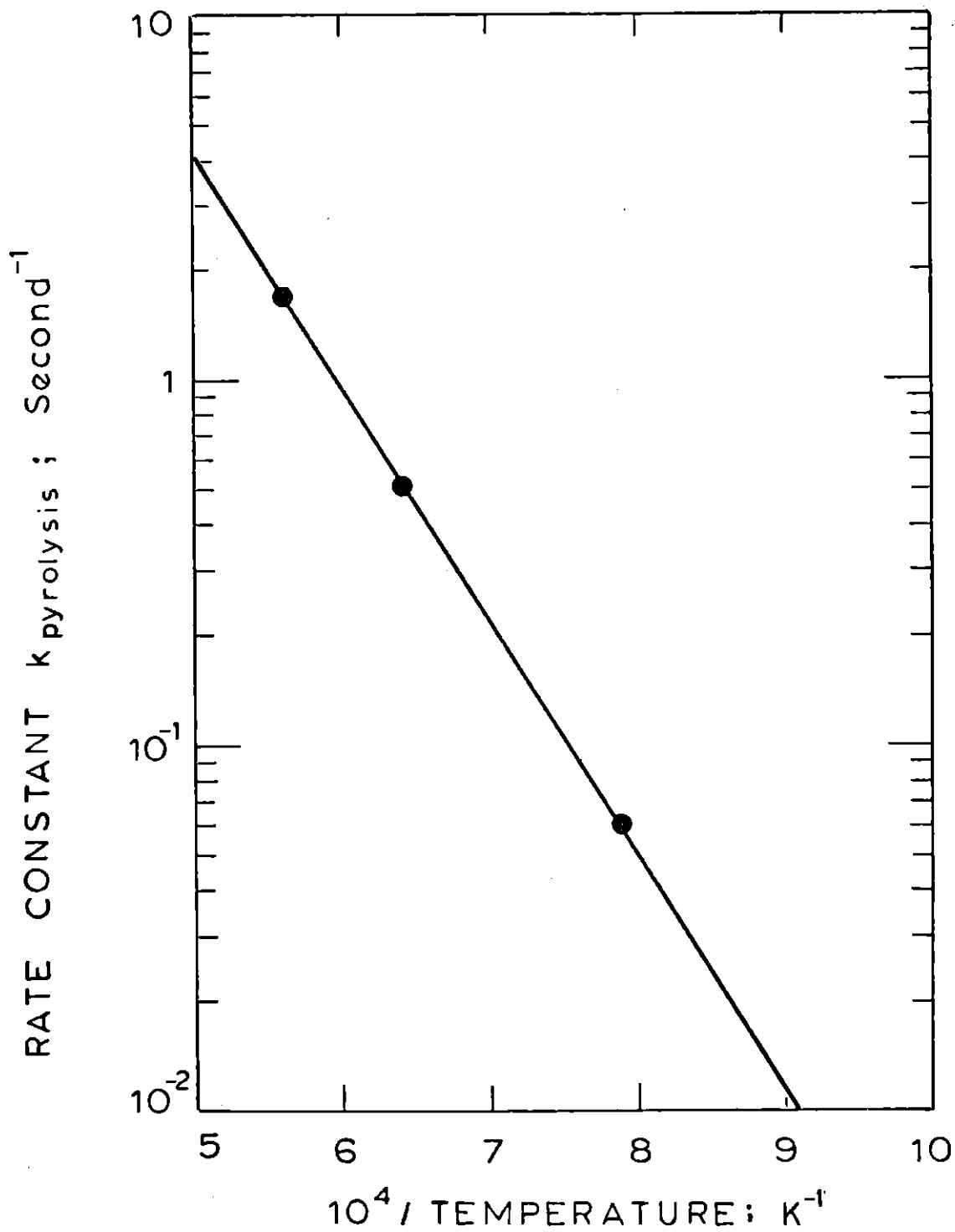
Figure 1.16

Arrhenius Plot of Pyrolysis Rate Constant for Char Nitrogen

$$k_{py} = 5.8 \times 10^3 \cdot \exp(-29,100/RT) \text{ sec}^{-1} \tag{1.16}$$

The comparison of present data with Pohl's coal-nitrogen pyrolysis data shows a good agreement (Figure 1.17).

In summary, the reaction rate of char-nitrogen during combustion can be described by the following rate expression:

$$\frac{dN}{dt} = -k_{py} \cdot N + \left(\frac{dC}{dt}\right) \cdot \frac{N}{C} \tag{1.17}$$

where k_{py} is given by Equation (1.16) and $\frac{dC}{dt}$ is the char oxidation rate.

1.3.3 Reduction of Nitric Oxide by Char

It is evident that the Char/NO_x reactions are important in determining the net NO_x emissions from fluidized bed coal combustors (Gibbs, Pereira and Beér, 1976). In parametric investigations of this study, the conversion efficiency of char-nitrogen to NO_x was found to be lower than that of volatile-nitrogen under corresponding conditions. This is possibly a consequence of the reduction of NO_x by char. It is essential to take into account the reduction of NO_x by char in modelling the char-nitrogen conversion to NO_x. In addition, a better understanding of the Char/NO_x reaction will, of course, provide information pertinent to the reduction of NO_x emissions by the modification of the combustion process.

Assuming a reaction first order in nitric oxide (Edward, 1972;
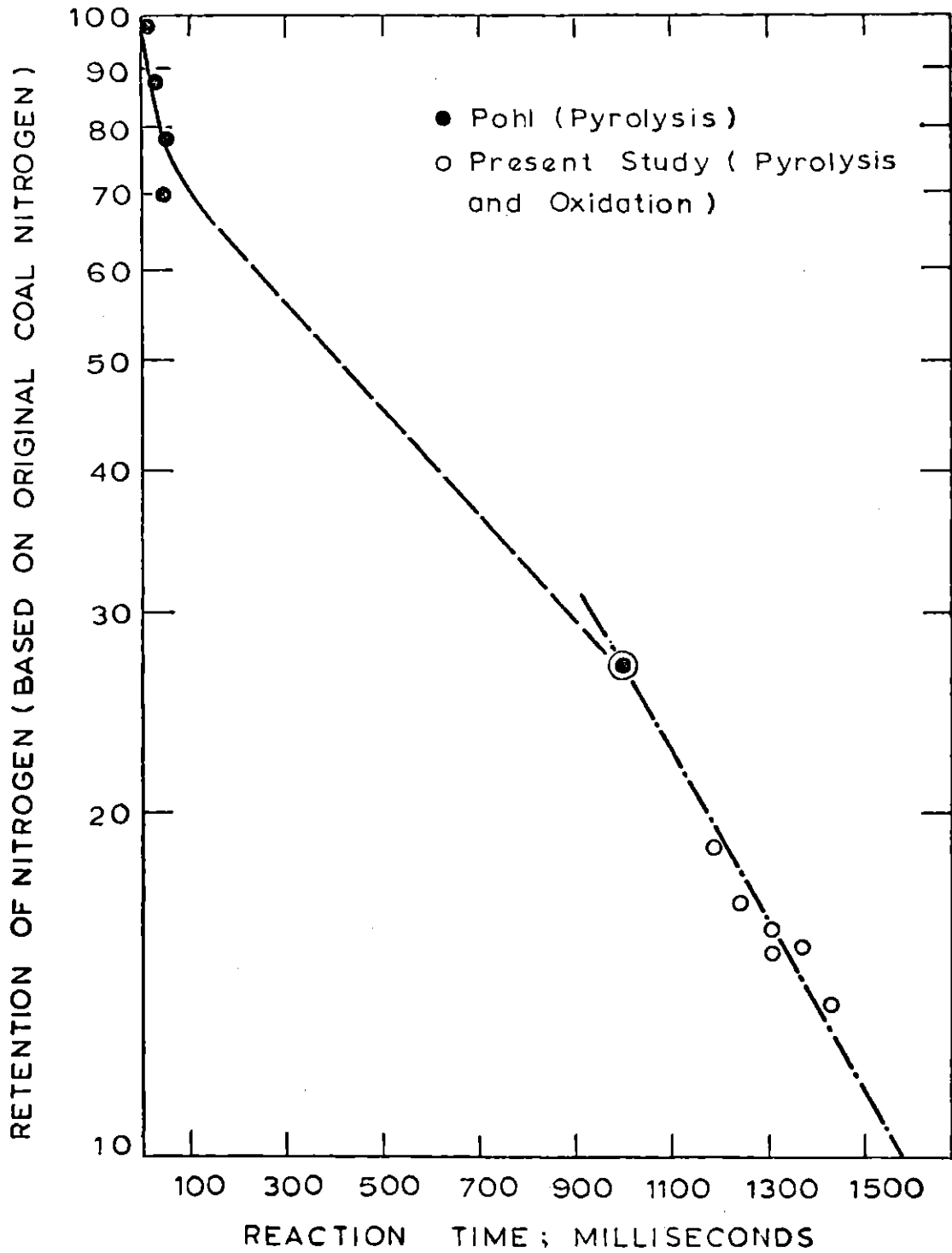
Figure 1.17

Retention of Fuel Nitrogen as Function of Reaction Time During
Pyrolysis and Oxidation

Pereira et al., 1976; Furnsawa et al., 1977) the rate constant may be given by:

$$(\eta \cdot k) = K \cdot \frac{1}{A_B \cdot \frac{W}{\tau}} \cdot \frac{u_{in}^2}{V} \cdot T_F \cdot \ln \frac{[NO]_{in}}{[NO]_{out}} \tag{1.18}$$

where

k   = intrinsic rate constant per unit B.E.T. surface area

η = effectiveness factor

A_B = specific B.E.T. surface area of char

W   = mass of char fed

τ = feeding time of char

u_{in} = volumetric flow rate of main gas

V   = working volume of furnace

T_F = furnace temperature

[NO]= concentration of NO_x

K   = 1.372×10^{-10} $\frac{g\text{-mole}}{l \cdot ppm \cdot K}$, is a constant

The values of $\frac{u_{in}^2}{W/\tau} \cdot \ln \frac{[NO]_{in}}{[NO]_{out}}$ were calculated from experimental data and were found to be independent of $[NO]_{in}$ (see Figure 1.18) implying that the char and NO_x reaction is indeed a first order reaction with respect to NO_x.

The effectiveness factor, η, and intrinsic rate constant, k, were evaluated from Equation (1.18) with following equations of η and ϕ_s, the Thiele modulus, by a trial-and-error method.
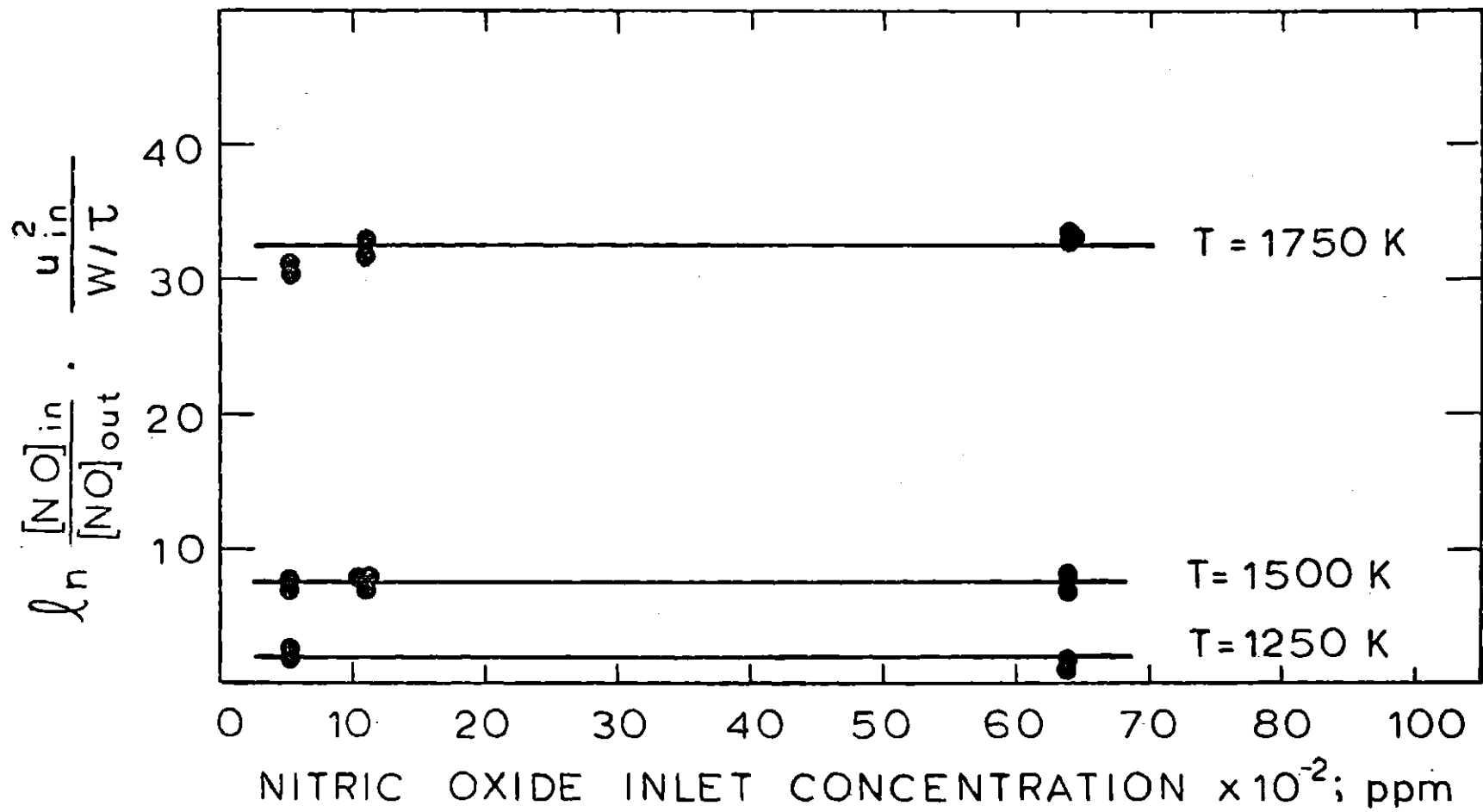
Figure 1.18

Test for a First-Order Kinetics of Nitric Oxide Reduction by Char.

$$\eta = \frac{1}{\phi_s} \left[\frac{1}{\tanh \ 3\phi_s} - \frac{1}{3\phi_s} \right] \qquad (1.19)$$

and

$$\phi_s = \frac{r_s}{3} \sqrt{\frac{k \cdot A_B \cdot \rho_B}{b \cdot D_e}} \qquad (1.20)$$

where

r_s = radius of particle

ρ_B = bulk density of particle

D_e = effective diffusivity

b = $4.1 \times 10^{-11} \ \dfrac{\text{g-mole}}{(\text{cm}^3)(\text{ppm})}$, is a conversion factor

A plot of k versus $1/T_F$ (Figure 1.19) yields an expression for k to be

$$k = 5.0 \times 10^{-5} \cdot \exp(-32,700/RT) \ \frac{\text{moles}}{(\text{sec})(\text{m}^2)(\text{ppm})}$$

The results obtained from present studies are in general agreement with the trend of high temperature results by Furusawa et al. (Figure 1.20).

Comparison between the Char/NO_x and Char/O_2 reaction shows that the intrinsic reaction rate for Char/NO_x is much slower than that for Char/O_2 system, but this is partially offset by differences in effectiveness factors.

Figure 1.21 was produced using the above results. The reduction of NO_x is strongly dependent upon the temperature level and char availability. A significant fraction of the NO_x can be reduced by
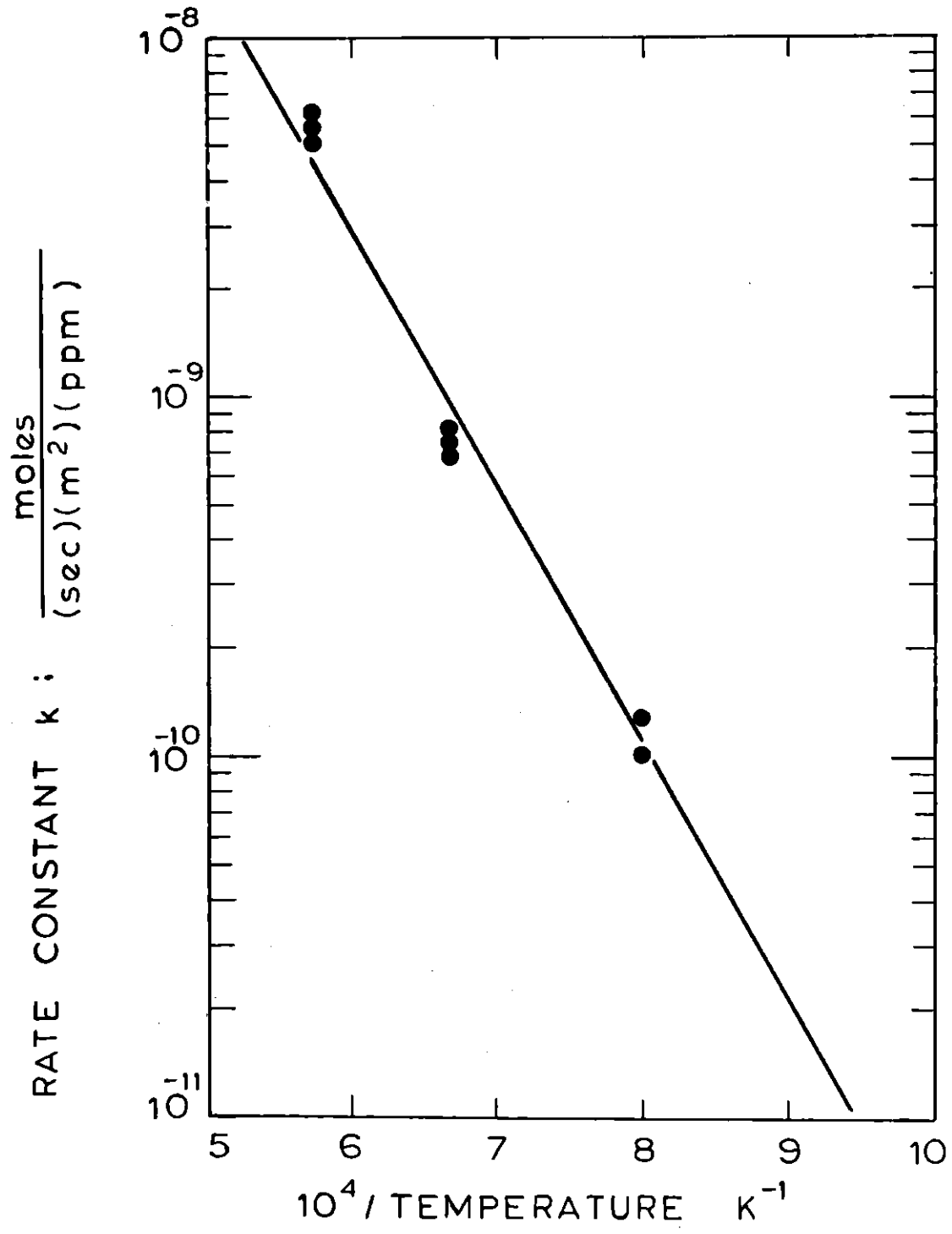
Figure 1.19

Arrhenius Plot of Intrinsic Rate Constant for Nitric Oxide Reduction by Char
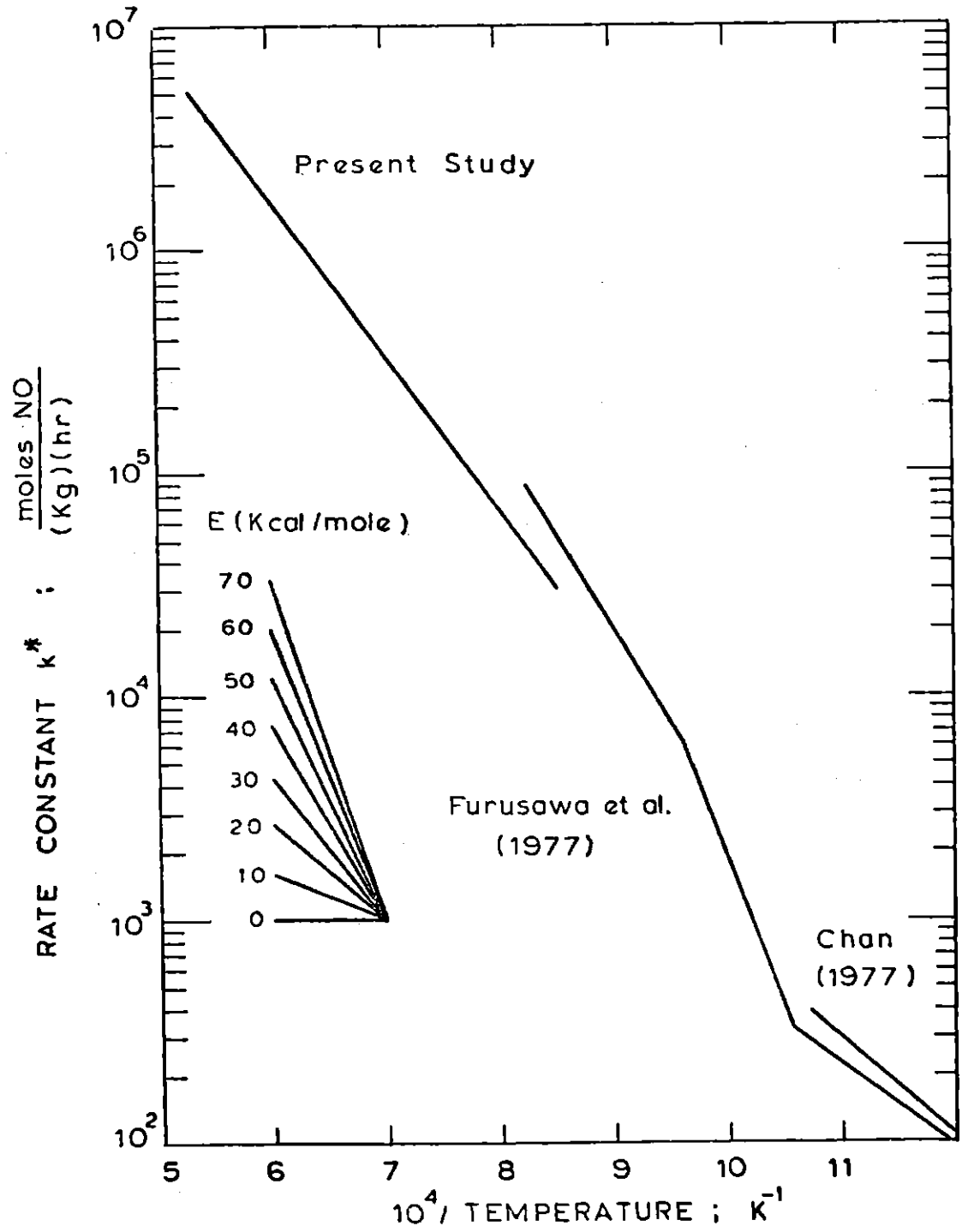
Figure 1.20

Comparison of Rate Constants for Nitric Oxide Reduction by Char
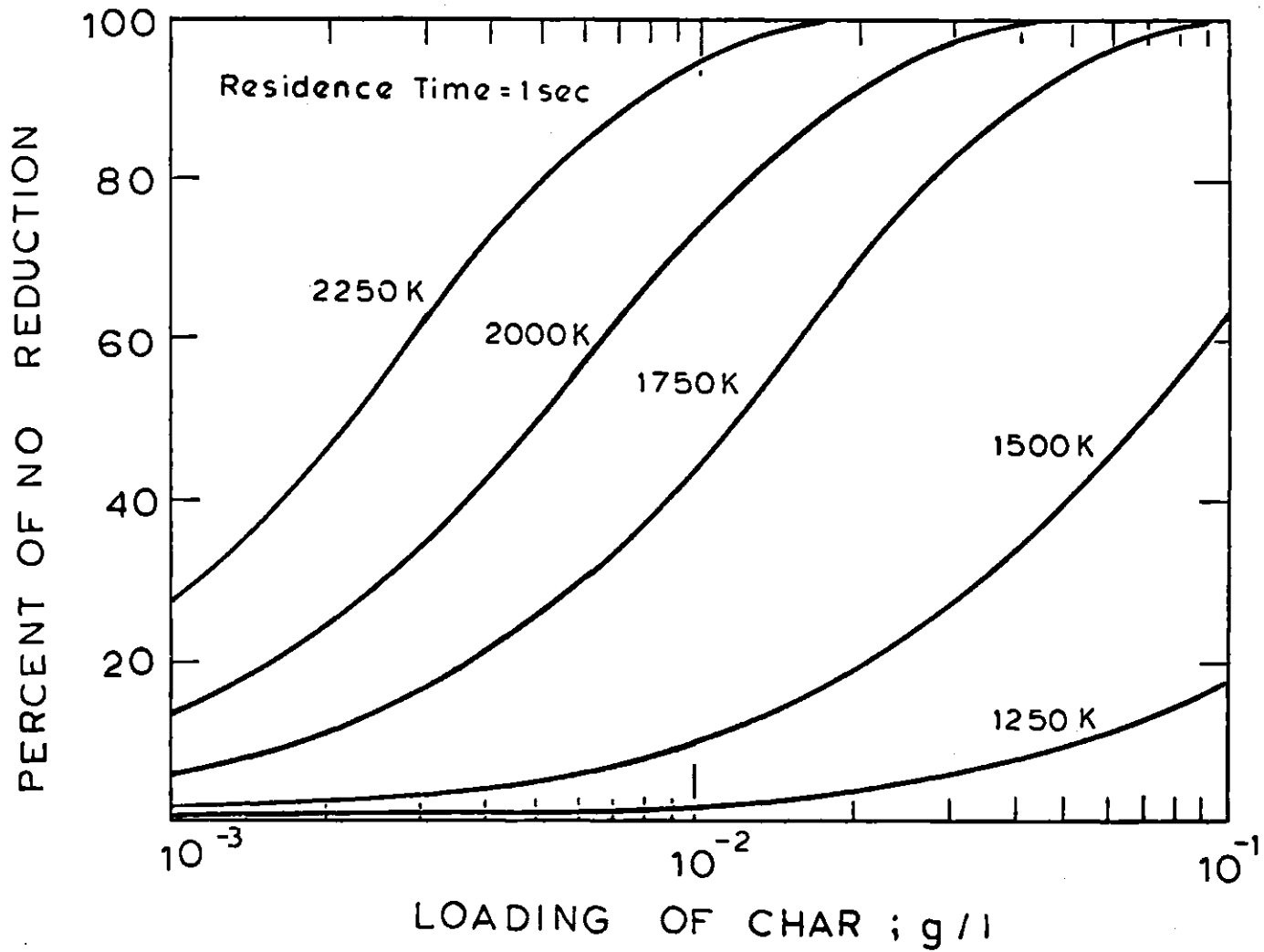
Figure 1.21

Potential Nitric Oxide Reduction as Function of Char Loading and Temperature

the contact with char at high temperature and/or long gas residence time. Brown et al. (1977) have observed that at a high fuel load, the increased first stage residence time had a major effect on NO_x reduction in coal fired boilers. The present model certainly provides an explanation to their experimental finding.

1.4 Conclusions

The major contributions of this thesis are the determination of the effects of temperature and fuel/oxygen equivalence ratio on the conversion of fuel nitrogen to NO_x and the elucidation of the roles played by the oxidation of char-nitrogen and the nitric oxide-char reaction on the overall coal-nitrogen conversion.

The data on coal and char oxidation show that the volatile-nitrogen accounts for the major fraction of the NO_x produced from coal-nitrogen at high temperature and low fuel/oxygen equivalence ratio. Increasing temperature increases the volatile contribution but decreases the efficiency with which it is converted to NO_x. For the combustor in this study, there is a net decrease in emissions with increases in both the temperature and the fuel/oxygen equivalence ratio in the first stage of a stage combustor.

The overall char burnout is found to be controlled primarily by internal pore diffusion. No selectivity between nitrogen and carbon loss is observed during oxidation but char-nitrogen is found to undergo pyrolysis in parallel with oxidation. The results indicate that the pyrolysis rate and the oxidation rate of the fuel-nitrogen are additive and separable during pulverized coal combustion.

The data on Char/NO_x experiments show that a significant fraction of NO_x can be reduced by the contact with char, especially at high temperature and/or long gas residence time.

CHAPTER 2

INTRODUCTION

As the U.S. oil production is declining, proved gas reserves are dwindling, and nuclear power is facing an uncertain future, coal is expected to play a more and more important role in the energy market. Furthermore, among all the energy resources, coal seems to be the most secure, because it is the most abundant domestic energy resource. The nation's prodigious coal reserves - on third of the world's known deposits - have hardly been tapped. Even at today's price and with today's mining methods, 437 billion tons of the fuel can be recovered in states from Texas to Alaska, from Pennsylvania to California. That is equal to a 340 year supply at the current rate of consumption. At the projected 1985 consumption levels, the coal reserves are still enough to last at least 200 years.

One of the major obstacles that prevent the extensive utilization of the enormous coal reserves is the emissions of nitric oxides (NO_x) from coal-burning facilities of current design. Of the five emitted pollutants for which National Ambient Air Quality Standards (NAAQS) have been promulgated (particulate matter, NO_x, SO_x, hydrocarbons, and CO, termed criteria pollutants), NO_x constitutes one of the most difficult problems to deal with. NO_x takes part in complex atmospheric reactions resulting in the formation of photochemical oxidants and other pollutants. Most of the anthropogenic NO_x emissions originate from combustion. Although combustion process modification is the least costly control technique, care must be taken that the controls should not produce such undesirable

results as lower fuel efficiency and increased hydrocarbon and CO emissions.

As a result of the rapid growth rate projected for combustion sources, combustion generated pollutant emissions are also expected to increase. Of the major pollutants, NO_x is the one the emission of which can be effectively controlled by combustion modifications. Sulfur emission has to be controlled either by burning low sulfur or desulfurized fuels or by scrubbing the flue gas. Organic particulates should not be emitted from a well designed plant and the inorganic particulates have to be precipitated from the flue gas.

In the following Sections, we shall present an overview on the dependence on coal as an energy resource and discuss NO_x as a health hazard. We shall also discuss briefly NO_x control technologies and, finally, the motivation for this study.

2.1 Coal - An Energy Resource

The United States has vast reserves of coal amounting to three times the energy contained in the Middle East's oil reserves, and currently accounting for more than 90% of U.S. proven energy reserves. The nation's coal industry began in the 18th century. Coal production increased steadily throughout the 19th century. By the turn of this century coal supplied 90% of the U.S. energy consumption. However, after more convenient and competitively priced oil and natural gas became available, coal consumption grew less rapidly than total energy consumption. The energy consumption supplied by coal dropped to 38% by 1950, and to less than 18% by 1974.

Today, more than 75% of national energy consumption is supplied by oil and gas, which constitute only less than 7% of the national energy

reserves (see Figure 2.1). The U.S. - with 6% of world population - uses 35% of world energy. Yet the Nation depends upon its least abundant energy resources to provide most of its energy needs. As a result of the oil embargo by the Organization of Petroleum Exporting Countries in late 1973, a national goal to double the production of coal by 1985 was announced by the federal government in early 1975.

Figure 2.2 shows the trend and the forecast of the national energy consumption. Energy demand grew at a rate of 3.6% in the 20 years before the 1973 embargo, and in 1975 the U.S. consumed about 73 quad-rillion Btu's. By 1985, as a result of higher prices, energy demand is expected to be much lower than the average growth rate of the last twenty years. Total domestic supply is forecasted to increase by 40% between 1974 and 1985 (see Figure 2.3) with a large role played by coal: coal production will increase to over one billion tons from 1974 levels of 611 million tons. Most of the new coal production will be used by electric utilities. Because net generation of electricity is expected to double by 1985, coal used for power generation is expected to increase from the 1974 annual level of 388 million tons to some 715 million tons in 1985, as shown in Table 2.1 (Federal Energy Administration, 1976).

Total U.S. coal resources, as shown in Figure 2.4, are well dispersed throughout the country. Additional deposits are located in Alaska. A coal reserve base has been established in 30 states. The total coal reserve base of 437 billion tons consists of about 28 billion tons of lignite, 168 billion tons of subbituminous coal, 233 billion tons of bituminous coal and 7 billion tons of anthracite. As shown in Table 2.2, of the total coal reserve base, about 202 billion tons occurs east of the

What Are the Roots of Our Energy Problem?

Coal ☐
Oil ▨
Gas ▨
Nuclear ▨
Other ▨

3% 4%
3%

90%

**Proved Reserves Economically
Recoverable with Existing Technology**

18%

4%

2%

46%

30%

**1974
Consumption Pattern**
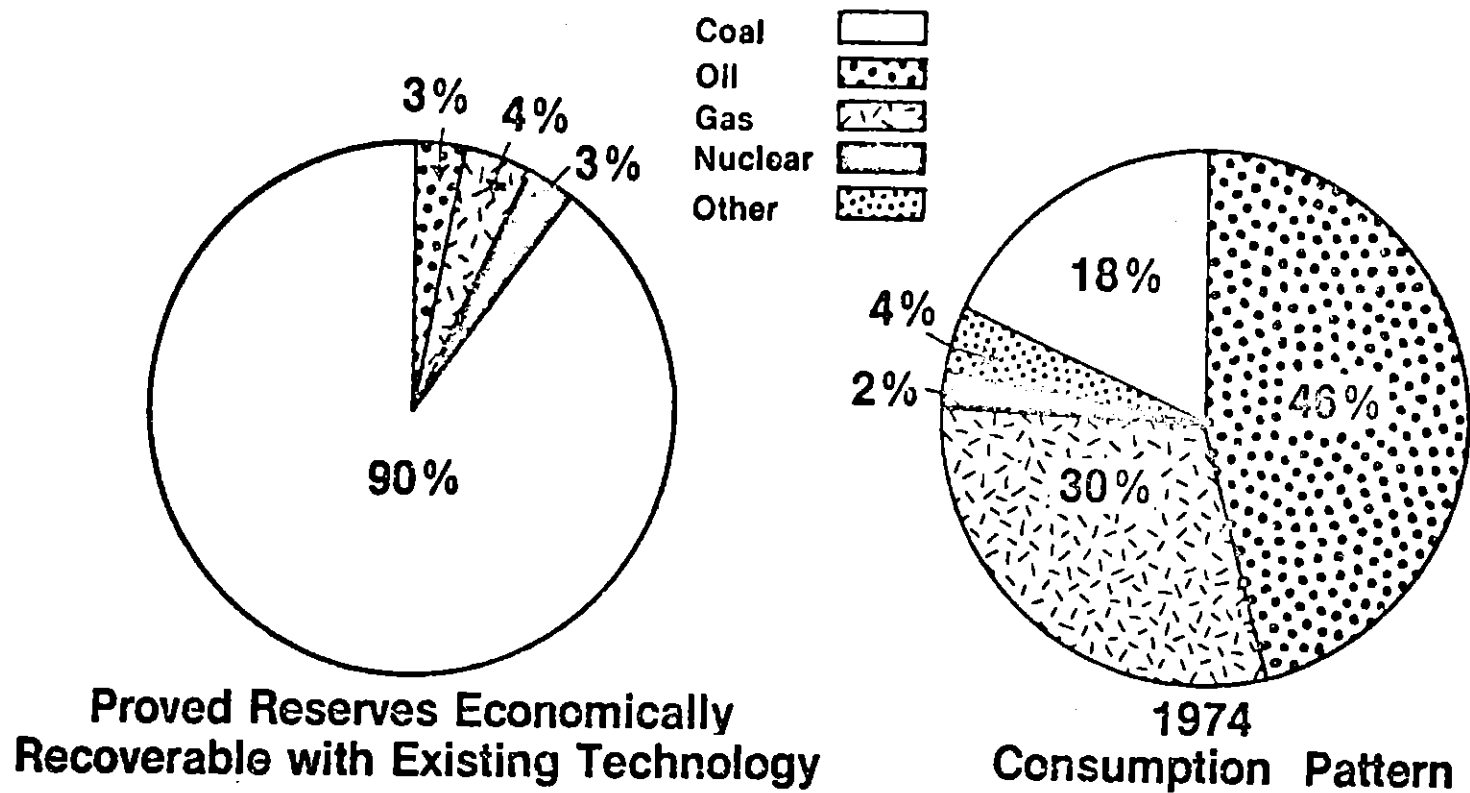
Figure 2.1

Proved Energy Reserves and Energy Consumption Pattern of the U.S.A.

(Federal Energy Administration, 1976).

How Much Energy Will the Nation Consume?

Quadrillion Btu
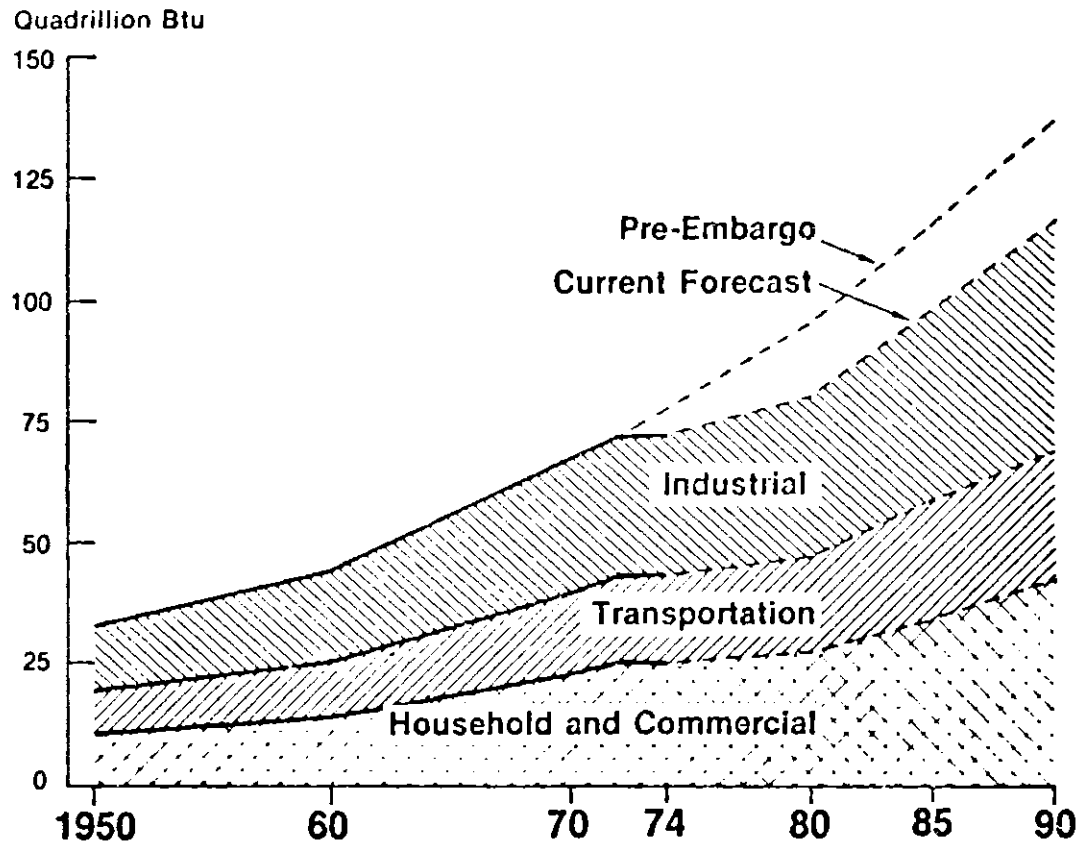
Figure 2.2

Annual Energy Consumption of the U.S.A. (Federal Energy Administration, 1976)

How Will the U.S. Meet Its Growing Energy Demands by 1985?
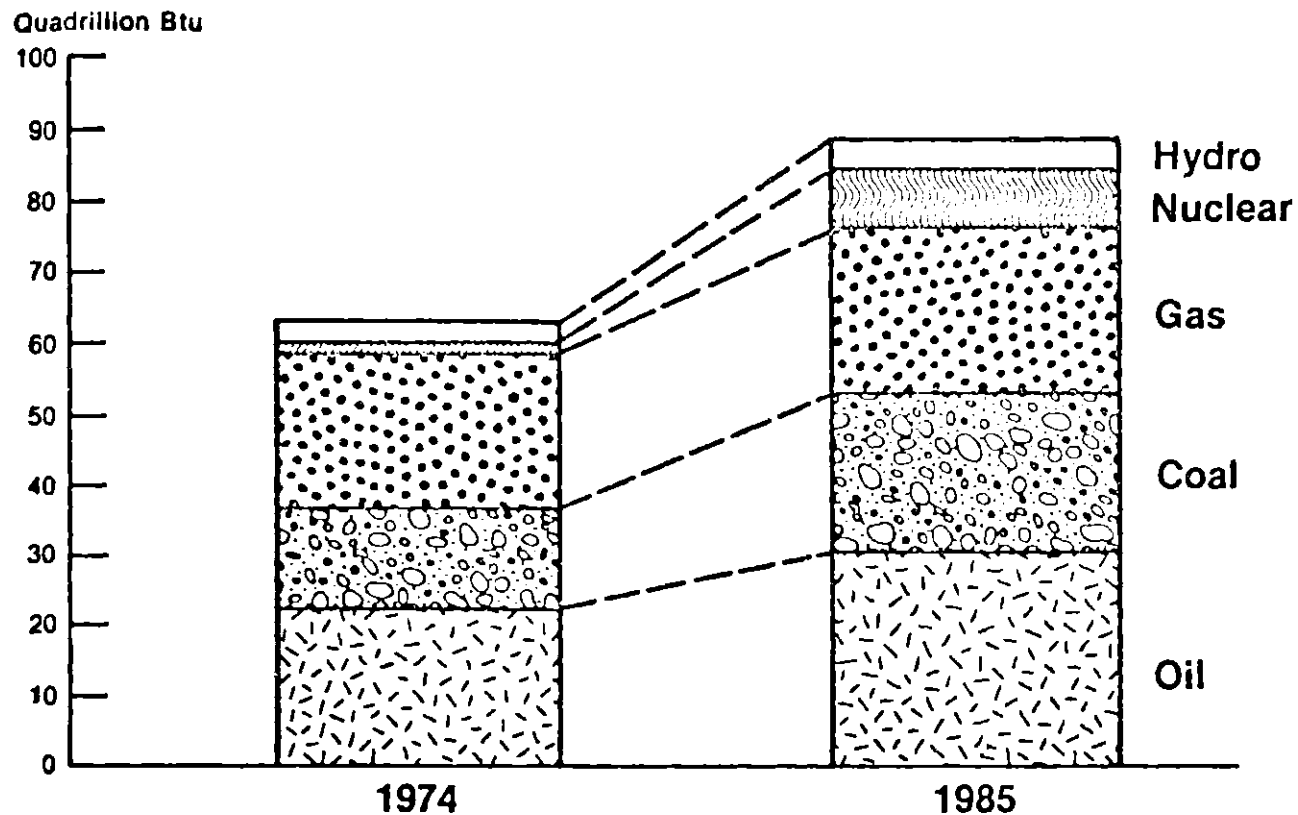
Figure 2.3

Domestic Energy Supply of the U.S.A. (Federal Energy Administration, 1976)

TABLE 2.1

COMPARISON OF 1974 LEVELS AND 1985
FORECASTS OF U.S. CONSUMPTIONS OF COAL
(Million Tons)

Sector	1974	1985	Absolute Increase	Compound Annual Percent Growth Rate
Electric Utilities	388	715	+327	5.7
Household/Commercial	9	5	- 4	-5.5
Industrial	64	124	+ 60	6.2
Coke and Gas	90	100	+ 10	1.0
Synthetics	-	16	+ 16	-
Exports	60	80	+ 20	2.6
Total	611	1,040	+429	5.0

Source: Federal Energy Administration

Coal Supply Regions

Legend

Bituminous Coal

Subbituminous Coal

Lignite

Anthracite

Regions
1. Northern Appalachia
2. Central Appalachia
3. Southern Appalachia
4. Midwest
5. Central West
6. Gulf
7. Eastern Northern
   Great Plains
8. Western Northern
   Great Plains
9. Rockies
10. Southwest
11. Northwest
12. Alaska (not shown)
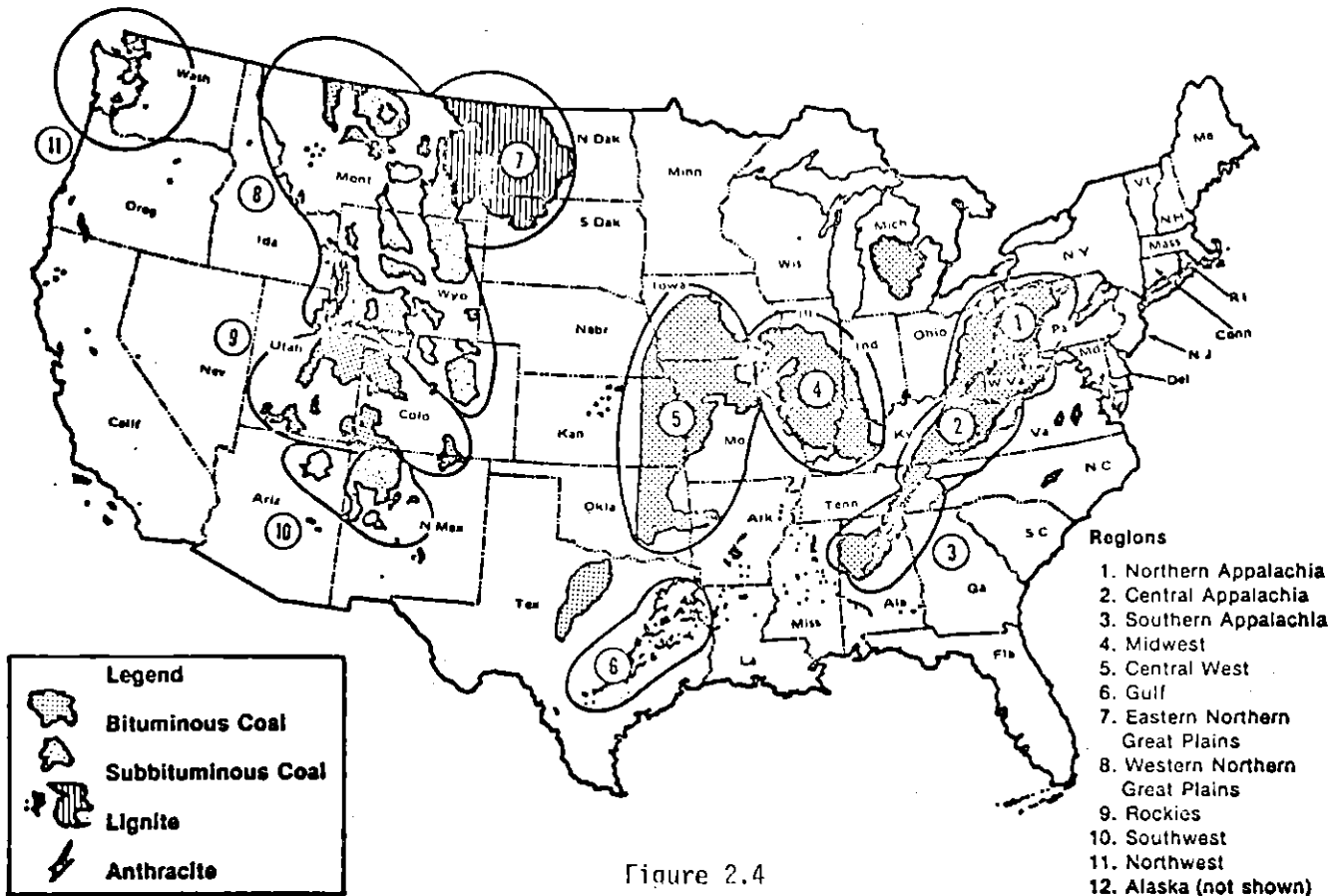
Figure 2.4

Coal Supply Regions of the Conterminous United States (Federal Energy Administration, 1976)

TABLE 2.2

DEMONSTRATED U.S. COAL RESERVE

	Billion Tons	Percent	Quadrillion Btu	Percent
East of Mississippi River	202.3	46.3	5,000	52.1
West of Mississippi River	234.4	53.7	4,600	47.9
Total U.S.	436.7	100.0	9,600	100.0

Source: Based upon Bureau of Mines data.

Mississippi River, which represent about 5,000 quadrillion Btu's, and about 234 billion tons occurs west of the river, which represent about 4,600 quadrillion Btu's (Scollon, 1977).

In summary, the U.S. has enormous coal reserves. Coal production is projected to increase from 611 million tons in 1974 to almost double the rate in 1985 in order to meet the growing U.S. energy demands. At these rates of consumption, the reserves are sufficient to last at least 200 years. Coal will undoubtedly play an important role in the future energy market.

2.2 Nitric Oxide - A Health Hazard

As mentioned earlier, one of the major drawbacks for coal burning is the emission of NO_x. Nitric Oxide (NO) is generally considered as non-toxic. However, in the presence of sunlight and ozone, it is readily converted to nitrogen dioxide (NO_2) which is corrosive and toxic. In addition, nitrogen dioxide will participate with ozone and atmospheric hydrocarbons in the complex chain reactions that lead to the production of photochemical smog.

The specific health hazards of NO_2 have been studied extensively by researchers. It is known that in living species, NO_2 irritates the sensory organs, inflames lungs, oxidizes lung tissue and changes lung morphology (Mueller and Hitchcock, 1969). It is suspected that NO_2 tends to settle on the hemoglobin in the blood and has a tendency to form dilute nitric acid when it comes in contact with the moisture in the lungs. Significant plant damage has also been attributed to NO_2.

Photochemical smog is formed when nitric oxides absorb sunlight then

react with atmospheric hydrocarbons to yield air pollutants such as
peroxyacyl nitrates, aldehydes and ozone. These products are known to
cause eye and throat irritation, decreased visibility, odor, and plant
damages (Patterson and Henein, 1972).

2.3 Nitric Oxide Control Technologies

Nitric oxides are harmful to human health. The Environmental
Protection Agency has established national air quality standards that
allow no more than an average of 0.055 ppm NO_x in ambient air. NO_x
emissions from new coal-fired facilities is limited to 0.7 pounds per
million Btu which translates into a stack gas concentration of 500 - 600
ppm in NO_x (Federal Register, 1971). The emphasis on the utilization of
coal will undoubtly increase the total NO_x emissions. More stringent EPA
regulations on the control of NO_x emissions are essential. The
improvements in the efficient use of the enormous U.S. coal reserves in
an environmentally acceptable manner therefore becomes an important
challenge.

We shall discuss, in detail, the NO_x formation mechanisms in the
Chapters that follow. In brief, NO_x is formed in stationary sources by the
following two mechanisms:

1. Thermal NO_x is formed by the fixation of the atmospheric
   nitrogen due to high temperature of the combustion processes.

2. Fuel NO_x is formed by the oxidation of chemically bound nitrogen
   in the fuel.

Thermal NO_x can be effectively eliminated by operating the coal combustor
at lower temperatures. Fuel NO_x is a problem more difficult to deal with.

This is the problem the author addresses in this thesis.

At present, the control technologies for NO_x emissions applicable to combustion sources can be summarized in following categories:

* Existing Clean Fuels

* Fuel Cleaning

* Combustion Modifications

* Flue Gas Cleaning

* Combinations of the above

The nitrogen content of American coals ranges from 0.5% to 2.0% by weight. Although not all of the nitrogen is converted to NO_x, the uncontrolled NO_x emissions still lie above the acceptable level. There is no economical method known at present that can remove fuel-nitrogen before the coal is burned or that can effectively scrub NO_x after it is formed from coal combustors. Fortunately, there exists a potential for reducing the fuel-nitrogen conversion to NO_x by modifications of the combustion processes. Combustion modifications have been the most economical and most promising approaches for reducing the NO_x emissions from coal-fired facilities.

There exists an urgent need to have a better understanding of the mechanisms of coal-nitrogen behavior during combustion in order to establish an optimum strategy for the control of NO_x emissions. This provides the motivation for this thesis work. The author hopes that this thesis will provide a better understanding on the fate of the coal-nitrogen and provide a basis for the development of the control technologies for NO_x emissions.

CHAPTER 3

PREVIOUS WORK

Coal combustion is a complicated high temperature process. The NO_x emissions during coal combustion can possibly be contributed by the oxidation of both atmospheric nitrogen and any nitrogen contained in the fuel. The review of past work will therefore first concentrate on the contribution of fuel NO_x and thermal NO_x. This is given in Section 3.1.

Regarding the combustion process, a coal particle undergoes complex physical and chemical changes during combustion. The processes involve both homogeneous and heterogeneous chemical reactions; multicomponent mass transfer; and conductive, convective and radiative heat transfer. Coal may first undergo rapid devolatilization by heating in the products of combustion recirculated to the burner. The volatiles may subsequently burn either in the boundary layers of individual particles or in the flames engulfing clouds of particles. The char will ultimately burn out in the tail of the flame. Alternatively, ignition may precede complete devolatilization and char and volatiles may burn contemporaneously. In summary, the combustion of pulverized coal particles occurs in three main stages: a stage of evolution of the volatile components, or devolatilization, followed by the homogeneous volatile combustion and then finally the heterogeneous combustion of residual char. Although the stages may overlap to some degree (Howard and Essenhigh, 1967a, 1967b), it is well recognized that the char combustion is generally of much longer duration. Based on this information, the conversion of coal-nitrogen to NO_x can

also be regarded as a three-stage process: coal-nitrogen devolatilization, volatile-nitrogen combustion and char-nitrogen combustion. The devolatilization prior to ignition and the distribution of nitrogen between char and volatiles will undoubtedly influence NO_x emission. The review on the coal-nitrogen devolatilization process will be given in Section 3.2; and the review on the contributions of volatile NO_x and char NO_x will be presented in Section 3.3.

Finally, since the destruction of NO_x is as important as the formation of NO_x in determining the net NO_x emission from coal combustors, a review on the reduction of NO_x by char will also be included.

3.1 Fuel NO_x and Thermal NO_x

An early investigation of the source of nitrogen for the production of NO_x during the fluidized bed combustion of coal has been made by Jonke et al. (1970). An experiment was performed in which after steady-state combustion had been reached with a synthetic air mixture of nitrogen and oxygen, argon was substituted for the nitrogen. They found that the NO_x level of the flue gas was not materially affected by the substitution of argon for the nitrogen. This indicated that the major source of nitrogen for the production of NO_x was the nitrogeneous content of coal. However, this conclusion derived from experiments at the low operating temperature of a fluidized bed may not necessarily apply at the high temperatures prevalent in pulverized coal flames.

Pershing (1976) and Pershing and Wendt (1976) have isolated fuel NO_x in pulverized coal flame using, instead of air, a synthetic oxidant mixture containing 21% O_2, 18% CO_2 and 61% Ar. Comparison between total

NO_x with preheated air as the oxidant and fuel NO_x with synthetic

mixture as the oxidant was accomplished under nearly identical conditions.

From the studies of four different coals and one coal char, they found

that, under typical combustion conditions, fuel NO_x contributed over 80%

of the total NO_x emissions. It should be noted, however, that the

combustor used by Pershing et al. was a relatively small one and was

subject to major heat loss through the walls. Estimates of the contribution

to total NO_x by the fuel-nitrogen are lower for larger combustors and

range from 30 to 55 percent (Habelt, 1977). These values obtained on

larger scale units are, however, subject to errors of interpretation.

In addition, Pershing et al. have also concluded that fuel NO_x formation

was relatively insensitive to flame temperature over a wide range of

practical interest.

An understanding of the formation of thermal NO_x will certainly

help to explain why the fuel NO_x was predominant in the systems mentioned

above. The reaction mechanism for the formation of thermal NO_x, which

arises from the fixation of atmospheric nitrogen, was first proposed by

Zeldovitch (1947). This mechanism has since been confirmed and modified

by a number of investigators (see Baulch, Drysdale and Lloyd, 1967-70).

The Zeldovitch mechanism is highly temperature dependent so that in a

typical pulverized coal flame, little thermal NO_x is expected due to the

comparatively low flame temperature in a small-scale combustor with cold

walls. This explains why little thermal NO_x was observed and fuel NO_x

contributed the major fraction of the total NO_x emission in most small-

scale coal-fired systems.

3.2 Devolatilization of Coal-Nitrogen

There are some data available in the literature on the distribution of the nitrogen in coal among pyrolysis products at coking conditions. (Feilder and Davis, 1934; Kirner, 1945; Hill, 1945.) The coking data, however, are not applicable to pulverized coal flames because of differences in heating rates, final temperatures, residence times, and particle interactions.

Since control of the nitrogen evolution provides one method of controlling total NO_x emissions, the mechanism and rates of devolatilization of coal-nitrogen have been extensively studied by Pohl (1976). The pyrolysis of the nitrogen content of coal was studied by rapidly heating dispersed pulverized particles of Montana lignite and Pittsburgh bituminous coal to temperatures of 1000 and 2100 K.

Time resolved measurements of nitrogen loss during pyrolysis were obtained and the evolution of nitrogen from coal was found to be kinetically controlled for conditions encountered in typical pulverized coal flames. The early stages of pyrolysis of coal-nitrogen was empirically correlated with a psuedo-first order Arrhenius-type rate equation.

A correlation between nitrogen loss and total solid weight loss during pyrolysis was also obtained. Little nitrogen was lost until 10-15% of the coal had been devolatilized. After this initial period associated with loss of side chains and scission of aliphatic bridges in coal, the rate of fractional nitrogen loss was found to be proportional to the rate of fractional total weight loss. This correlation, if it is found to have general validity provides a base for evaluating the

kinetics of nitrogen evolution from that of the more readily determined
total volatile evolution.

Another important feature from Pohl's studies is the asymptotic
behavior of devolatilization. When coal was slowly heated in crucibles
to different temperatures, most of the volatile matter evolution
occured at temperatures below that of the ASTM Proximate Analysis test
(1023 K) whereas most of the nitrogen was evolved at higher temperatures.
Although carbon formed a stable compound in char, no comparable stabilized
nitrogen structures were formed, consequently, nitrogen could continue
to be released until it was completely eliminated from char.

Pohl's studies represent the most complete and best available
information on the kinetics of coal-nitrogen devolatilization.

3.3 Char NO_x and Volatile NO_x

At present, there is limited information on the contribution of the
nitrogen devolatilized from the coal and the nitrogen oxidized from the
char to total NO_x emissions. By the use of fragmentary data,
Sternling and Wendt (1972) drew up a schematic diagram for the
distribution of coal-nitrogen between volatiles and char during pyrolysis
and oxidation. They indicated that a significant portion of the nitrogen
in the coal may not be volatilized but will appear in the char; hence the
oxidation of nitrogen in the char may contribute significantly to total
NO_x emissions.

Coal char combustion is a complicated process. Since the char
structure is porous, both internal and external combustion would occur
(Anson, Moles and Street, 1971). In addition, pore diffusion may sometimes

play an important role in the combustion process (Smith and Tyler, 1972, 1974; Mandel, 1977). Physical and chemical characteristics that influence the conversion of fuel nitrogen to NO_x during coal char combustion were theoretically examined by Wendt and Schulze (1976). They showed that diffusion-reaction interactions were important in determining the selectivity of the char particle toward NO_x production. Their model predicted that char combustion was a potentially rich source of NO_x.

The work by Blair et al. (1976) has also shown that a large fraction of nitrogen may remain in the char after devolatilization, and may be responsible for the major portion of the NO_x emissions. The results on the behavior of fuel-nitrogen under simulated combustion conditions by Pohl and Sarofim (1976) and Song, Beér and Sarofim (1977) also support this picture for temperatures below 1750 K but the trend of the data suggests that much of the fuel-nitrogen may be volatilized at higher temperature so that volatile-nitrogen may become the major contribution to total NO_x emissions.

By means of a fluidized bed combustor, Pereira and Beér (1975) and Pereira (1975) have assessed the influence of temperature on the relative contributions of char-nitrogen and volatile-nitrogen to the total NO_x emissions. They found that the char-nitrogen contribution to the total NO_x emissions predominated at low temperatures, whereas at higher temperatures the contribution of the volatile fraction became more important.

In summary, results from past work have suggested that the relative importances of volatile-nitrogen and char-nitrogen contribution to fuel NO_x are temperature dependent. Char-nitrogen is important when temperature

is low and volatile-nitrogen is important when temperature is high. However, the information available has been only qualitative and there has been no information obtained at conditions encountered in pulverized coal flames.

3.4 Reduction of NO_x by Char

Since the destruction of NO_x is as important as the formation of NO_x in determining the net NO_x emission from coal combustors, we shall devote this Section to the reduction of NO_x by char.

In an experimental effort to investigate the NO_x emissions from a fluidized bed coal combustor, Gibbs, Pereira and Beér (1976) observed a reaction between NO_x and char during the combustion of coal. Although the char was known to react easily with NO in the absence of oxygen (Edwards, 1972), it was not expected up until then that this reaction could also occur under oxidizing conditions. An investigation was then conducted to explore the reaction between NO_x and char in a fluidized bed operating over a temperature range of approximately 600 to 900 C. They reported that the reaction had a relatively low activation energy (about 16 Kcal/mole) and a reaction order of unity with respect to NO_x. They also found that the nitric oxide reduction was strongly dependent on the char particle size with increasing conversion as particle size decreased.

These observations were partially supported by the recent work done in Japan (Furusawa, Kunii, Oguma and Yamada, 1977). The Japanese researchers have conducted a kinetic study of NO_x reduction in a fixed bed reactor with a dilute mixture of carboneceous materials (e.g., char

or activated carbon) over a wide range of temperature (750 - 1250 K).
They also found that the reduction of NO_x was first order with respect
to NO_x concentration. Interestingly enough, they observed three
temperature ranges with different activation energies: 17.3 Kcal/mole
for 773 K to 993 K; 57.1 Kcal/mole for 993 K to 1056 K; and 39.7 Kcal/mole
for 1056 K to 1183 K. Evidently, in modelling NO_x emission from coal
combustion systems, any extrapolation as well as interpolation of
Char/NO_x kinetics has to be done with great care.

Apparently, the Char/NO_x reaction is analogous to Char/O_2 reaction,
and in fact, NO_x may compete with O_2 for the char gasification reaction.
In determining the net NO_x emissions from a coal combustor, the Char/NO_x
reaction should not be neglected. A better understanding on the Char/NO_x
reaction will, of course, provide information pertinent to the reduction
of NO_x emission by the modification of the combustion processes.

CHAPTER 4

GENERAL SCOPE OF THE THESIS

The overall objectives of this thesis work were twofold. First of all, it was aimed to provide an engineering and parametric overview on the NO_x emissions during coal combustion. It was desired to identify and investigate those factors and parameters which are important in the formation of NO_x in pulverized coal flame. These studies were directed at finding the range of practical conditions under which NO_x formation was minimized. The second half of this thesis work was devoted to developing a better understanding of the kinetics of the processes that control the formation and destruction of NO_x during the combustion of coal, in order to provide quantitative guidelines for the designer.

In order to achieve the various goals of the study, two types of investigations were conducted in this thesis work: parametric investigations of the gross NO_x emissions and kinetic studies. The parametric investigations included the determinations of the effects of both the fuel/oxygen equivalence ratio and the temperature on NO_x emissions, and also the identification of the separate contributions of char-nitrogen and volatile-nitrogen to total NO_x emissions. The kinetic investigations included the studies of the intrinsic kinetics of formation of NO_x during coal char combustion and the intrinsic kinetics of reduction of NO_x by char.

The approaches were both experimental and theoretical. The experimental data were obtained under simulated coal combustion conditions

to facilitate the direct application of the results to real systems. Theoretical models were derived to generalize the experimental results and to predict the rates of both the fuel-nitrogen consumption and NO_x formation during coal combustion. These theoretical models can provide the fundamental information necessary for the design of combustion process modifications for NO_x control.

The experimental apparatus and procedures will be described in Chapter 5. The parametric investigations are discussed in Chapter 6. The kinetic studies of the formation of NO_x during coal char combustion are presented in Chapter 7, while the kinetic studies of the reduction of NO_x by char in Chapter 8. Each of Chapters 6, 7 and 8 is designed to be self-contained. The format in each chapter will start with a brief review on past work, it is then followed by the presentations of experimental results, the derivation of theoretical models, and finally the conclusions and the discussions on practical implications. The information contained in the individual chapter is therefore inter-related with that in other chapters, but can also be treated independently. The overall conclusions of this thesis work are presented in Chapter 9. Finally, suggestions for the improvement of the experimental procedures and recommendations for future studies are given in Chapter 10.

CHAPTER 5

EXPERIMENTAL APPARATUS AND PROCEDURES

5.1 Experimental Apparatus

Flow furnaces have been widely used for coal studies because of their similarity to actual coal combustor systems. A wide range of simulations can be achieved by controlling both gas and wall temperatures, consequently, the results may be readily applicable to real systems. A flow furnace system was chosen for this study because of the flexibility it provided for carrying out both parametric studies and kinetic studies on the fate of the fuel-nitrogen during coal combustion. The system consists of a temperature controlled tubular furnace, a coal/char particle feeder, particle collector, a gas preheater, and a vacuum system. The basic design of this system is given by Kobayashi (1976).

5.1.1 The Furnace

The schematic of the furnace system is shown in Figures 5.1 and 5.2. Figure 5.1 shows the furnace in laminar-flow mode and Figure 5.2 shows the furnace in free-fall mode (see Sections 5.1.3 and 5.2). The system is built around an ASTRO model 1000A furnace (ASTRO Industries, Inc., Santa Barbara, California). The furnace is a graphite resistance furnace, i.e., the heating is done by supplying electricity to a 3 1/2 in I.D., 12 in long graphite resistance heating element. The furnace shell is anodized aluminum with water cooling channels in the central section of the shell. Thermal insulation between the heating element and central

Char and Carrier Gas

Main Gas
from Preheater

Thermocouple

Alumina Honeycomb
Flow Straightener

Water Cooled Flanges

Alumina Muffle Tube

Power and
Water

Power and
Water

Quartz
Observation
Port

Graphite
Heating Element

Sintered
Bronze Filter

Water Cooled
Collecter

Water Cooled
Flanges

Ball Valve

Ball Valve

Exhaust

Water

Quenching Gas

Vacuum
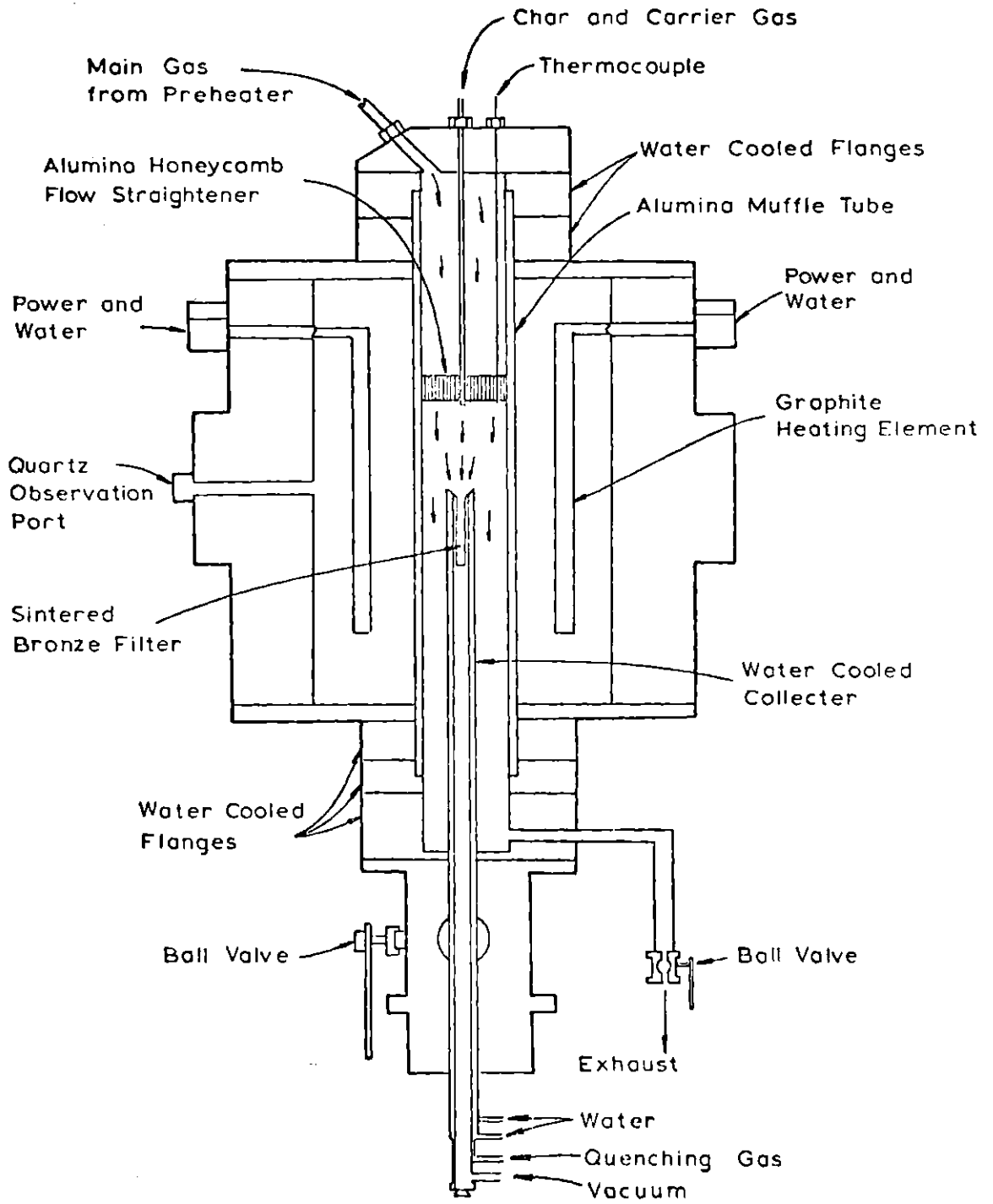
Figure 5.1

Furnace with Collector Probe
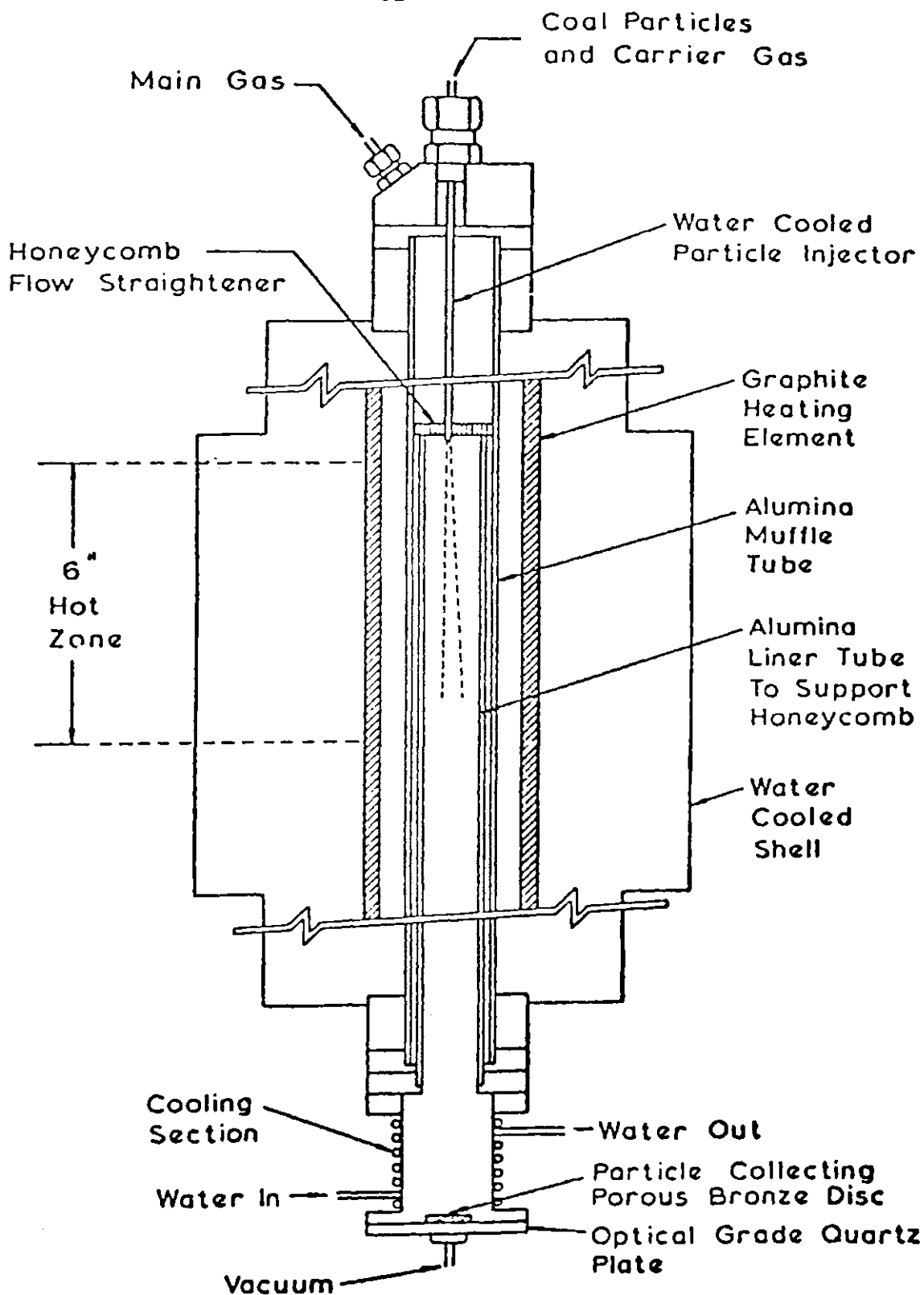
Figure 5.2

Furnace with Bronze Disc Collector

shell is provided by carbon powder. The insulation pack is retained by a radiation shield which surrounds the tubular heating element. Two coaxial aluminum oxide muffle tubes are used as reaction chambers, which permit operating the furnace in an oxidizing atmosphere. The outer alumina muffle tube, 24 in long, 3 in O.D., 2 1/2 in I.D., is used to shield the graphite heating element from the reaction zone. The inner alumina muffle tube, 15 in long, 2 1/4 in O.D., 2 in I.D., is used to support a ceramic honeycomb gas flow straightener. The honeycomb, made by E.I. du Pont de Nemours and Co. (Wilmington, Delaware) with a trade name of TORVEX, is 1 in thick and has a nominal pore diameter of 1/16 in.

The furnace is equipped with a 14 KVA power supply (230 V and 65 A) which consists of a stepdown transformer, a manually operated SCR power controller, and an automatic temperature programmer. The temperature programmer allows temperature changes to be made at desired rates. This feature is particularly important when using the alumina muffle tubes, since the alumina tubes are so sensitive to temperature changes that the heating rates and cooling rates must be slow enough to avoid thermal shock to the material. The furnace temperature is controlled and monitored by a boron-graphite/graphite thermocouple which is located in the center of the furnace just outside the heating element. The wall temperature of the outer muffle tube can also be checked by an optical pyrometer through an observation port with a diameter of 1/2 in. The temperature within the reaction zone immediately below the honeycomb is monitored by a platinum/platinum-rhodium thermocouple to indicate whether there is proper heating of the main gas. Since the melting temperatures of alumina muffle tube and honeycomb are 2100 K and

1900 K, respectively, the maximum operating temperature is set at 1750 K for the reason of safety.

5.1.2 Coal/Char Feeder

The coal/char feeder is composed of two sections: the particle-feeding control section and the water-cooled particle injection probe. The feeding control section, as depicted in Figure 5.3, employs a mechanical vibrator, partial fluidization of the particles, and an adjustable needle valve to obtain uniform feed rates of particles. The particles are then transported by a carrier gas and injected along the axis of the furnace through the water-cooled injection probe.

The main body of the control section is made of polished plexiglas to facilitate the direct visual inspections of coal level and feed rate. The plexiglas section is 3 1/2 in long and 1/2 in I.D. and is capable of loading up to 3 grams of pulverized coal/char sample. A 1/8 in O.D. stainless steel needle valve (i.e., a stainless steel tubing with a closed, tapered end) extends axially through this part down to another smaller plexiglas section which has been machined internally to form a cone-shaped funnel. The feed rate is controlled by the needle valve opening, the vibrator strength and the carrier gas flow rate. The carrier gas is introduced through the hollow needle valve and injected radially through six equally spaced 0.010 in holes near the tip of the needle valve just next to the tapered end. The carrier gas flows at high velocity (but low flow rates) through these holes so as to fluidize the particles locally, thus preventing packing and clogging in the narrow region. An adjustable mechanical vibrator which is attached

Carrier Gas

Needle
Valve
Adjustment
Lever

Char Feed
Port

Feed Rate
Control
Needle Valve

Plexiglas Body

Char

Vibrator

Char and
Carrier Gas
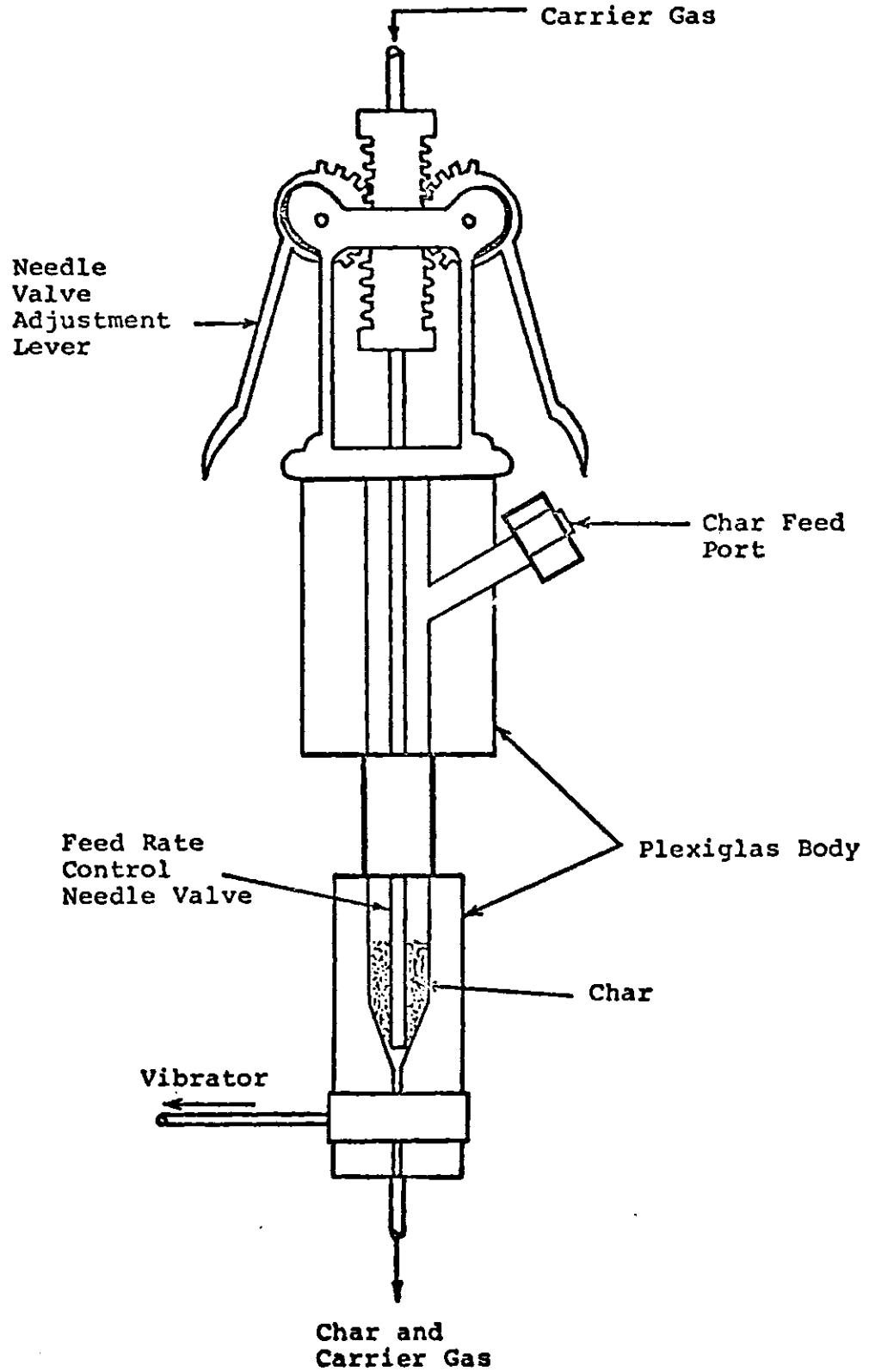
Figure 5.3

Coal/Char Feeder

to the throat of the funnel oscillates the entire feeder assembly to help the feeding.

The particles are then carried by both gravity and the carrier gas into the water-cooled injection probe which is connected to the bottom of the feed control section. The water-cooled particle injection probe consists of three concentric stainless steel tubes together with 1/4 in O.D. in outermost tube and 1/16 in O.D. in innermost tube. The annular space between the tubes is used for circulating water to cool the probe which carries the particles in its innermost tube. The injection probe extends axially into the center of the furnace with its tip about 1/2 in below the bottom level of the honeycomb.

The feed rate can be adjusted between 0.01 gm/min and 1.0 gm/min. In normal operations of this study, about 1 gm of coal or char samples are fed at 0.15 gm/min with carrier gas flow rate about 30 cc/min.

5.1.3 Particle Collection Systems

The furnace can be operated in two different modes: laminar-flow mode and free-fall mode. Accordingly, two different particle collection systems are used. In the laminar-flow mode, the particles are injected along the axis of the furnace and carried down by the laminar flow stream of the main gas, and finally the reacted particles are quenched and collected in the water-cooled collector probe. In free-fall mode, the particles are allowed to fall freely by gravity through the hot zone of the furnace then onto the bronze disc collector placed in the cooled section of the furnace.

5.1.3.1 Collector Probe Used in Laminar-Flow Mode Experiments

Figure 5.4 shows the design of the particle collector probe used in laminar-flow mode experiments. It consists of three concentric copper tubes with 1 3/8 in O.D. in outermost tube and 1/2 in I.D. in innermost tube. The two outer passages are used to circulate the external cooling water and the center passage is used to withdraw the quenched gaseous and solid reaction products. Eight 1/8 in O.D. copper tubes pass through the space between the inner two tubes to carry the cool quenching gas. The quenching gas is injected toward the axis through the porous bronze at the bevelled portion of the collection filters. The sintered bronze filters (specially manufactured by Thermet, Inc., Gloucester, Massachusetts) are used to retain the reacted char while the quenched gases are drawn through the filter and the center passage of the probe by the vacuum system of the furnace. The bronze filter is 0.740 in O.D. at the open end, 0.4 in O.D. and 4 in long at the straight section, and the wall thickness is 0.060 in. The average particle size of the sintered bronze shot is about 15 microns and the average pore size of the bronze filters is about 5 microns.

Water has been tried in the quenching system. However, based on the following reasons, the gas quenching has been proved to be more advantageous than the water quenching in the present studies:

(1) With water quenching, the bronze collecting filter quickly becomes clogged due to the tendency of water to wash small ash particles off the char surface into the filter pores. With gas quenching, the tendency of the ash particles being washed away is minimized.

Char and
Hot Gas

Sintered
Bronze
Filter

Water
OUT

Water
IN

Quenching
Gas

Vacuum
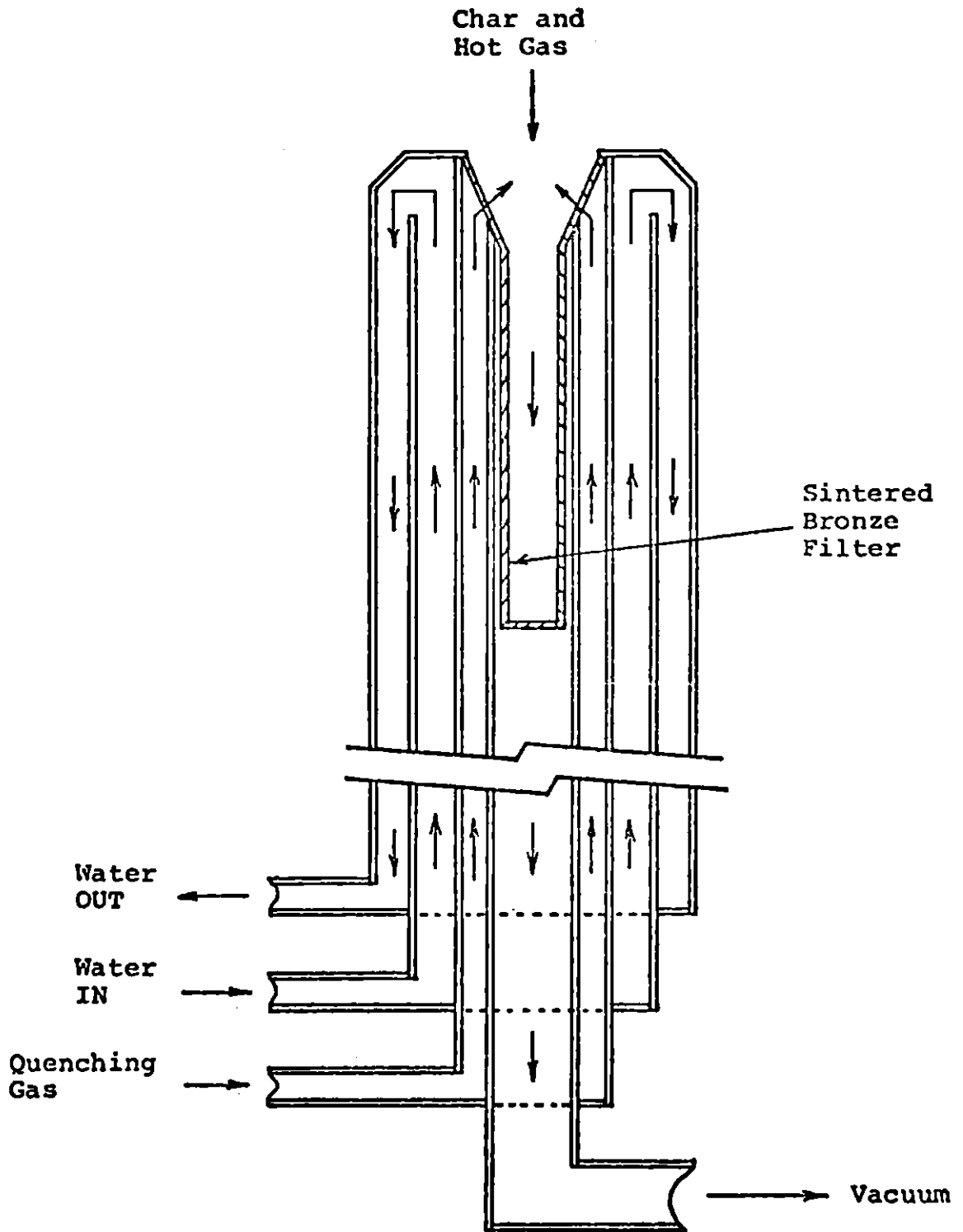
Figure 5.4

Particle Collector

(2) The use of gas quenching simplifies the experimental arrangements and procedures. First of all, with gas quenching, large reservoir required to separate gases from water is eliminated. Secondly, with gas quenching, there is no need to dry the filter and collected sample before weighing and other analysis.

(3) Elimination of the water quenching assures higher accuracies of gas phase analyses by avoiding the possibilities of gas losses due to dissolution in the excess water.

5.1.3.2 Bronze Disc Collector Used in Free-Fall Mode Experiments

Figure 5.2 shows the furnace in free-fall mode. In free-fall mode, the char particles are collected in a 3 in diameter, 1/8 in thick sintered bronze disc at the bottom of the cooling section of the furnace. The sintered bronze discs were manufactured by Thermet, Inc., Gloucester, Massachusetts. They have an average pore diameter of about 5 microns. The gas exits through a 1/4 in pipe fitting under the center of the bronze disc.

5.1.4 Gas Preheater

In most of the experiments, the main gas is introduced to the furnace at room temperature. The main gas then passes through the honeycomb gas straightener and enters the reaction zone. Heat transfer calculations revealed that at the maximum gas flow rate of 6 1/min (measured at room temperature) the main gas temperature would approach

that of the honeycomb. These predictions were confirmed by the direct gas
temperature measurement with the platinum/platinum-rhodium thermocouple
extending just below the honeycomb as described in Section 5.1.1 Therefore,
the honeycomb, in addition to serving as a gas flow straightener, also
serves as a main gas preheater. Nvertheless, the system has been equipped
with a packed bed gas preheater for use in experiments with higher gas
flow rate. The preheater, located at the upstream of the furnace main gas
inlet, is a 18 in long, 1 in O.D. stainless steel tube packed with 3/16 in
alumina pellets. A Lindberg "Hevi-Duty" model 55081-A tubular furnace
(120 V, 8.5 A) (Lindberg, Inc., Watertown, Wisconsin) is used as the heat
source. The stainless steel tube is placed in the tubular furnace in a
vertical position with 12 in of its length enclosed by the furnace. It
is capable of reaching a temperature of 1000 C.

5.1.5 Vacuum System

The vacuum system consists of two Cenco "Megavac" pumps connected in
parallel. These pumps (115 V and 6 A) are rated at 1/3 h.p., with
individual maximum capacities of 57 1/min at 0 psig. The suction rate
is regulated by a control valve located downstream of the furnace. All
vacuum lines are 1/2 in I.D. or larger to minimize the pressure drop.

5.2 Experimental Procedures

5.2.1 Parametric Investigations

In the parametric studies, coal and char oxidation experiments
under a fixed residence time of one second are carried out in the furnace
in a free-fall mode. In this mode, the particles are allowed to fall

freely through the hot zone and then onto the bronze disc collector placed in the cooled section of the furnace. The time for the particles travelling through the hot zone is about one second. The chars used in the oxidation studies are prepared by pyrolyzing the coal at the temperature and residence time corresponding to those of the coal oxidation experiments. The procedure for the oxidation experiments is as follows.

The furnace is heated to the desired temperature level at a heating rate of 250 C/hr to 350 C/hr, using the temperature controller and programmer. The wall temperature is also measured by a Land optical pyrometer and by the platinum/platinum-rhodium thermocouple extending just below the honeycomb. Once the furnace has reached the final steady state temperature, a pre-weighed bronze disc collector is placed at the bottom flange. About 1 gram of coal (or char) is weighed and placed in the feeder. The main gas is then introduced into the furnace. As soon as the main gas flow becomes steady, the feeder vibrator is turned on and the particles are fed to the furnace with a helium carrier gas of 30 cc/min. The total particles are fed fairly uniformly for 6 to 7 minutes or at a rate of 0.15 gm/min. The main gas is a simulated air mixture, i.e., 21% oxygen in helium mixture. The main gas flow rate is varied between 1 l/min and 3 l/min from run to run in order to obtain different fuel/oxygen equivalence ratios. The off-gas is withdrawn continuously from the furnace for gas phase analyses. After all the particles are fed, the bronze disc collector is removed and weighed and the solid weight loss of the coal (or the char) is obtained. The collected char is transferred to a sample bottle for further analyses

of chemical composition and for physical characterizations.

5.2.2 Kinetic Studies

Two different kinetic studies are conducted in this thesis work: a kinetic study of the Char/O_2 reaction and a kinetic study of the Char/NO_x reaction. The char used for these kinetic studies are specially prepared to meet specific requirements. We shall present the procedures for the preparation of the char in Section 5.2.2.1. The procedures for Char/O_2 experiments and the procedures for Char/NO_x experiments are presented in Sections 5.2.2.2 and 5.2.2.3, respectively.

5.2.2.1 Preparation of Char

In selecting char for the kinetic studies, two criteria have to be met. First, the char produced should be relatively "volatile-free", or more specifically, it should have reached asymptotic solid weight loss due to pyrolysis. When this char is subjected to further Char/O_2 or Char/NO_x studies, there should be no or very little volatile interference. Secondly, the pyrolyzed char produced should have retained a significant portion of the nitrogen from the original coal, so that the fate of the char-nitrogen during oxidation can be accurately studied.

In order to meet the above criteria, the char is specially produced by pyrolyzing lignite coal particles at a furnace temperature of 1750 K for a residence time of one second. The char production is made in the furnace in the free-fall mode of operation with a minor modification to permit a direct and continuous collection of the char

in a flask. During the char production process, 3 l/min helium gas is used as the main gas. The char so produced is then size-graded to select particles in the 38 to 44 micron size range for further experiments.

5.2.2.2 Char/O_2 Experiment

The kinetic studies of Char/O_2 reaction are carried out in the furnace in a laminar-flow mode. In this mode, the char particles are injected along the axis of the furnace and then carried down by the laminar-flow stream of the main gas. The oxidant stream of oxygen in helium is supplied through the honeycomb straightener at a sufficiently fast rate to prevent significant depletion of the oxygen during reaction. The reacted particles are quenched and collected in the water-cooled collector probe. The residence time of the particles can be varied by adjusting the distance between the feeder tip and the collector probe. The experimental procedures for the kinetic studies of Char/O_2 reaction are as follows.

The furnace is first heated using the temperature controller and programmer as described in Section 5.2.1. About 1 gram of char is weighed and loaded to the feeder after the furnace has reached the desired temperature. The quenching gas, argon, is set to about 25 l/min after a pre-weighed bronze filter is placed in the collector probe. The vacuum is adjusted continuously so that the furnace pressure is maintained at about 0 psig as the collector probe is put into muffle tube. The collector probe is then raised into the furnace and secured at a certain distance from the char feeder. The main gas, a mixture of oxygen and helium with a desired oxygen partial pressure, is then

-104-

supplied to the furnace. The main gas flow rate is always set at 6 l/min
(based on room temperature and atmospheric pressure). By the adjustment
of a side tube regulating rotameter and the main vacuum valve, half of
the main gas fed to the furnace is withdrawn through the collector probe
and another half of the main gas is removed from the bottom of the
furnace to ensure efficient quenching and proper collection of the
reacted particles. The furnace pressure is monitored and maintained at a
slightly positive pressure (less than 1 psig) throughout the run again
by the adjustment of the vacuum. After all the gas flow rates and
furnace pressure have reached steady state, the feeder vibrator is turned
on and the char particles are fed to the furnace with a helium carrier
gas of 30 cc/min. The particle feeding rate is, as in free-fall mode,
consistantly at about 0.15 gm/min. As soon as the feeding is finished,
the main gas is turned off and the collector probe is removed from the
furnace. The quenching gas and vacuum are then turned off and the
bronze filter is quickly removed from the probe and weighed and the
solid weight loss of the char is obtained. Finally, the collected char
is transferred to a sample bottle for further analyses.

5.2.2.3 Char/NO$_x$ Experiment

The kinetic studies of Char/NO$_x$ reaction are carried out in the
furnace in a free-fall mode as the parametric studies described in
Section 5.2.1. Certified gas of NO$_x$ in helium or argon, supplied by
Matheson Gas Company (Gloucester, Massachusetts), is used as a main gas.
The main gas flow rate is typically set at 3 l/min. A chemiluminescent

NO-NO_x Gas Analyzer and a chart recorder are used to monitor the NO_x concentration in the off-gas from the furnace throughout the run (see Section 5.3.1).

The main gas is first introduced into the furnace through the honeycomb straightener. About 2 to 3 minutes is the typical length of the time for the NO_x concentration in the off-gas to stabilize and reach the same level as that in the inlet gas. After steady state has been reached, the feeder is turned on and char particles are fed along the furnace axis. A sudden drop of NO_x concentration in off-gas is observed as soon as the particles are fed. The concentration of NO_x in the off-gas decreases to a certain steady level during the run. When the char feeding is finished, the NO_x concentration in off-gas starts to go back to its original level with certain time lag. After the NO_x concentration in the off-gas has returned to its original level and stabilized, the main NO_x gas is turned off and a secondary helium gas is introduced into the furnace to purge the system until no more NO_x can be detected. The NO_x concentration in the off-gas from the furnace is monitored continuously using a chart recorder. Finally, the secondary helium gas is turned off and residual char is removed from the sintered bronze disc filter for analysis.

A summary of operating conditions for all experiments is shown in Table 5.1.

5.3 Gas Phase Analyses

The species of primary interest in the gas phase during the course of this thesis work is, of course, NO_x. Other prevailing

TABLE 5.1

SUMMARY OF OPERATING CONDITIONS

1. Parametric Studies
   Furnace Temperature (K):   1250   1500   1750
   Fuel/O_2 Equivalence Ratio (ϕ): 0.2   ~ 4
   Main Gas Flow Rate (ℓ/min):   varied in accordance with ϕ
   Carrier Gas Flow Rate (cc/min):   30

2. Char/O_2 Kinetic Studies
   Furnace Temperature (K):   1250   1500   1750
   Partial Pressure of Oxygen (atm):   0.2   0.4
   Main Gas Flow Rate (ℓ/min):   6
   Quenching Gas Flow Rate (ℓ/min): 25
   Side-tube Gas Flow Rate (ℓ/min): 3
   Carrier Gas Flow Rate (cc/min):   30

3. Char/NO_x Kinetic Studies
   Furnace Temperature (K):   1250   1500   1750
   NO_x Concentration (ppm):   530   1100   6400
   Main Gas Flow Rate (ℓ/min):   3
   Carrier Gas Flow Rate (cc/min):   30

nitrogen-containing compounds in the gas phase include N_2, NH_3 and HCN. In addition to nitrogenous species, CO, CO_2 and hydrocarbon compounds are also of interest in the coal combustion system. The concentrations of all the species mentioned above are measured by different techniques:

1. Nitric oxide emission is monitored using a chemiluminescent detector.

2. Ammonia concentration is measured by colorimetric analysis.

3. Hydrogen cyanide concentration is determined using a specific ion electrode.

4. Molecular nitrogen and methane are analyzed by gas chromatography.

5. Carbon monoxide and carbon dioxide are analyzed by both gas chromatography and non-dispersive infrared analysis.

We shall discuss all the techniques of measurements in detail.

5.3.1   Chemiluminescent Gas Analysis of NO_x

A Thermo Electron Model 10B Rack Mounted Chemiluminescent $NO-NO_x$ Gas Analyzer (Thermo Electron Corp., Waltham, Massachusetts) is used for the analysis of nitric oxide (NO_x). Combustion gases are withdrawn continuously from the furnace, passed through a filter to remove soot and tar, then fed into the analyzer for NO_x analysis. For the purpose of systematic measurement, any nitrogen dioxide (NO_2) present is converted to nitric oxide (NO) by a molybdenum converter prior to nitric oxide detection, although the concentration of nitrogen dioxide (NO_2) is always negligible (i.e., less than 3% of NO concentration) in our combustion system.

This instrument has a typical response time of 1.7 seconds and an

operating range of 2.5 to 10,000 ppm with an accuracy of ±1% of full-scale. The meter response to NO_x is recorded on a strip chart recorder and integrated over time for the total yield. This technique allows the fraction of the nitrogen in the coal that is converted to NO_x to be determined.

The chemiluminescence meter is calibrated at the operating conditions used during actual sampling using nitrogen gas as a zero gas and a series of certified nitrogen oxide in helium calibration gases supplied by Matheson Gas Company (Gloucester, Massachusetts). The concentrations of calibration gases are confirmed by independent Saltzman analysis for the total nitrogen oxides in accordance with ASTM procedures (D 1607-69).

5.3.2 Colorimetric Analysis of NH_3

A gas sampling unit is used to collect NH_3 from the furnace off-gases. The basic gas sampling unit consists of two bubblers containing 0.1 N H_2SO_4 solution, a flow regulator to control the flow rate, and a wet test meter to measure the total volume of gas. The gas sampling system is first checked for its collection efficiency by passing a known concentration and known volume of NH_3 through the bubbler. Off-gases from the furnace are then bubbled through the bubbler containing fresh 0.1 N H_2SO_4 solution to absorb NH_3. A sample aliquot from the bubbler is then tested with a Nessler reagent in accordance with ASTM procedures (D 1426-74) for the ammonia content.

5.3.3 Standard Specific Ion Electrode Analysis of HCN

Hydrogen cyanide from furnace off-gases is first collected in a gas sampling unit. The gas sampling unit is basically identical to the unit used for NH_3 sampling except that the absorbing agent in the bubbler is now changed to 0.1 N NaOH solution. After absorption has been completed, an aliquot of 0.01 N $Pb(NO_3)_2$ is added to the sample solution for the removal of the potential interference by S^{--} ion originated from coal. The cyanide content in the sample solution is then measured by an Orion cyanide ion electrode model 94-06 (Orion Research, Inc., Cambridge, Massachusetts). The electrode is calibrated frequently against a series of standard NaCN solutions prepared daily. The reproducibility of the electrode is ±2%.

5.3.4 Gas Chromatographic Analysis of N_2, CO, CO_2 and CH_4

A five-layer material gas sampling bag manufactured by Calibrated Instruments, Inc. (Ardsley, New York) is used to collect the off-gas from furnace. The sampling bag is then connected to a gas chromatographic system and a known volume of gas from the bag is introduced into a sample loop for gas chromatographic analyses. The gas chromatographic system is a Fisher/Hamilton Model 29 Gas Partitioner manufactured by Fisher Scientific Company (Pittsburgh, Pennsylvania). This instrument is equipped with two columns. Column No. 1 is a 6 ft x 1/4 in aluminum tubing packed with 30% Di-2-ethylhexylsebacate (DEHS) on 60/80 mesh Chromosorb P. Column No. 2 is a 6 1/2 ft x 3/16 in aluminum tubing packed with 40/60 mesh Molecular Sieve 5 A. Both columns are operated at room temperature. Alternatively, the packing materials in both

columns can be simultaneously replaced by Porapak Q, with Column No. 1 operating at room temperature and Column No. 2 operating at dry ice temperature, i.e., -78 C. The gas chromatograph is calibrated against a standard gas before and after each sample run to ensure a good accuracy. The standard gas, supplied by Matheson Gas Company (Gloucester, Massachusetts) consists of known concentrations of CO, CO_2, CH_4, N_2, and H_2 in a helium mixture. Total CO, CO_2, CH_4, and N_2 emissions from the furnace can be determined by comparing the gas chromatographic response to that of the standard gas.

5.3.5 Non-Dispersive Infrared Analyses of CO and CO_2

The concentrations of CO and CO_2 are also measured by Beckman non-dispersive infrared analyzers (Beckman Instruments, Inc. Fullterton, California). Model 315 A is used for CO_2 analysis and Model 315 B for CO. These analyzers allow automatic and continuous concentration determinations of CO and CO_2 in a complex gas mixture. The analysis is based on a differential measurement of the absorption of infrared energy by the particular component of interest. These instruments are frequently calibrated against a dry nitrogen zero standard gas and a series of certified carbon monoxide in argon calibration gases and certified carbon dioxide in argon calibration gases. The repeatability of the instrument is ±2% of the full scale. The off-gases from the furnace are withdrawn, diluted with a secondary argon stream if necessary, and then introduced directly into these analyzers for a continuous monitoring of CO and CO_2 concentrations. The meter response is recorded on a strip chart recorder as a function of time. Since the

meter response is nonlinear, the total yield of CO or CO_2 is determined by a differential graphical integration. The non-dispersive infrared analyses of CO and CO_2 provide a second check on the analyses of CO and CO_2 by gas chromatography.

5.4 Proximate Analysis

The proximate analysis of coal was developed as a simple means for determining the distribution of products obtained during heating under standard conditions. It is the most commonly used type of analysis for characterizing coals in connection with their utilization. The proximate analysis includes the determinations of: (1) water or moisture; (2) ash; (3) volatile matter; and (4) fixed carbon. Brief descriptions of each procedure are given as follows.

5.4.1 Moisture

A Labline Model 3620ST drying oven is used for the determination of the moisture content. Coors ceramic crucibles containing the samples are heated in the oven for one hour at a temperature of 110 C, i.e., a temperature slightly higher than the boiling point of water. The oven is continuously purged with nitrogen to sweep the water vapor away from the samples when the samples are being dried. Finally, the moisture content of the sample is determined by measuring the loss in weight after heating.

5.4.2 Ash

The ash content is determined using a home-made magnesium brick furnace. The heat is supplied to the furnace by four silicon carbide electrodes which are connected in parallel to a Variac. Coors ceramic crucibles containing the samples are first placed in the furnace at room temperature. The Variac is set to heat the furnace gradually so that the temperature reaches 500 C in one hour. The Variac is then readjusted so that the temperature reaches 750 C at the end of the second hour. The samples are continuously heated to constant weight at 750 C. The furnace is purged with an ample supply of air at all times. Finally, the ash content is determined by weighing the residue remaining in the crucible after burning under these rigidly controlled conditions mentioned above.

5.4.3 Volatile Matter

A Hoskin Model 303 cylindrical furnace with a continuous purge of nitrogen is used for the determination of volatile matter. A loosely covered platinum crucible containing the samples to be analyzed is suspended in the hot zone of the furnace which is maintained at a temperature of 950 ± 20 C. After heating for exactly 7 minutes, the crucible is removed from the furnace and allowed to cool. The sample is weighed as soon as it is cold. The percentage loss of weight minus the percentage moisture equals the volatile matter.

5.4.4 Fixed Carbon

The fixed carbon is a calculated figure obtained by subtracting

from 100 the sum of the percentage of moisture, ash and volatile matter.

5.5 Elemental Analysis

The ultimate analysis of the raw coals, the original char used for
Char/O_2 or Char/NO_x studies, and selective residual char samples were
performed by the Galbraith Laboratories, Inc., Knoxville, Tennessee.
The ultimate analysis includes the determinations of carbon, hydrogen,
nitrogen and sulfur. The oxygen content is obtained by difference.
Only brief summaries of each individual analysis method will be given
here.

5.5.1 Carbon and Hydrogen

A weighed quantity of dry sample is burned in a stream of oxygen
at 800 to 900 C and the products of combustion passed over heated cupric
oxide, which insures complete conversion of all of the carbon to carbon
dioxide and all of the hydrogen to water. After the purification from
interfering substances, the combustion products are passed through a
train for the absorption of CO_2 and H_2O. The percentages of carbon and
hydrogen in the sample can then be calculated from the increases in
weight of the absorbants used to collect the water and carbon dioxide.
The expected error by this method is about 0.5%.

5.5.2 Nitrogen

The Kjeldahl method (or it is often referred to as the Kjeldahl-
Wilfarth-Gunning method) is used for the determination of nitrogen
content in the sample. In this procedure, nitrogen is converted into

ammonium salts by destructive digestion of the sample with a hot, catalyzed mixture of concentrated sulfuric acid and potassium sulfate. A 24-hour digestion time is specially requested for all the analyses to ensure a complete digestion, although a digestion period of 3 to 6 hours is suggested by ASTM procedures (D 3179-73). After the complete digestion of the sample, the ammonium salts are then subsequently decomposed in a hot alkaline solution from which the ammonia is recovered by distillation into a acid solution. Finally, the ammonia content is then determined titrimetrically. The expected error of the Kjeldahl method is about 5%.

5.5.3 Total Sulfur

The method used for the total sulfur determination is based on the combustion of the sulfur compounds to form sulfate ions. Then the concentration of sulfate ions is determined either gravimetrically or volumetrically. This method gives an expected error of 2%.

5.5.4 Oxygen

No direct oxygen analysis was requested during the course of the thesis work. Instead, the oxygen content was determined indirectly by subtracting ash and all other elements from 100%. This procedure can lead to rather substantial errors in the oxygen concentration because mineral matter changes weight when sulfides and carbonates react during ashing.

5.6 Physical Characterization of Char

Physical characterization of the original char used for Char/O_2 or Char/NO_x studies and selective residual char samples were performed by the Quantachrome Corp., Greenvale, New York. The physical characterization includes the determinations of specific B.E.T. surface areas, total pore volumes, average pore sizes and true powder densities. The Quantasorb Surface Area Analyzer is used for the determinations of specific B.E.T. surface areas, total pore volumes and average pore sizes. The Null-Pycnometer is used for the measurements of true powder densities. Brief descriptions on the principle of operations are given as follows.

5.6.1 Specific B.E.T. Surface Area

Mixtures of helium and nitrogen gas are passed through a small U-shaped cell containing the sample. At liquid nitrogen temperature, helium will not adsorb on any surface while nitrogen will physically adsorb on all substances. The amount of nitrogen adsorbed at various partial pressures can then be used to calculate the sample's surface area and pore structure.

Adsorption and desorption occur when the sample is immersed into and then withdrawn from a liquid nitrogen filled Dewar Flask. Changes in the ratio of He to N_2 in the flowing stream, due to adsorption and desorption, are sensed by a specially designed thermal conductivity detector. The signals delivered by the detector are nearly Gaussian in shape. The instantaneous signal height is proportional to the rate of adsorption or desorption and the total integrated area under the curve is proportional to the quantity of gas adsorbed. This area is

automatically digitally integrated by the Quantasorb Surface Area
Analyzer.

In this manner, the quantity of adsorbate that corresponds to a
molecular monolayer on the solid surface can, therefore, be obtained
by the application of B.E.T. equation (i.e., by either multi-point
B.E.T. analysis or single-point B.E.T. analysis) (see Gregg and Sing,
1967). Combining this with the cross-sectional area occupied per
adsorbed molecule, usually taken to be about 16.2 $\overset{o}{A}^2$ for N_2, gives the
total surface area of the sample. Finally, the specific B.E.T. surface
area is obtained by dividing the total surface area by the total weight
of the sample analyzed. All the specific B.E.T. surface areas reported
in this thesis work are obtained by the single-point B.E.T. analysis.

5.6.2 Total Pore Volume

Vapors in equilibrium with liquid contained in fine capillaries
or pores will have depressed vapor pressures. In fact, if the pore is
adequately small in diameter, the vapor will condense at pressures far
below normal. As indicated by the Kelvin Equation (see Gregg and Sing,
1967), nitrogen gas will condense into all pores with radii less than
500 $\overset{o}{A}$ at a relative pressure (defined as the ratio of the gaseous pressure
to the saturated vapor pressure over the liquid phase at the same
temperature) of 0.99. Based on this principle, the total pore volume
of the sample can be measured by the following procedures.

After thoroughly outgassing a sample, adsorb a concentration of
adsorbate (N_2) corresponding to a relative pressure of 0.99 (the
practical range is 0.96 - 0.99). When the adsorption is complete,

remove the liquid nitrogen bath and let the adsorbate desorb.
Calibrating the signal with pure adsorbate gives the volume adsorbed in
terms of gaseous volume of N_2. Finally, converting the volume of gaseous
nitrogen adsorbed (or desorbed) to the volume of liquid nitrogen held
in the pores yields the total pore volume of the sample.

5.6.3 Average Pore Size

The exact pore size is difficult to determine unless a careful
study is made regarding the behaviors of both complete adsorption and
desorption isotherms. However, a logically defined average-pore-diameter
can be calculated with prior knowledge of the surface area and total
pore volume by assuming that cylindrical pores constitute the nature of
the entire surface. With this assumption and a knowledge of simple
geometry, the average pore diameter can therefore be calculated as four
times the ratio of total pore volume to total surface area. The average
pore diameters of char samples reported in this thesis are obtained in
this manner.

5.6.4 True Powder Density

The true powder density of the char is measured by the Null-
Pycnometer. The Null-Pycnometer uses a differential and null principle
to rapidly and accurately measure the true powder volume of the samples.
Operation is based on a gas displacement method which is achieved by
increasing the pressure on the sample side of a sensitive differential
gauge and then observing the pressure required to zero or null the
differential gauge when pressure is applied to the opposite side.

Helium gas is used since it exactly obeys the ideal gas equation. The readings of the pressure required to null the differential gauge, once with sample in the cell and once with the cell empty, are then used to calculate the powder volume, and in turn, the powder density.

5.7 Chemical and Physical Properties of Coal and Char Used for Study

Two coals were used in this study: Montana lignite-A and Montana subbituminous coal. The Montana lignite-A from the Savage mine in Richland county, Montana is a low rank, low sulfur, non-caking western coal. The Montana subbituminous coal containing significant moisture is from Powder River region, Montana.

The Montana lignite was received as 1/8 inch particles. These particles were ground in a ball mill and separated through roto-tapped Tyler screens to produce a 38 to 44 micron size range for further studies. Figure 5.5 shows the lignite particle size frequency distribution. The cumulative mass distribution was found to fit well with the Rossin-Rammler (1939) distribution function. This is shown in Figure 5.6.

The Montana subbituminous coal was pulverized prior to shipment to M.I.T. The subbituminous coal was also size-graded to select particles in 38 to 44 micron size range for oxidation experiments.

The Montana lignite-A was used to produce char for both parametric and kinetic studies (see Sections 5.2 and 6.3). The char produced by pyrolyzing lignite at a temperature of 1250 K for a residence time of 1 second is called 1250 K lignite char and the char produced at 1750 K for 1 second is called 1750 K lignite char. In the parametric studies,

RAW LIGNITE
FREQUENCY DISTRIBUTION

x = 47.6
σ = 15.2
s = 3.42
b = 1.33 × 10^{-6}
798 Particles

FREQUENCY (ARBITRARY UNITS)

DIAMETER (MICRON)
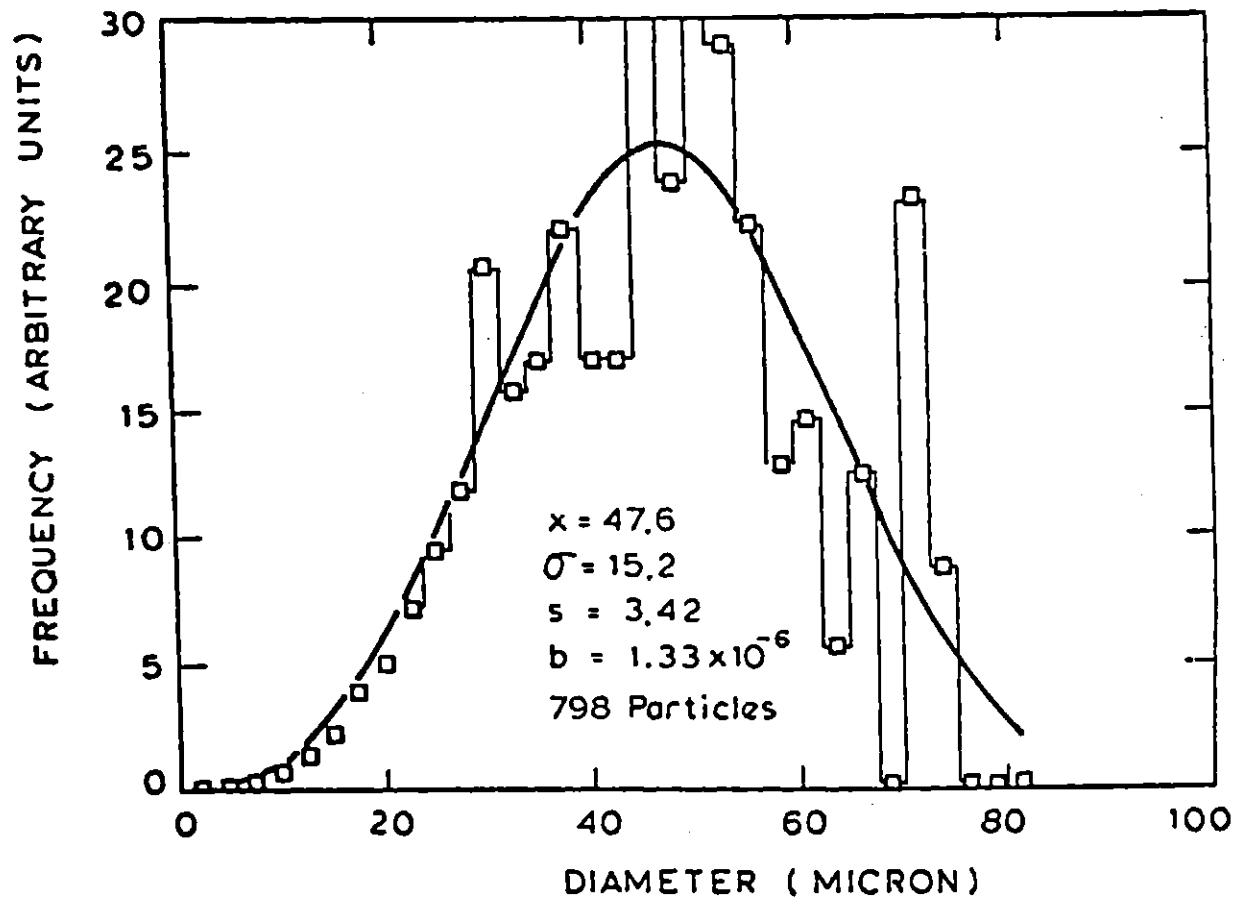
Figure 5.5

Particle Size Distribution of Raw Lignite

RAW LIGNITE
ROSIN-RAMMLER DISTRIBUTION

$\bar{x} = 52.3$

$s = 3.42$

$b = 1.33 \times 10^{-6}$
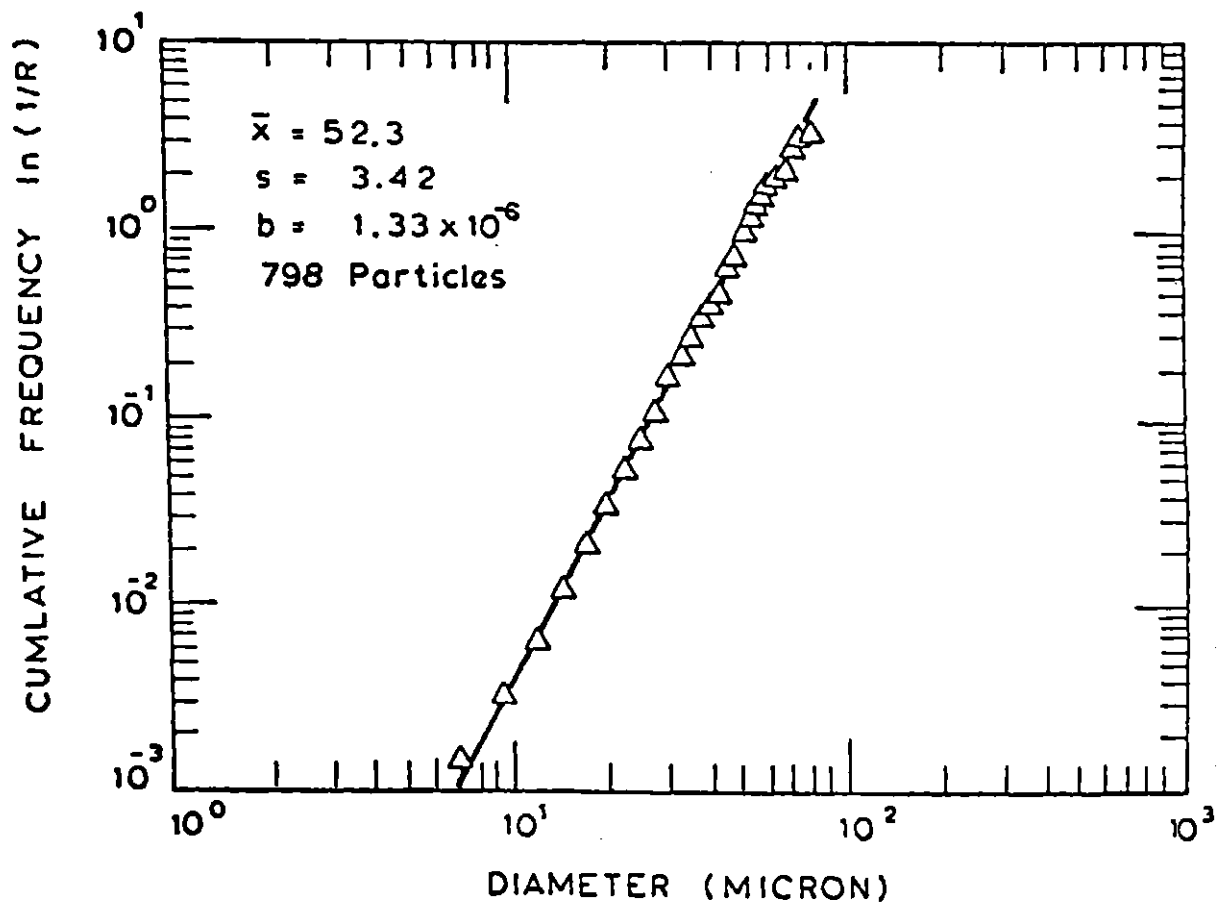
798 Particles

Figure 5.6

Rosin-Rammler Distribution of Raw Lignite

both 1250 K lignite char and 1750 K lignite char were used as produced. In kinetic studies, the 1750 K lignite char was size-graded to select particles in the 38 to 44 micron size range for further experiments, however, the final average particle size was found to be 30 microns. Figure 5.7 shows the particle size distribution of the 1750 K lignite char particles.

Both proximate and ultimate analyses of the coals and chars used for the study were performed in accordance with the procedures described in Sections 5.4 and 5.5. The chemical properties of the coals and chars are summarized in Table 5.2.

Physical characterizations of the original char used for Char/O_2 or Char/NO_X kinetic studies were performed according to the procedures presented in Section 5.6. The specific B.E.T. surface area, pore volume, average pore size, and powder density of the 1750 K lignite char are summarized in Table 5.3.
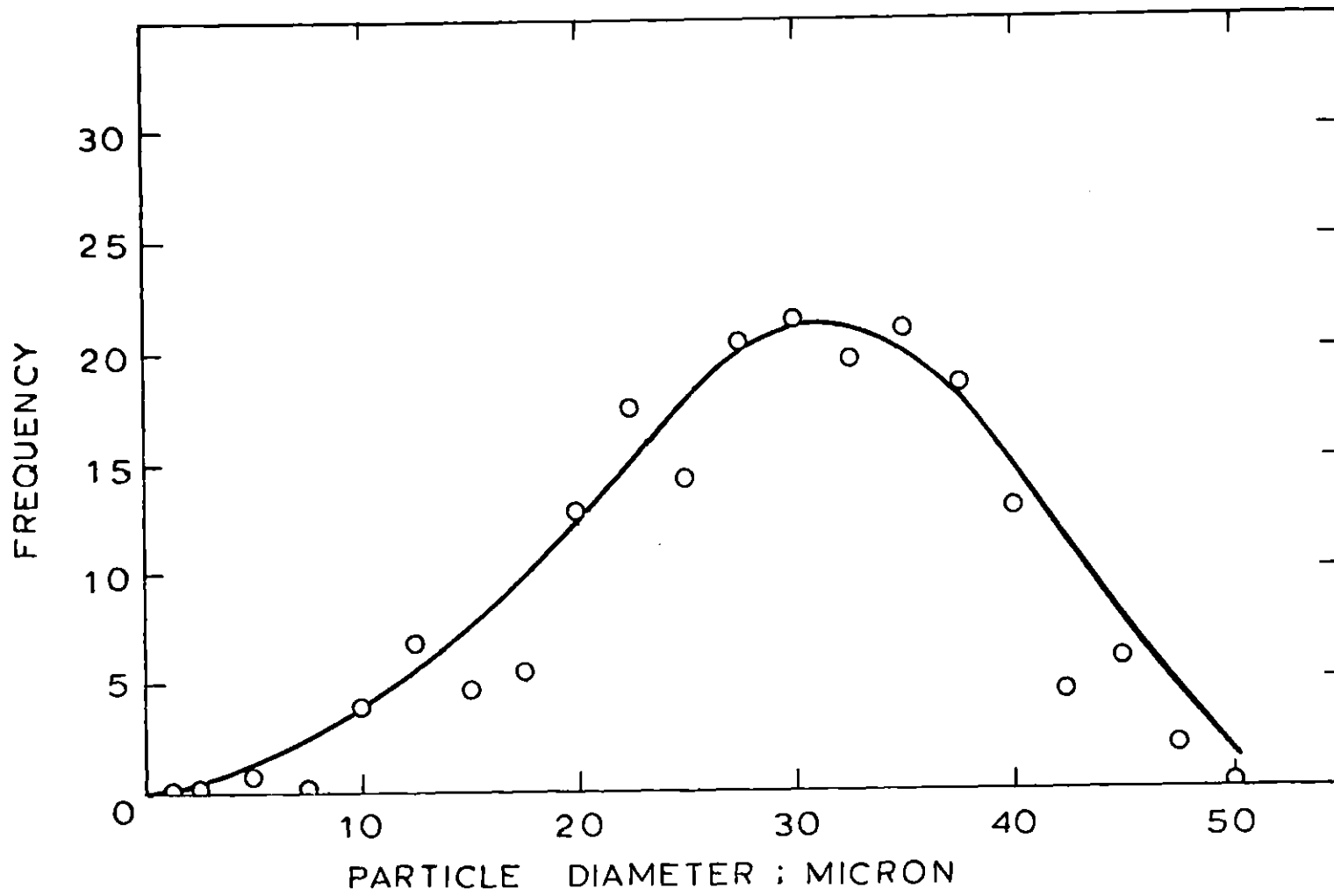
Figure 5.7

Particle Size Distribution of 1750 Lignite Char

TABLE 5.2

CHEMICAL PROPERTIES OF COALS AND CHARS

| Type | Specification | Proximate Analysis A.R. Wt% | | | Ultimate Analysis A.R. Wt% | | | | |
		VM	H_2O	Ash	C	H	N	S	O (by Diff.)
Montana Lignite-A	Savage	36.20	13.60	7.80	54.50	4.96	0.88	0.84	17.42
Montana Sub-Bituminous	Powder River Region	35.16	21.23	9.34	53.26	3.35	0.87	0.78	11.17
1250 K Lignite Char		NM*	4.20	12.08	66.94	2.09	1.02	0.56	13.11
1750 K Lignite Char**		NM	2.02	18.03	76.42	0.69	0.55	1.06	1.23
1750 K Lignite Char***		NM	2.10	19.00	76.11	0.36	0.58	1.11	0.74

*NM = Not Measured

**Used in parametric studies

***Used in Char/O_2 and Char/NO_x kinetic studies

TABLE 5.3

PHYSICAL PROPERTIES OF 1750 K LIGNITE CHAR

Type	Average Particle Diameter μ	B.E.T. Surface Area m^2/g	Pore Volume cm^3/g	Average Pore Diameter $\overset{\circ}{A}$	Bulk Density g/cm^3
1750 LC-1*	30	110.0	0.160	57.7	1.71
1750 LC-3*	30	121.6	0.157	51.6	1.71
1750 LC-4**	30	175.0	0.184	42.2	1.64

*Used in Char/O_2 kinetic studies

**Used in Char/NO_x kinetic studies

CHAPTER 6

PARAMETRIC INVESTIGATIONS

6.1 Introduction

When a pulverized coal particle is injected into a hot furnace, it may first undergo rapid devolatilization by heating in the products of combustion recirculated to the burner. The volatiles may subsequently burn either in the boundary layers of individual particles or in the flames engulfing clouds of particles and the char will ultimately burn out in the tail of the flame. Alternatively, ignition may precede complete devolatilization so that char and volatiles may burn concurrently. Based on these models of the coal combustion and other fragmentary data, conceptual paths that could be taken by the coal nitrogen during combustion can be depicted as shown in Figure 6.1.

The nitrogen in the coal, upon heating, may first be volatilized to become volatile-nitrogen. The volatile-nitrogen compounds yield transient species such as N, NH, NH_2, CN, etc. (Pereira, 1975) during their decomposition within the non-equilibrium flame reaction zone, which are then oxidized to form NO_x or other nitrogeneous species. The nitrogen in the coal could also be retained in the char during pyrolysis to become char-nitrogen. Since the char is going to be consumed either partially or completely during the final char burnout process, the char-nitrogen will ulatimately be oxidized to form NO_x or to be reduced to form N_2 and other nitrogenous species. The original char-nitrogen could also be further retained in the unburned char.

PYROLYSIS

OXIDATION

NOx

N$_2$ + Others

Char-Nitrogen

Coal-
Nitrogen

Volatile-Nitrogen

NH$_i$, Amines

NOx

CN, Cyanides

N$_2$ + Others
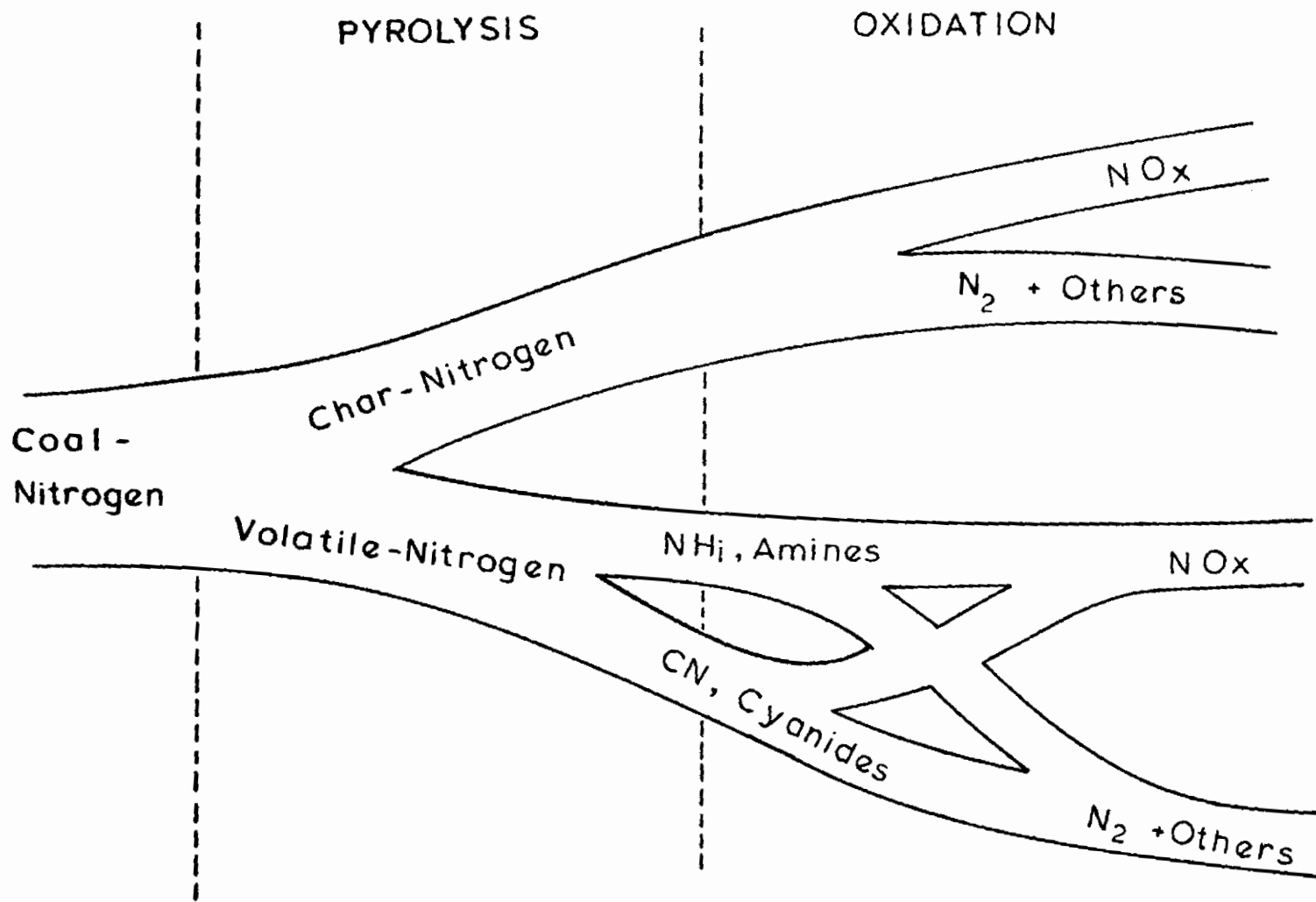
Figure 6.1

Conceptual Paths of Coal-Nitrogen During Combustion

In viewing the conceptual paths of coal-nitrogen, several questions arise:

1. What is the contribution of the coal-nitrogen to NO_x? What fraction of the nitrogen in the coal is converted to NO_x?

2. What is the distribution of the coal-nitrogen between volatiles and char? Is the coal-nitrogen oxidized as volatiles or in char?

3. For low NO_x emission, is it preferable for the coal-nitrogen to go to the char or volatiles? What are the effects of stoichiometry and temperature on NO_x formation? How do combustion modifications affect the split of nitrogen between volatiles and char?

Answers to these questions are essential to the studies of the fate of the coal-nitrogen during coal combustion. Answers to these questions are also pertinent to the design of low NO_x emission coal combustion systems. Consequently, these questions underlay the approach and design for the parametric investigations.

In view of the above considerations, the following goals were selected for the parametric investigations:

1. To determine the effect of the fuel/oxygen equivalence

ratio* on NO_x emissions.

2. To determine the effect of the temperature on NO_x emissions.

3. To identify the individual contribution of char-nitrogen and volatile-nitrogen to the total NO_x emissions.

The information obtained would then be very useful for the development of control strategies for coal combustion systems.

In order to achieve the various goals of these parametric investigations, five different types of experiments were designed to simulate industrial coal combustion conditions as indicated in the following tabulation.

	Experiment	Reaction Time	ϕ	Temperature
(1)	Oxidation of Montana Lignite	~1 sec	0.2-4.0	1250, 1750 K
(2)	Pyrolysis of Montana Lignite	~1 sec	—	1250, 1750 K
(3)	Oxidation of 1250 K Lignite Char	~1 sec	0.2-4.0	1250 K
(4)	Oxidation of 1750 K Lignite Char	~1 sec	0.2-4.0	1750 K
(5)	Oxidation of Montana Sub-bituminous Coal	~1 sec	0.7-1.3	1250, 1500 1750 K

*For the purpose of this study, the fuel/oxygen equivalence ratio (ϕ) is defined as follows:

$$\phi \equiv \frac{(F_f/F_o)_{actual}}{(F_f/F_o)_{stoichiometric}} = \frac{(F_o)_{stoichiometric}}{(F_o)_{actual}}$$

where F_f is the feed-rate of the fuel and F_0 is the feed-rate of the oxygen. The values of $(F_0)_{stoichiometric}$ were obtained by calculating the total amount of the oxygen which was required to oxidize completely all the elements in the fuel to form the most stable oxides of every element, then subtracting the amount of the oxygen which existed in the original fuel used for the study.

The premise of conducting oxidation experiments on both coal and char produced by pyrolysis of the coal at the temperature and residence time corresponding to those of the oxidation experiments, was that if the volatile-nitrogen conversion and the char-nitrogen conversion could be treated independently, then the volatile-nitrogen contribution to NO_x could be obtained by subtracting the char-nitrogen contribution to NO_x from the overall NO_x emissions obtained from the oxidation experiments of coal.

6.2 Oxidation of Lignite

In order to avoid the complication by thermal NO_x, arising from the fixation of atmospheric nitrogen, simulated air (i.e., 21% oxygen in helium) was used for all the oxidation experiments. Montana lignite particles with a nominal size of 38 to 44 microns were burned in this simulated air at varying fuel/oxygen equivalence ratios at two different temperature levels according to the procedures described in Chapter 5. The unburned char was recovered. The nitrogen retained in the unburned char was determined by elemental analysis. The conversion of coal-nitrogen to NO_x was obtained by measuring the concentration of the off gas from the furnace.

The results obtained from oxidizing raw coals at various fuel/oxygen equivalence ratios in a furnace temperature of 1250 K and a residence time of 1 second are shown in Figure 6.2. As shown at the top of the figure is the total solid weight loss (on a dry-ash-free basis) as a function of fuel/oxygen equivalence ratio. The solid weight loss was nearly 100% at very fuel lean conditions, however, it started to decrease
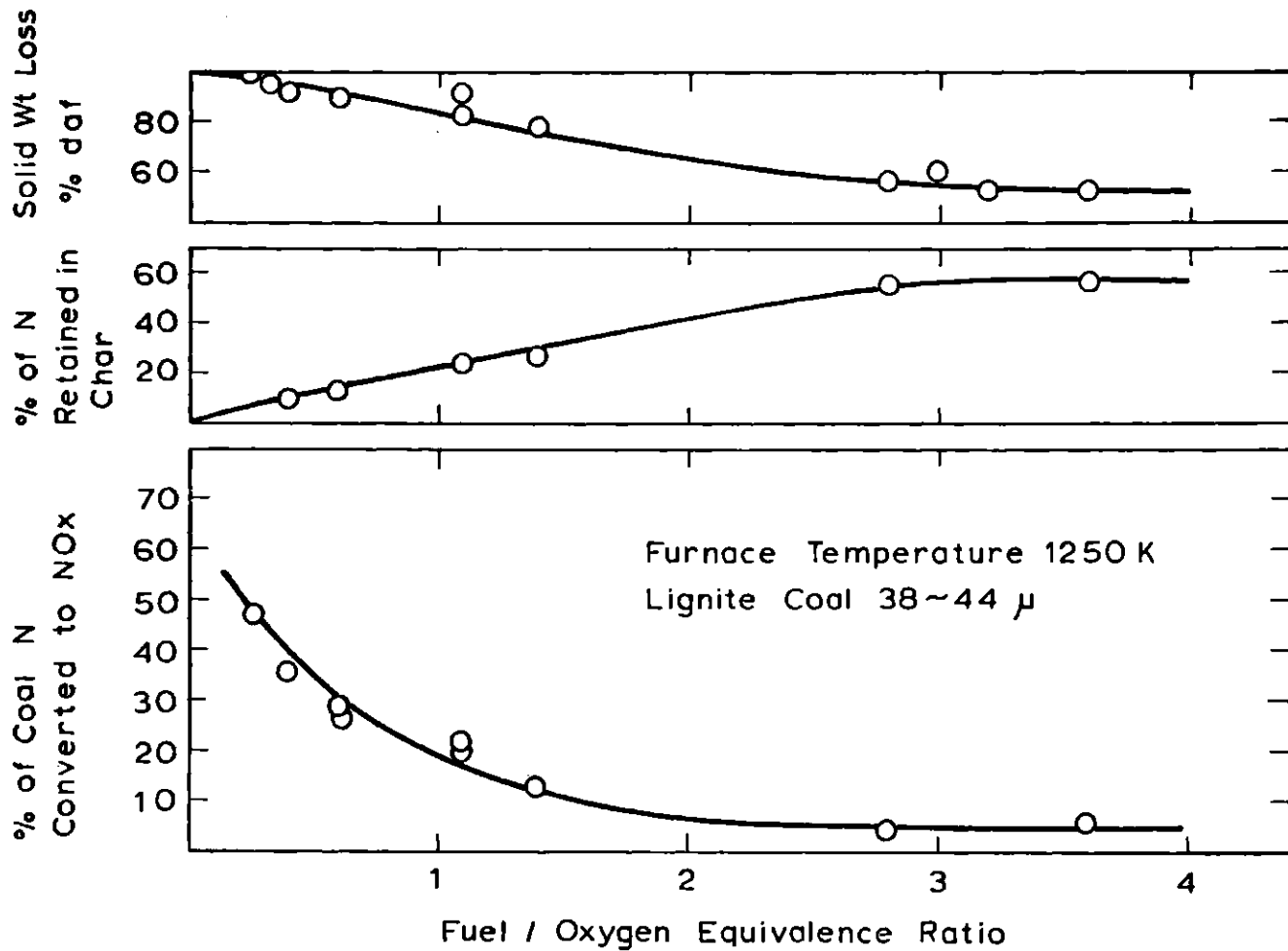
Figure 6.2

Fate of Coal Nitrogen During Oxidation: Conversion to Nitric Oxide (Bottom); Retention by Unburned Char (Middle); and Combustion Efficiency (Top). Montana Lignite at 1250 K.

as the fuel/oxygen equivalence ratio started to increase. The solid weight loss continued to decrease until an asymptotic value of about 50% at a fuel/oxygen equivalence ratio of about 3 was obtained. The solid weight loss could also be viewed as a solid combustion efficiency. As expected, the combustion efficiency was very high at very fuel lean conditions. The combustion efficiency became poorer and poorer as the flame became richer and richer.

In the center of the figure shows the fraction of the original coal nitrogen retained by any unburned char as a function of fuel/oxygen equivalence ratio. The nitrogen retention curve is complementary to the solid weight loss curve. When solid burnout was complete, there was obviously no nitrogen retained in the char. The nitrogen retained in the unburned char increased as the solid burnout decreased or as the fuel/oxygen equivalence ratio increased. The retention reached an asymptotic value of about 55% at fuel/oxygen equivalence ratios above 3.

In the bottom of the figure is the conversion curve of coal-nitrogen to NO_x. Again it was correlated with fuel/oxygen equivalence ratio. The coal-nitrogen conversion to NO_x was found to decrease monotonically with increasing fuel/oxygen equivalence ratios. At very fuel lean conditions, about 60% of the original coal-nitrogen was converted to NO_x. The conversion decreased to about 22% at fuel/oxygen equivalence ratio of 0.8. At stoichiometric condition, conversion is about 18%. The conversion reached an asymptotic value of about 5% at fuel/oxygen equivalence ratios above 2.

Similar results obtained in a furnace temperature of 1750 K are shown in Figure 6.3. The trends of the results at 1750 K were more or

Fuel / Oxygen Equivalence Ratio
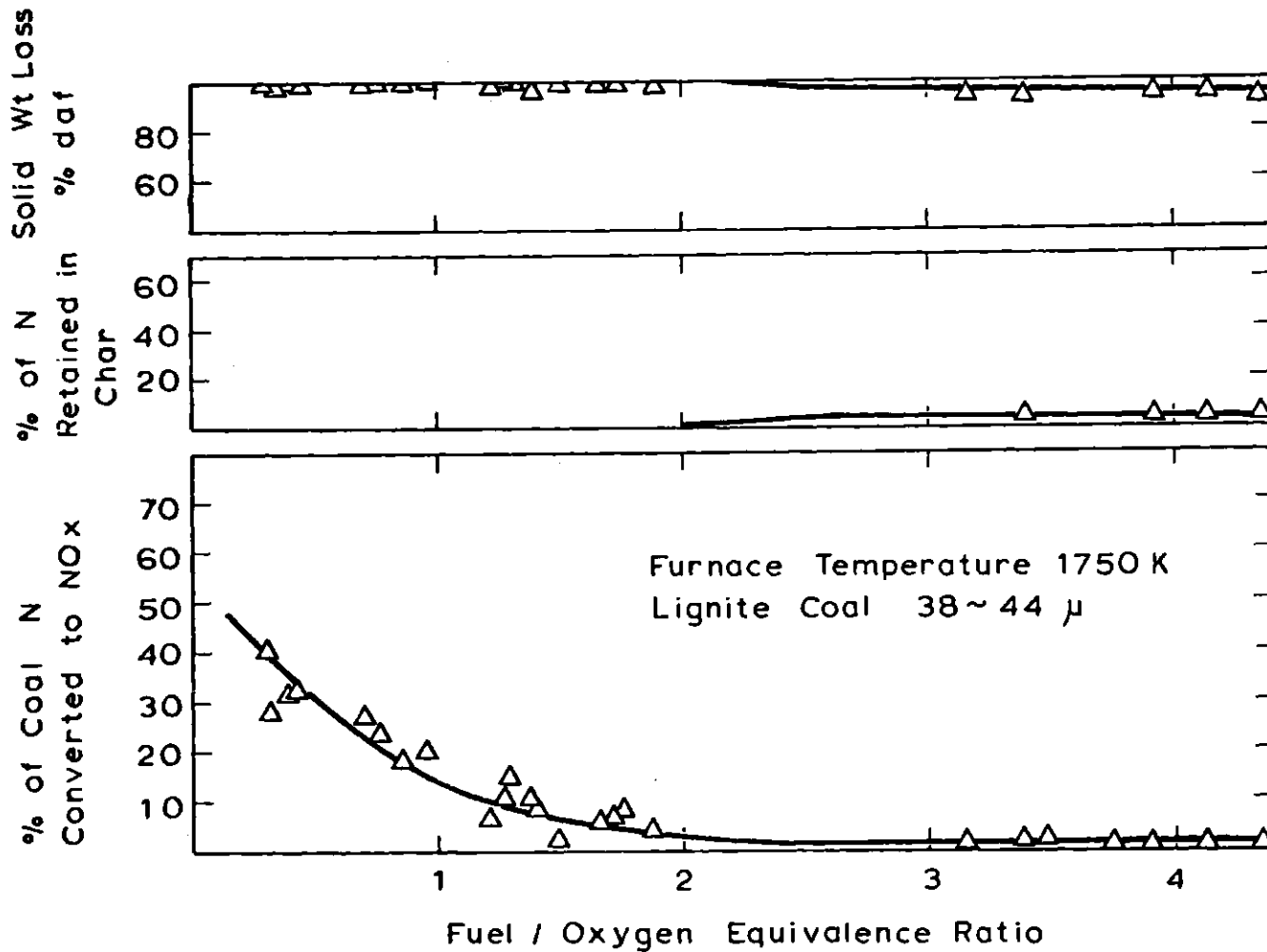
Figure 6.3

Fate of Coal Nitrogen During Oxidation: Conversion to Nitric Oxide (Bottom); Retention by Unburned Char

(Middle); and Combustion Efficiency (Top). Montana Lignite at 1750 K.

less the same as those at 1250 K. However, there were also some apparent differences between the oxidation of coal at 1250 K and 1750 K:

1. The solid weight loss at 1750 K was much higher than that at 1250 K especially at high fuel/oxygen equivalence ratio. At 1750 K, the solid burnout was complete even at a fuel/oxygen equivalence ratio of 2 and even at a very rich condition, say fuel/oxygen equivalence ratio of 4, the solid weight loss was still 95%.

2. Since the solid weight loss was much higher at higher temperature, therefore, the retention of the nitrogen in the unburned char was correspondingly lower than that at lower temperature. Only about 5% of the original coal-nitrogen was retained in unburned char at a fuel/oxygen equivalence ratio of 4.

3. At 1750 K, the conversion efficiency of coal-nitrogen to NO_x was marginally lower, say about 5 percent absolute, than that at 1250 K. The conversion to NO_x was about 55% at very lean conditions and decreased to an asymptotic conversion efficiency of about 1% at very rich conditions.

6.3 Pyrolysis of Lignite

The purpose of the pyrolysis experiments was to produce char at different temperature levels for use in further oxidation experiments. The char was prepared by the pyrolysis of the coal at the temperature and residence time corresponding to those of oxidation experiments. The details for the production of char for use in oxidation experiments

were outlined in Chapter 5. The char produced by pyrolyzing lignite at a temperature of 1250 K and residence time of 1 second will be designated 1250 K lignite char and the char produced at 1750 K and 1 second will be designated 1750 K lignite char. The characterizations of 1250 K lignite char and 1750 K lignite char are tabulated in Table 5.2. It is of interest at this time to point out that the nitrogen content (as received weight percent) of 1250 K lignite char was 1.02% and this value represented a retention of 75% of the original nitrogen in the raw lignite. The 1750 K lignite char had nitrogen content of 0.55 weight percent and that represented 27% nitrogen retention from the raw lignite. They were in good agreement with the values previously reported by Pohl (1976).

6.4 Oxidation of Lignite Char

Section 6.3 described the production of lignite char. The char so produced was then subjected to further oxidation experiments at each corresponding temperature. Figure 6.4 shows the oxidation results of 1250 K lignite char at a furnace temperature of 1250 K and a residence time of 1 second. Figure 6.5 is the results of 1750 K lignite char at 1750 K. Both results showed similar trends, but with some differences, to oxidations of the raw coal at corresponding temperature.

The solid weight loss of lignite char was lower than the solid weight loss of raw coal at a given condition. This was because the char had already been devolatilized at the corresponding temperature for 1 second and had very little volatile matter left to lose. While for the case of raw coal, the solid weight loss was due to not only
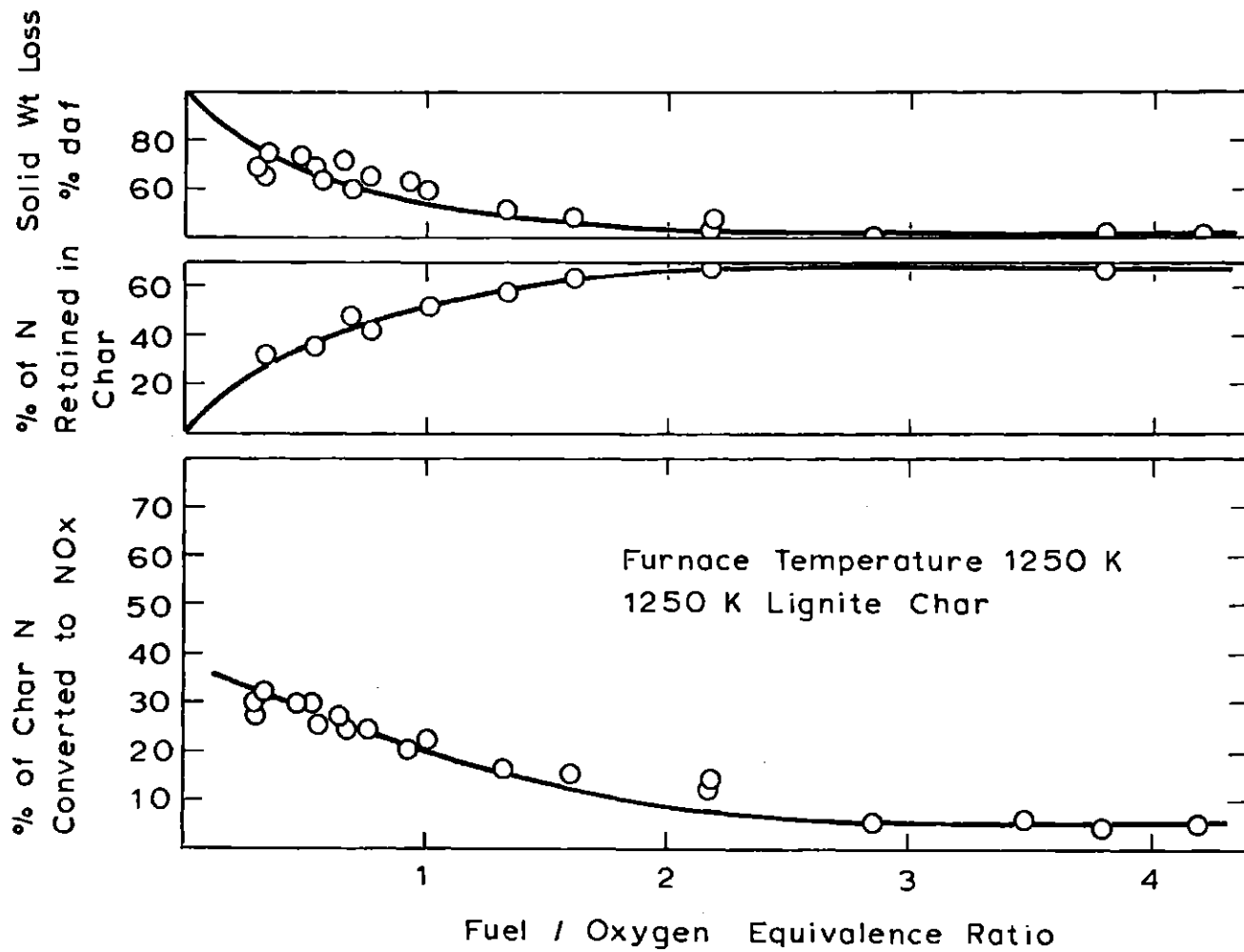
Figure 6.4

Fate of Char Nitrogen During Oxidation: Conversion to Nitric Oxide (Bottom); Retention by Unburned Char

(Middle); and Combustion Efficiency (Top). Char from Montana Lignite Pyrolyzed and Oxidized at 1250 K.
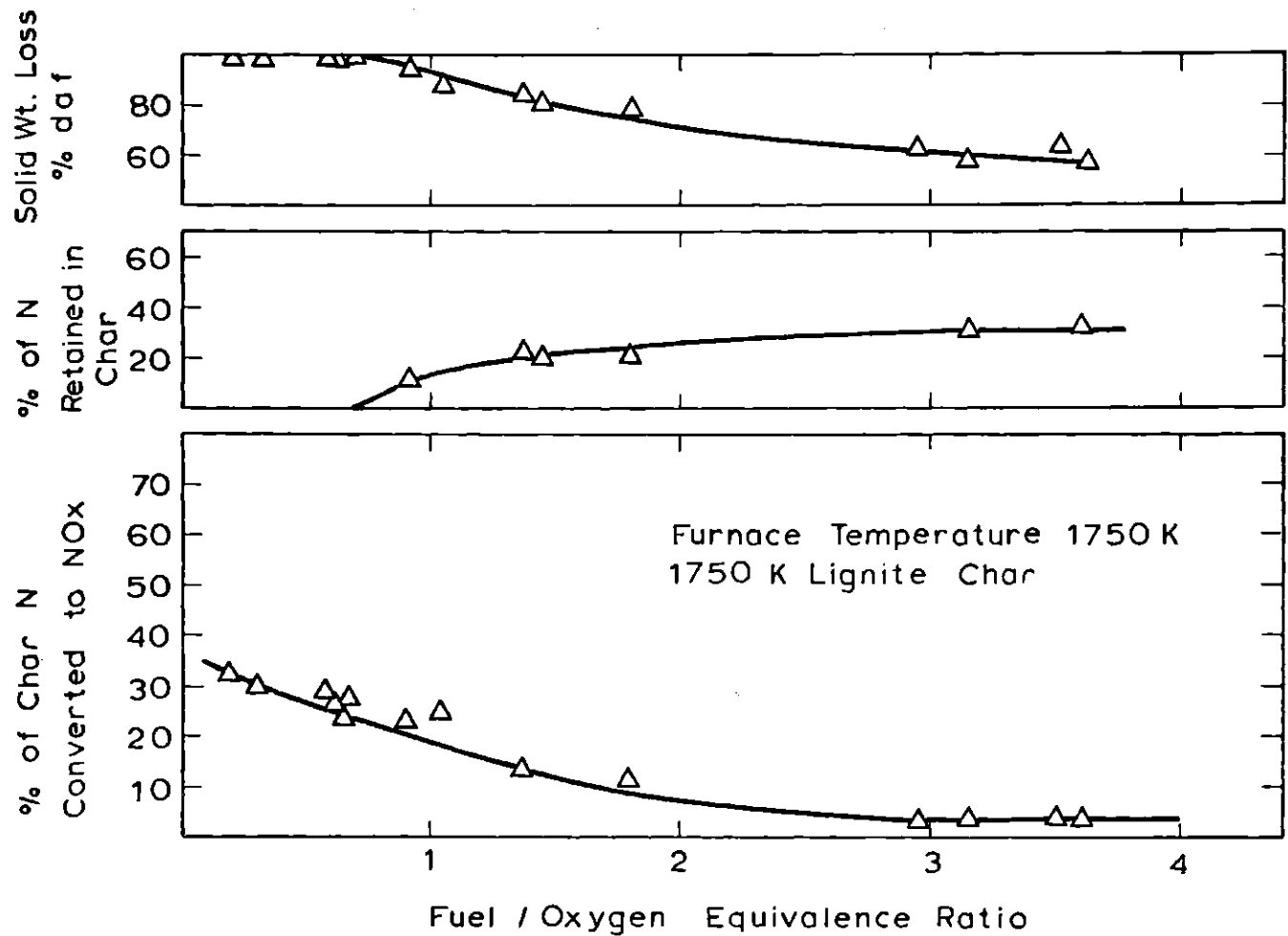
Figure 6.5

Fate of Char Nitrogen During Oxidation: Conversion to Nitric Oxide (Bottom); Retention by Unburned Char (Middle); and Combustion Efficiency (Top). Char from Montana Lignite Pyrolyzed and Oxidized at 1750 K

oxidation but also pyrolysis. Since there was more unburned char remaining during the oxidation of lignite char at any given condition, the retention of the nitrogen in the residual char was also found to be higher than that found for raw coal.

The conversion of char-nitrogen to NO_x followed a trend similar to the one observed for oxidation of raw coal. Both char-nitrogen and coal-nitrogen conversion to NO_x were found to decrease monotonically with increasing fuel/oxygen equivalence ratios. However, as can be seen from Figures 6.2 to 6.5, at fuel lean conditions, the conversion to NO_x of char-nitrogen was much lower than the corresponding values for coal-nitrogen,while at high fuel/oxygen equivalence ratio, the difference between char-nitrogen and coal-nitrogen conversion became less apparent. At 1250 K and at strongly lean condition, for example, the conversion of coal-nitrogen to NO_x was about 60% while the conversion of char-nitrogen to NO_x was slightly less than 40%.

6.5 Oxidation of Montana Sub-Bituminous Coal

In Section 6.2, it has been pointed out that at 1750 K the conversion efficiency of coal-nitrogen to NO_x was marginally lower than that at 1250 K. The effect of temperature on fuel nitrogen oxidation was small and it was feared that the results might be influenced by day-to-day variations in operating conditions. In order to critically test the effect of temperature on the conversion of coal-nitrogen to NO_x, a series of experiments were conducted in which the fuel/oxygen ratios were fixed and the furnace temperature was varied. The data shown in Figure 6.6 were obtained for a Montana sub-bituminous coal in this
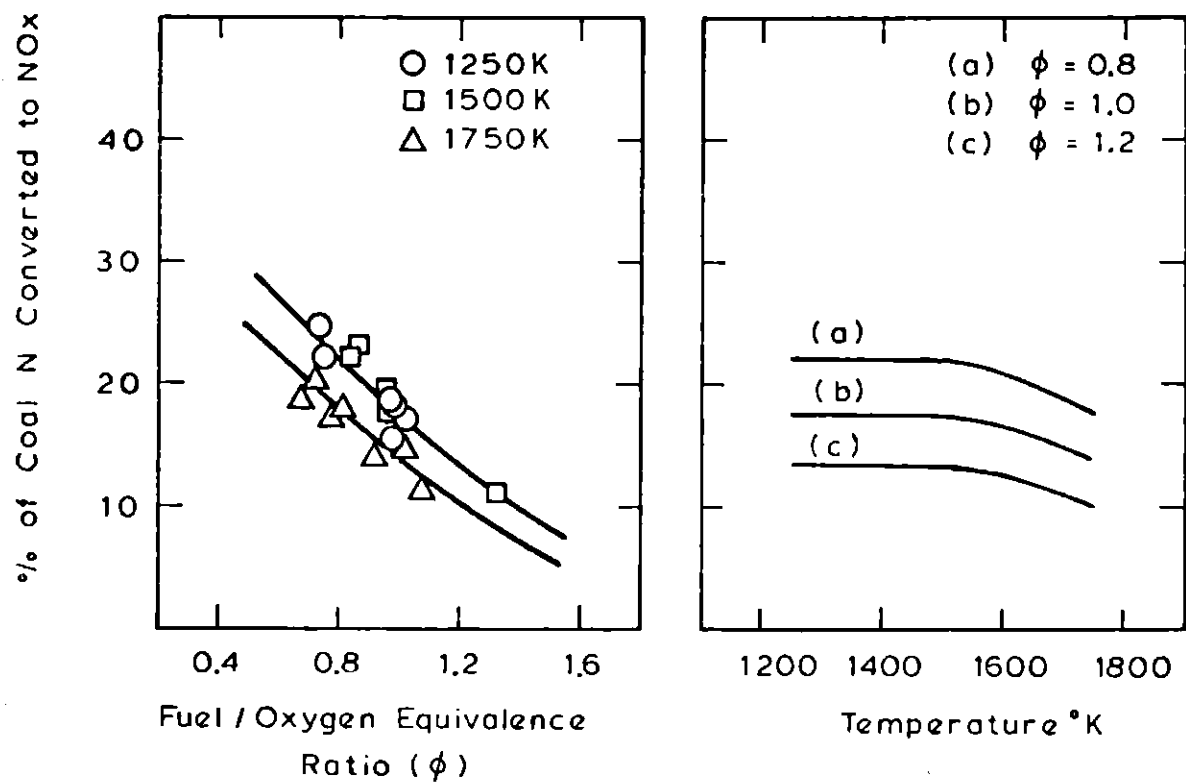
Figure 6.6

Effects of Temperature and Fuel/Oxygen Equivalence Ratio on Conversion of Coal Nitrogen to Nitric Oxide.

Montana Sub-Bituminous Coal.

manner. The fuel/oxygen equivalence ratios were fixed in a range of 0.7 to 1.3 because it is the range of interest to practical coal combustors. On the left of Figure 6.6 is the conversions of coal-nitrogen to NO_x as a function of fuel/oxygen equivalence ratio obtained at furnace temperatures of 1250 K, 1500 K, and 1750 K, respectively. No distinction could be made for data obtained at 1250 K and 1500 K, although the conversion at 1750 K was lower as compared to the conversion at 1250 K or 1500 K at any given fuel/oxygen equivalence ratio. Comparisons of data obtained at 1250 K with those in Figure 6.2 and data at 1750 K with those in Figure 6.3 show very little differences even though different coals were involved. This is consistent with the findings of Pershing (1976) and results obtained by Pohl (1976).

The information on the left-hand diagram of Figure 6.6 was translated into the right-hand diagram which shows the conversion of coal-nitrogen to NO_x as a function of temperature at three specific fuel/oxygen equivalence ratios of 0.8, 1.0 and 1.2, the ratios of interest to practical combustors, to emphasize the temperature effect on the conversion efficiency of coal-nitrogen to NO_x. The NO_x yields were essentially the same at 1250 K and 1500 K for all three fuel/oxygen equivalence ratios, while they decreased by about 25% for the lower fuel/oxygen equivalence ratio and by about 20% for the higher fuel/oxygen ratio, as the temperature was increased from 1500 K to 1750 K.

6.6 Contribution of Volatile-Nitrogen and Char-Nitrogen to Nitric Oxide

In order to identify the individual contribution of char-nitrogen and volatile-nitrogen to the total NO_x emission, the experiments were

designed, as indicated in previous sections, in such a way that overall

contribution of coal and contribution of char, produced by pyrolysis

of the coal at the temperature and residence time corresponding to those

of the oxidation experiments, were obtained directly. Then the volatile-

nitrogen contribution could be obtained by subtracting the char-nitrogen

contribution to NO_x from overall coal-nitrogen contribution. Figure 6.2

shows the conversion to NO_x of lignite at 1250 K and Figure 6.4 shows

the conversion to NO_x of 1250 K lignite char at 1250 K. Therefore, the

data from Figures 6.2 and 6.4 can be used to estimate the fraction of

the NO_x emissions that are contributed by the volatiles and char for a

pulverized coal combustion system at 1250 K. In the same manner, the

contribution to NO_x of volatiles and char at furnace temperature of

1750 K can be estimated by manipulating the data from Figures 6.3 and

6.5.

A simplified scheme that represents the fate of the fuel nitrogen

during combustion of coal has been suggested previously (Pohl, 1976;

Pohl and Sarofim, 1976 and Song, Beér and Sarofim, 1977), and is

summarized on the next page:
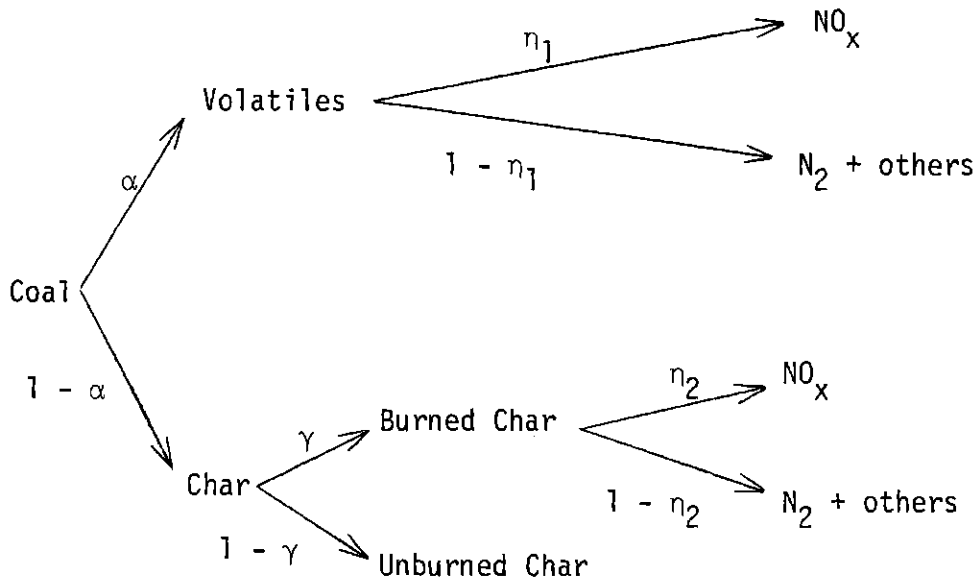
By a first order approximation which assumes that the volatile-nitrogen conversion to NO_x and char-nitrogen conversion to NO_x are independent, the overall conversion, η^*, of coal-nitrogen to NO_x is then given by:

$$\underset{\substack{\text{overall} \\ \text{conversion} \\ \text{to } NO_x}}{\eta^*} = \underset{\substack{\text{volatile} \\ \text{contribution}}}{\alpha\eta_1} + \underset{\substack{\text{char} \\ \text{contribution}}}{(1 - \alpha)\gamma\eta_2}$$

where

α = fraction of the coal-nitrogen that is released as volatiles

$1-\alpha$ = fraction of the coal-nitrogen that is retained in the char

γ = fraction of the char-nitrogen that is consumed

$\gamma\eta_2$ = fraction of the char-nitrogen that is converted to NO_x

η_1 = fraction of the volatile-nitrogen that is converted to NO_x

η^* = overall conversion of coal-nitrogen to NO_x

The values of $(1-\alpha)$ have been found to be 0.75 at a temperature of 1250 K and 0.27 at 1750 K (see Section 6.3). The values of η^* were reported as functions of fuel/oxygen equivalence ratio in Figures 6.2 and 6.3 for 1250 K and 1750 K, respectively, and the values of $\gamma\eta_2$ in Figures 6.4 and 6.5. The values of η_1, the efficiency of conversion to NO_x of the volatile-nitrogen, and $\frac{\alpha\eta_1}{\eta^*}$, the percentage of the total NO_x contributed by volatile-nitrogen have been derived from the above information for temperatures of 1750 K and 1250 K and are reported in Figure 6.7. The efficiency of conversion to NO_x of volatile-nitrogen (bottom diagram of Figure 6.7) and the contribution to the total emissions of the volatile-nitrogen (top diagram of Figure 6.7) were found to decrease monotonically with increasing fuel/oxygen equivalence ratios. As fuel/oxygen equivalence ratio increased from 0.2 to 2, the contribution to the total NO_x by the volatile-nitrogen decreased from about 80% to 40% at 1750 K, and from about 50% to 10% at 1250 K. As expected, the contribution to NO_x by the volatiles increased with temperatures. The conversion to NO_x of the volatile-nitrogen, however, decreased with increasing temperature. These two effects tend to compensate and partially explain the small dependence on temperature of the conversion to NO_x of coal-nitrogen. In this study, a small net decrease was observed (see Section 6.5). In an independent study, Pershing (1976) has found practically no effect of temperature on the conversion of coal-nitrogen to NO_x.
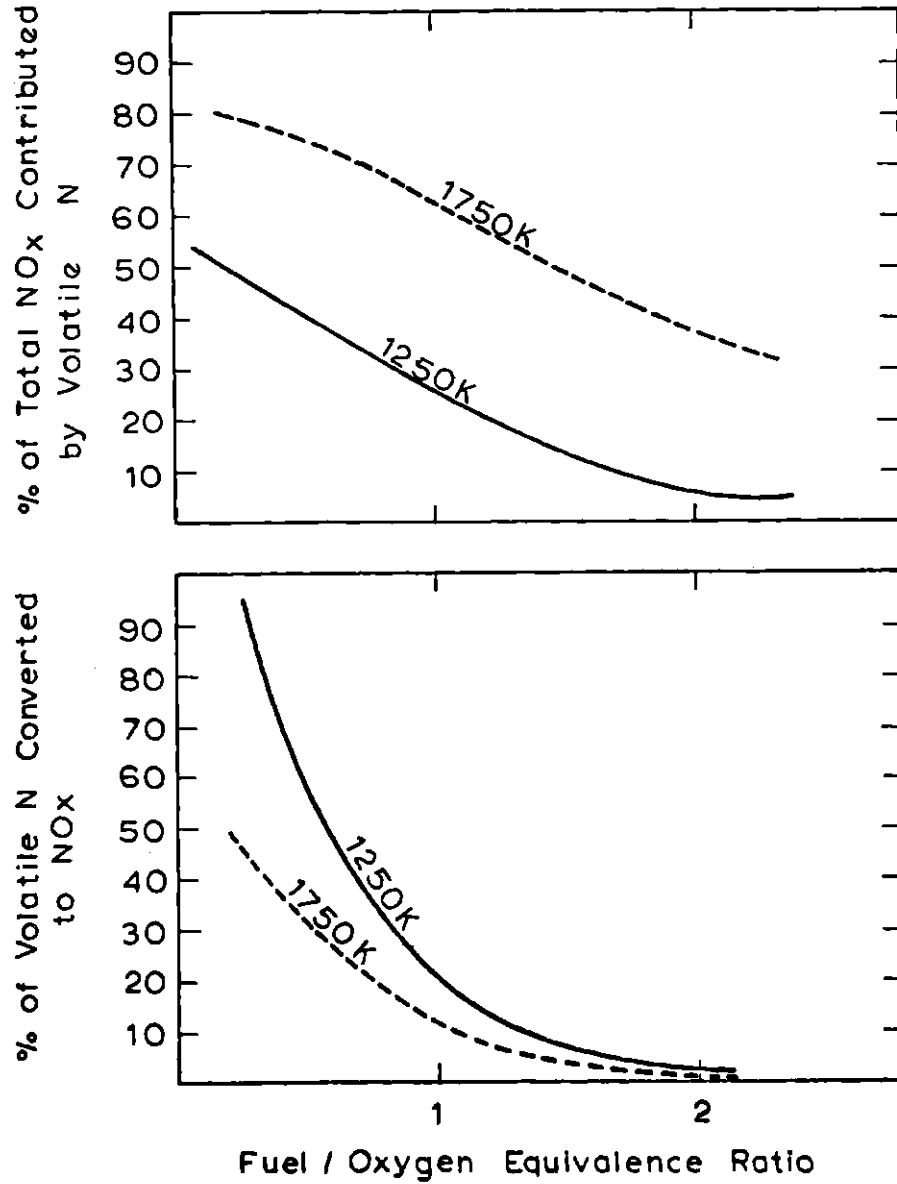
Figure 6.7

Fate of Volatile Nitrogen During Oxidation: Total Nitric Oxide Contributed by Volatiles (Top); Conversion Efficiency of Volatiles to Nitric Oxide (Bottom).

We shall address the analogy between the combustion of coal-volatiles and the ordinary gaseous flames in Chapter 7. Nevertheless it is of interest to note here that our results of volatile combustion are in good agreement with the generalizations derived from studies on idealized laboratory flame systems (Fenimore, 1972; Sarofim, Williams, Modell and Slater, 1975; etc.). Our results showed that the volatile-nitrogen conversion efficiency decreased with increases in fuel/oxygen equivalence ratio. This result is in general agreement with those reported in flame studies. We have demonstrated that the volatile-nitrogen conversion to NO_x decreased as the temperature increased. This is because the volatile phase has a higher volatile-nitrogen concentration at higher temperature for any given fuel/oxygen equivalence ratio, and this in turn results in a lower conversion to NO_x which is consistent with flame studies that show that the conversion of fuel-nitrogen to NO_x decreases with increases in concentration of fuel-nitrogen.

6.7 Practical Implications

Nitric oxide produced by the oxidation of bound nitrogen in coal is a consequence of the oxidation of both nitrogenous compounds evolved with coal volatiles and nitrogen retained by char residue. The interactions between the devolatilization and oxidation steps in pulverized coal combustion complicate the development of NO_x control strategy. For any given temperature, the conversion efficiency to NO_x by volatile-nitrogen is usually higher than the conversion efficiency by char-nitrogen. This is very distinctly demonstrated especially at fuel lean conditions. With increasing temperature, the extent of

coal-nitrogen devolatilization increases but the conversion of the volatile-nitrogen to NO_x decreases. These two effects tend to compensate each other and partially lead to the small dependence on temperature of the total coal-nitrogen conversion to NO_x. Although the results from this study revealed that the total NO_x yields were decreased by about 20% as the furnace temperature was increased from 1500 to 1750 K, it is evident that the combustion modication by changing temperature alone does not have a very significant effect on the total NO_x emissions.

The conversion of fuel-bound nitrogen is most strongly dependent upon oxygen availability. Our results have shown that the conversion efficiencies to NO_x of both volatile-nitrogen and char-nitrogen decreased very significantly with increasing fuel/oxygen equivalence ratio. Our results have suggested that the reduction of NO_x emissions from pulverized coal combustors can be accomplished by modications of combustion processes by varying the fuel/oxygen equivalence ratio and temperature at different stages of the combustion process. It is optimal to operate the first stage of a combustor at high temperature and fuel-rich conditions to favor the completion of the devolatilization. The residual char with little nitrogen content (the nitrogen content of residual char depends on the extent of nitrogen-devolatilization at first stage) is then transported to the second stage of the combustor to complete the combustion at relatively fuel lean conditions and low temperature. In this manner, a staged pulverized coal combustor will significantly reduce the NO_x emissions while maintaining a high combustion efficiency.

6.8 Conclusions

Montana lignite was burned in 21% oxygen in helium mixture at
furnace temperatures of 1250 K and 1750 K. It has been found that the
conversion of coal-nitrogen to NO_x decreased monotonically with fuel/
oxygen equivalence ratios. Oxidation experiments were also carried out
on char in order to identify the separate contributions to NO_x emission
of the volatiles and char. The char used in the oxidation studies was
prepared by pyrolysis of coal at the temperature and residence time
corresponding to those of oxidation experiments. The conversion to NO_x
of char-nitrogen was also found to follow a trend similar to that
observed for oxidation of raw coal. However, the char-nitrogen
conversion to NO_x was lower than the corresponding values for the coal-
nitrogen.

Volatile-nitrogen contribution and char-nitrogen contribution were
obtained by a first order approximation which assumed that the volatile-
nitrogen conversion to NO_x and char-nitrogen conversion were independent.
It was found that volatilized nitrogen compounds accounted for a major
fraction of NO_x produced from coal-nitrogen especially at high
temperatures and low fuel/oxygen equivalence ratios. Nevertheless,
the char-nitrogen contribution could not be neglected particularly at
high fuel/oxygen equivalence ratios and low temperatures. Increasing
temperature increased the volatile contribution but decreased the
efficiency with which it was converted to NO_x. These two effects tended
to compensate each other and partially explained the small dependence
on temperature of the conversion of coal-nitrogen. For the combustor

in this study, there was a net decrease in emissions with increases in temperature above 1500 K, suggesting that NO_x emissions could be reduced by increases in both the temperature and the fuel/oxygen equivalence ratio in the first stage of a staged combustor.

CHAPTER 7

KINETIC STUDY I. FORMATION OF
NITRIC OXIDE DURING COAL CHAR COMBUSTION

7.1 Introduction

In Chapter 6 we examined the conversion of coal-nitrogen to NO_x and identified the separate contribution of char-nitrogen and volatile-nitrogen to total NO_x emissions. We also determined the effects of both the fuel/oxygen equivalence ratio and the temperature on NO_x emissions. The question arises, however, of what the reaction mechanism of the coal-nitrogen conversion to NO_x is.

An approach to this problem might be through a close examination of the coal combustion processes. The combustion of pulverized coal particles can be imaged to occur in three main stages: a stage of evolution of the volatile components, or devolatilization, followed by the homogeneous volatile combustion and then finally the heterogeneous combustion of residual char. Although the stages may overlap to some degree (Howard and Essenhigh 1967a, 1967b), it is clear the char combustion is generally of much longer duration. Based on the above information, the conversion of coal-nitrogen to NO_x can, therefore, also be regarded as a three-stage process: coal-nitrogen devolatilization, volatile-nitrogen combustion and char-nitrogen combustion.

We shall discuss coal-nitrogen devolatilization in Section 7.1.1, volatile-nitrogen combustion in Section 7.1.2 and char-nitrogen combustion in the sections follow.

7.1.1 Coal-Nitrogen Devolatilization

The control of the nitrogen evolution provides one method of controlling total NO_x emissions. The mechanism and rates of nitrogen devolatilization from coal have been extensively studied by Pohl (1976). The pyrolysis of the nitrogen content of coal was studied by rapidly heating dispersed pulverized particles of Montana lignite and Pittsburgh bituminous coal to temperatures of 1000 and 2100 K. This study provides the most complete information on the kinetics of coal-nitrogen devolatilization.

Time resolved measurements of the nitrogen retention from Pohl's studies are presented in Figure 7.1. The data at times up to 300 milliseconds were obtained using the fast flow furnace and the data at one second were obtained in the drop tube furnace. Evolution of the nitrogen from coal was kinetically controlled for conditions encountered in typical pulverized coal flames. The early stages of pyrolysis of the two coals studied can be empirically correlated by a psuedo-first order rate constant with the value

$$k = 9.3 \times 10^3 \cdot \exp\ (-22,700/RT)\ \sec^{-1}$$

Correlation between nitrogen retention and solid weight loss (dry-ash-free) was also obtained and is shown in Figure 7.2. A linear correlation was found between fractional total solid weight loss and fractional nitrogen loss for the two coals studied. Nitrogen evolution paralleled that of the total volatiles with the notable exception that little nitrogen was released until 10 to 15% of the coal had been

RETENTION OF NITROGEN IN PYROLIZED CHARS
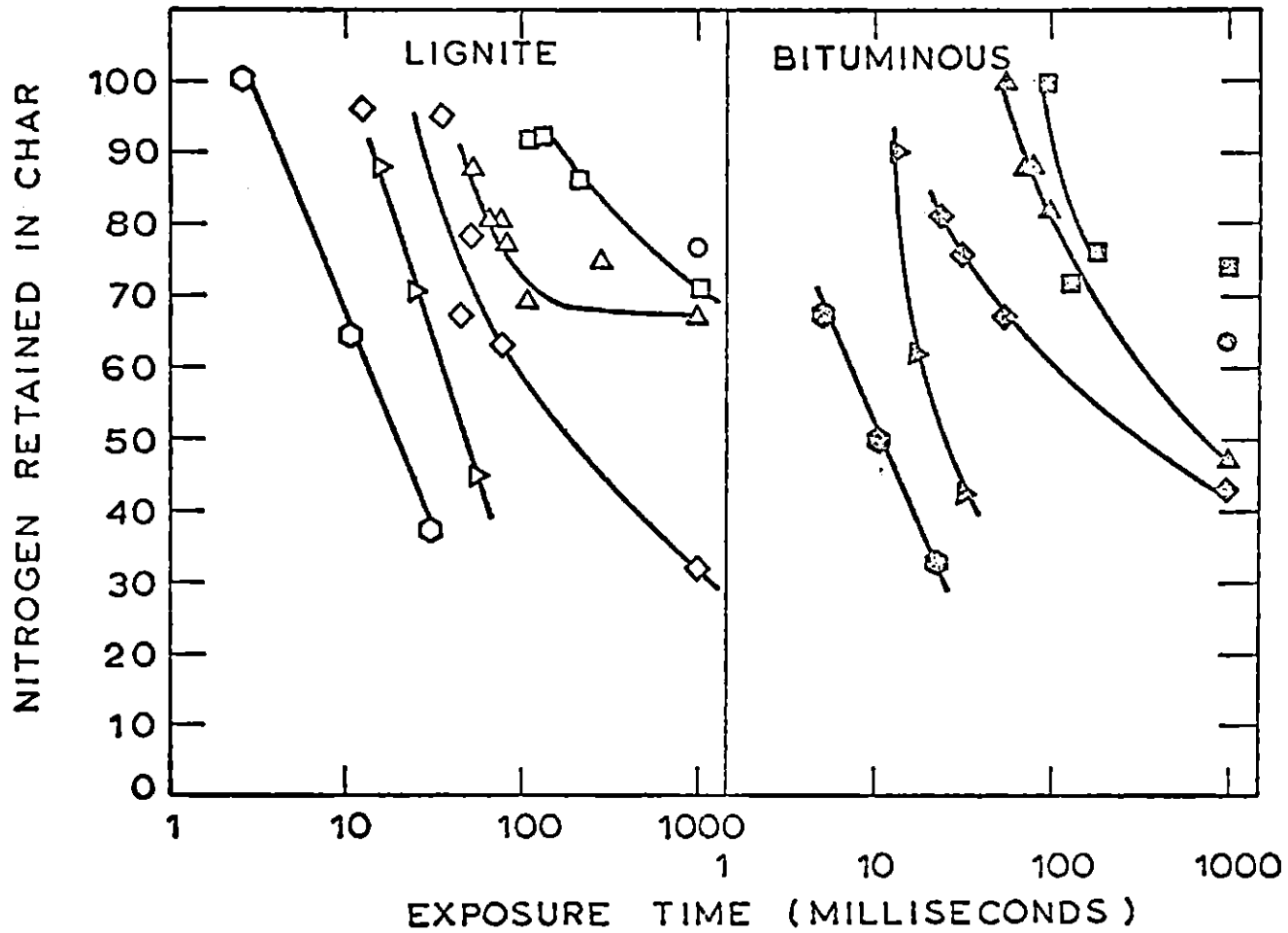
Figure 7.1

Retention of Nitrogen in Devolatilized Lignite and Bituminous Coal Chars (Pohl, 1976)

NITROGEN LOSS vs WEIGHT LOSS
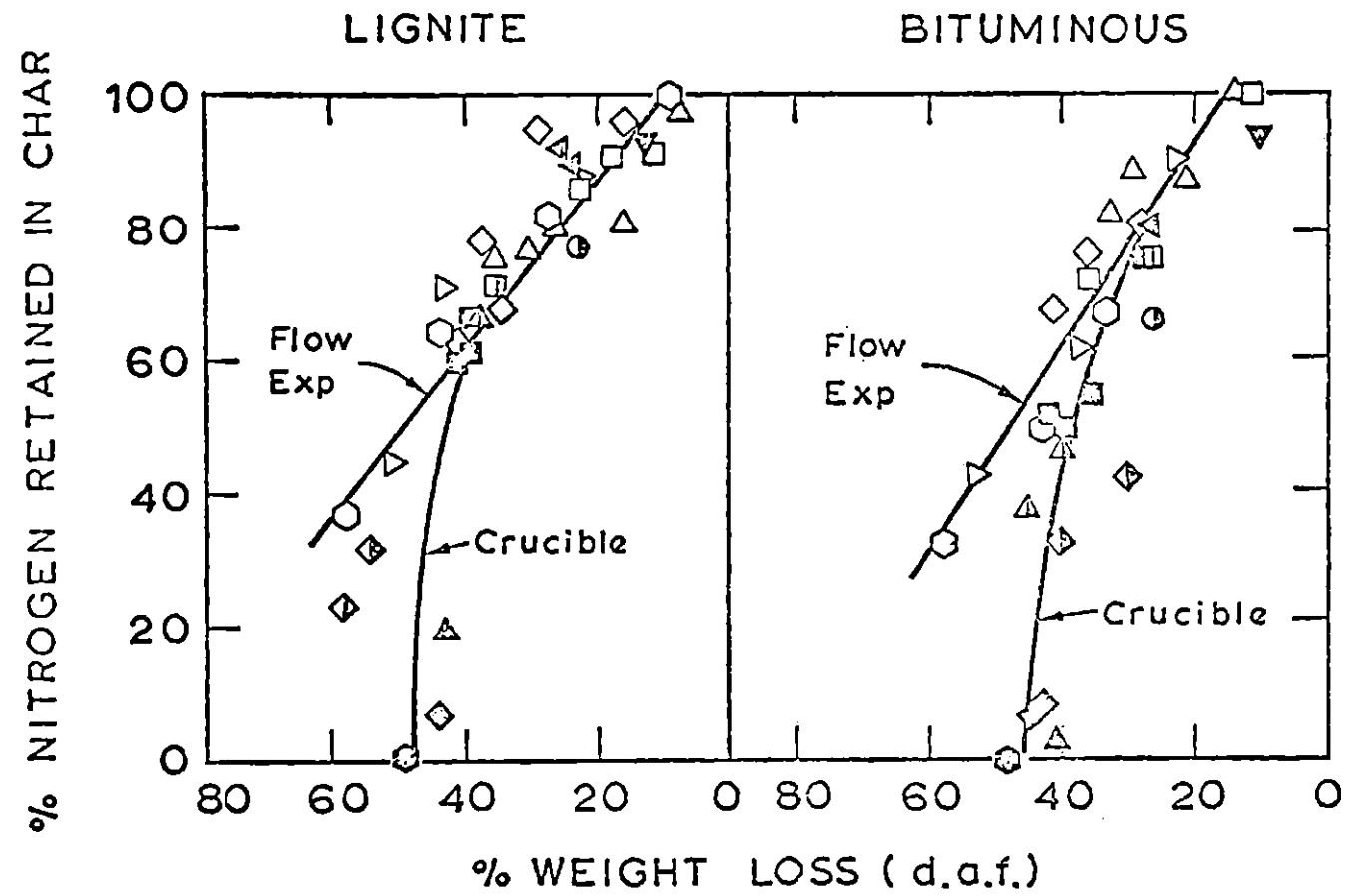
Figure 7.2

Correlation Between Nitrogen Loss and Total Weight Loss During Pyrolysis of Coal (Pohl, 1976)

devolatilized. After the initial delay, the nitrogen loss became more rapid than total weight loss. The slope of the nitrogen loss versus total weight loss was 1.25 for the lignite and 1.50 for the bituminous coal studied. This correlation, if it is found to have general validity provides a base for evaluating the kinetics of nitrogen evolution from that of the more readily determined total volatile evolution.

Another important feature from Pohl's studies is the asymptotic behavior of devolatilization. Measurements were made of the various elements retained in char produced by heating samples of coal in crucibles until the weight approached a constant value. Heating times varied from 20 minutes at 2100 K to 12 hours at 600 K. The results from the lignite samples held in crucibles are summarized in Figure 7.3. When coal was slowly heated in crucibles to different temperatures, most of the volatile matter evolution occured at temperatures below that of the ASTM Proximate Analysis test (1023 K) whereas most of the nitrogen was evolved at higher temperatures. Although carbon formed a stable compound in char, no comparable stabilized nitrogen structures were formed, consequently, nitrogen could continue to be released until it was completely eliminated from char.

7.1.2 Volatile-Nitrogen Combustion

As soon as the volatiles are released from the coal, they will counter-diffuse and mix with the air. The temperature in this study generally exceeded the spontaneous ignition value, and therefore the volatiles are expected to burn in a mode that is governed by the rate
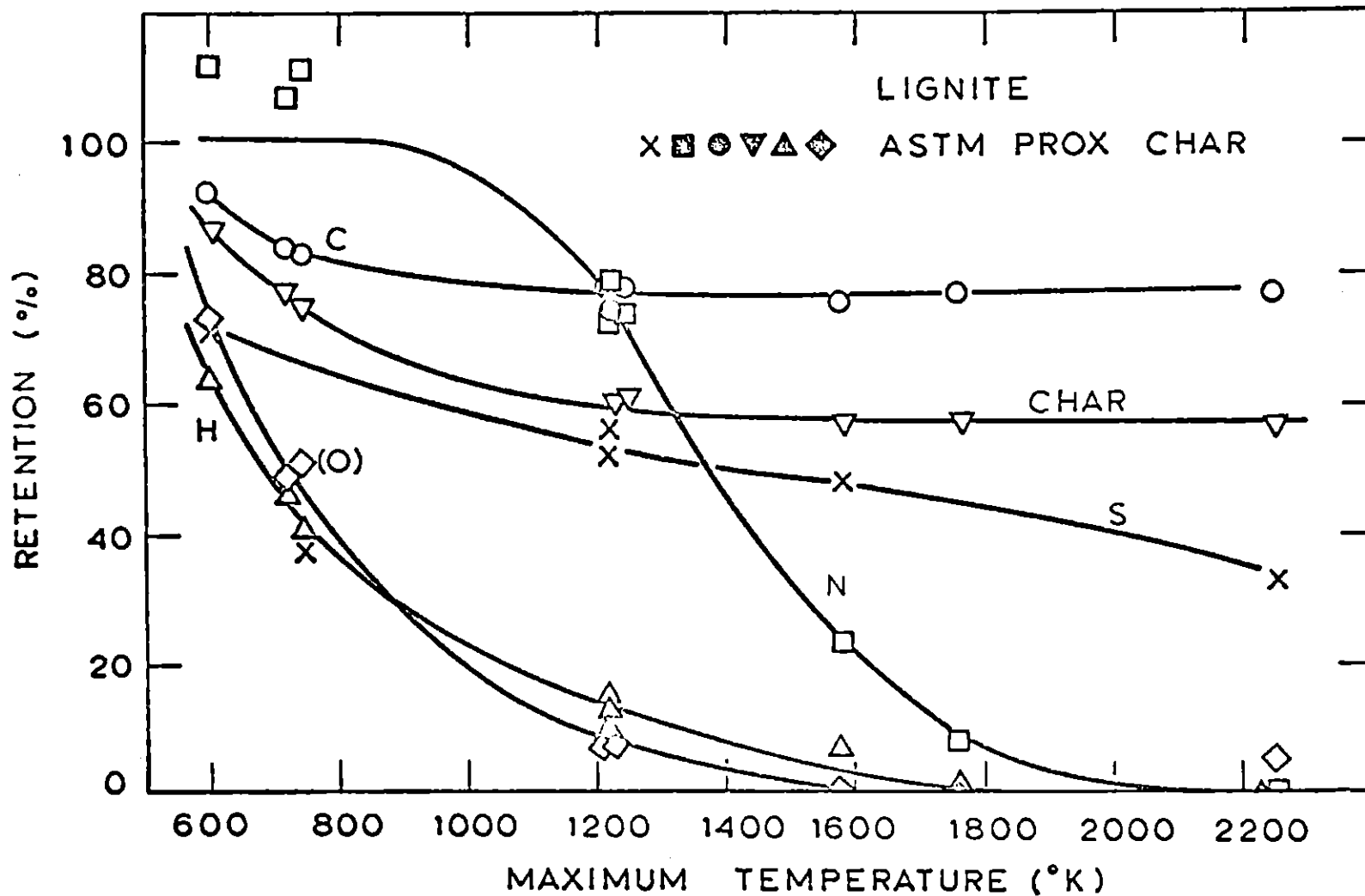
Figure 7.3

Asymptotic Retentions of Elements in Char in Crucible Experiment, Montana Lignite (Pohl, 1976)

of release of volatiles. At very high rates of release, a detached

diffusion flame will be produced. At low rates of volatile evolution,

the volatiles will be consumed at the particle surface simultaneously

with the char. Under certain conditions volatiles may premix with the

char to yield a mixture outside the flamability limits and then ignition

will be delayed until the composition of the mixture is brought into

the flammable range by further mixing with volatiles or oxygen.

It is apparent that the processes that occur during the combustion

of coal volatiles are analogous to those occuring in gaseous flames.

Therefore, the data that have been obtained by the addition of model

nitrogen compounds to laboratory premixed or diffusion flames are per-

tinent to the understanding of the oxidation of volatile-nitrogen.

The earliest flame study performed by Shaw and Thomas (1965) is

only historically significant and the data must be reinterpretated to

include in the fuel equivalence ratio the amount of oxygen necessary

to burn the nitrogen additive. Subsequent studies by Fenimore (1971, 1972)

De Soete (1972) and Sarofim, Williams, Modell and Slater (1975) have

reached the following conclusions:

1. The conversion of fuel-nitrogen to NO_x is close to unity
   under fuel lean conditions but decreases dramatically
   under fuel rich conditions.

2. An increase in fuel nitrogen concentration results in an
   increase in total NO_x emissions but a decrease in the
   conversion efficiency to NO_x.

3. The conversion increases only slightly with increasing
   flame temperature.

These conclusions, derived from studies on idealized laboratory systems, are also supported by the results obtained on practical industrial combustion systems (Martin and Berkau, 1972; Turner et al., 1972; and Bartok et al., 1972).

The flame study of nitrogen compound has been a widely studied topic in the past and at present there exists a large amount of information in the literature. Since it is not within the scope of this study, no further discussion will be presented.

7.1.3 Char-Nitrogen Combustion

This section is concerned with the kinetics of char-nitrogen oxidation.

We have addressed, in Chapter 6, the problem of combustion process modification by staged combustion for reducing NO_x emission. The results of parametric investigations discussed in Chapter 6 suggested that it was optimal to operate the first stage of a combustor at high temperature and under fuel-rich conditions. In staged combustion, the addition of oxygen required to complete the coal combustion is delayed until after much of fuel nitrogen has reacted, thus it involves char burnout in the late stage of the combustion (Pershing et al., 1975; Armento et al., 1975). Char combustion has recently been identified by a number of investigators as a potentially high source of NO_x emission and thus can not be ignored (Wendt et al., 1974; Pohl, 1976). The contribution to NO_x emission by the nitrogen in the char increases with decreasing combustion temperature and with increasing fuel/oxygen equivalence ratio (see Chapter 6) and complicates the development of

control strategies.

Since the char structure is porous, both internal and external combustion would occur (Anson et al., 1971). In addition to chemical reactions, external gas film and ash layer diffusion and internal pore diffusion may sometimes also play important roles in the combustion process (Mulcahy and Smith, 1969). It is therefore, important to identify the control regimes of the char burnout process in order to obtain the intrinsic kinetics.

In considering the kinetics of char-nitrogen combustion, a pressing problem is to supply a quantitative answer to the question: "During char combustion, are both nitrogen and carbon in char equally vulnerable to the attack by oxygen?" More specifically, the selectivity of oxygen attacking nitrogen and carbon in a char particle has to be considered.

So far, all our considerations have been focussed on the formation of NO_x during the combustion of coal char. There exist, however, also processes which lead to the partial or total reduction of NO_x. Recently, in an experimental effort to investigate the NO_x emissions from char and volatiles, Gibbs, Pereira and Beér (1976) observed a reaction between NO_x and char during the combustion of coal in a fluidized bed. Although the char was known to react easily with NO_x in the absence of oxygen (Edwards, 1972), it was not expected that the same reaction would occur under oxidizing conditions. The reduction of NO_x by char which may begin soon after NO_x is formed within a pore may reduce a significant fraction of the NO_x formed before it entirely diffuses out of the porous

char structure. Another destruction reaction to be considered is the reaction between NO_x and CO. The homogeneous reaction between NO_x and CO is probably not very important. However, this reaction may be significantly enhanced if it is heterogeneously catalyzed by char.

In view of all the above consideration, the formation and destruction of NO_x during the combustion of coal char can be summarized as follows.

$$Char(C,N) \xrightarrow{\text{oxidation}} CO + NO$$

$$2 \; NO + Char \longrightarrow N_2 + 2 \; CO$$

$$2 \; NO + 2 \; CO \xrightarrow{\text{Char}} N_2 + 2 \; CO_2$$
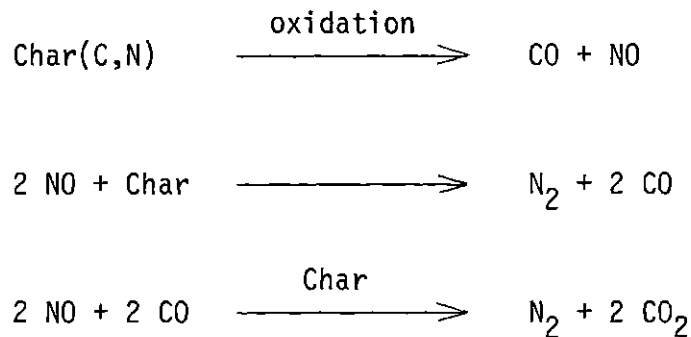
In this chapter we shall deal in detail with the kinetics of oxygen/char reaction. In Chapter 8 we shall consider NO/char reaction. Finally, since the NO/CO reaction is not within the scope of this thesis work, it is recommended for further investigations.

7.2 Scope and Objectives

For the kinetic study of the formation of NO_x during coal char combustion, the goals are:

1. To evaluate the effects of external and pore diffusion processes in order to obtain the intrinsic kinetics of char/oxygen reaction.

2. To study the selectivity of oxygen attacking nitrogen and carbon in a char particle.

3. To determine experimentally the kinetics parameters for char-nitrogen oxidation.

The char used for this study was produced by the pyrolysis of Montana lignite particles at a temperature of 1750 K for a residence time of one second. The char was purposely produced at this temperature and residence time because:

i. the char so produced has reached asymptotic solid weight loss (about 59% d.a.f.) due to pyrolysis. Therefore, when this char is subjected to oxidation at the same or lower temperatures and shorter residence times, there will be very little volatile loss.

ii. the char so produced retains a significant portion of the nitrogen from the original coal (about 27% of the original nitrogen content), to permit char-nitrogen oxidation studies.

The char so produced was designated 1750 K lignite char. Its characterizations are given in Tables 5.2 and 5.3.

7.3 Results

Time-resolved weight loss measurements of char during oxidation were made by the rapid quenching of samples taken at different distances from the char injector according to the procedures described in Chapter 5. The oxidant stream of oxygen in helium was supplied through a honeycomb gas straightener at a rate sufficiently fast to

prevent significant depletion of the oxygen during reaction. Oxidation experiments were carried out at temperatures of 1250 K, 1500 K, and 1750 K and oxygen partial pressures of 0.2 atm and 0.4 atm.

Time-resolved weight loss measurements are tabulated in Appendix B. Figure 7.4 summarizes these results in a semi-logarithmic plot of Char Retention versus Reaction Time. The time history of the retention at a temperature of 1250 K and oxygen partial pressure of 0.2 atm was a straight line. When the temperature and/or oxygen partial pressure increased, the retention appeared to level off after the retention became less than about 55%. Since the slopes of this semi-logarithmic plot represent the reaction rate per unit mass of char, the "leveling-off" phenomenon indicated the decrease of reactivity of char with the extent of burnout. This phenomenon will be discussed in detail in Section 7.7. Broken straight lines were drawn for the entire range of the data of 0.4 atm at both 1500 K and 1750 K to indicate some uncertainties on the initial rate.

Selected char samples were further analyzed to determine both physical characteristics (B.E.T. surface area, average pore size, etc.) and chemical compositions (ash, carbon, hydrogen, sulfur, and nitrogen content). These results are summarized in Appendix B. The specific B.E.T. surface area and average pore diameter of solid products were measured as a function of percent char burnout (d.a.f.). Figure 7.5 shows the behaviors of the normalized specific B.E.T. surface area and the normalized average pore diameter. (They were normalized against the initial properties of the original char). Up to approximately 45 percent char burnout, the specific B.E.T. surface area increased
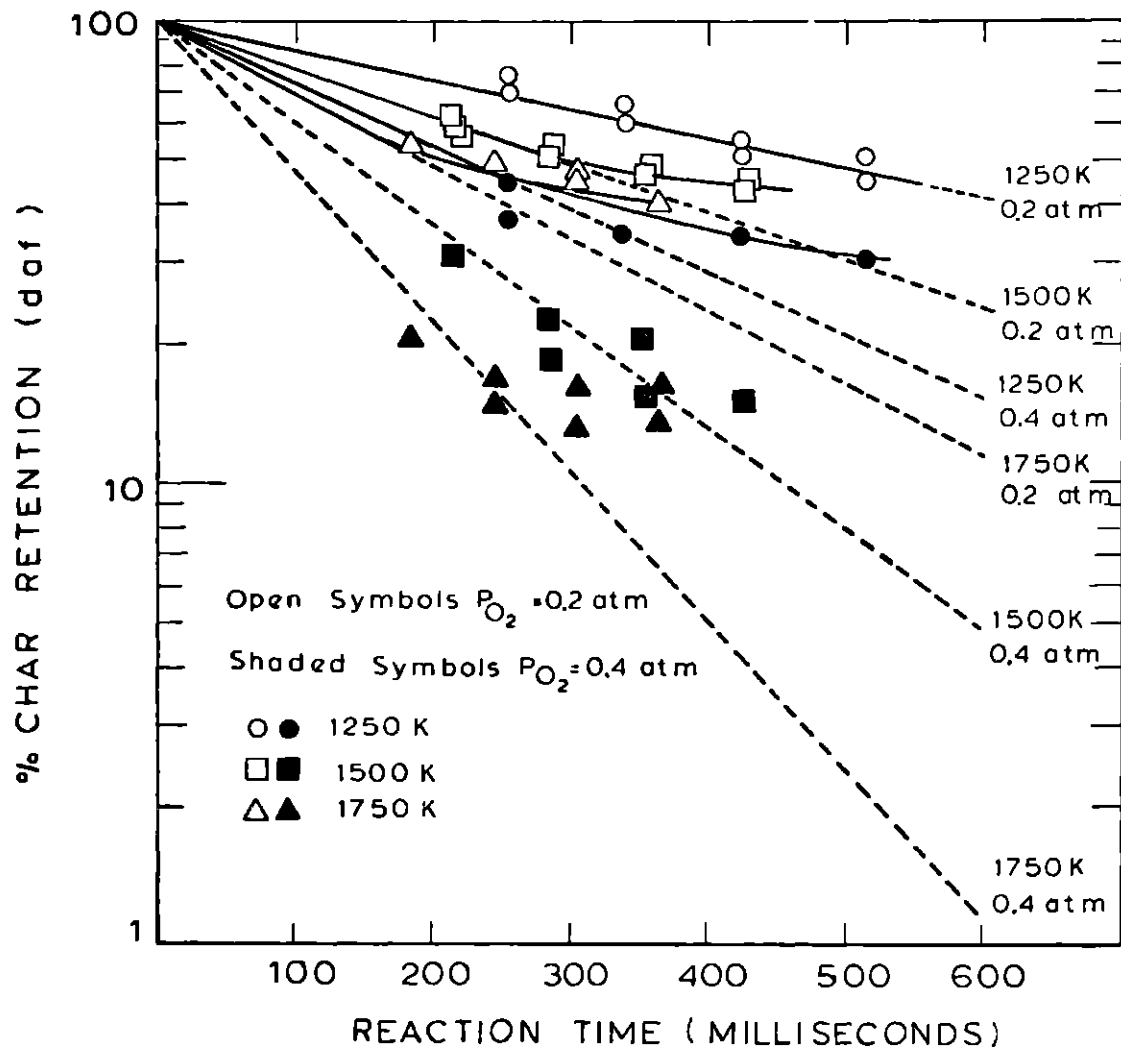
Figure 7.4

Retention of Char as Function of Reaction Time During Oxidation
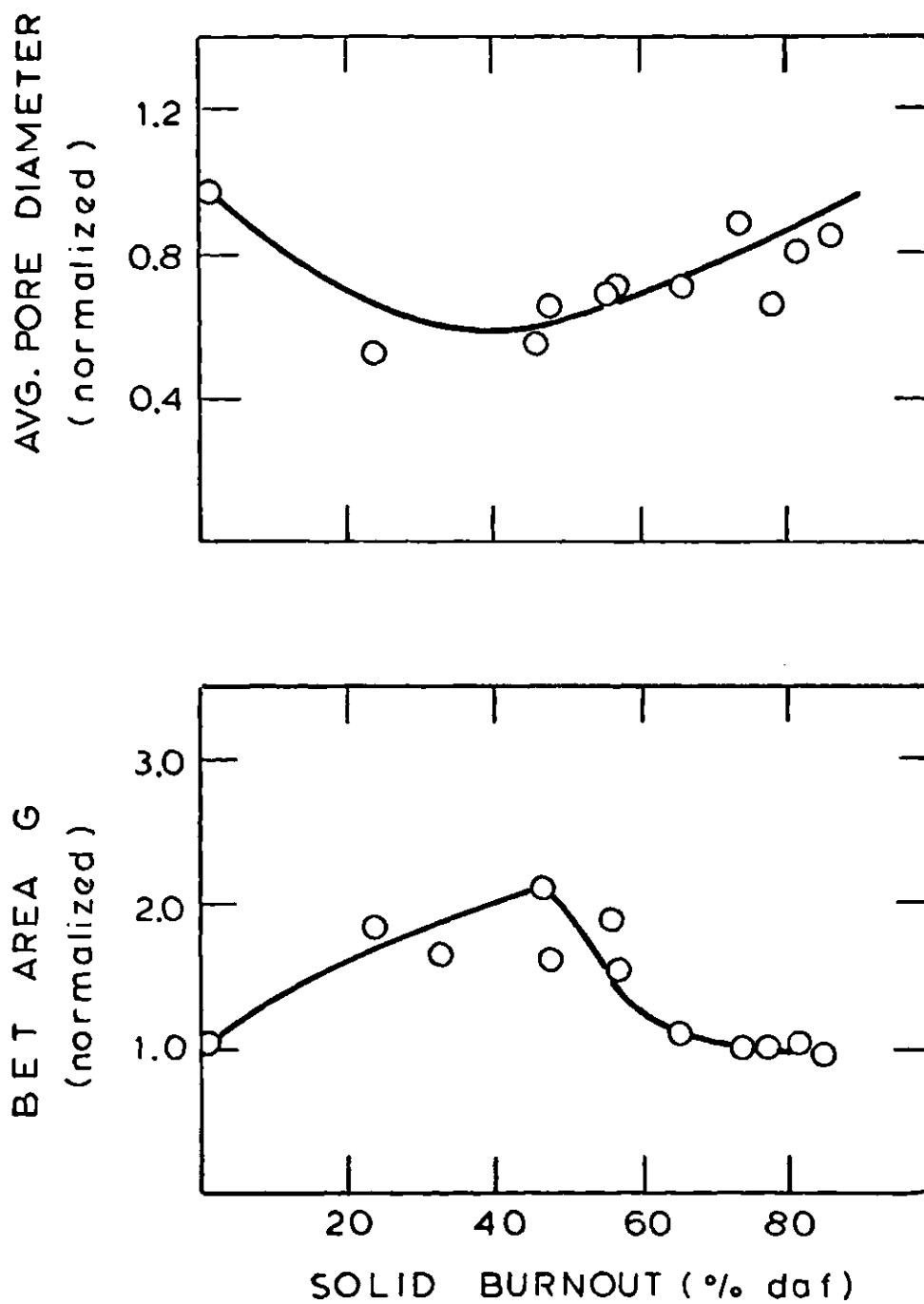
Figure 7.5

Average Pore Diameter and Specific B.E.T. Surface Area as Functions of

Solid Burnout During Char Oxidation

and the average pore diameter decreased, implying the opening-up of small pores in the initial stages of combustion. In the latter stages, the char burned both externally and internally at approximately constant diameter until, at an advanced stage, it fragmented as has been observed previously (Anson, Moles and Street, 1971). This is corroborated by our data showing decreasing specific B.E.T. surface area and increasing average pore diameter in the latter half of the burnout process, which can be interpreted in terms of the destruction of the micropores.

The variation of nitrogen to carbon ratio was also obtained as a function of reaction time. This is shown in Figure 7.6, where the nitrogen/carbon ratio is expressed in terms of the percentage of the original nitrogen/carbon ratio in the 1750 K lignite char. For the temperatures of 1250 K and 1500 K, data for both oxygen partial pressures of 0.2 atm and 0.4 atm were included in the figure. For 1750 K, only data for an oxygen partial pressure of 0.2 atm were reported.

As can be seen, little difference is apparent in the nitrogen to carbon ratio obtained at the two oxygen partial pressures studied at both 1250 K and 1500 K. The time history of this nitrogen to carbon ratio was found to be linear, for any given temperature, on this semi-logarithmic plot. At 1250 K and for both 0.2 atm and 0.4 atm oxygen partial pressures, the nitrogen/carbon ratio remained very close to its initial value; however, the ratio was found to decrease with increasing temperature. As can be seen in Figure 7.6, for a reaction time of 500 milliseconds, the nitrogen/carbon ratio remained at about 97% of the original ratio at 1250 K. It decreased to about 78% at 1500 K and dropped to about 43% at 1750 K.
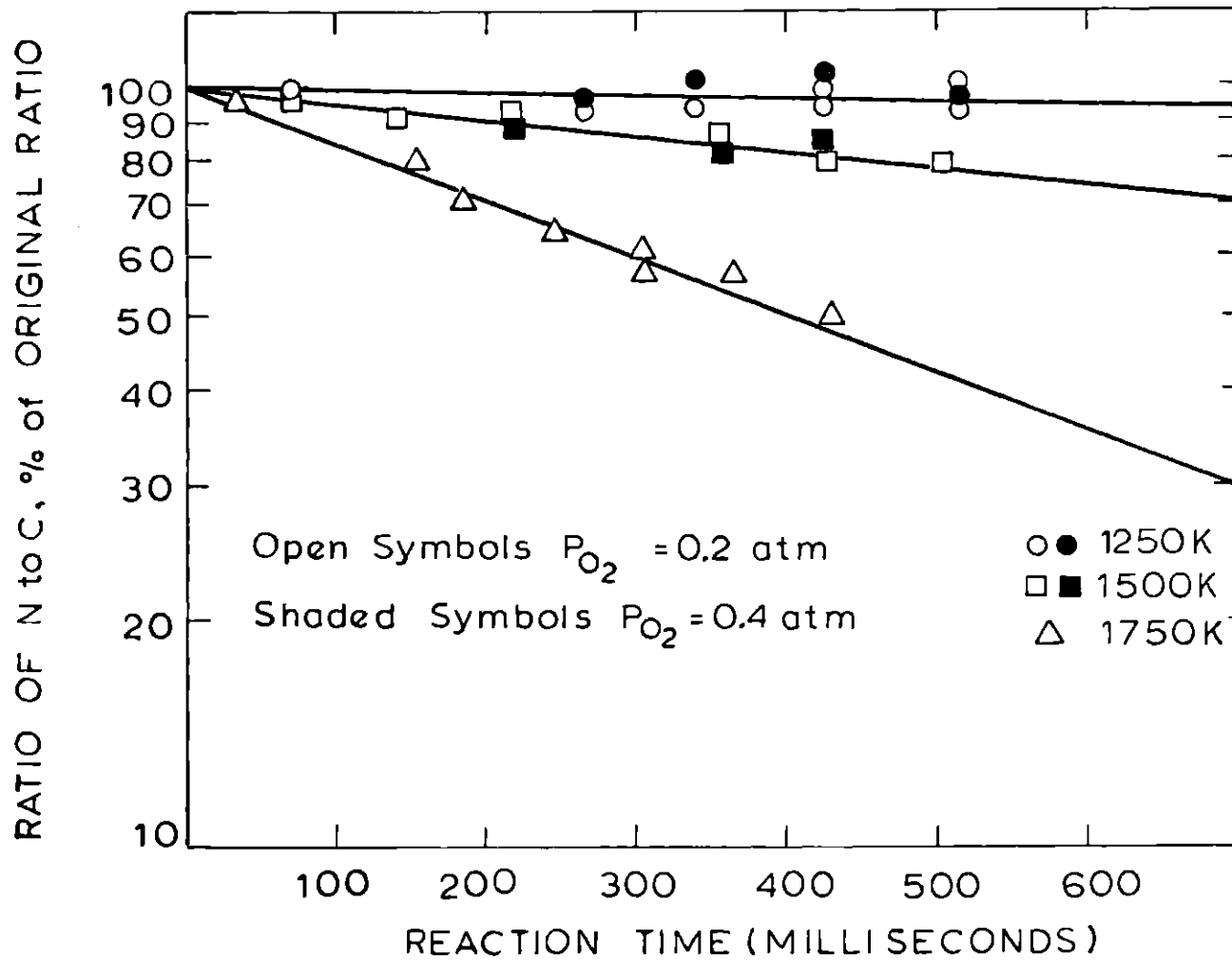
Figure 7.6

Ratio of Nitrogen to Carbon as Function of Reaction Time During Char Oxidation

7.4 Apparent Kinetics of Char/Oxygen Reaction*

Curves in Figure 7.4 show the time history of solid char retention in char/oxygen experiments. As indicated in the last section, the "leveling-off" phenomenon was observed, implying a decrease in reactivity of the char in the late stages of burnout. As a first attempt to determine the apparent kinetics, the initial rates of reaction will be used by measuring the initial slopes of these curves. We shall address the problem of the change in reactivity of char later in Section 7.7.

7.4.1 Initial Rates

Figure 7.4 provides the time history of solid retention in a semi-logarithmic plot. The slope of a tangent to any curve at any time in Figure 7.4 is therefore:

$$\text{slope} = \frac{d(\ln Z)}{dt} = \frac{1}{W}\frac{dW}{dt} \qquad (7.1)$$

where

Z = % char retention, d.a.f.

W = mass of the char

$\frac{dW}{dt}$ = consumption rate of char

Since the slope represents the reaction per unit mass of char, the initial rate can be calculated by determining the initial slope of the tangent to the curve. The initial rate of reaction can also

---

*The calculation approach in Sections 7.4 and 7.5 are analogous to the one used by Mandel (1977).

be expressed in various forms for the convenience of different calculations as follows.

Per unit particle,

$$R_p = -\frac{4\pi}{3} r_s^3 \, \rho_B \, \frac{1}{M_C} \frac{d(\ln Z)}{dt} \tag{7.2}$$

Per unit specific B.E.T. surface area,

$$R_B = -\frac{1}{M_C} \frac{1}{A_B} \frac{d(\ln Z)}{dt} \tag{7.3}$$

Per unit external surface area,

$$R_E = -\frac{1}{3} r_s \, \rho_B \, \frac{1}{M_C} \frac{d(\ln Z)}{dt} \tag{7.4}$$

where

R_p = char oxidation rate per particle

R_B = char oxidation rate per unit B.E.T. surface area

R_E = char oxidation rate per unit external surface area

r_s = radius of particle

ρ_B = bulk density of char

M_C = molecular weight of carbon

A_B = specific B.E.T. surface area of char

Values for r_s, ρ_B and A_B are given in Table 5.3.

Table 7.1 summarizes the initial rates of reaction in term of Equations (7.2), (7.3) and (7.4) for different experimental conditions.

TABLE 7.1

INITIAL RATES OF REACTION FOR CHAR/OXYGEN EXPERIMENTS

P_{O_2}	T_F	dZ/dt	R_P	R_B	R_E
atm	K	sec^{-1}	$\dfrac{g\text{-moles}}{sec \cdot particle}$	$\dfrac{g\text{-moles}}{sec \cdot cm^2}$	$\dfrac{g\text{-moles}}{sec \cdot cm^2}$
0.2	1250	-1.460	2.941×10^{-9}	1.049×10^{-7}	1.041×10^{-4}
0.2	1500	-2.372	4.780×10^{-9}	1.704×10^{-7}	1.691×10^{-4}
0.2	1750	-3.596	7.245×10^{-9}	2.583×10^{-7}	2.563×10^{-4}
0.4	1250	-3.090	6.225×10^{-9}	2.220×10^{-7}	2.203×10^{-4}
0.4	1500	-5.009	1.009×10^{-8}	3.599×10^{-7}	3.570×10^{-4}
0.4	1750	-7.513	1.513×10^{-8}	5.397×10^{-7}	5.355×10^{-4}

7.4.2 Approximate Particle Temperatures

No direct measurement was made on the particle temperature though it was our original intention to measure the particle temperature by two-color pyrometry. Fortunately, the particle temperature can be calculated to a certain degree of accuracy if it is known what the primary product of the reaction is (Ayling and Smith, 1972).

The rate of heat generation within a particle is given by

$$\dot{Q}_g = R_P \cdot \Delta H_r \qquad (7.5)$$

where

R_P = rate of reaction

ΔH_r = heat of reaction

The rate of heat loss by a particle is governed by the combined effects of the heat loss by convection and the heat loss by radiation:

$$\dot{Q}_1 = h_t A_E (T_P - T_F) + 4\sigma A_E T_{Avg}^3 (T_P - T_F) \qquad (7.6)$$

where

h_t = external heat transfer coefficient between the particle surface and the main gas

A_E = external surface area of the particle

σ = Stefan-Boltzmann constant

T_P = particle temperature

$$T_F = \text{main gas temperature}$$

$$T_{Avg} = (T_P + T_F)/2$$

At steady state,

$$\dot{Q}_g = -\dot{Q}_l \qquad (7.7)$$

Therefore, T_P can be solved by combining Equations (7.5) and (7.6):

$$T_P = T_F - \frac{R_p \cdot \Delta H_r}{A_E (h_t + 4\sigma T_{Avg}^3)} \qquad (7.8)$$

The value of ΔH_r in Equation (7.8) depends on whether CO or CO_2 is the primary product.

Ayling and Smith (1972) have developed a two-color radiation pyrometer to measure the particle surface temperature for their char burnout experiments. They found that the measured particle temperatures were in satisfactory agreement with what would be calculated if CO rather than CO_2 were the primary product based on their observed rates of reaction. On this basis, with the lack of direct particle temperature measurement and gas analyses, the primary product is assumed to be CO, and therefore, ΔH_r = -26.6 kcal/g-mole. (The value of ΔH_r will of course vary slightly with combustion temperature. However, the allowance for this small variation is not included in our analysis.)

To evaluate h_t, the following correlation for forced-convection heat transfer can be used (Bird, Stewart and Lightfoot, 1960):

$$Nu = \frac{h_t \cdot d_s}{\lambda_g} = 2 + 0.60 \cdot (Re)^{1/2} \cdot (Pr)^{1/3} \qquad (7.9)$$

Assuming $N_u \approx 2$, then

$$h_t = \lambda_g/r_s \qquad (7.10)$$

where

λ_g = thermal conductivity of the gas to be evaluated at

T_{Avg} (see Appendix G)

Therefore, Equation (7.8) becomes

$$T_p = T_F + \frac{26.6 \times 10^3 \cdot R_p}{4\pi \; r_s^2 \; (\lambda_g/r_s + 4\sigma \; T_{Avg}^3)} \qquad (7.11)$$

For given rates, T_p may be found by an iterative solution assuming values for T_{Avg}. Table 7.2 summarizes the particle temperatures using Equation (7.11) and the initial rates from Table 7.1.

7.4.3 Surface Oxygen Concentration

The most commonly used rate expression for a gas-solid system is a power law kinetic expression:

$$\begin{aligned} Rate &= f \; (temperature, \; composition) \\ &= k(T) \cdot C_s^{\;n} \\ &= k_0 \cdot exp \; (-E/RT) \cdot C_s^{\;n} \qquad (7.12) \end{aligned}$$

TABLE 7.2

APPROXIMATE PARTICLE TEMPERATURES FOR CHAR/OXYGEN EXPERIMENTS

P_{O_2}	T_F	λ_g	T_p
atm	K	$\dfrac{cal}{cm \cdot sec \cdot K}$	K
0.2	1250	7.53×10^{-4}	1255
0.2	1500	8.60×10^{-4}	1508
0.2	1750	9.65×10^{-4}	1760
0.4	1250	5.62×10^{-4}	1265
0.4	1500	6.33×10^{-4}	1522
0.4	1750	7.05×10^{-4}	1779

where C_s is gas concentration at the solid surface. Therefore, our next task is to evaluate the true value of the surface oxygen concentration, C_s.

A mass balance on an external spherical shell in the boundary gas film region leads to

$$\frac{d}{dr} \left(r^2 \dot{N}_r \right) = 0 \qquad (7.13)$$

where $\dot{N}_r$ is the mole flux of O_2 per unit area through an external shell of radius r. From Fick's First Law, $\dot{N}_r$ may be given as

$$\dot{N}_r = \frac{-\alpha D_g}{\alpha + C_r} \frac{dC_r}{dr} \qquad (7.14)$$

and

$$\alpha = \frac{P_t}{R \cdot T_{Avg}} \qquad (7.15)$$

where

C_r = oxygen concentration at radius r

D_g = binary gas diffusivity for O_2-He (see Appendix E)

P_t = total system pressure

R = gas constant

substituting Equation (7.14) into (7.13), we have

$$\frac{d}{dr}\left[\frac{r^2}{\alpha + C_r}\frac{dC_r}{dr}\right] = 0 \qquad (7.16)$$

As CO has been assumed to be the primary product, the total rate of O_2 transport to the particle surface shall equal half of the observed reaction rate. Equation (7.16) may now be solved using the following boundary conditions:

B.C. 1 $\quad \dot{N}_r = \frac{-\alpha D_g}{\alpha + C_r}\frac{dC_r}{dr} = -\frac{1}{2}\frac{R_p}{4\pi\, r_s^{\,2}} \qquad$ at $r = r_s$

$$(7.17)$$

B.C. 2 $\quad C_r = C_g \qquad\qquad\qquad$ at $r = \infty$

where C_g is the oxygen concentration at the outer edge of the boundary layer evaluated at T_{Avg}, or

$$C_g = \frac{P_{O_2}}{R\, T_{Avg}} \qquad (7.18)$$

and P_{O_2} is, of course, the oxygen partial pressure in the main gas. This gives:

$$C_r = (\alpha + C_g)e^{-\frac{R_p}{8\pi r\alpha D_g}} - \alpha \qquad (7.19)$$

At the particle surface $r = r_s$ and $C_r = C_s$, we then have

$$C_s = (\alpha + C_g)\, e^{-\frac{R_p}{8\pi r_s\alpha D_g}} - \alpha \qquad (7.20)$$

Therefore, for the rates given in Table 7.1, values of C_s may be obtained at the experimental conditions used. Table 7.3 summarizes the calculations.

7.4.4 Apparent Kinetics

Having estimated particle temperatures and surface oxygen concentrations, the apparent reaction order, n, rate constants, k, and activation energy, E, of the rate expression given by Equation (7.12) can be found for the oxidation reaction of 1750 K lignite char.

The calculation involved iterative solutions and was rather tedious. Figure 7.7 shows the flow diagram for the computation scheme. The results are summarized in Table 7.4 and Figure 7.8. The apparent rate constant based on the consumption rate of char per unit external surface area, for the oxidation reaction of 1750 K lignite char was

$$k_E = 5.0 \times 10^3 \exp{(-11,200/RT)} \ \frac{cm}{sec} \left(\frac{g\text{-moles}}{cm^3} \right)^{0.01} \qquad (7.21)$$

7.5 Effectiveness Factor and Intrinsic Kinetics

In section 7.4 we have identified the resistance due to the external diffusion of oxygen to the particle surface and obtained the apparent kinetics. We shall now deal with the resistance due to the internal pore diffusion in order to determine the intrinsic reaction kinetics. To measure how much the reaction rate is lowered because of the resistance to pore diffusion, it is common practice to

TABLE 7.3

SURFACE OXYGEN CONCENTRATIONS FOR CHAR/OXYGEN EXPERIMENTS

P_{O_2} atm	T_F K	α $\dfrac{\text{g-moles}}{\text{cm}^3}$	C_g $\dfrac{\text{g-moles}}{\text{cm}^3}$	D_g $\dfrac{\text{cm}^2}{\text{sec}}$	C_s $\dfrac{\text{g-moles}}{\text{cm}^3}$
0.2	1250	9.727×10^{-6}	1.945×10^{-6}	7.65	1.933×10^{-6}
0.2	1500	8.104×10^{-6}	1.621×10^{-6}	10.95	1.607×10^{-6}
0.2	1750	6.945×10^{-6}	1.389×10^{-6}	14.25	1.373×10^{-6}
0.4	1250	9.688×10^{-6}	3.875×10^{-6}	7.80	3.845×10^{-6}
0.4	1500	8.066×10^{-6}	3.226×10^{-6}	11.10	3.192×10^{-6}
0.4	1750	6.905×10^{-6}	2.762×10^{-6}	14.40	2.723×10^{-6}

Estimate

$$n_i = \ln\left[\frac{R_{P;P_{O_2},1;T_{F,i}}}{R_{P;P_{O_2},2;T_{F,i}}}\right] \bigg/ \ln\left[\frac{C_{s;P_{O_2},1;T_{F,i}}}{C_{s;P_{O_2},2;T_{F,i}}}\right]$$

$$\bar{n} = \frac{1}{3}\sum_i^3 n_i$$

$$k_{P,j} = R_{P,j}/(C_{s,j})^{\bar{n}}$$

Plot $k_{P,j}$ vs. $1/T_{P,j}$ and evaluate E from slope

$$n_{calculated,i} = \left[\ln\left(\frac{R_{P;P_{O_2},1;T_{F,i}}}{R_{P;P_{O_2},2;T_{F,i}}}\right) + \frac{E}{R}\left(\frac{1}{T_{P,i1}} - \frac{1}{T_{P,i2}}\right)\right] \bigg/ \ln\left(\frac{C_{s;P_{O_2},1;T_{F,i}}}{C_{s;P_{O_2},2;T_{F,i}}}\right)$$

$$\bar{n}_{calculated} = \frac{1}{3}\sum_i^3 n_{calculated,i}$$

Check: $\bar{n}_{calculated} \overset{?}{=} \bar{n}$

NO   YES

Let $\bar{n} = \bar{n}_{calculated}$

Stop Calculation

$$\bar{n} \; ; \; k_{P,j} \; ; \; E$$

Figure 7.7

Flow Diagram for the Computations of Apparent Kinetic Constants for

Char/Oxygen Reaction

TABLE 7.4

APPARENT KINETIC CONSTANTS FOR CHAR/OXYGEN REACTION

P_{O_2}	T_F	k_E	$10^4/T_p$
atm	K	$\dfrac{cm}{sec}\left(\dfrac{g\text{-moles}}{cm^3}\right)^{0.01}$	K^{-1}
0.2	1250	47.22	7.968
0.2	1500	92.08	6.631
0.2	1750	163.10	5.682
0.4	1250	50.58	7.905
0.4	1500	98.55	6.570
0.4	1750	173.01	5.621

$$k_{E,0} = 5.0 \times 10^3 \ \frac{cm}{sec}\left(\frac{g\text{-moles}}{cm^3}\right)^{0.01}$$

$$n = 0.99$$

$$E = 11,200 \ \frac{cal}{g\text{-mole}}$$
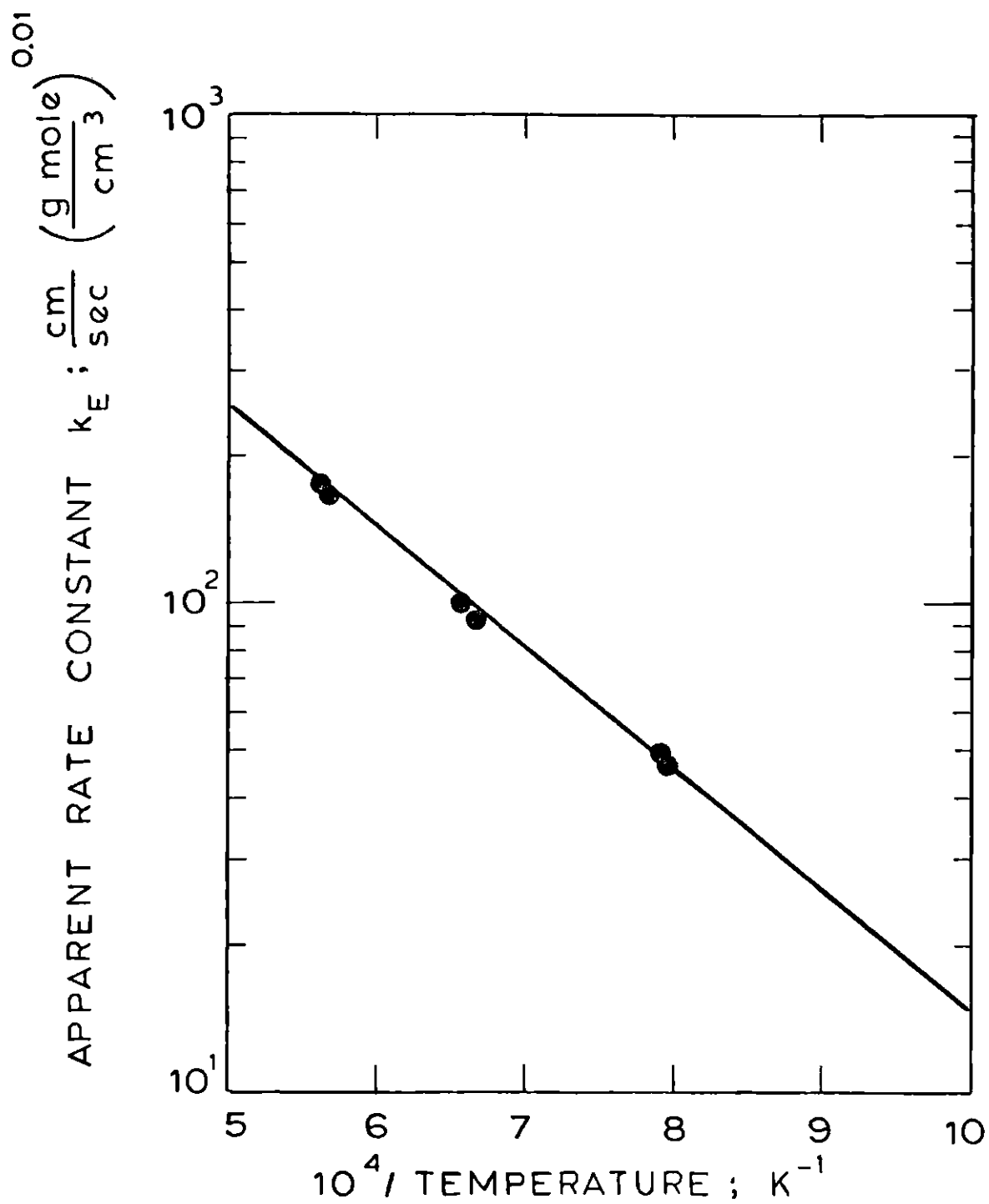
Figure 7.8

Arrhenius Plot of Apparent Rate Constant for Char Oxidation

estimate the effectiveness factor, η, which is defined as follows:

$$\eta = \frac{\text{Observed Rate}}{\text{Rate in Absence of Pore Diffusion Limitation}}$$

$$= \frac{R_p}{V_s \cdot k_v \cdot C_s^{\,m}} \qquad (7.22)$$

where

R_p = observed reaction rate per particle

V_s = volume of the particle

k_v = intrinsic rate constant per unit volume of particle

m = intrinsic reaction order

By determining a value for η, the intrinsic rate constant can be obtained from the experimentally-determined rates reported in Section 7.4.1.

For simplicity, a flat-plate geometry will be used for the mathematical analysis. Considering pore-diffusion and reaction in a flat plate of porous char, the differential equation to be solved is

$$D_e \frac{d^2C}{dr^2} = k_v\, C^m \qquad (7.23)$$

where C is the oxygen concentration within the porous structure at a distance r from the center of the particle, and D_e is the effective pore diffusivity. The boundary conditions are:

B.C. 1 $\quad$ $C = C_s$ $\qquad$ at $r = r_s$

$$(7.24)$$

B.C. 2 $\quad$ $\dfrac{dC}{dr} = 0$ $\qquad$ at $r = 0$

For the sake of convenience, the system equation is often written in dimensionless form by letting

$$\xi = \frac{C}{C_s} \qquad \text{and} \qquad \psi = \frac{r}{r_s} \qquad (7.25)$$

and

$$\phi = r_s \sqrt{\frac{k_v}{D_e} \cdot C_s^{m-1}} \qquad (7.26)$$

so that the system equation becomes

$$\frac{d^2\xi}{d\psi^2} = \phi^2 \xi^m \qquad (7.27)$$

with boundary conditions

B.C. 1 $\quad$ $\xi = 1$ $\qquad$ at $\psi = 1$

$$(7.28)$$

B.C. 2 $\quad$ $\dfrac{d\xi}{d\psi} = 0$ $\qquad$ at $\psi = 0$

Note that ϕ is often called the Thiele modulus. Solving Equation (7.28) for $\dfrac{d\xi}{d\psi}$, utilizing the second boundary condition, gives

$$\frac{d\xi}{d\psi} = \phi \cdot \left(\frac{2}{m+1}\right)^{1/2} \cdot (\xi^{m+1} - \xi_0^{m+1})^{1/2} \qquad (7.29)$$

where ξ_0 is the dimensionless concentration at the center of the particle. Note that for pore diffusion control, $\xi_0 \to 0$ and Equation (7.29) reduces to

$$\frac{d\xi}{d\psi} = \phi \cdot \left(\frac{2}{m+1}\right)^{1/2} \cdot \xi^{\frac{m+1}{2}} \qquad (7.30)$$

At steady-state, the rate of reaction must equal the flux of reactant at the particle surface. Therefore,

$$\frac{1}{A_E} R_P = D_e \cdot \left. \frac{dc}{dr} \right|_{r=r_s} \qquad (7.31)^*$$

Where A_E is the external surface area.

---

*To be consistent with Equation (7.17), a factor of 1/2 should be applied to the left hand side of Equation (7.31) to account for the earlier assumption that CO is the primary product of reaction at both external and internal reaction surfaces. However, the factor of 1/2 is no longer necessary if the reaction is assumed to proceed to completion by the sequential reaction of CO with O_2:

$$CO + \frac{1}{2} O_2 \longrightarrow CO_2$$
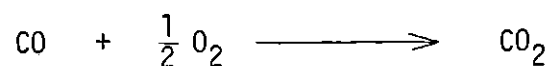
Or in dimensionless form

$$\gamma_s = \left.\frac{d\xi}{d\psi}\right|_{\psi=1} \tag{7.32}$$

where $\gamma_s = \frac{r_s R_p}{A_E \cdot D_e \cdot C_s}$ is the dimensionless reaction rate. Substituting

Equation (7.32) into (7.30) and utilizing the first boundary condition,

yields

$$\gamma_s = \phi \left(\frac{2}{m+1}\right)^{1/2} \tag{7.33}$$

Analogous to Equation (7.22), the effectiveness factor is given in

dimensionless terms as

$$\eta = \frac{\gamma_s}{\phi^2} \cdot \beta_s \tag{7.34}$$

where $\quad \beta_s = \frac{A_E r_s}{V_s}$

manipulating Equation (7.34), gives

$$\eta\phi^2 = \phi \beta_s \left(\frac{2}{m+1}\right)^{1/2} = \left(\frac{2}{m+1}\right) \beta_s^2 \frac{1}{\eta} \tag{7.35}$$

Note that $\eta\phi^2$ can also be expressed as

$$\eta\phi^2 = \frac{3 R_p}{4\pi r_s D_e C_s} \tag{7.36}$$

by combining the definition of η (Equation (7.22)) and ϕ (Equation (7.26)). Finally, combining Equations (7.22), (7.35), and (7.36) yields

$$R_E = \frac{R_P}{A_E} = \left[\left(\frac{2}{m+1}\right) D_e \, k_v \, C_s^{m+1}\right]^{1/2} \tag{7.37}$$

where R_E is the observed reaction rate per unit external surface area. Thus, the mth-order reaction behaves like a reaction of order $(m+1)/2$, i.e., the apparent reaction order observed in Section 7.4. In addition the temperature dependency of reactions is affected by strong pore resistance. From Equation (7.37) the observed rate constant for an mth-order reaction is

$$k_{ob} = \left(\frac{2}{m+1} \cdot k_v \cdot D_e\right)^{1/2} \tag{7.38}$$

Taking logs and differentiating with respect to temperature gives

$$\frac{d(\ln k_{ob})}{dT} = \frac{1}{2}\left[\frac{d(\ln k_v)}{dT} + \frac{d(\ln D_e)}{dT}\right] \tag{7.39}$$

With Arrhenius temperature dependencies for both reaction and diffusion we have

$$k_v = k_{v,o} \exp\left(-\frac{E_v}{RT}\right)$$

and

$$D_e = D_{e,o} \exp\left(-\frac{E_D}{RT}\right)$$

and replacing in Equation (7.39) gives

$$E_{ob} = \frac{E_v + E_D}{2} \tag{7.40}$$

Since E_v is generally much larger than E_D, we have

$$E_{ob} \cong \frac{E_v}{2} \tag{7.41}$$

In Section 7.4.4, the apparent reaction order was found to be 0.99. Therefore, the true order of the oxidation reaction of 1750 K lignite char is $m = 0.98$.

Solving Equation (7.37) for k_v gives

$$k_v = 0.99 \frac{R_E^2}{D_e \cdot C_s^{1.98}} \qquad \frac{1}{sec}\left(\frac{g\text{-moles}}{cm^3}\right)^{0.02} \tag{7.42}$$

The intrinsic reaction rate constant based on unit specific B.E.T. surface area can also be obtained

$$k_B = \frac{k_v}{\rho_B \cdot A_B}$$

$$= 0.99 \frac{R_E^2}{\rho_B \cdot A_B \cdot D_e \cdot C_s^{1.98}} \qquad \frac{cm}{sec}\left(\frac{g\text{-moles}}{cm^3}\right)^{0.02} \tag{7.43}$$

Substituting Equation (7.42) into Equation (7.22) gives

$$\eta = \frac{3}{r_s} \left[\frac{C_s\ D_E}{0.99\ R_E} \right] \tag{7.44}$$

Note that values for D_e are determined in Appendix F assuming Knudsen diffusion in fine pores. Table 7.5 and Figure 7.9 summarize the results of intrinsic kinetic constants and effectiveness factors for the oxidation reaction of 1750 K lignite char. The intrinsic activation energy obtained from Figure 7.9 was 22,100 cal/g-mole. As expected, this was approximately twice the apparent activation energy observed in Section 7.4.4. The intrinsic rate constant, based on the consumption rate of char per unit B.E.T. surface area, for the oxidation reaction of 1750 K lignite char was therefore given by

$$k_B = 2.8 \times 10^3 \ \exp(-22,100/RT) \ \frac{cm}{sec} \left(\frac{g\text{-moles}}{cm^3} \right)^{0.02} \tag{7.45}$$

7.6 Comparison of the Intrinsic Kinetics of Present Study with Those of Others

The intrinsic kinetic parameters of Char/O_2 reaction have been obtained through the development of a pore diffusion model. It is of interest to compare the intrinsic kinetics obtained from the present study with those of others.

Smith (1971a,1971b) studied the kinetics of combustion of four pulverized fuels (i.e., petroleum, coke, anthracite, bituminous coal char and semi-anthracite) at temperatures between 1200 K and 2270 K. He observed that particle combustion rates were controlled by the

TABLE 7.5

INTRINSIC KINETICS FOR CHAR/OXYGEN REACTION

P_{O_2} atm	T_F K	D_e $\frac{cm^2}{sec}$	η	k_B $\frac{cm}{sec}\left(\frac{g\text{-moles}}{cm^3}\right)^{0.02}$	$10^4/T_P$ K^{-1}
0.2	1250	2.257×10^{-3}	8.466×10^{-2}	4.930×10^{-1}	7.968
0.2	1500	2.474×10^{-3}	4.749×10^{-2}	1.711	6.631
0.2	1750	2.673×10^{-3}	2.892×10^{-2}	4.967	5.682
0.4	1250	2.266×10^{-3}	7.989×10^{-2}	5.635×10^{-1}	7.905
0.4	1500	2.486×10^{-3}	4.490×10^{-2}	1.950	6.570
0.4	1750	2.688×10^{-3}	2.761×10^{-2}	5.558	5.621

$$k_{B,0} = 2.8\times10^3 \ \frac{cm}{sec}\left(\frac{g\text{-moles}}{cm^3}\right)^{0.02}$$

$$m = 0.98$$

$$E = 22,100 \ \frac{cal}{g\text{-mole}}$$
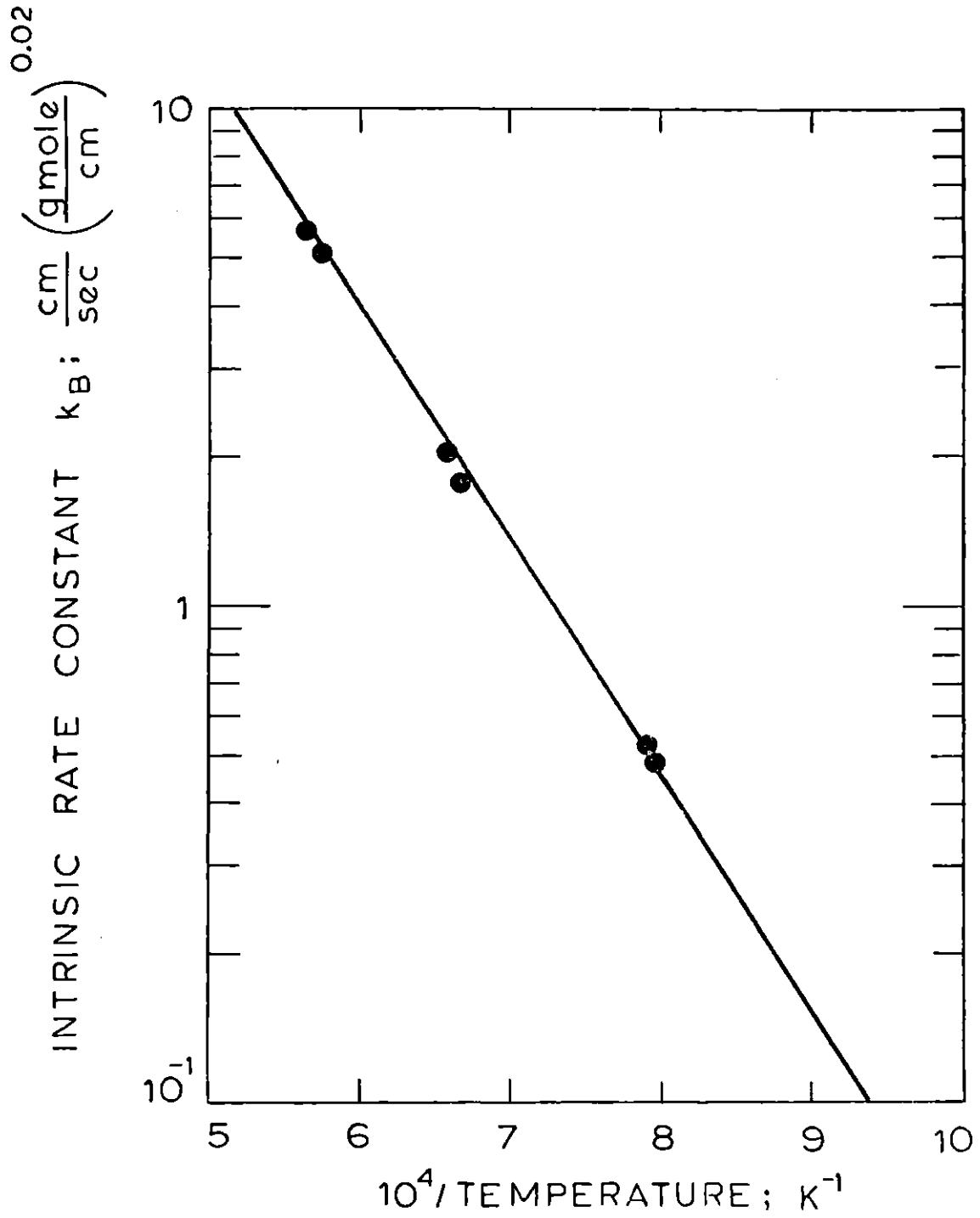
Figure 7.9

Arrhenius Plot of Intrinsic Rate Constant for Char Oxidation

combined effects of oxygen diffusion into the pore structure of the particles and reaction at the pore walls. The apparent activation energies were found to be in the range of 16 to 18 Kcal/mole which corresponded to intrinsic activation energies of 32 to 36 Kcal/mole. Other studies on the combustion of pulverized coal and pulverized coal char have given intrinsic activation energies ranging from 30 to 50 Kcal/mole (Field, 1969, 1970; Smith and Taylor, 1972, 1974). Field, Gill, Morgan and Hawksley (1967) have reviewed the data on carbon oxidation rates determined between 900 and 1650 K in four investigations and shown that the rates could be correlated by an empirical expression with an activation energy of 35.7 Kcal/mole. Although the intrinsic activation energy of 22.1 Kcal/mole obtained from the present study is somewhat lower than these values mentioned above, it is comparable to the intrinsic activation energy of 25.2 Kcal/mole found in a separate MIT study of oxidation of a pulverized Montana Rosebud coal char (Mandel, 1977). The influence of impurities which exist in the coal chars could account for the low activation energies.
(Thring and Essenhigh, 1963; Field, 1969; Mulcahy and Smith, 1969.)

The intrinsic rates from the present study should also be compared with those of others. Smith and Tyler (1974) have studied the reactivity of a pulverized brown coal char to oxygen and correlated the intrinsic oxidation rate per B.E.T. surface area of the char, R_B, with temperature over the range 630 to 1812 K by the empirical relation:

$$R_B = 1.34 \exp(-32,600/RT_p) \ g/(cm^2 \ sec)$$

taking the true order to be zero over the whole temperature range. At 1760 K, this yields an intrinsic reaction rate of 1.198×10^{-5} g-moles/ (cm^2 sec). The intrinsic rate of present study at 1760 K calculated from Equation (7.44) with $C_s = 1.373 \times 10^{-6}$ g-mole/cm^3 and $m = 0.98$ (see Table 7.3) is 9.070×10^{-6} g-mole/(cm^2 sec). Thus, the rate calculated from present study is different from the rate of Smith and Tyler merely by a factor of 1.3 under above conditions. Rates calculated under other conditions within the range of present study also show similarly good agreement with those calculated from the rate expression of Smith and Tyler.

In summary, the intrinsic activation energy found in the present study appears slightly low, nevertheless, the overall reaction rates are comparable to those found by Smith and Tyler for a pulverized brown coal char over a wide range of temperatures.

7.7 Change in Reactivity of Char During Combustion

In Figure 7.4 the retentions of char under different experimental conditions were plotted. As indicated before, the retentions appeared to level off after the retentions became less than 55%. To make it easier to be visualized, this problem can be restated from the point of view of solid weight loss. The solid weight loss appeared to level off considerably after the char reached a certain extent of burnout. This indicated the decrease of the reactivity of the char during the burnout process. In order to investigate this phenomenon quantitatively, the rates (or equivalently, the slopes) were taken at different stages

of burnout under different experimental conditions (i.e., 1250 K, 0.2 atm; 1500 K, 0.2 atm; 1750 K, 0.2 atm; and 1250 K, 0.4 atm). The rates were then normalized individually by the initial rates under the same experimental conditions. Thus, the relative reactivities, R*, of char as a function of solid burnout (d.a.f.) were obtained. The R* is given by R* = (d ln Z/dt)/(d ln Z/dt)i. Table 7.6 and Figure 7.10 summarize the results. Interestingly enough, the reactivity of char remained constant in the first half of the burnout process, i.e., from the beginning of the combustion to approximately 45% of total solid burnout. The reactivity then decreased dramatically in the second half of burnout process. From 45% to 50% burnout (d.a.f.), the reactivity dropped to almost only half of the initial reactivity. From 50% to 60% burnout (d.a.f.), the reactivity dropped further down to almost a quarter of the original reactivity. In order to monitor the entire process of the char combustion, it is therefore essential to couple the initial intrinsic kinetics discussed in Section 7.5, with the variation of reactivity of char during the burnout process.

The decrease in reactivity with the progress of the reaction could not be explained simply by the change in B.E.T. surface area alone. (See Figure 7.5 for the behavior of the normalized specific B.E.T. surface area.) It can, however, be a consequence of several other factors. Some of the possible reasons are:

1. The build-up of a "protective" ash layer on the particle external surface inhibits oxygen diffusion to the unreacted core at the center of the particle.

TABLE 7.6

RELATIVE REACTIVITIES OF CHAR DURING OXIDATION

Solid Burnout % d.a.f.	R*			
T (K)	1250	1500	1750	1250
P_{O_2} (atm)	0.2	0.2	0.2	0.4
0	1	1	1	1
10	1	1	1	1
20	1	1	1	1
30	1	1	1	1
40	1	1	1	1
45	1	1	1	1
50	1	0.524	0.480	0.571
55	-	0.326	0.316	0.357
60	-	-	0.916	0.253
65	-	-	-	0.215
70	-	-	-	-
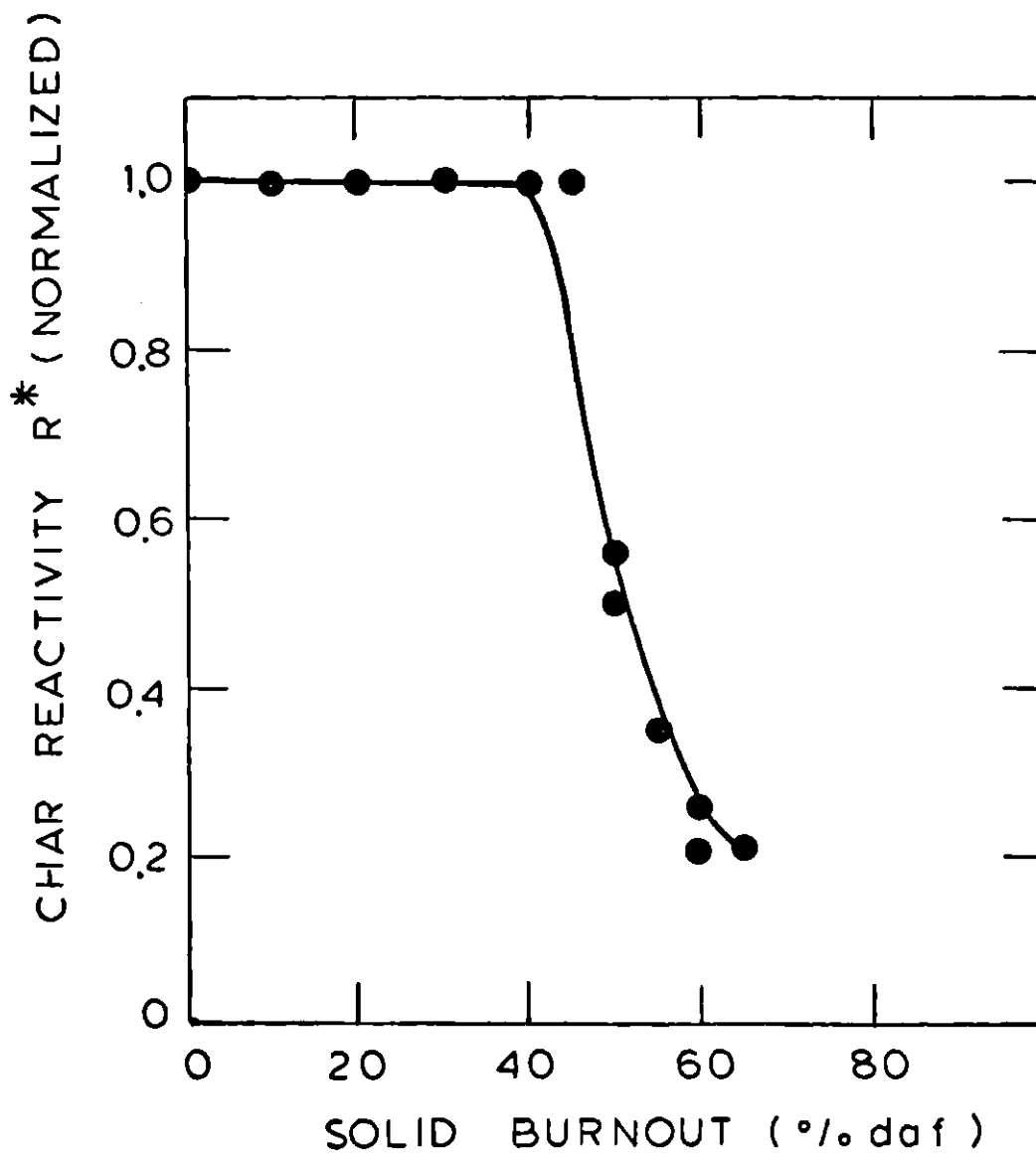
Figure 7.10

Char Reactivity as Function of Solid Burnout During Oxidation

2. Poisoning by ash or metals or other contaminants at the pore
    mouth diminishes the overall activity. The diffusion through
    this poisoned mouth can, in the case of a fast reaction, become
    rate determining, hence the addition of a small amount of
    poison can cut down the overall activity by a large factor.

3. Particle surface annealing with time causes the deactivation
    of char.

4. The consumption, destruction, deterioration, or transformation
    of the active sites, localized in certain spots, due to
    reaction results in a decrease in reactivity.

No attempt was made to test the last two hypotheses. A mathematical
model was set up to check the validity of the ash-layer build-up theory.
The ash-layer build-up model can predict a marked drop in reactivity,
but only with an unreasonably thick build-up of an ash layer. The ash-
layer build-up model has therefore been discarded.

A pore-mouth poisoning model has been successfully proved to be
able to rationalize the behavior of the char reactivity as a function
of burnout and has been shown physically consistent with the combustion
processes. We shall discuss the pore-mouth poisoning model in the
next section.

7.8 Pore-Mouth Poisoning of Char

In Section 7.5 we have dealt with the problem of diffusion-
reaction in porous char with a simplified flat-plate geometry. In the
development of the pore-mouth poisoning model, a somewhat more realistic

geometry, utilizing single cylindrical pore, will be used for a rigorous treatment. Since the intrinsic reaction order for the oxidation of 1750 K lignite char is 0.98 (see Section 7.5), a first-order reaction kinetics can be used without losing any accuracy.

7.8.1 Reaction in Single Pore

Consider a single cylindrical pore, as shown in Figure 7.11(a), with a first-order reaction (with respect to oxygen) taking place at the walls of the pore:

Starting with the material balance for the elementary slice of the pore, and rearranging the balance, we obtain

$$\frac{d^2C}{dx^2} - \frac{2\,k_B}{D_K\,r_p}\,C = 0 \qquad\qquad (7.46)$$

where

k_B = intrinsic rate constant per unit B.E.T. surface area

r_p = pore radius

D_K = Knudsen pore diffusivity (see Appendix F).

Examining the physical limits of the conceptual pore, we find

B.C. 1 $\qquad C = C_s \qquad$ at $x = 0$ $\qquad\qquad (7.47)$

B.C. 2 $\qquad \dfrac{dC}{dx} = 0 \qquad$ at $x = L$ $\qquad\qquad (7.48)$
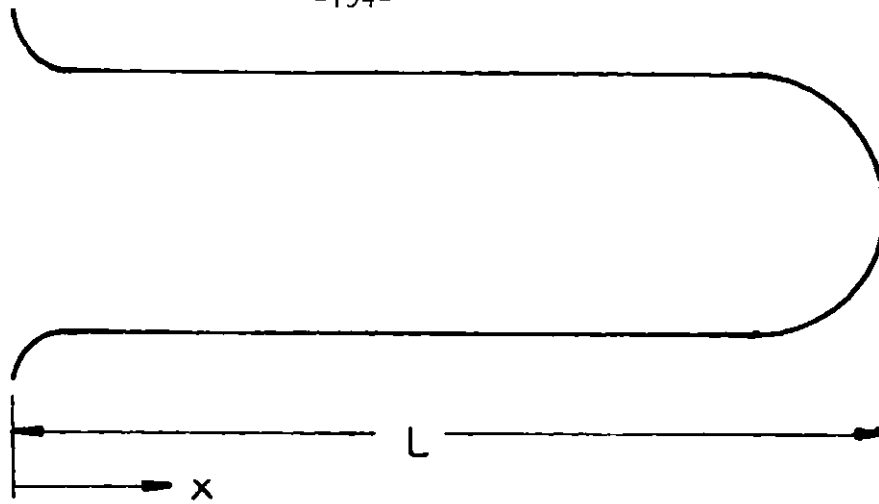
(a) Unpoisoned Pore
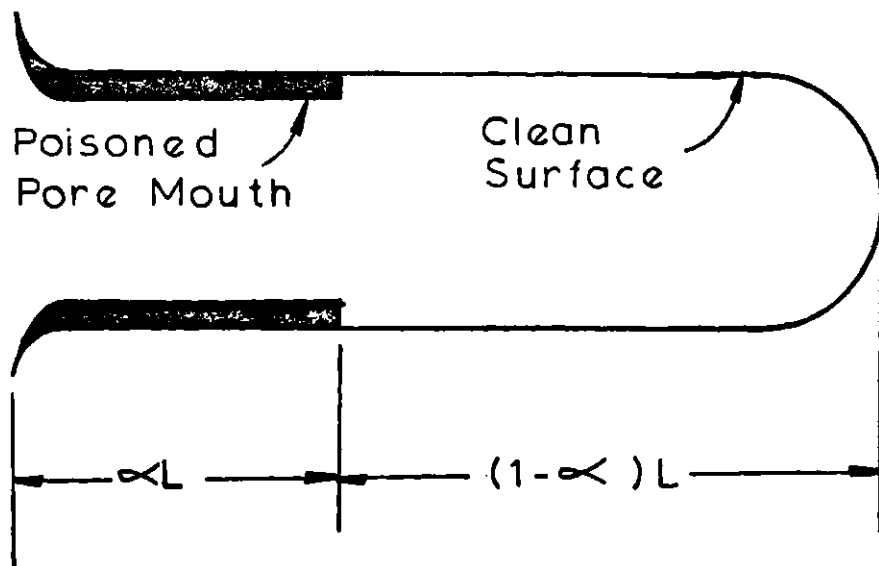
(b) Poisoned Pore

Figure 7.11

Representation of a Single Cylindrical Pore

(a) Unpoisoned (b) Poisoned near Mouth of Pore

Solving Equation (7.46) with the boundary conditions given by Equations (7.47) and (7.48) we obtain

$$\frac{C}{C_s} = \frac{\cosh \left[\phi\left(1 - \frac{x}{L}\right)\right]}{\cosh \phi} \tag{7.49}$$

where

$$\phi = L \sqrt{\frac{2 \, k_B}{r_p \, D_K}} \tag{7.50}$$

$$= \text{Thiele modulus}$$

Note that, at steady state, the rate of reaction, R, must equal the flux of reactant at $x = 0$. Thus

$$R = \pi \, r_p{}^2 \, D_K \left(-\frac{dC}{dx}\right)_{x=0} \tag{7.51}$$

$$= \pi \, r_p{}^2 \, D_K \cdot \frac{\phi C_s}{L} \cdot \tanh \phi \tag{7.52}$$

$$= \pi \, r_p \, C_s \sqrt{2 \, r_p k_B D_K} \quad \tanh \phi \tag{7.53}$$

By definition, the effectiveness factor η, is then given by:

$$\eta = \frac{\pi \, r_p{}^2 D_K \cdot \dfrac{\phi \, C_s}{L} \cdot \tanh \phi}{2 \, \pi \, r_p \cdot L \cdot k_B \cdot C_s}$$

$$= \frac{\tanh \phi}{\phi} \tag{7.54}$$

Note that, $\tanh \phi \rightarrow 1$ for ϕ larger than 2, thus

$$\eta = \frac{1}{\phi} \qquad \text{for } \phi > 2 \qquad (7.55)$$

7.8.2 Reaction with Poisoned Pore Mouth (after Wheeler, 1951, 1955)

We shall now consider the reaction with a poisoned pore mouth. Looking at Figure 7.11(b), we assume that the concentration of reactant at the pore mouth is again C_s, and we wish to find the rate of reaction in a pore which has its initial length αL poisoned. We assume the transport of reactant through the poisoned portion to be by diffusion. Under steady state conditions this will occur with a linear concentration gradient, i.e.,

$$\frac{dC}{dx} = \frac{\Delta C}{\Delta L} = \frac{C_s - C_1}{\alpha L} \qquad (7.56)$$

where C_1 is the (unknown) concentration at the end of the poisoned region. The rate of this diffusion through the poisoned length αL must equal the rate of reaction in the clean region of length $(1 - \alpha)L$, and this rate for first order reaction is given by Equation (7.53) with C_1 substituted for C_s. Thus

$$\begin{pmatrix} \text{Rate of Diffusion} \\ \text{thru Poisoned Section} \end{pmatrix} = \begin{pmatrix} \text{Rate of Reaction} \\ \text{on the Clean Section} \end{pmatrix} \qquad (7.57)$$

or in symbols

$$\pi \, r_p^{\,2} \, D_K \, \frac{C_s - C_1}{\alpha L} = \pi \, r_p \, C_1 \cdot \sqrt{2 \, r_p \cdot k_B \cdot D_K} \;\; \tanh \, [\phi_0 (1-\alpha)] \qquad (7.58)$$

Note that ϕ_0 is the value of ϕ for the unpoisoned pore, so that $\phi_0 (1-\alpha)$ is the value of ϕ for the unpoisoned portion of length L $(1-\alpha)$.

Solving Equation (7.58) for C_1 and substituting this value back into the expression for the rate of diffusion through the poisoned section, i.e., left hand side of Equation (7.58), gives the desired rate in the poisoned pore:

$$R_{po} = \frac{\pi \, r_p \, C_s \, \sqrt{2 \, r_p \, k_B \, D_K} \cdot \tanh \, [\phi_0 (1-\alpha)]}{1 + \alpha \phi_0 \cdot \tanh \, [\phi_0 (1-\alpha)]} \qquad (7.59)$$

The ratio (F) of the activity of the poisoned pore (R_{po}) to that of the unpoisoned pore (R_{un}) is then given by

$$F = \frac{R_{po}}{R_{un}}$$

$$= \left[\frac{\tanh \, [\phi_0 (1-\alpha)]}{\tanh \, \phi_0} \right] \left[\frac{1}{1 + \alpha \phi_0 \, \tanh \, [\phi_0 (1-\alpha)]} \right] \qquad (7.60)$$

For a reactive solid with small pores, ϕ_0 is very large. Assuming that ϕ_0 and $\phi_0 (1-\alpha) \gg 2$, we can approximate $\tanh \, [\phi_0 (1-\alpha)]$ and $\tanh \, \phi_0$ by unity. Therefore

$$F = \frac{1}{1 + \alpha \phi_0} = \frac{1}{1 + \alpha \, \frac{1}{\eta_0}} \qquad (7.61)$$

F can be obtained as function of α if η_0, the unpoisoned effectiveness factor is known. We have calculated η in Section 7.5 based on the initial rates. Since in the pore-mouth poisoning model it is arbitrarily assumed that the pores in the original char are not poisoned, therefore, the values of η in Table 7.5 can be regarded as values for η_0. The average value of $\frac{1}{\eta_0}$ for the conditions of interest, i.e., 1250 K, 0.2 atm; 1500 K, 0.2 atm; 1750 K, 0.2 atm; and 1250 K, 0.4 atm, are estimated to be 20. Thus, for our system,

$$F = \frac{1}{1 + 20\alpha} \tag{7.62}$$

Figure 7.12 is the plot of α versus F.

7.8.3 Validity of Pore-Mouth Poisoning Model

Having obtained the model of pore-mouth poisoning, we can now relate the reaction rate of char at any time, $R_{B,t}$, to the initial rate, $R_{B,i}$, as:

$$R_{B,t} = R_{B,i} \cdot F(\alpha) \cdot G(\beta)$$

or

$$R^* = \frac{R_{B,t}}{R_{B,i}} = F(\alpha) \cdot G(\beta) \tag{7.63}$$

where

$$\beta = \% \text{ char burnout, d.a.f.}$$
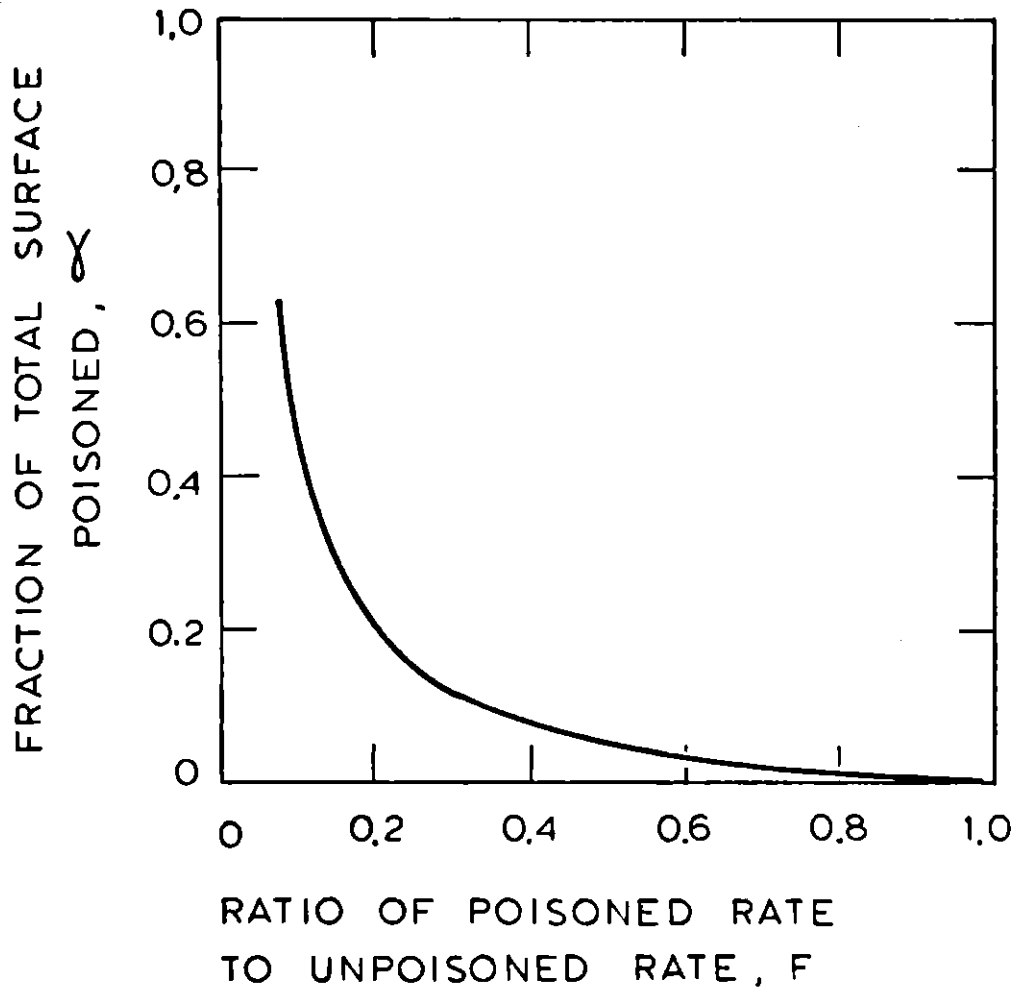
Figure 7.12

Ratio of Poisoned Rate to Unpoisoned Rate as Function of Fraction Total

Surface Poisoned

R^* = $R^*(\beta)$, the overall relative reactivity as shown in Figure 7.10.

$G(\beta)$ = normalized B.E.T. area as shown in Figure 7.5.

$F(\alpha)$ = poisoning effect as given by Equation (7.62).

Assuming the poisoning phenomenon is related to the ash released during char burnout process, the fraction α of a pore that is poisoned should be proportional to the ash-released (H) per unit B.E.T. surface area. In other words, the pore-mouth poisoning model would be valid if it can be proved that

$$\alpha = K \frac{H}{G} \tag{7.64}$$

where K is a constant. We shall prove Equation (7.64) as follows.

Since R^* and G have been determined experimentally as functions of burnout as shown in Figure 7.10 and Figure 7.5, respectively, F can then be obtained also as a function of burnout by rearranging Equation (7.63) i.e.,

$$F(\beta) = \frac{R^*(\beta)}{G(\beta)} \tag{7.65}$$

Figure 7.13 summarizes the results. Coupling the information from Figure 7.13, F = $F(\beta)$, and Figure 7.12, α = $\alpha(F)$, gives

$$\alpha = \alpha(\beta)$$
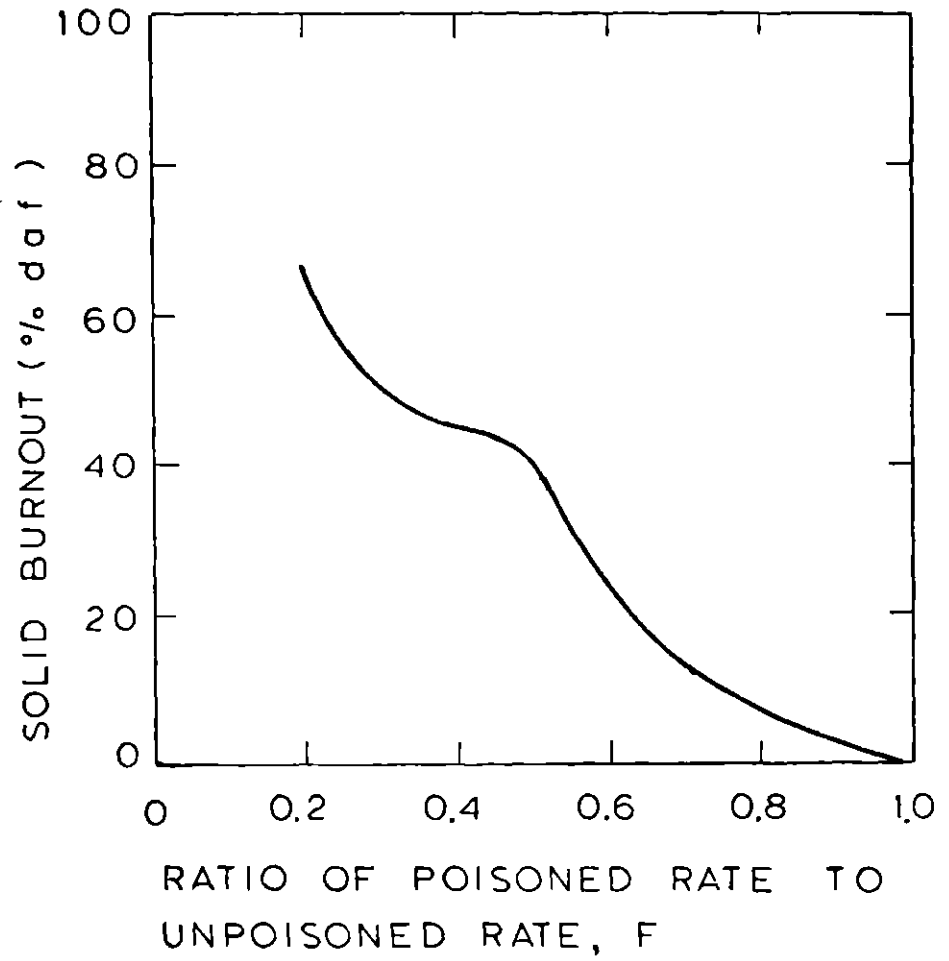
Figure 7.13

Ratio of Poisoned Rate to Unpoisoned Rate as Function of Solid Burnout

The results are shown in Figure 7.14. Noting that $G = G(\beta)$, shown in Figure 7.5 and

$$H = (\text{Ash Content of Char Used}) \times \beta$$

therefore, we have

$$\frac{H}{G} = 0.19\left(\frac{\beta}{G}\right)$$

Figure 7.15 shows the plot of $\frac{H}{G}$ versus β or Burnout. Finally, by coupling the information from Figure 7.14, $\alpha = \alpha(\beta)$, and Figure 7.15, $\frac{H}{G} = f(\beta)$ we obtain

$$\alpha = \alpha\left(\frac{H}{G}\right)$$

This is shown in Figure 7.16. A linear correlation was found for $\alpha = \alpha\left(\frac{H}{G}\right)$, therefore, we have proved that

$$\alpha = K \frac{H}{G} \tag{7.64}$$

Thus, the pore-mouth poisoning model is physically consistent and provides one hypothesis for the decrease in char reactivity with increasing char burnout.

In summary, the reaction rate of char at any time can be related to the initial rate by
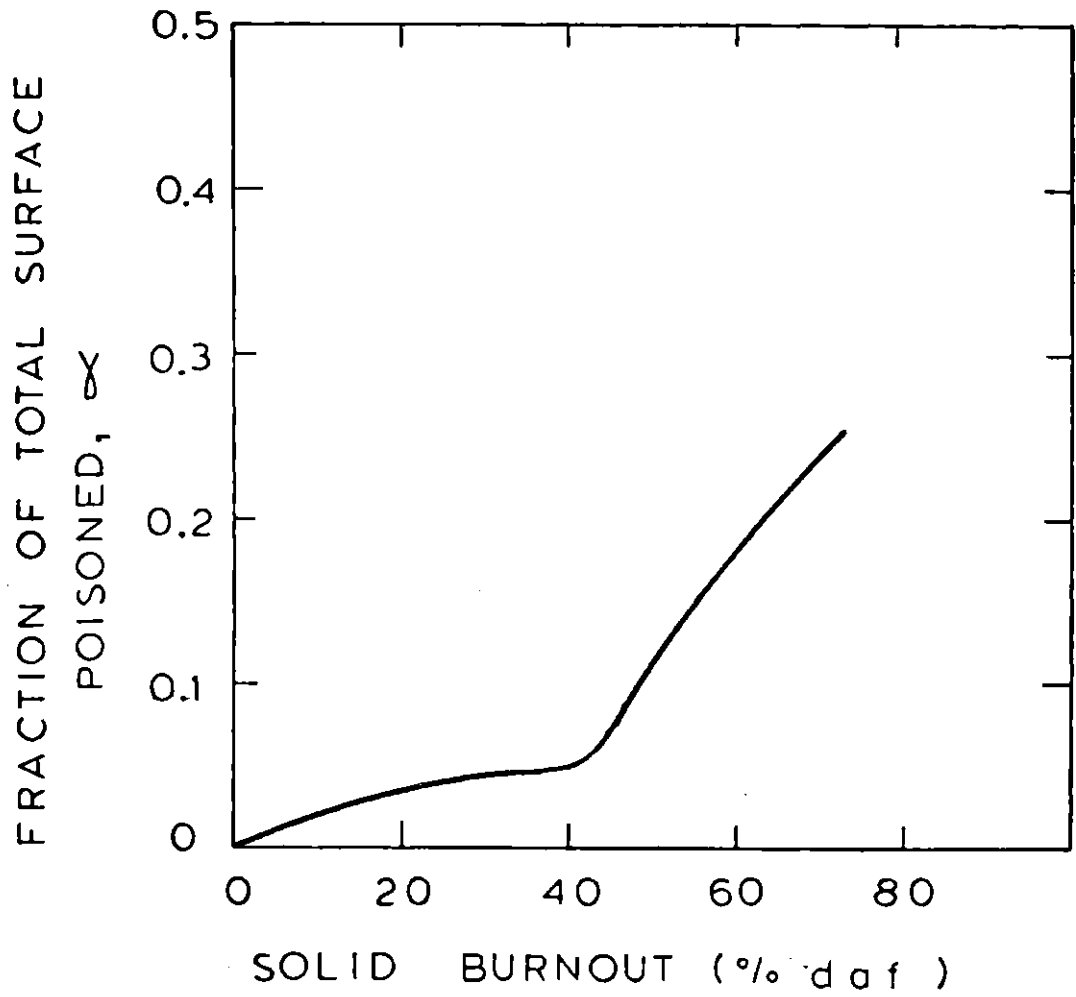
Figure 7.14

Fraction of Total Surface Poisoned as Function of Solid Burnout
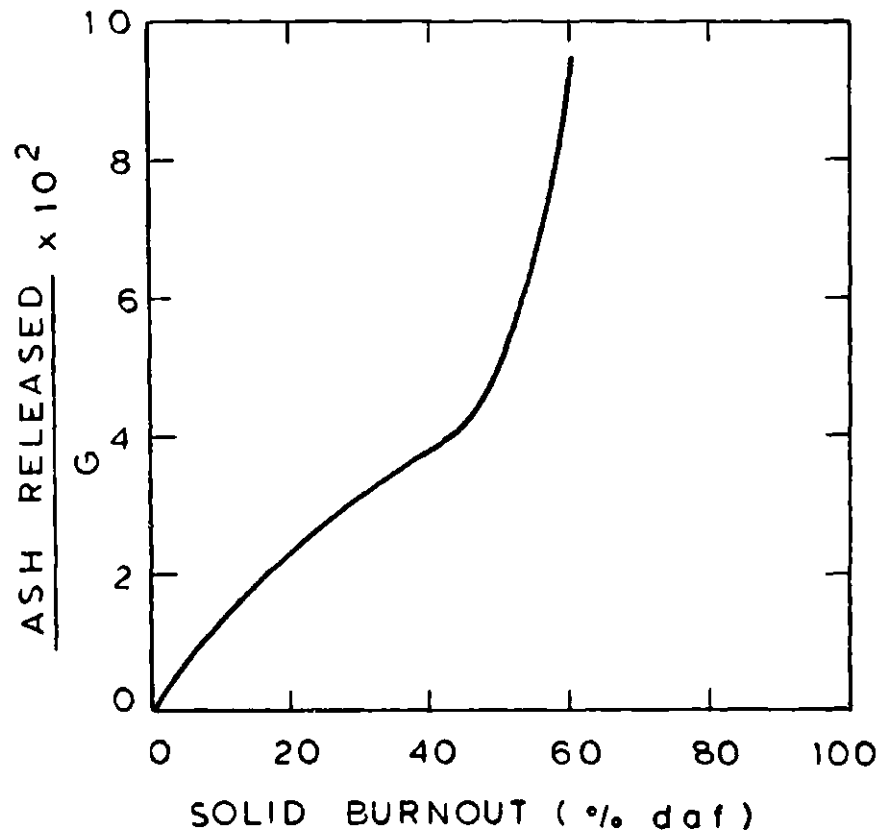
Figure 7.15

Ash Released per (Normalized) B.E.T. Surface Area as Function of Solid Burnout
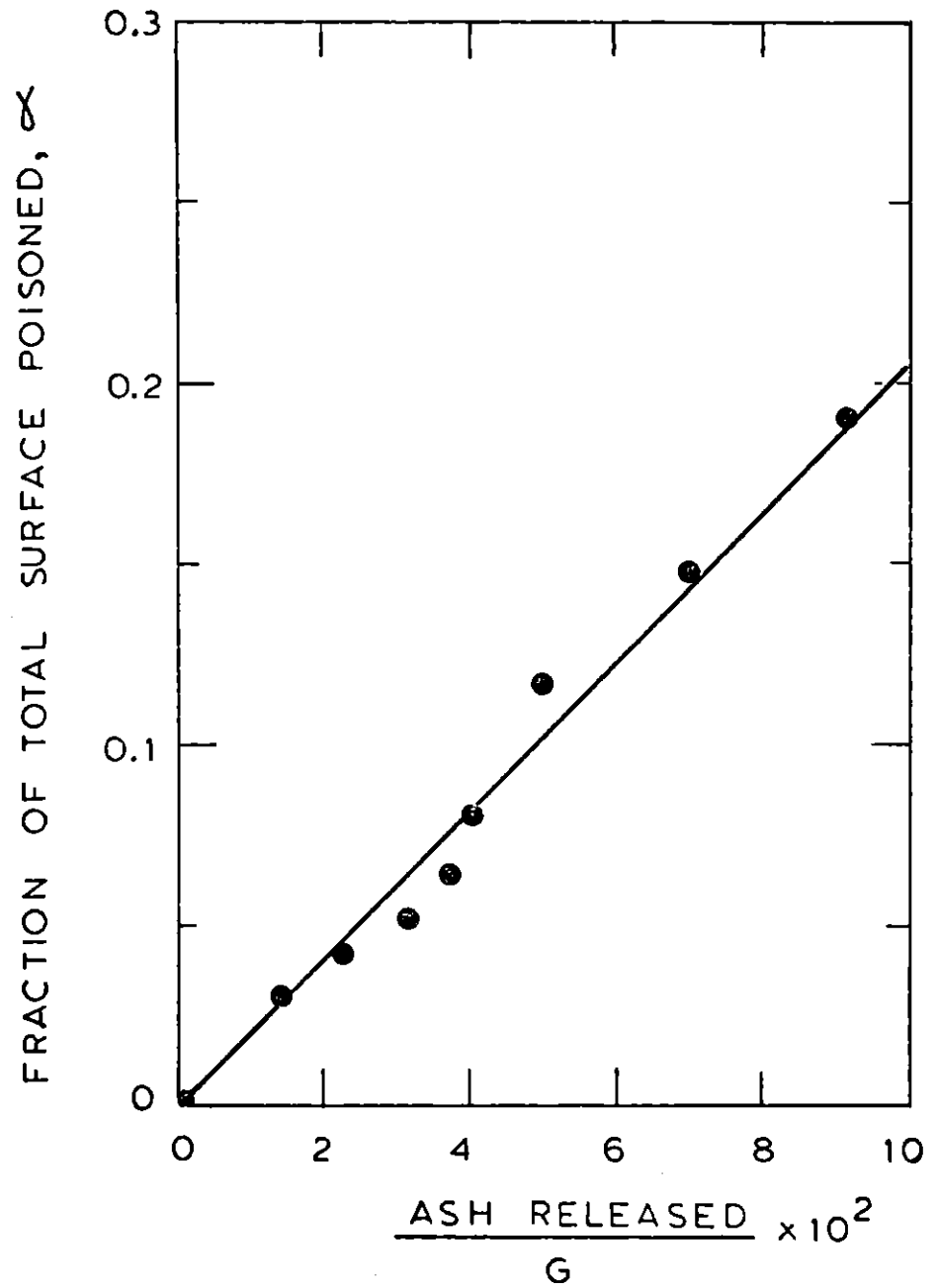
Figure 7.16

Linear Correlation Between Fraction of Total Surface Poisoned and Ash

Released per (Normalized) B.E.T. Surface Area

$$R_{B,t} = R_{B,i} \cdot F(\beta) \cdot G(\beta) \tag{7.65}$$

where G can be found experimentally, F can be estimated from the pore-mouth poisoning model, and $R_{B,i}$ can be estimated from initial intrinsic rate constant for a char.

7.9 Kinetics of Char-Nitrogen Combustion

Having discussed the overall char burnout kinetics in previous Sections, we shall now consider the behavior of char-nitrogen during coal char combustion.

The following observations can be drawn from the variation with time of the nitrogen/carbon ratio in char, as shown in Figure 7.6.

1. The nitrogen to carbon ratio decreased with increases in temperature during char burnout.

2. The nitrogen to carbon ratio was insensitive to oxygen partial pressure during char burnout.

3. A plot of the logarithm of the nitrogen/carbon ratio versus reaction time yields a straight line.

In order to explain the behavior described above, we should first examine the characteristics of the char used. The char was produced by pyrolyzing lignite particles at 1750 K for a residence time of one second in the drop tube furnace. It has been previously shown (Pohl, 1976) that during coal pyrolysis, the carbon loss reached an asymptotic value within a time of 100 milliseconds at 1750 K, the temperature used to produce the char in this study, but that nitrogen release

continued for longer times. The rationalization of these results was
that while carbon is present in relatively stable compounds in the char,
no comparable stabilized nitrogen structures are formed; consequently,
char-nitrogen continues to be released until it is completely eliminated
from char. Therefore, when a char particle is oxidized, nitrogen loss
will be due to both devolatilization and oxidation, but the carbon loss
will be exclusively due to oxidation.

Since the pyrolysis loss and oxidation loss of char-nitrogen are
additive, the consumption rate of char-nitrogen can be written as

$$
\begin{pmatrix} \text{total consumption-rate} \\ \text{of char-nitrogen} \end{pmatrix} = \begin{pmatrix} \text{consumption-rate of} \\ \text{char-nitrogen due} \\ \text{to pyrolysis} \end{pmatrix} +
$$

$$
\begin{pmatrix} \text{consumption-rate of} \\ \text{char-nitrogen due} \\ \text{to oxidation} \end{pmatrix} \qquad (7.67)
$$

or in symbols

$$
\frac{dN}{dt} = \left(\frac{\partial N}{\partial t}\right)_{\text{pyrolysis}} + \left(\frac{\partial N}{\partial t}\right)_{\text{oxidation}} \qquad (7.68)
$$

Assuming the fuel-nitrogen is uniformly distributed throughout the
char, the oxidation rate of the nitrogen should therefore equal the
product of the instant oxidation rate of the carbon and the mole ratio

of the fuel nitrogen to carbon in the char in that instant (Wendt and Schulze, 1976). We have

$$\left(\frac{\partial N}{\partial t}\right)_{oxidation} = \left(\frac{\partial C}{\partial t}\right)_{oxidation} \cdot \left(\frac{N}{C}\right) \qquad (7.69)$$

As it has been mentioned earlier, the carbon loss during combustion is exclusively due to oxidation, i.e.,

$$\frac{dC}{dt} = \left(\frac{dC}{dt}\right)_{oxidation} = \left(\frac{\partial C}{\partial t}\right)_{oxidation} \qquad (7.70)$$

Combining Equations (7.68), (7.69), and (7.70), gives

$$\frac{dN}{dt} = \left(\frac{\partial N}{\partial t}\right)_{pyrolysis} + \left(\frac{dC}{dt}\right) \cdot \left(\frac{N}{C}\right) \qquad (7.71)$$

A first-order fuel-nitrogen pyrolysis kinetics (Pohl, 1976) gives

$$\left(\frac{\partial N}{\partial t}\right)_{pyrolysis} = -k_{py} \cdot N \qquad (7.72)$$

Substituting Equation (7.72) into Equation (7.71) yields

$$\frac{dN}{dt} = -k_{py} \cdot N + \left(\frac{N}{C}\right) \cdot \left(\frac{dC}{dt}\right) \qquad (7.73)$$

As indicated by Equation (7.73), in order to describe the reaction rate of char-nitrogen during combustion, $\frac{dN}{dt}$, both k_{py}, the rate constant of char-nitrogen devolatilization, and $\frac{dC}{dt}$, the carbon oxidation rate,

have to be determined. In previous Sections, char oxidation kinetics has been obtained. Since the intrinsic oxidation rate of the char was obtained on a dry-ash-free basis and a dry-ash-free char is virtually carbon (note that 1750 K lignite char has a carbon content of 96.46% d.a.f.), the reaction rate of char can with good approximation be regarded as the reaction rate of carbon. The carbon oxidation rate, $\frac{dC}{dt}$, can therefore be obtained directly from Equation (7.65). Our immediate task here is then to find char-nitrogen pyrolysis rate constant, k_{py}. It can be obtained from the time dependence of nitrogen to carbon ratio. The slopes of the lines in Figure 7.6 yields $d \ln(N/C)/dt$. This may be equated to k_{py} as follows:

$$\frac{d}{dt}\left(\frac{N}{C}\right) = \frac{1}{C}\left[\frac{dN}{dt} - \left(\frac{N}{C}\right)\cdot\left(\frac{dC}{dt}\right)\right] \tag{7.74}$$

Multiplying both sides by C and rearranging the terms, we obtain

$$\frac{dN}{dt} = C \frac{d}{dt}\left(\frac{N}{C}\right) + \left(\frac{N}{C}\right)\cdot\left(\frac{dC}{dt}\right) \tag{7.75}$$

Comparing Equation (7.73) and (7.75), gives

$$C \frac{d}{dt}\left(\frac{N}{C}\right) = -k_{py} \cdot N \tag{7.76}$$

Upon rearrangement, we have

$$\frac{1}{(N/C)} \frac{d}{dt} (N/C) = -k_{py} \tag{7.77}$$

or

$$\frac{d}{dt} \left[\ln\left(\frac{N}{C}\right) \right] = -k_{py} \tag{7.78}$$

In this manner, we can obtain k_{py} by determining the slope of the semi-logarithmic plot of N/C versus time. The results are tabulated in Table 7.7. Finally, an Arrhenius-type correlation for the pyrolysis of char-nitrogen can be obtained by plotting $\ln k_{py}$ versus $1/T_p$. (Note that the particle temperature, T_p is slightly different from the gas temperature, T_F, see Section 7.4.2). This is shown in Figure 7.17. The char-nitrogen pyrolysis rate constant is therefore given by the following expression:

$$k_{py} = 5.8 \times 10^3 \cdot \exp\left[\frac{-29,100}{RT}\right] \text{ sec}^{-1} \tag{7.79}$$

The kinetics of pyrolysis so obtained can be compared with that obtained by Pohl (Section 7.1.1).

It should be noted that Pohl's pyrolysis kinetics were derived from the initial stage of coal-nitrogen devolatilization while in this study the data were obtained on char that has already lost 73% of the coal-nitrogen during the char production process. Pohl's pyrolysis kinetics has an activation energy of 22.7 Kcal/mole which is slightly lower than the activation energy obtained in this study, i.e., 29.1 Kcal/mole. This

TABLE 7.7

PYROLYSIS RATE CONSTANTS OF CHAR-NITROGEN

T_F K	P_{O_2} atm	k_{py} sec^{-1}
1250	0.2	0.06
1250	0.4	0.06
1500	0.2	0.51
1500	0.4	0.51
1750	0.2	1.72
1750	0.4	1.72

$k_{py,0} = 5.8 \times 10^3 \ sec^{-1}$

$E = 29,100 \ \frac{cal}{g\text{-}mole}$
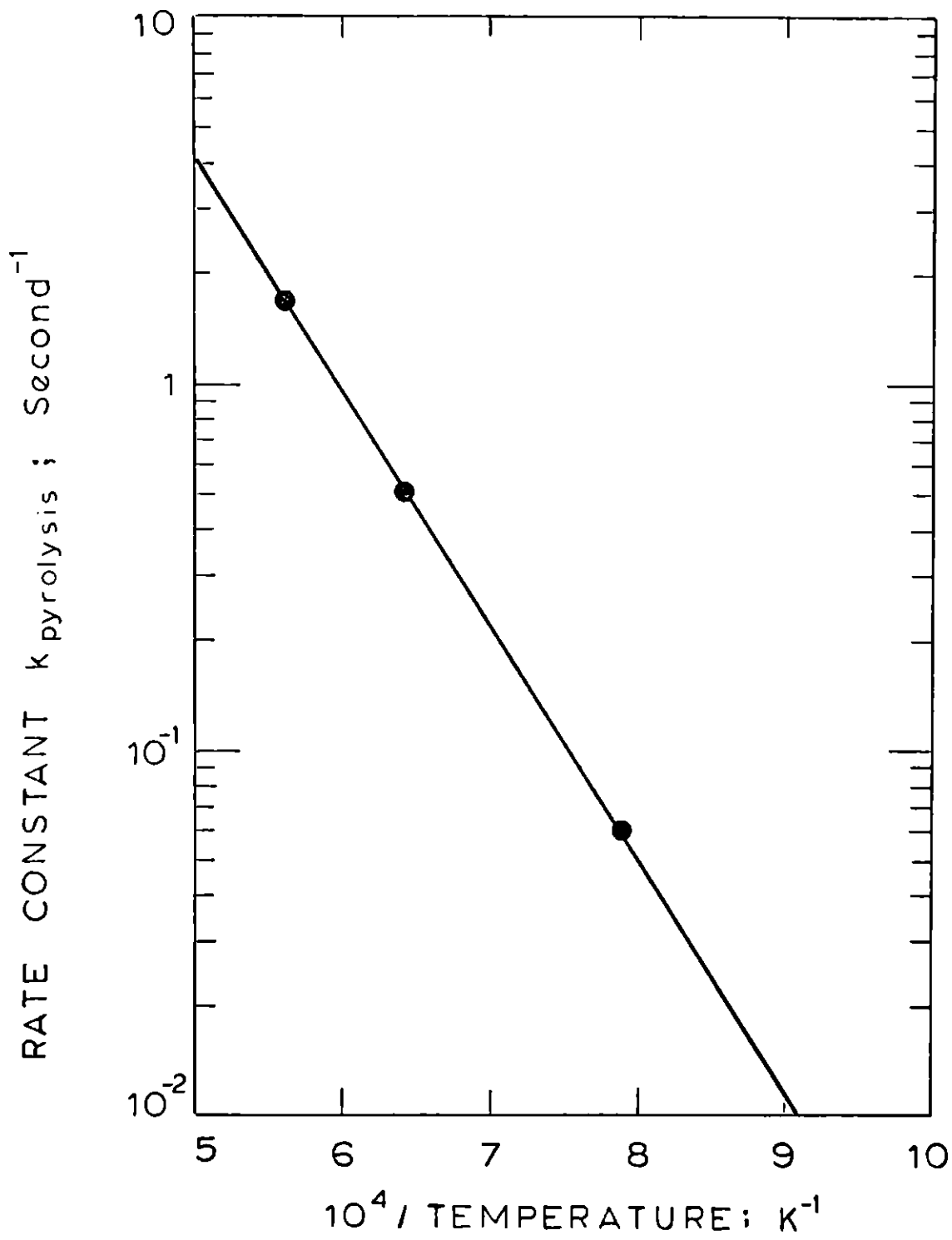
Figure 7.17

Arrhenius Plot of Pyrolysis Rate Constant for Char Nitrogen

difference may be explained by the fact that pyrolysis can be modelled by parallel reactions with different activation energies (Anthony, 1974; Anthony, Howard, Hottel and Meissner, 1975). The activation energies for the initial stages of devolatilization are expected to be low. As the devolatilization proceeds toward completion, the pyrolysis rate slows down as a consequence of the increase in the activation energy of the controlling reaction. This explains why the observed activation energy (in fact, that is the average activation energy) in Pohl's studies was found to be slightly lower than the observed activation energy in this study.

Pohl's time-resolved measurements extended to a time of 1 second while the measurements in this study started from a time of 1 second. Both sets of data should be compared at the transition time of 1 second. The data on nitrogen retention in Figure 7.6 are combined with those obtained by Pohl (1976). The combined results are shown in Figure 7.18. Pohl's data points in Figure 7.18 are directly reproduced from Figure 7.1. The data points of this study in Figure 7.18 are obtained by translating the information in Figure 7.6 in the following manner:

1. Multiplying $(N/C)_f/(N/C)_i$ in Figure 7.6 by 0.27 to obtain the values for nitrogen retention based on original coal-nitrogen. (Note that the fresh char has retained 27% of the original coal-nitrogen).

2. Adding 1000 milliseconds to the time scale in Figure 7.6 because, before the oxidation, the char has been pyrolyzed for
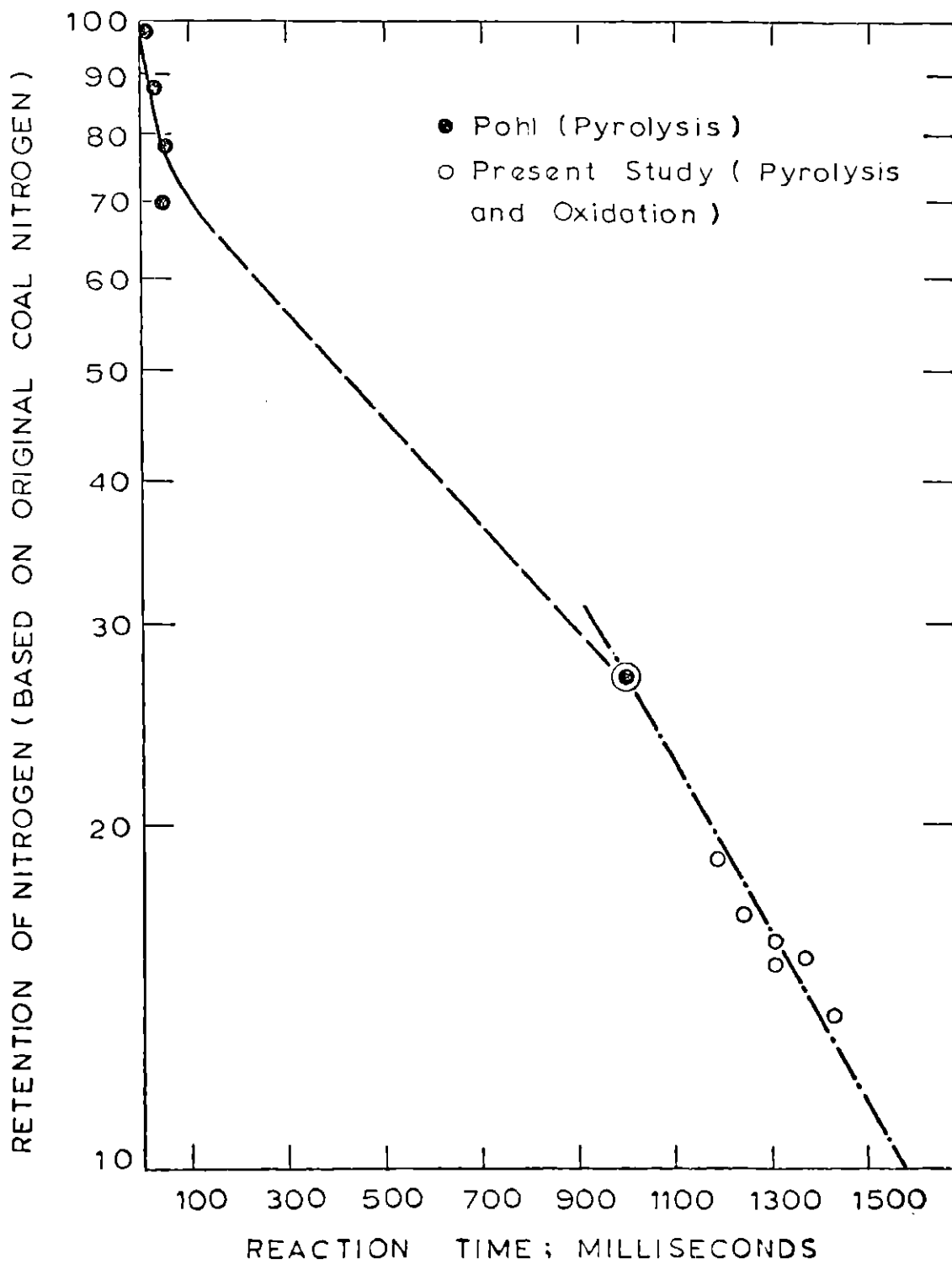
Figure 7.18

Retention of Fuel Nitrogen as Function of Reaction Time

During Pyrolysis and Oxidation

1 second during the char production process.
Only the results obtained at furnace temperature of 1750 K are compared in Figure 7.18. As expected, there is a good agreement between the absolute value of the pyrolysis kinetics constant obtained in this study and the constant obtained by Pohl. The absolute value of the pyrolysis kinetic constant obtained in this study at 1750 K and 1000 milliseconds is 1.72 $\sec^{-1}$ while the kinetic constant from Pohl's study has been calculated to be 1.06 $\sec^{-1}$ at the same reaction time.

The good agreement between the pyrolysis kinetics obtained from combustion experiments with the corresponding values from pyrolysis experiments indicates that combustion experiments can be designed to yield data on both pyrolysis kinetics and oxidation kinetics for coal-nitrogen. Therefore, separate studies of coal-nitrogen devolatilization can be bypassed.

In summary, the reaction rate of char-nitrogen during combustion, $\frac{dN}{dt}$, can be described by the following rate expression:

$$\frac{dN}{dt} = -k_{py} \cdot N + \left(\frac{dC}{dt}\right) \cdot \left(\frac{N}{C}\right) \tag{7.80}$$

where k_{py} is given by Equation (7.79) and $\frac{dC}{dt}$ is the oxidation rate of carbon, given by Equation (7.66).

7.10 Conclusions

Char burnout experiments were conducted to determine parameters of the char-nitrogen oxidation kinetics. The char used was produced by

pyrolyzing lignite particles at 1750 K for one second so that it was practically "volatile-free" but retained a significant portion of the nitrogen from the coal and therefore, was suitable for char-nitrogen oxidation studies. Time-resolved weight loss measurements were obtained at temperatures of 1250 K, 1500 K and 1750 K and oxygen partial pressures of 0.2 atm and 0.4 atm. Selected char samples were further analyzed for both physical characteristics and chemical compositions.

For the overall char burnout process, pore diffusion has been identified as the rate determining step. A pore diffusion model was developed and the effectiveness factors based on the initial rates were found to have values between about 0.03 and 0.09 over the entire range of conditions studied. From the model, an intrinsic reaction order with respect to oxygen was found to be 0.98. This reaction order was used to calculate an activation energy of 22,100 cal/g-mole. The overall intrinsic rate constant per unit B.E.T. surface area for the char oxidation was determined as

$$k_B = 2.8 \times 10^3 \cdot \exp\left(-\frac{22,100}{RT}\right) \ \frac{cm}{sec}\left(\frac{g\text{-moles}}{cm^3}\right)^{0.02}$$

From the variation during combustion of the B.E.T. surface area and the average pore diameter, it was evident that in the initial stage of the combustion, small pores were opening up, while in the latter stage, the char burned both externally and internally at an approximately constant diameter until it fragmented. The reactivity of the char

remained constant in the early stage of the burnout process but dropped dramatically in the late stage. This behavior was successfully explained by a pore-mouth poisoning model which has proved to be physically consistent with the combustion process. The reaction rate of char at any time could be determined from its initial reaction rate with a correction of reactivity change due to both the poisoning in the pore mouth and the change in total B.E.T. surface area.

As to the behavior of char-nitrogen during combustion, there was no selectivity between nitrogen and carbon loss during oxidation. The char-nitrogen, however, could undergo pyrolysis in parallel with oxidation.

Parameters of the kinetics of char-nitrogen evolution were obtained from experimentally determined, time resolved nitrogen to carbon ratios in the residual char during combustion. The first-order pyrolysis rate constant of char-nitrogen was given by the following expression:

$$k_{py} = 5.8 \times 10^3 \cdot \exp\left(\frac{-29,100}{RT}\right) \ \sec^{-1}$$

This kinetic constant of char-nitrogen pyrolysis obtained from combustion experiments has been found to be in a good agreement with that obtained from pure pyrolysis studies.

The oxidation rate of char-nitrogen was correlated to the oxidation rate of carbon, $\frac{dC}{dt}$, with a factor equal to the mole ratio of the fuel nitrogen to carbon, i.e.,

$$\left(\frac{\partial N}{\partial t}\right)_{oxidation} = \left(\frac{dC}{dt}\right) \cdot \left(\frac{N}{C}\right)$$

Since the pyrolysis rate and the oxidation rate of char-nitrogen are additive, the total consumption rate of char-nitrogen during combustion, $\frac{dN}{dt}$, is finally described by the following formula:

$$\frac{dN}{dt} = -k_{py} \cdot N + \left(\frac{dC}{dt}\right) \cdot \left(\frac{N}{C}\right)$$

CHAPTER 8

KINETIC STUDY II. REDUCTION

OF NITRIC OXIDE BY CHAR

Having focused our attention on the formation kinetics of NO_x from

char in the last Chapter, we shall consider in this Chapter the destruc-

tion kinetic of NO_x - more specifically, the reduction kinetics of NO_x

by char.

8.1 Previous Work

In an experimental effort to investigate the NO_x emission from a

fluidized bed coal combustor, Gibbs, Pereira and Beér (1976) have observed

a reaction between NO_x and char resulting in significant reduction of

NO_x during the combustion of coal. Although the char was known to react

with NO_x in the absence of oxygen (Edwards, 1972), it was not expected

up until then that the reaction would occur also in the presence of

oxygen. So they decided to further explore this problem - the reduction

of NO_x by char in fluidized bed combustor under simulated conditions,

and have reached the following conclusions:

The reaction between NO_x and char in fluidized bed,

1. had a relatively low activation energy (16 kcal/g-mole)

2. was first order with respect to NO_x

3. was strongly dependent on the char particle size.

The above generalizations were partially supported by Furusawa, Kunii,

Oguma and Yamada (1977), who studied the reduction of NO_x in a fixed
bed reactor with a dilute mixture of carboneceous materials (e.g., char
or activated carbon) in the temperature range of 750 to 1250 K. They
also found that the reduction of NO_x was first order with respect to
NO_x concentration. Interestingly enough, they observed three tempera-
ture ranges with different activation energies. The activation energies
for the reaction between NO_x and a Taiheiyo coal char are tabulated
below:

Temperature Range K	Activation Energy Kcal/mole
1183 - 1056	39.7
1056 - 993	57.1
993 - 773	17.3

We shall provide, in Section 8.9, a comparison of these results with
those from the present study and the results from a recent parallel
study at M.I.T. (Chan, 1977).

Figure 8.1, which is reproduced from Furusawa et al., summarizes
the NO_x reduction rate constants from different investigators.

8.2 Objectives and Scope

It is evident that the NO/Char reactions are important in deter-
mining the net NO_x emissions from fluidized bed coal combustors. In
Chapter 6, the conversion efficiency of char-nitrogen to NO_x was found
to be lower than that of volatile-nitrogen under corresponding conditions.
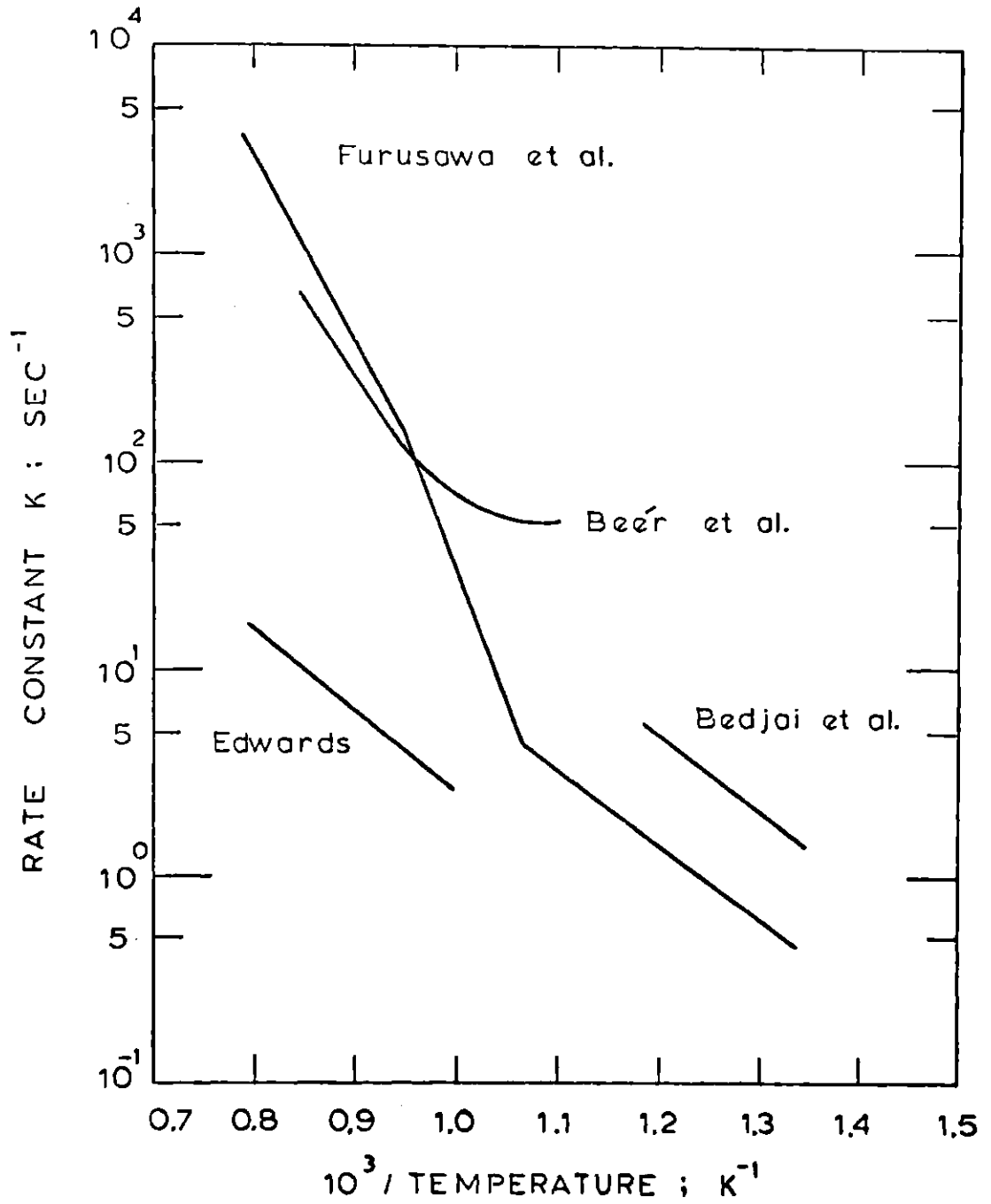
Figure 8.1

Summary of Past Work on the Rate Constants for Nitric Oxide Reduction by Char

(Furusawa et al., 1977)

This is possible by a consequence of the reduction of NO_x by char. In modelling the char-nitrogen conversion to NO_x, it is therefore essential to take into account the reduction of NO_x by char, which may begin soon after NO_x is formed on the pore walls and before it diffuses out of the porous char structure. In addition, a better understanding of the NO/Char reaction will, of course, provide information pertinent to the reduction of NO_x emissions by combustion modification.

Most of the previous studies have been carried out at relatively low temperatures (< 1250 K) in either fluidized beds or fixed beds. It has, therefore, been our intention to obtain kinetic information at temperature levels and for time intervals of interest in pulverized coal combustors.

Our immediate goal for this NO/Char study is to obtain kinetic data that would facilitate the determinations of reaction order, activation energy and effectiveness factor and thus to develop a kinetic model for the reduction of NO_x by char. To this end, the experiments were conducted under the following conditions:

Temperature K	NO_x Concentration, ppm, with balance gas of He or Ar		
1250	530 (He)	6400 (He)	
1500	530 (He)	6400 (He)	1100 (Ar)
1750	530 (He)	6400 (He)	1100 (Ar)

Three different inlet concentrations of NO_x were employed to enable

the determination of the reaction order. In addition, helium and argon were used as the inert constituents in the oxidant stream to test the effect of the diluent. Experiments were conducted at three temperature levels to facilitate the calculation of activation energy.

8.3 Kinetic Model of the Reduction of Nitric Oxide by Char in a Flow Furnace

It has been shown that the reaction between NO_x and char is thermodynamically favorable (Edward, 1972) and the favorable products are N_2, CO and CO_2. The overall reaction can be written as (Chan, 1977; Pereira, 1975)

$$(a+b)\ C + (a+2b)\ NO \rightarrow a\ CO + b\ CO_2 + \left[\frac{a}{2} + b\right] N_2 \qquad (8.1)$$
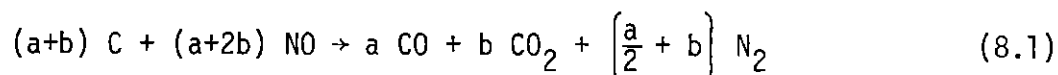
Apparently, the Char/NO_x reaction is analogous to the Char/O_2 reaction that has been dealt with in the last Chapter. In fact, NO may compete with O_2 for the char gasification reaction.

As it has been discussed in Chapter 7, the overall reaction process in a gas-solid system involves several steps. In developing a rate expression for a single porous solid particle, we must account for the various processes that may cause resistance to the reaction. For our present system, we may visualize these resistances as follows.

1. External gas film diffusion resistance

2. Internal pore diffusion resistance

3. Surface reaction resistance.

Both external gas film diffusion and internal pore diffusion have to
be determined in order to obtain the intrinsic reaction kinetics. In
the previous Chapter, on the Char/O_2 system, the surface oxygen concen-
trations were first evaluated in order to obtain the apparent kinetics,
then the effectiveness factors were calculated and finally the intrinsic
kinetics were determined. For the Char/NO system, we shall use a similar
approach with following modifications:

1. The external gas film diffusion resistance is first assumed to
   be negligible, the validity of this assumption will be tested
   as described in Section 8.7.

2. The internal pore diffusion resistance will be incorporated
   in the intrinsic kinetics rate expression by employing the
   effectiveness factor, η, defined as

$$\eta = \frac{\text{Apparent Rate}}{\text{Intrinsic Rate}} \tag{8.2}$$

8.3.1 The Rate Equation for the Reduction of Nitric Oxide by Char

For Char/NO reaction, a simple empirical rate expression is given
as:

$$-r_{NO} = k \cdot \eta \cdot [NO]^n \tag{8.3}$$

where

$-r_{NO}$ = consumption rate of NO per unit B.E.T. surface area
of char

k   = intrinsic rate constant for Char/NO reaction

η   = effectiveness factor due to internal pore diffusion of
     the system

[NO]= NO_x concentration in ppm

n   = reaction order with respect to [NO]

Since it has been suggested in most of the previous work that Char/NO reaction is a first order reaction (Edward, 1972; Pereira et al., 1976; Furursawa et al., 1977), n is assumed to be unity. The validity of this assumption will be checked later (see Section 8.5). Therefore,

$$-r_{NO} = \eta \cdot k \cdot [NO] \qquad (8.4)$$

8.3.2 Flow Furnace Reactor Model

Since our empirical rate expression, Equation (8.4), is relatively simple, an integral reactor analysis method will be employed here. Furthermore, a plug-flow approximation for the gas is assumed. The material balance of NO_x across a differential cross sectional segment of the furnace, at steady state, can be written as

$$F_{NO} = (F_{NO} + dF_{NO}) + (-r_{NO}) \cdot dA \qquad (8.5)$$

where

F_{NO} = input molar flow rate of NO_x to the segment

$F_{NO} + dF_{NO}$= output molar flow rate of NO_x from the segment

$$dA = \text{total B.E.T. surface area of char in this segment}$$

Noting that

$$dF_{NO} = d[F_{NO,in} (1 - X_{NO})] = -F_{NO,in} \, dX_{NO} \qquad (8.6)$$

where

$$F_{NO,in} = \text{inlet molar flow rate of } NO_x \text{ to the furnace}$$

$$X_{NO} = \text{conversion of } NO_x$$

We obtain on replacement

$$dA = F_{NO,in} \frac{dX_{NO}}{-r_{NO}} \qquad (8.7)$$

Since the density of the present system can be considered as constant, we have

$$dX_{NO} = d\left(\frac{c_{NO,in} - c_{NO}}{c_{NO,in}}\right)$$

$$= d\left(\frac{[NO]_{in} - [NO]}{[NO]_{in}}\right)$$

$$= -\frac{d[NO]}{[NO]_{in}} \qquad (8.8)$$

where

$C_{NO,in}$ = inlet molar concentration of NO_x in moles per volume gas

C_{NO} = concentration of NO_x in moles per volume gas

$[NO]_{in}$ = inlet concentration of NO_x in ppm

$[NO]$ = concentration of NO_x in ppm

Also note that

$$F_{NO,in} = C_{NO,in} \cdot u_{in} \tag{8.9}$$

where

u_{in} = volumetric flow rate of NO_x to the furnace

Substituting Equations (8.4), (8.8), (8.9) into Equation (8.7), we have

$$dA = \frac{C_{NO,in}}{[NO]_{in}} \cdot u_{in} \cdot \frac{1}{(\eta \cdot k)} \cdot \left(-\frac{d[NO]}{[NO]}\right) \tag{8.10}$$

If the ideal gas law is assumed to hold, we can relate $C_{NO,in}$, in mole/liter, to $[NO]_{in}$ by

$$C_{NO,in} \cdot (22.4) \cdot \left(\frac{298}{273}\right) \cdot 10^6 = [NO]_{in}$$

or

$$C_{NO,in} \cdot (2,445 \times 10^7) = [NO]_{in} \qquad (8.11)$$

Combining Equations (8.10) and (8.11), we have

$$dA = \frac{1}{2,445 \times 10^7} \cdot u_{in} \cdot \frac{1}{(n \cdot k)} \cdot (-d \ln[NO]) \qquad (8.12)$$

Now, as to the B.E.T. surface area, dA, of the char in this differential segment, it can be expressed as follows:

$$dA = A_B \cdot dW$$

$$= A_B \cdot \frac{W}{\tau} \cdot dt_g \qquad (8.13)$$

where

A_B = specific B.E.T. surface area of char used

dW = weight of char in the segment

W = total weight of char fed to the furnace

τ = total time required to feed W to the furnace

dt_g = residence time of NO_x in the segment

Note that a steady state feeding rate of char has been assumed in Equation (8.13). Substituting Equation (8.13) into Equation (8.12), we obtain

$$A_B \cdot \left(\frac{W}{\tau}\right) \cdot dt_g = - \frac{1}{2.445 \times 10^7} \cdot u_{in} \cdot \frac{1}{(\eta \cdot k)} \cdot d \ln[NO] \tag{8.14}$$

Equation (8.14) may be integrated and with the substitution of the following expression for t_g,

$$t_g = \frac{V}{u_{in} \cdot \frac{T_F}{273 + 25}} \tag{8.15}$$

where V is the effective volume of the furnace and T_F is the furnace temperature, and upon rearrangement, we finally obtain

$$(\eta \cdot k) = \frac{1}{7.286 \times 10^9} \cdot \frac{1}{A_B \cdot \frac{W}{\tau}} \cdot \frac{u_{in}^2}{V} \cdot T_F \cdot \ln \frac{[NO]_{in}}{[NO]_{out}} \tag{8.16}$$

Providing that

1) Char/NO reaction is a first order reaction

2) external gas film diffusion resistance is insignificant

Equation (8.16) can be used to evaluate the products of intrinsic rate constant and effectiveness factors, i.e., $(\eta \cdot k)$, under different conditions.

8.4 Experimental Results

Data on Char/NO reaction were obtained in the flow furnace, according to the procedures described in Chapter 5. The char was produced by the pyrolysis of a Montana lignite at a temperature of 1750 K for a residence time of one second, i.e., the same char used in Char/O_2

kinetic studies. Nitric oxide reduction experiments were carried out at temperatures of 1250 K, 1500 K and 1750 K, and inlet NO_x concentrations of 530 ppm, 1100 ppm, and 6400 ppm, with helium or argon as the inert constituent in the oxidant stream. No significant difference was observed between the results with helium and argon as a diluent. As indicated earlier, three different inlet concentrations of NO_x were employed to enable the determination of the reaction order and three different temperature levels were investigated to facilitate the calculation of activation energy.

The results were summarized in Table 8.1.

8.5 Test for the First Order Reaction Between Nitric Oxide and Char

A reaction mechanism is first order if the conversion of the reactant is independent of the inlet concentration. According to Equation (8.16), the values of

$$\frac{u_{in}^2}{W/\tau} \cdot \ln \frac{[NO]_{in}}{[NO]_{out}}$$

at any given temperature, should be independent of the inlet concentration of NO_x, i.e., $[NO]_{in}$, if the assumption that the Char/NO reaction is first order with respect to NO_x is valid. Table 8.2 and Figure 8.2 summarize the results of calculations. According to Figure 8.2, at any given temperature, the values of

TABLE 8.1

EXPERIMENTAL RESULTS OF CHAR/NITRIC OXIDE STUDY

T_F	$[NO]_{in}$	$[NO]_{out}$	u_{in}	W	τ
K	ppm	ppm	1/min	g	min
1250	530	447	3	0.6097	1
	530	459	3	0.6073	1
	6400	5800	3	0.6042	1.2
	6400	5800	3	0.6100	1.2
1500	530	311	3	0.6194	1
	530	320	3	0.6130	1
	6400	3810	3	0.6117	1
	6400	4030	3	0.6171	1
	1100	675	2.86	0.8059	1.5
	1100	766	3.15	0.4550	1
	1100	824	3.40	0.4343	1
1750	530	66.5	3	0.6086	1
	530	65.5	3	0.6121	1
	6400	877	3	0.6110	1.15
	6400	1574	3	0.6116	1.6
	6400	1145	3	0.6058	1.3
	1100	388	3.35	0.4636	1.3
	1100	413	3.30	0.4306	1.3

TABLE 8.2

CALCULATED RESULTS FOR CHAR/NITRIC OXIDE EXPERIMENTS

T_F K	$[NO]_{in}$ ppm	$\dfrac{u_{in}^2}{W/\bar{\tau}} \cdot \ln \dfrac{[NO]_{in}}{[NO]_{out}}$ $1^2/(min)(g)$
1250	530	2.52
	530	2.11
	6400	1.77
	6400	1.74
1500	530	7.74
	530	7.41
	6400	7.62
	6400	6.75
	1100	7.44
	1100	7.88
	1100	7.71
1750	530	30.75
	530	30.72
	6400	33.66
	6400	33.03
	6400	33.24
	1100	32.77
	1100	32.25
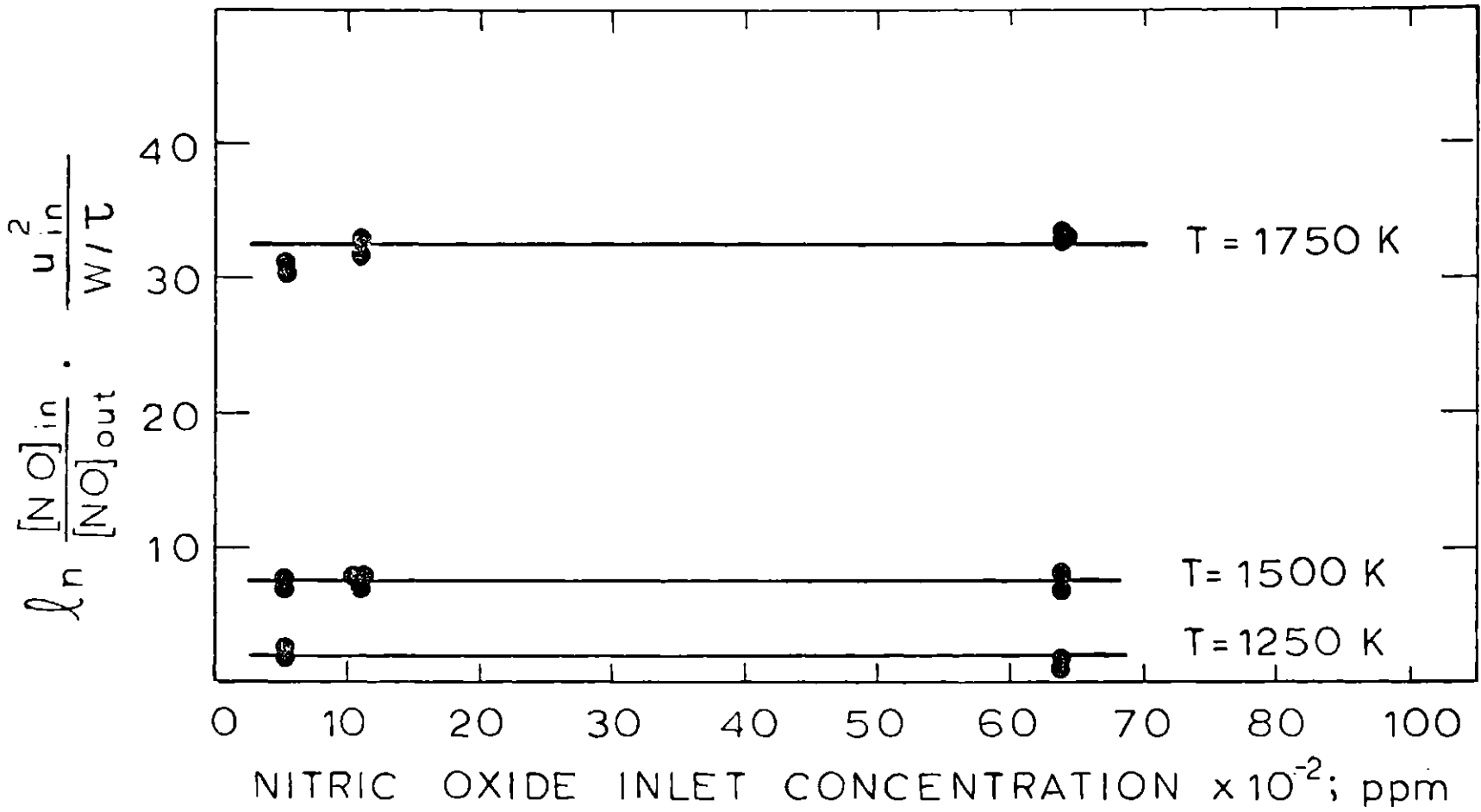
Figure 8.2

Test for a First-Order Kinetics of Nitric Oxide Reduction by Char

$$\frac{u_{in}^2}{W/\tau} \cdot \ln \frac{[NO]_{in}}{[NO]_{out}}$$

are independent of $[NO]_{in}$. Therefore, the char and NO_x reaction is indeed a first order reaction with respect to nitric oxide.

8.6 Estimation of Effectiveness Factors and Intrinsic Rate Constants

8.6.1 Calculation of $(\eta \cdot k)$

We have developed a kinetic model of the reduction of NO_x by char in a flow furnace in Section 8.3. The values of the product of the effectiveness factor, η, and the intrinsic rate constant, k, under different experimental conditions, can therefore be evaluated by Equation (8.16) and the results tabulated in Table 8.1. The results of $(\eta \cdot k)$ under different conditions were summarized in Table 8.3.

8.6.2 Estimation of η and k

Our next task is to estimate the effectiveness factors, η, under different conditions so that the intrinsic rate constants can be calculated by the expression

$$k = \frac{(\eta \cdot k)}{\eta} \tag{8.17}$$

For a first-order reaction on a spherical porous pellet, the effectiveness factor, η, is given by (Smith, 1970)

TABLE 8.3

RESULTS OF PRODUCTS OF η AND k

T_F K	$[NO]_{in}$ ppm	$(\eta \cdot k) \times 10^{10}$ $\dfrac{moles}{(sec)(m^2)(ppm)}$
1250	530	1.233 ± 0.140
	6400	0.926 ± 0.006
1500	530	4.811 ± 0.154
	6400	4.562 ± 0.401
	1100	4.873 ± 0.140
1750	530	22.77 ± 0.02
	6400	24.67 ± 0.23
	1100	24.08 ± 0.28

$$\eta = \frac{1}{\phi_s} \left[\frac{1}{\tanh 3\phi_s} - \frac{1}{3\phi_s} \right] \tag{8.18}$$

and ϕ_s is the Thiele-type modulus for a spherical particle, and is defined as

$$\phi_s = \frac{r_s}{3} \sqrt{\frac{k \cdot A_B \cdot \rho_B}{b \cdot D_e}} \tag{8.19}$$

where

r_s = radius of particle

k = intrinsic rate constant

A_B = specific B.E.T. surface area of char

ρ_B = bulk density of char

D_e = effective pore diffusivity (see Appendix F)

b = $4.1 \times 10^{-11} \dfrac{\text{g-mole}}{(\text{cm}^3)(\text{ppm})}$, is a conversion factor

Therefore, with Equations (8.17), (8.18), and (8.19) and values of $(\eta \cdot k)$ in Table 8.3, the effectiveness factors, η, and the intrinsic rate constants, k, can now be evaluated by trial-and-error and an iterative solution. Figure 8.3 shows the flow diagram for the computation scheme. The results were summarized in Table 8.4.

The effectiveness factor for the NO/Char system was close to unity at 1250 K. It decreased to 0.8 at 1500 K and decreased further to 0.4 at 1750 K. The decrease in effectiveness factor with increasing temperature implied the transition from a regime of chemical reaction

Evaluate $(\eta \cdot k)$ from Equation (8.16)

$\downarrow$

$\eta_{assumed} = 1$

$\downarrow$

$$k = \frac{(\eta \cdot k)}{\eta_{assumed}}$$

$\downarrow$

$$\phi_s = \frac{r_s}{3} \sqrt{\frac{k \cdot A_B \cdot \rho_B}{b \cdot D_e}}$$

$\downarrow$

$$\eta_{calculated} = \frac{1}{\phi_s}\left[\frac{1}{\tanh 3\phi_s} - \frac{1}{3\phi_s}\right]$$

$\downarrow$

Check: $\eta_{calculated} \overset{?}{=} \eta_{assumed}$

NO   YES
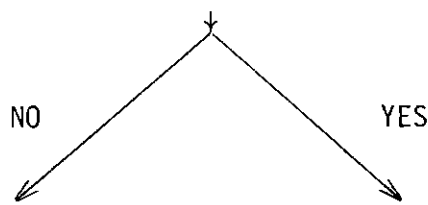
Let $\eta_{assumed} \equiv \eta_{calculated}$ Stop Calculation

$$\eta = \eta_{assumed}; \quad k = \frac{\eta \cdot k}{\eta_{assumed}}$$
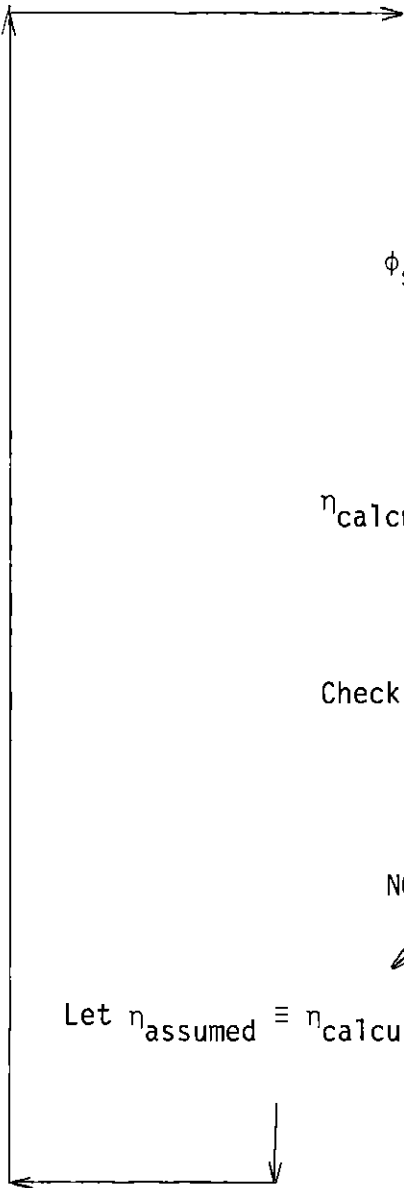
Figure 8.3

Flow Diagram for the Computations of Effectiveness Factors and Intrinsic
Rate Constants for Char/NO_x Reaction

TABLE 8.4

INTRINSIC RATE CONSTANTS AND EFFECTIVENESS FACTORS FOR CHAR/NITRIC

OXIDE REACTION

T_F K	$[NO]_{in}$ ppm	η	$k \times 10^{10}$ $\dfrac{moles}{(sec)(m^2)(ppm)}$
1250	530	0.94	1.312
	6400	0.94	0.986
1500	530	0.80	6.015
	6400	0.80	5.702
	1100	0.80	6.092
1750	530	0.40	56.92
	6400	0.40	61.67
	1100	0.40	60.22

control to a regime of internal pore diffusion control as the temperature of the system increased.

8.7 External Gas Film Diffusion Versus Chemical Reaction

In developing the kinetic model of the reduction of NO_x by char in a flow furnace, we have assumed that the external gas film diffusion resistance is negligible as compared to that of surface reaction (see Section 8.3). Our task in this Section is therefore to check the validity of that assumption. We shall estimate the external mass transfer coefficients for the NO/Char system for any given condition, then compare their magnitudes with those of the corresponding intrinsic rate constant obtained in Section 8.6 to prove the insignificance of the external mass transfer resistance.

To evaluate the external mass transfer coefficient of a gas-solid system, the following correlation for a flow past single spheres can be used (Bird, Stewart and Lightfoot, 1960).

$$Sh = \frac{k_g d_s}{D_g} = 2 + 0.6 \, (Sc)^{1/3} \, (Re)^{1/2} \qquad (8.20)$$

where

k_g = external mass transfer coefficient

d_s = diameter of spherical particle

D_g = bulk diffusivity of the fluid system

Sc = Schmidt number

Re = Reynolds number

Sh = Sherwood number

Since the bulk diffusivity, D_g, for NO-He system can be calculated by the Chapman-Enskog formula (see Appendix E), the external mass transfer coefficient, k_g, can therefore be estimated by the following expressions:

$$k_g \geq \frac{2D_g}{d_s} \tag{8.21}$$

or

$$(k_g)_{lower\ bound} = \frac{2D_g}{d_s} \tag{8.22}$$

The results of k_g and their comparisons with the rate constants, k, and the products of η and k were summarized in Table 8.5. Note that, for the purpose of comparison, the unit of the rate constant, k, has been converted to the same unit as that of k_g by the following expression:

$$k'\left[\frac{cm}{sec}\right] = k \ \frac{moles}{(sec)(m^2)(ppm)} \times 22400\left[\frac{cm^3}{mole}\right] \times \frac{T_F}{273} \times \frac{m^2}{10^4 \ cm^2} \times \frac{1 \ ppm}{10^{-6}}$$

As can be seen from Table 8.5, the external mass transfer coefficients are about six to seven orders of magnitude larger than the reaction rate constants.

This proves the validity of our early assumption that the external gas film diffusion resistance is negligible as compared to that of the surface chemical reaction. Therefore, the reaction rate

TABLE 8.5

COMPARISON OF KINETIC RATE CONSTANTS WITH

EXTERNAL MASS TRANSFER COEFFICIENTS

T_F K	k' $\dfrac{cm}{sec}$	$\eta \cdot k'$ $\dfrac{cm}{sec}$	k_g $\dfrac{cm}{sec}$
1250	1.178×10^{-3}	1.107×10^{-3}	5233
1500	7.371×10^{-3}	5.897×10^{-3}	7106
1750	8.558×10^{-2}	3.423×10^{-2}	9273

Note: The unit of the kinetic rate constant, k, has been converted to the

same unit as that of k_g by the following expression:

$$k' \frac{cm}{sec} = k \frac{mole}{(sec)(m^2)(ppm)} \times 22400 \frac{cm^3}{mole} \times \frac{T_F}{273} \times \frac{1 \ m^2}{10^4 \ cm^2} \times \frac{1 \ ppm}{10^{-6}}$$

constants obtained in Section 8.6 are indeed the true intrinsic kinetic rate constants for the conditions under investigation.

8.8 Intrinsic Activation Energy

Our kinetic model of the reduction of NO_x by char in a flow furnace has provided the possibility of the interpretation of our experimental results and the estimation of the intrinsic kinetic rate constants. The intrinsic activation energy of the reduction of NO_x by char can therefore be obtained from the slope of a plot of ln k versus $\frac{1}{T_F}$. This is shown in Figure 8.4.

The intrinsic activation energy of the reduction of NO_x by char has been estimated to be 32,700 cal/g-mole. The reduction rate constant per unit B.E.T. surface area is given by the following expression:

$$k = 5.0 \times 10^{-5} \exp(-32,700/RT) \quad \frac{moles}{(sec)(m^2)(ppm)} \qquad (8.23)$$

8.9 Comparison of the Intrinsic Kinetics of Present Study with that of Previous Work

As we have mentioned earlier, most of the previous work has heavily concentrated on a rather low temperature range and most of the kinetic data were obtained in either a fluidized bed or a fixed bed. No kinetic information on the reduction of NO_x by char obtained in a flow furnace under high temperature conditions pertinent to the pulverized coal combustors is available in the literature. The results
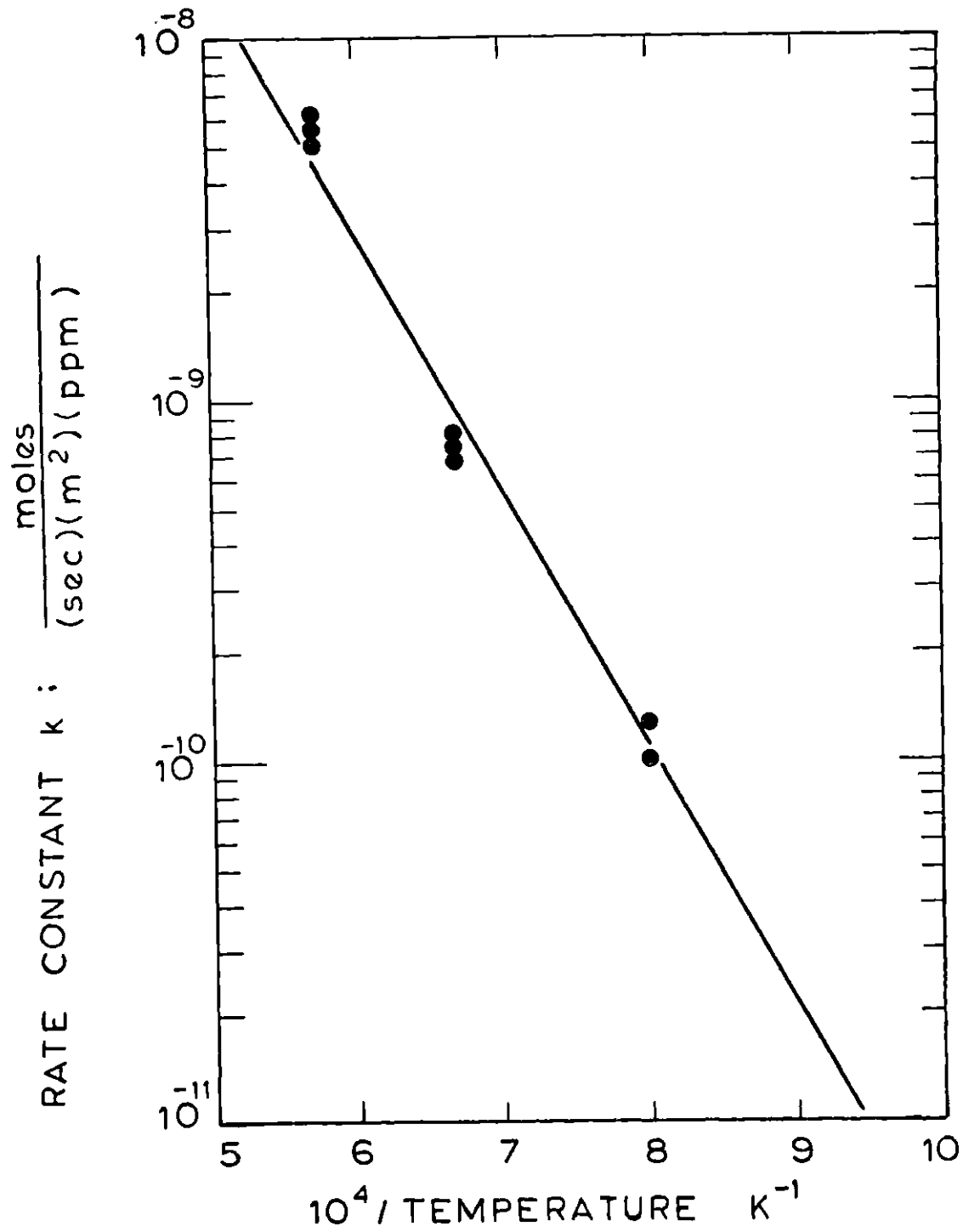
Figure 8.4

Arrhenius Plot of Intrinsic Rate Constant for Nitric Oxide Reduction by Char

obtained by Furusawa et al. in a fixed bed reactor represented the most complete information for the temperature conditions encountered in most of the fluidized bed coal combustors. Their results covered three different temperature ranges with different activation energies (see Section 8.1).

It is of interest to compare, in Figure 8.5*, the trend of the results from the present studies with that of the results by Furusawa et al. and the results obtained from a recent parallel study done at M.I.T. (Chan, 1977).

The results obtained from the present studies show an excellent agreement with the trend of high temperature results (1056 - 1183 K) by Furusawa et al. On the other hand, the results obtained from the parallel study at M.I.T. by Chan match well with the low temperature results (773 - 993 K) obtained by Furusawa et al.

In the light of the significant variation of intrinsic parameters with temperature it can be concluded that in modelling NO_x emission from coal combustion systems, the extrapolation as well as interpolation of NO/Char kinetics has to be done with great care.

---

*For the purpose of comparison, the unit of the rate constant, k, obtained from the present studies has been converted to $\frac{moles}{(hr)\ (Kg)}$ by the following expression:

$$k^* \frac{moles}{(hr)\ (Kg)} = k \frac{moles}{(sec)(m^2)(ppm)} \times 175\ \frac{m^2}{gm} \times \frac{10^3\ gm}{1\ Kg} \times \frac{3600\ sec}{1\ hr} \times \frac{1\ ppm}{10^{-6}}$$
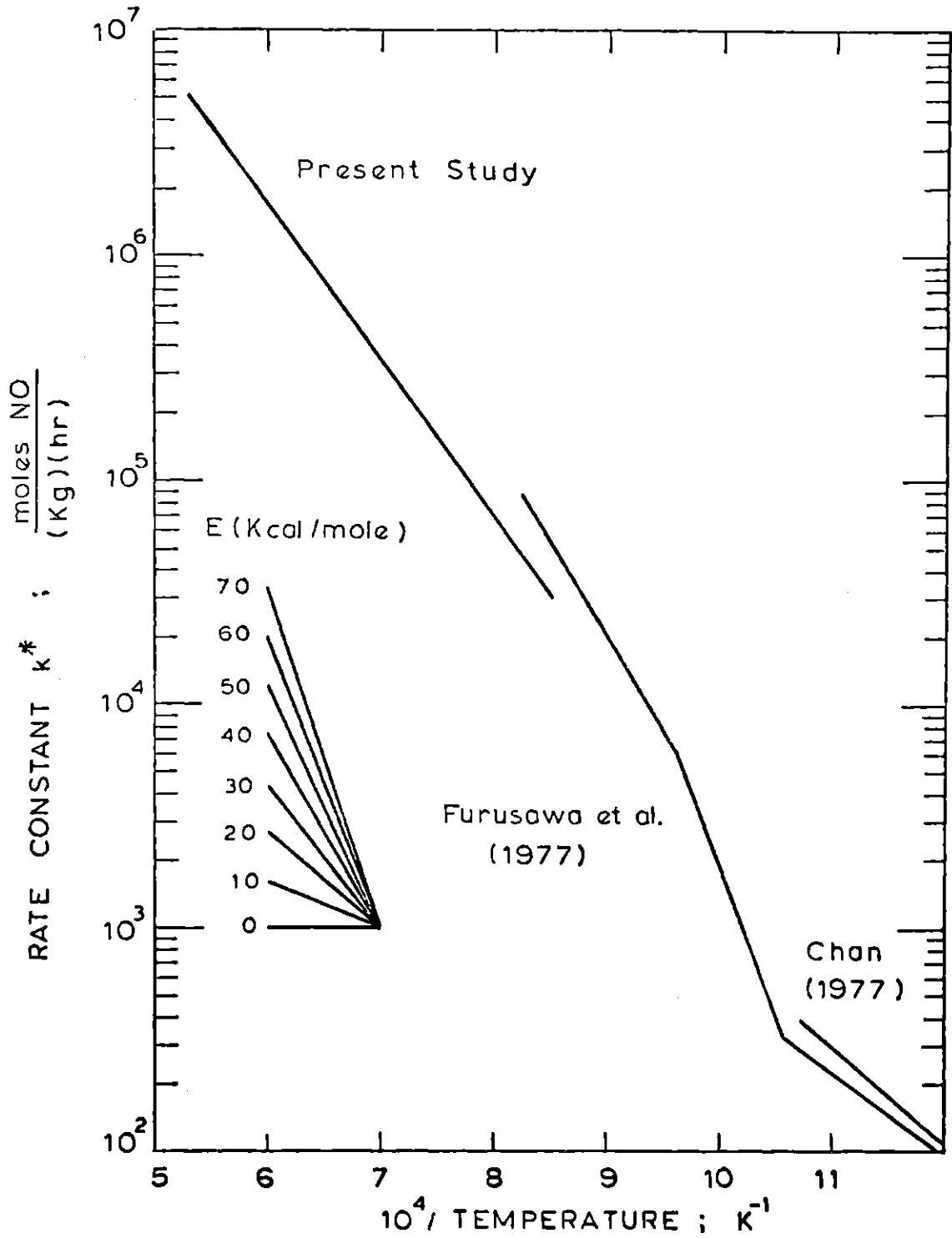
Figure 8.5

Comparison of Rate Constants for Nitric Oxide Reduction by Char

8.10 Comparison of Char/NO$_x$ Reaction with Char/O$_2$ Reaction

It is of interest to compare the intrinsic reactivity of Char to NO$_x$ reported in this Chapter with that of Char to oxygen reported in Chapter 7.

The intrinsic rate constants per B.E.T. surface area and the orders for both reactions are summarized below:

For Char/O$_2$ reaction:

$$k_B = 2.8 \times 10^3 \exp(-22,100/RT) \quad \frac{cm}{sec}\left(\frac{g\text{-moles}}{cm^3}\right)^{0.02}$$

$$m = 0.98$$

For Char/NO$_x$ reaction:

$$k = 5.0 \times 10^{-5} \exp(-32,700/RT) \quad \frac{moles}{(sec)(m^2)(ppm)}$$

$$n = 1.0$$

As expected, the activation energy is higher for Char/NO$_x$ reaction than that for Char/O$_2$ reaction.

To compare the absolute reaction rates, let us consider a reaction system at 1500 K and a total pressure of 1 atm. Let us also assume that the partial pressures for both O$_2$ and NO$_x$ are 0.1 atm respectively. Thus, the absolute rates can be calculated to be

1.814×10^{-6} moles $C/(cm^2$ sec) for Char/O_2 reaction and 8.594×10^{-9} moles $C/(cm^2$ sec) for Char/NO_x reaction. As can be seen, the rate for Char/O_2 reaction is about two orders of magnitude higher than the rate for Char/NO_x reaction under the conditions specified above.

It is to be noted that the effectiveness factors for both reactions are distinctly different, and effectiveness factors have to be taken into account when considering the overall reaction rates. For the conditions specified above, the effectiveness factors are about 0.04 for Char/O_2 reaction in this study and about 0.8 for Char/NO_x reaction. In addition, the reactivity of char to O_2 decreased with char burnout while no decrease in the reactivity of char to NO_x was observed, for there was no appreciable consumption of char in the Char/NO_x study.

In summary, the Char/NO_x reaction is analogous to the Char/O_2 reaction. The NO_x might compete with O_2 for the char gasification reaction, although the intrinsic rate for Char/NO_x is much slower than that for Char/O_2 reaction.

8.11 Practical Implications

This Chapter has been devoted to the study of the reaction between NO_x and char. The purpose of the study was to gain insight into the kinetics of NO_x reduction by char under conditions encountered in pulverized coal flames. The results from this study indicate that NO_x can, indeed, significantly be reduced by the contact with char, but the importance of this reduction under practical conditions has yet to be established.

The reduction of NO_x is strongly dependent upon temperature level and char availability. Figure 8.6 shows the effects of temperature and char loading using data obtained from this study. The residence time of gas has been assumed to be one second.

This figure predicts that at 1750 K, about 40% of NO_x can be reduced with a practical char loading (i.e., $5 \times 10^{-3} \sim 10^{-2}$ g/l). At lower temperature levels, i.e., 1500 K or 1250 K, however, the reductions of NO_x are not so significant as that at 1750 K. To reach 40% reduction of NO_x at these low temperature levels, it requires an unrealistically high char loading, unless the residence time can be extended to a longer duration.

Brown, Mason and Neubauer (1977), who studied staging parameters for NO_x control in coal fired boilers, have observed that, at a high load, the increased first stage residence time had a major effect on NO_x reduction. Our model certainly provides an explanation to their experimental finding.

The kinetics obtained in the present study have also been extrapolated to reasonably higher temperatures. Figure 8.6 also shows the NO_x reduction at 2000 K and 2250 K using the extrapolated rate constants and effectiveness factors. The NO_x reduction is very significant at these high temperature levels even with low char loading. It is hoped that this information can provide a useful guideline for the designers of high temperature combustion systems, e.g., coal-fired magnetohydrodynamic (MHD) power generation combustors.
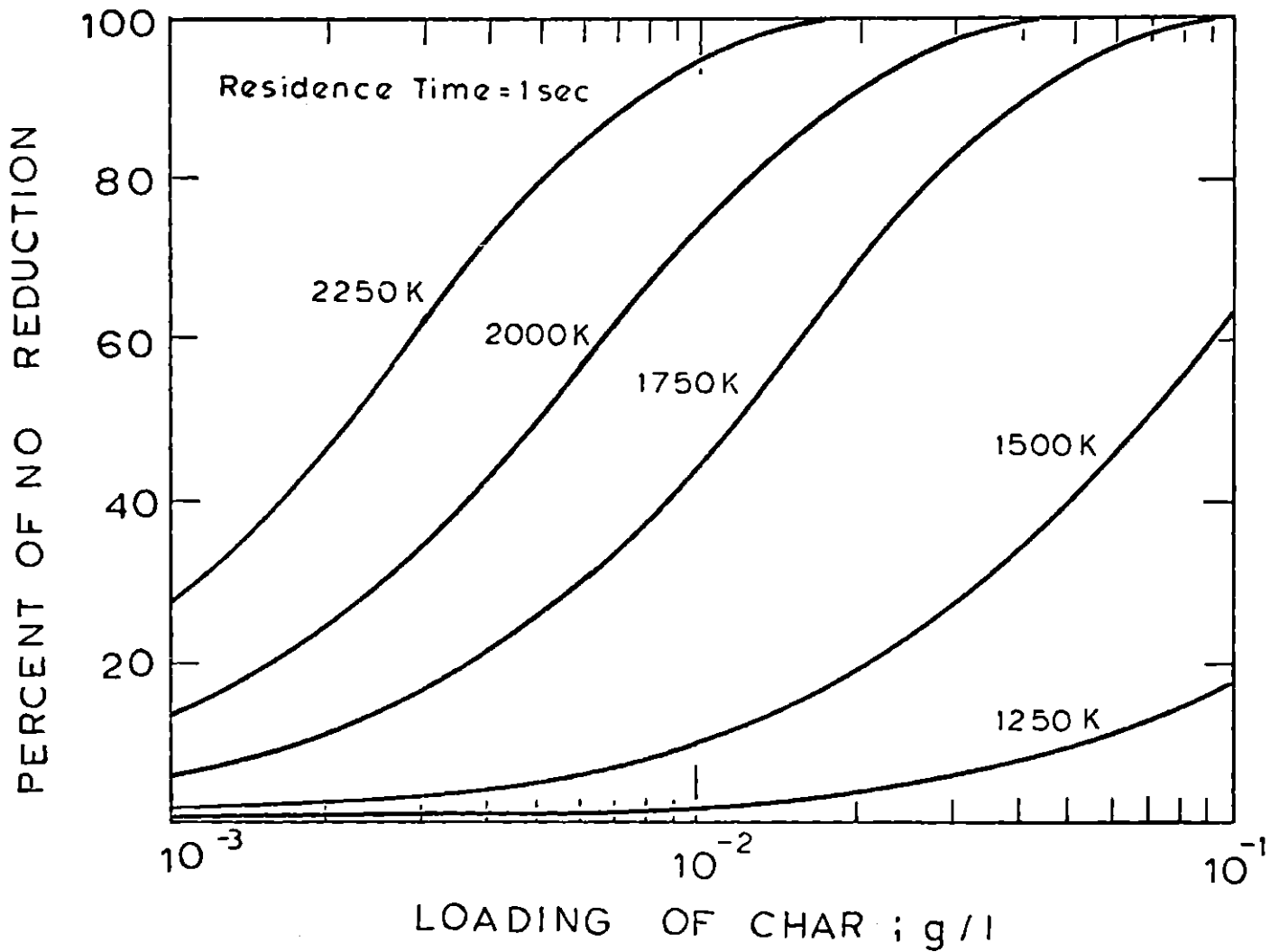
Figure 8.6

Potential Nitric Oxide Reduction as Function of Char Loading and Temperature

8.12 Conclusions

It has been shown that the NO/Char reaction plays an important role in determining the net NO_x emissions from a combustion system, therefore, for the completion of the modelling of NO_x emissions from coal combustors, it is necessary to take into account the reduction of NO_x by char.

Experiments were conducted in the flow furnace under high temperature conditions pertinent to the pulverized coal combustors to enable the calculation of kinetic constants for the model. The following conclusions have been reached from the present studies.

1. The external gas film diffusion resistance is of no significance in the NO/Char system under conditions of interest in pulverized coal combustors.

2. Reduction of NO_x by char is a first order reaction with respect to NO_x.

3. The effectiveness factor for the NO/Char system is close to unity at a temperature as low as 1250 K. It decreases as the temperature increases. This implies the transition from a regime of chemical reaction control to a regime of internal pore diffusion control as the temperature of the sytem increases.

4. The activation energy for the NO/Char reaction is calculated to be 32,700 cal/g-mole and the intrinsic rate constant per unit B.E.T. surface area is given by

$$k = 5.0 \times 10^{-5} \exp (-32,700/RT) \frac{moles}{(sec)(m^2)(ppm)}$$

5. The present results appear to fit the overall trend of previous
   work, although no previous data have been obtained in a
   temperature range as high as that of the present studies.

CHAPTER 9

CONCLUSIONS

The major contributions of this thesis are the determination of the effects of temperature and fuel/oxygen equivalence ratio on the conversion of fuel nitrogen to NO_x and the elucidation of the roles played by the oxidation of char-nitrogen and the nitric oxide-char reactions on the overall coal-nitrogen conversion. Data developed during this thesis work allow the following conclusions to be drawn:

A. Coal-Nitrogen Conversion

1. The conversion of coal-nitrogen to NO_x decreased monotonically with increasing fuel/oxygen equivalence ratios.

2. The conversion of char-nitrogen to NO_x followed a trend similar to that of the raw coal, however, the char-nitrogen conversion efficiencies were lower than the corresponding values for the coal-nitrogen.

3. Volatilized nitrogen compounds accounted for a major fraction of NO_x produced from coal-nitrogen especially at high temperatures and low fuel/oxygen equivalence ratios.

4. The char-nitrogen contributions to NO_x emission could not be neglected particularly at high fuel/oxygen equivalence ratios and low temperatures.

5. Increasing temperature increased the volatile contribution to NO_x but decreased the efficiency with which it was converted to

NO_x.

6. For the fuel/oxygen equivalence ratios in a range of interest to practical coal combustors, the total coal-nitrogen conversion to NO_x remained constant when the temperature increased from 1250 K to 1500 K, while it decreased by about 20% to 25% when the temperature increased from 1500 K to 1750 K.

B. Coal Char Oxidation

1. For the overall char burnout process, the internal pore diffusion was identified to be the rate determining step. A pore diffusion model was developed and the effectiveness factors based on the initial rates were found to have values between about 0.03 and 0.09 over the entire range of conditions studied.

2. From the model, an intrinsic reaction order with respect to oxygen was found to be 0.98. This reaction order was used to calculate an activation energy of 22,100 cal/g-mole. The overall intrinsic rate constant per unit B.E.T. surface area for the char oxidation was determined as

$$k_B = 2.8 \times 10^3 \exp\left(-\frac{22100}{RT}\right) \quad \frac{cm}{sec} \left(\frac{g\text{-moles}}{cm^3}\right)^{0.02}$$

3. The reactivity of the char remained constant in the early stage of the burnout process but dropped dramatically in the late stage. This behavior was successfully explained by a pore-mouth poisoning model.

4. There was no selectivity between nitrogen and carbon loss during oxidation but the char-nitrogen could undergo pyrolysis in parallel with oxidation.

5. A first-order pyrolysis rate constant of char-nitrogen was obtained from the time-resolved nitrogen to carbon ratio in the residual char during combustion, and was given by the following expression:

$$k_{py} = 5.8 \times 10^3 \cdot \exp\left(\frac{29,100}{RT}\right) \quad \sec^{-1}$$

6. The oxidation rate of char-nitrogen was correlated to the oxidation rate of carbon, $\frac{dC}{dt}$, with a factor equal to the mole ratio of the fuel nitrogen to carbon, i.e.

$$\left(\frac{\partial N}{\partial t}\right)_{oxidation} = \left(\frac{dC}{dt}\right) \cdot \left(\frac{N}{C}\right)$$

7. The pyrolysis rate and the oxidation rate of char-nitrogen were found to be additive. The total consumption rate of char-nitrogen during combustion, $\frac{dN}{dt}$, was successfully described by the following formula:

$$\frac{dN}{dt} = -k_{py} \cdot N + \left(\frac{dC}{dt}\right) \cdot \left(\frac{N}{C}\right)$$

C. Reduction of Nitric Oxide by Char

1. The external gas film diffusion resistance was of no significance in the NO/Char system under conditions of interest in pulverized coal combustions.

2. Reduction of NO_x by char was a first order reaction with respect to NO_x.

3. The effectiveness factor of the NO/Char system was close to unity at a temperature as low as 1250 K. It decreased as the temperature increased. This implied the transition from a regime of chemical reaction control to a regime of internal pore diffusion control as the temperature of the system increased.

4. The activation energy for NO/Char reaction was found to be 32,700 cal/g-mole and the rate constant per unit B.E.T. surface area was given by

$$k = 5.0 \times 10^{-5} \exp\left(\frac{-32,700}{RT}\right) \qquad \frac{moles}{(sec)(m^2)(ppm)}$$

CHAPTER 10

RECOMMENDATIONS

The results of this investigation have provided numerous
suggestions for the improvement of the experimental procedures and
recommendations for future studies. They are listed as follows.

A. Suggestions for the Improvement of the Experimental Procedures

   1. The particle surface temperature should be measured by a
       two-color pyrometer or other technique which is adaptable
       to the furnace system.

   2. The particle velocities and residence times under any
       experimental conditions should be determined experimentally
       by some practical techniques.

B. Subjects Recommended for Future Studies

   1. The interactions between volatile-nitrogen and char-nitrogen
       should be studied to check the validity of the first order
       approximation in our parametric studies which assumes no
       interference between volatile-nitrogen and char-nitrogen. Or
       more specifically, the dependence between volatile-nitrogen
       conversion and char-nitrogen conversion should be investigated.

   2. In addition to the pore-mouth poisoning model, other possible
       rationalizations that can explain realistically the dramatic

change of char reactivities during combustion should also be investigated. Experiments should be designed in such a way that the hypothesis of surface annealing or active sites change can be tested.

3. The importance of the char-catalyzed reaction between NO_x and CO should be assessed. The kinetic data should be obtained for the modelling of NO_x emissions from coal combustors.

4. Kinetic studies of the reduction of NO_x by coal should be carried out to explore the perturbations on the overall NO_x destruction mechanism in coal combustors.

5. The models for the competing NO_x formation and NO_x destruction reactions should be used to explain the experimental observations on the net conversion of coal-nitrogen to NO_x.

6. Data on kinetics of both devolatilization and oxidation of coal-nitrogen should be obtained directly from time-resolved combustion experiments of other coals in order to verify the generality of the hypothesis formulated in this study that the pyrolysis rate and the oxidation rate of the coal-nitrogen are additive and separable during pulverized coal combustion.

APPENDIX A

RESULTS OF PARAMETRIC INVESTIGATIONS

The experimental data of the parametric investigations are summarized in Tables A.1 to A.5. Tables A.1 and A.2 are the results of oxidation experiments of Montana lignite at 1250 K and 1750 K, respectively. Table A.3 is the results of oxidation experiments of 1250 K lignite char at 1250 K and Table A.4 the results of 1750 K lignite char at 1750 K. Nitrogen analysis was performed only on selective residual char samples. Table A.5 summarizes the results of oxidation experiments of Montana sub-bituminous coal.

TABLE A.1

RESULTS OF OXIDATION EXPERIMENTS OF MONTANA LIGNITE AT 1250 K

Run Number	ϕ	Solid Weight Loss % d.a.f.	% of Fuel-N Converted to NO_x	% of Fuel-N Retained in Char
YLL-201	3.22	53.02		
YLL-204	1.36	78.12	13.35	26.51
YLL-205	1.12	85.07		
YLL-206	0.33	94.50		
YLL-209	2.78	56.16	4.70	55.87
YLL-211	3.58	52.04	5.41	56.88
YLL-213	2.98	59.50		
YLL-218	0.23	100.00	45.35	
YLL-220	0.38	92.07	35.05	10.72
YLL-221	0.61	84.05	26.29	
YLL-222	1.04	84.13	19.42	24.19
YLL-223	1.10	91.50	20.78	
YLL-224	0.59	90.11	27.67	13.67

TABLE A.2

RESULTS OF OXIDATION EXPERIMENTS OF MONTANA LIGNITE AT 1750 K

Run Number	ϕ	Solid Weight Loss, % d.a.f.	% of Fuel-N Converted to NO_x	% of Fuel-N Retained in Char
YLL-013	3.16	95.31	0.30	
YLL-014	0.31	100.00	40.34	
YLL-015	1.37	100.00	11.00	
YLL-016	1.21	100.00	6.69	
YLL-017	3.75	95.70	0.64	4.45
YLL-018	0.96	99.40	20.35	
YLL-019	0.43	100.00	32.95	
YLL-020	1.49	100.00	0.51	
YLL-251	1.29	100.00	15.95	
YLL-252	1.73	93.21	7.86	
YLL-253	1.67	100.00	5.69	
YLL-254	1.27	100.00	10.22	
YLL-256	0.75	100.00	23.67	
YLL-257	0.38	100.00	30.51	
YLL-258	0.85	100.00	18.35	
YLL-259	0.31	100.00	28.41	
YLL-260	0.70	100.00	27.17	
YLL-261	1.88	100.00	4.75	
YLL-262	1.72	100.00	6.95	
YLL-263	8.36	89.50	0.20	
YLL-264	3.38	95.25	0.54	3.37
YLL-266	1.38	94.50	9.42	
YLL-267	4.14	96.13	0.87	3.90
YLL-268	4.35	94.51	0.65	4.03
YLL-269	5.34	93.02	0.57	
YLL-270	3.92	97.06	0.65	2.70
YLL-271	3.49	98.15	0.53	

TABLE A.3

RESULTS OF OXIDATION EXPERIMENTS OF 1250 K LIGNITE CHAR AT 1250 K

Run Number	ϕ	Solid Weight Loss, % d.a.f.	% of Fuel-N Converted to NO_x	% of Fuel-N Retained in Char
YLL-281	0.30	69.61	29.89	
YLL-282	0.57	63.64	25.81	
YLL-284	0.31	65.96	27.77	
YLL-285	0.48	73.03	30.00	
YLL-286	0.69	60.65	24.18	48.55
YLL-287	1.01	59.67	22.27	52.14
YLL-289	0.66	70.19	27.69	
YLL-290	0.77	64.75	24.38	42.83
YLL-291	0.93	63.25	20.32	
YLL-292	2.18	43.14	12.63	68.46
YLL-293	1.61	47.82	15.29	64.51
YLL-294	2.19	47.25	14.10	
YLL-295	1.33	51.56	16.37	58.30
YLL-297	2.85	40.31	5.68	
YLL-300	3.48		6.57	
YLL-302	3.80	42.47	4.86	68.51
YLL-304	4.20	42.99	5.04	
YLL-305	0.54	69.85	29.34	36.59
YLL-306	0.34	75.11	32.06	33.56

TABLE A.4

RESULTS OF OXIDATION EXPERIMENTS OF 1750 K LIGNITE CHAR AT 1750 K

Run Number	ϕ	Solid Weight Loss, % d.a.f.	% of Fuel-N Contained to NO_x	% of Fuel-N Retained in Char
YLL-231	1.44	80.23	27.16	19.22
YLL-232	1.05	87.16	24.48	20.58
YLL-233	0.65	100.00	23.25	
YLL-234	0.63	100.00	25.56	
YLL-235	0.66	100.00	26.56	
YLL-236	0.59	100.00	28.83	
YLL-237	0.92	95.01	23.12	12.01
YLL-238	3.61	56.74	3.35	34.44
YLL-239	1.37	84.86	13.68	
YLL-240	2.97	64.12	2.91	22.08
YLL-241	3.16	62.12	3.58	30.69
YLL-242	3.52	63.70	3.16	
YLL-243	10.02	40.49	1.63	
YLL-244	6.34	50.44	2.88	
YLL-245	0.31	100.00	29.60	
YLL-246	0.19	100.00	31.47	
YLL-247	1.80	78.92	11.37	20.93

TABLE A.5

RESULTS OF OXIDATION EXPERIMENTS OF MONTANA SUB-BITUMINOUS COAL

Run Number	Temperature K	ϕ	Solid Weight Loss % d.a.f.	% of Fuel-N Converted to NO_x
YLL-404	1250	0.98	60.67	15.25
YLL-405	1250	0.75	78.97	22.43
YLL-406	1250	0.58	76.62	22.59
YLL-407	1250	0.76	65.55	18.77
YLL-408	1250	0.74	82.73	24.87
YLL-409	1250	0.97	69.94	18.88
YLL-410	1250	1.01	67.16	17.39
YLL-411	1250	0.99	68.26	18.32
YLL-421	1500	0.85	87.51	22.72
YLL-422	1500	0.54	74.16	
YLL-423	1500	0.83	85.19	22.01
YLL-424	1500	1.32	63.07	11.41
YLL-426	1500	0.96	80.20	19.42
YLL-427	1500	0.97	79.04	18.57
YLL-428	1500	0.79	78.84	19.18
YLL-431	1750	1.08	87.12	11.48
YLL-432	1750	0.43	96.46	
YLL-433	1750	0.68	97.09	18.80
YLL-434	1750	0.91	92.80	14.09
YLL-435	1750	0.73	99.02	20.17
YLL-436	1750	0.79	96.15	17.02
YLL-437	1750	0.81	97.22	17.72
YLL-438	1750	1.01	92.61	14.59

APPENDIX B

RESULTS OF CHAR/OXYGEN EXPERIMENTS

Tables B.1 to B.3 summarize the results on the solid weight loss
of 1750 K lignite char oxidation experiments at various temperatures
and oxygen partial pressures. The distances between the tip of the
feeder and the mouth of the collector probe were converted to residence
times according to the definition in Appendix D. Tables B.4 to B.6
are the results of the ultimate analysis of selective char samples
from oxidation experiments. Table B.7 is the physical characterization
of selective char samples.

TABLE B.1

RESULTS OF OXIDATION EXPERIMENTS OF 1750 K LIGNITE CHAR AT 1250 K

Run Number	P_{O_2} atm	Distance in	Solid Weight Loss % d.a.f.	Char Batch Number
TLR-256	0.2	5	46.73	LC-1
TLR-258	0.2	5	52.69	LC-1
TLR-260	0.2	6	47.12	LC-1
TLR-261	0.2	3	25.77	LC-1
TLR-262	0.2	4	35.56	LC-1
TLR-263	0.2	5	44.83	LC-1
TLR-264	0.2	6	52.34	LC-1
TLR-265	0.2	3	21.17	LC-1
TLR-266	0.2	4	31.44	LC-1
TLR-312	0.4	3	62.53	LC-3
TLR-313	0.4	6	69.21	LC-3
TLR-314	0.4	5	58.52	LC-3
TLR-315	0.4	5	63.74	LC-3
TLR-316	0.4	3	55.48	LC-3
TLR-321	0.4	4	65.96	LC-3

TABLE B.2

RESULTS OF OXIDATION EXPERIMENTS OF 1750 K LIGNITE CHAR AT 1500 K

Run Number	P_{O_2} atm	Distance in	Solid Weight Loss % d.a.f.	Char Batch Number
TLR-213	0.2	5	41.44	LC-6
TLR-214	0.2	5	49.16	LC-6
TLR-215	0.2	5	44.25	LC-6
TLR-216	0.2	5	41.39	LC-6
TLR-223	0.2	4	43.93	LC-6
TLR-224	0.2	3	30.32	LC-6
TLR-225	0.2	6	54.14	LC-6
TLR-231	0.2	5	50.33	LC-6
TLR-232	0.2	4	48.94	LC-6
TLR-236	0.2	3	37.18	LC-6
TLR-245	0.2	3	42.90	LC-1
TLR-246	0.2	4	41.70	LC-1
TLR-248	0.2	6	53.85	LC-1
TLR-251	0.2	3	28.67	LC-1
TLR-211	0.4	5	79.06	LC-6
TLR-212	0.4	3	69.94	LC-6
TLR-292	0.4	4	78.43	LC-3
TLR-301	0.4	5	84.32	LC-3
TLR-303	0.4	6	89.87	LC-3
TLR-305	0.4	4	81.48	LC-3
TLR-306	0.4	3	79.92	LC-3
TLR-308	0.4	6	84.28	LC-3

TABLE B.3

RESULTS OF OXIDATION EXPERIMENTS OF 1750 K LIGNITE CHAR AT 1750 K

Run Number	P_{O_2} atm	Distance in	Solid Weight Loss % d.a.f.	Char Batch Number
TLR-271	0.2	6	58.34	LC-1
TLR-272	0.2	4	51.88	LC-1
TLR-274	0.2	3	47.54	LC-1
TLR-276	0.2	5	51.23	LC-1
TLR-277	0.2	5	54.59	LC-1
TLR-203	0.4	5	82.32	LC-6
TLR-204	0.4	5	78.63	LC-6
TLR-208	0.4	5	83.81	LC-6
TLR-280	0.4	3	78.42	LC-3
TLR-281	0.4	4	85.79	LC-3
TLR-283	0.4	6	84.26	LC-3
TLR-284	0.4	5	79.70	LC-3
TLR-285	0.4	6	85.15	LC-3
TLR-287	0.4	4	84.41	LC-3
TLR-288	0.4	5	86.87	LC-3

TABLE B.4

CHEMICAL PROPERTIES OF CHAR SAMPLES FROM OXIDATION EXPERIMENTS AT 1250 K

Run Number	P_{O_2} atm	Distance in	Ultimate Analysis Wt% (dry)				Char Batch Number
			C	H	N	S	
TLR-148	0.2	1	75.75	0.82	0.65	1.15	LC-5
TLR-147	0.2	3	66.18	0.45	0.54	1.12	LC-5
TLR-175	0.2	4	61.44	0.53	0.50	1.07	LC-5
TLR-144	0.2	5	51.87	0.19	0.44	1.03	LC-5
TLR-256	0.2	5	69.46	0.86	0.53	1.17	LC-1
TLR-264	0.2	6	67.49	0.72	0.53	1.38	LC-1
TLR-173	0.2	6	53.89	0.64	0.44	1.16	LC-5
TLR-316	0.4	3	75.72	0.10	0.53	2.36	LC-3
TLR-321	0.4	4	59.73	0.26	0.45	1.20	LC-3
TLR-315	0.4	5	61.77	0.23	0.51	1.35	LC-3
TLR-314	0.4	5	64.20	0.98	0.49	1.17	LC-3
TLR-313	0.4	6	61.22	0.24	0.45	1.15	LC-3
LC-1			77.86	0.46	0.595	1.16	
LC-3			77.84	0.38	0.567	1.16	
LC-5			74.86	0.88	0.660	1.33	

TABLE B.5

CHEMICAL PROPERTIES OF CHAR SAMPLES FROM OXIDATION EXPERIMENTS AT 1500 K

Run Number	P_{O_2} atm	Distance in	Ultimate Analysis Wt% (dry) C	H	N	S	Char Batch Number
TLR-134	0.2	3	58.47	0.43	0.49	1.15	LC-5
TLR-153	0.2	5	46.44	0.33	0.35	0.88	LC-5
TLR-156	0.2	6	37.22	0.20	0.28	0.71	LC-5
TLR-151	0.2	7	53.38	0.30	0.38	1.06	LC-5
TLR-306	0.4	3	46.35	0.37	0.29	1.64	LC-3
TLR-301	0.4	5	49.49	0.22	0.28	0.93	LC-3
TLR-211	0.4	5	59.16	0.94	0.38	0.96	LC-6
TLR-308	0.4	6	49.68	0.17	0.31	1.14	LC-3
LC-3			77.84	0.38	0.567	1.16	
LC-5			74.86	0.88	0.660	1.33	
LC-6			79.38	0.34	0.620	0.92	

TABLE B.6

CHEMICAL PROPERTIES OF CHAR SAMPLES FROM OXIDATION EXPERIMENTS AT 1750 K

Run Number	P_{O_2} atm	Distance in	Ultimate Analysis Wt% (dry)				Char Batch Number
			C	H	N	S	
TLR-126	0.2	0.5	72.91	0.70	0.63	1.09	LC-5
TLR-119	0.2	2.5	68.63	0.26	0.50	1.45	LC-5
TLR-165	0.2	3	52.38	0.14	0.32	0.90	LC-5
TLR-167	0.2	4	54.54	0.21	0.30	1.08	LC-5
TLR-164	0.2	5	59.53	0.23	0.31	1.06	LC-5
TLR-277	0.2	5	65.80	0.68	0.28	1.24	LC-1
TLR-271	0.2	6	64.78	0.61	0.28	1.35	LC-1
TLR-124	0.2	6.5	46.84	0.10	0.21	1.15	LC-5
TLR-162	0.2	7	44.69	0.15	0.20	0.98	LC-5
LC-1			77.86	0.46	0.595	1.16	
LC-5			74.86	0.88	0.660	1.33	

TABLE B.7

PHYSICAL PROPERTIES OF CHAR SAMPLES FROM OXIDATION EXPERIMENTS

Run Number	P_{O_2} atm	T_F K	Distance in	B.E.T. Surface Area m^2/g	Pore Volume cm^3/g	Average Pore Diameter $\overset{\circ}{A}$	Char Batch Number
TLR-261	0.2	1250	3	208.0	0.160	30.8	LC-1
TLR-249	0.2	1500	3	149.1	0.255	68.4	LC-1
TLR-252	0.2	1500	5	177.2	0.172	38.8	LC-1
TLR-273	0.2	1750	3	234.1	0.193	33.0	LC-1
TLR-277	0.2	1750	5	213.1	0.211	39.6	LC-1
TLR-316	0.4	1250	3	187.9	0.171	36.4	LC-3
TLR-315	0.4	1250	5	136.2	0.125	36.7	LC-3
TLR-290	0.4	1500	3	126.2	0.145	46.0	LC-3
TLR-293	0.4	1500	5	136.4	0.142	41.8	LC-3
TLR-280	0.4	1750	3	127.7	0.108	33.8	LC-3
TLR-284	0.4	1750	5	130.9	0.139	42.5	LC-3

APPENDIX C

RESULTS OF CHAR/NITRIC OXIDE EXPERIMENTS

The results of nitric oxide reduction experiments at various temperature and nitric oxide inlet concentrations are summarized in Table C.1.

TABLE C.1

RESULTS OF NITRIC OXIDE REDUCTION EXPERIMENTS

Run Number	T_F K	$[NO]_{in}$ ppm	$[NO]_{out}$ ppm	u_{in} 1/min	W g	τ min	Char Batch Number
RLR-203	1250	530	447	3	0.6097	1	LC-4
RLR-204	1250	530	459	3	0.6073	1	LC-4
RLR-207	1250	6400	5800	3	0.6042	1.2	LC-4
RLR-208	1250	6400	5800	3	0.6100	1.2	LC-4
RLR-216	1500	530	311	3	0.6194	1	LC-4
RLR-217	1500	530	320	3	0.6130	1	LC-4
RLR-212	1500	6400	3810	3	0.6117	1	LC-4
RLR-213	1500	6400	4030	3	0.6171	1	LC-4
RLR-102	1500	1100	675	2.86	0.8059	1.5	LC-4
RLR-103	1500	1100	766	3.15	0.4550	1	LC-4
RLR-104	1500	1100	824	3.40	0.4343	1	LC-4
RLR-223	1750	530	66.5	3	0.6086	1	LC-4
RLR-224	1750	530	65.5	3	0.6121	1	LC-4
RLR-226	1750	6400	877	3	0.6110	1.15	LC-4
RLR-227	1750	6400	1574	3	0.6116	1.6	LC-4
RLR-228	1750	6400	1145	3	0.6058	1.3	LC-4
RLR-111	1750	1100	388	3.35	0.4636	1.3	LC-4
RLR-112	1750	1100	413	3.30	0.4306	1.3	LC-4

APPENDIX D

CALCULATION OF REACTION TIMES IN CHAR/OXYGEN REACTION

The reaction time is defined as the length of the duration in which char particles expose to gas concentrations and the high temperature environment of the furnace. In the kinetic study of Char/O_2 reaction, it is the traveling time of char particles from the tip of the feeder to the mouth of the collector probe. As soon as the particles are injected into the hot environment of the furnace, they could be accelerated or decelerated by the main gas flow stream, depending upon the relative initial particle velocity. In laminar flow experiments, the char particles are entrained and accelerated by the faster main gas flow, and approach the centerline velocity of the main gas flow. Kobayashi (1976), using essentially the same system, was able to measure the particle velocities directly by a laser doppler anemometer through several observation ports along the furnace axis which gave visual access to the inside of the muffle tube. He concluded that the average particle velocity could be approximated by 1.4 times the average main gas velocity. The rationalization is as follows.

In laminar flow, the velocity profile is parabolic and the average main gas velocity, $<v_z>_g$ is given by:

$$\langle v_z \rangle_g = \frac{\int_0^{2\pi} \int_0^R v_z \, r \, dr \, d\theta}{\int_0^{2\pi} \int_0^R r \, dr \, d\theta} \tag{D.1}$$

Due to the velocity gradient of the fluid, particles near the wall receive aerodynamic lift toward the center of the tube resulting in a centralized particle flow field. Assuming that the particles are uniformly distributed within 0.8 radius of the muffle tube, the average particle velocity can then be given as:

$$\langle v_z \rangle_p = \frac{\int_0^{2\pi} \int_0^{0.8R} v_z \, r \, dr \, d\theta}{\int_0^{2\pi} \int_0^{0.8R} r \, dr \, d\theta} \tag{D.2}$$

The velocity distribution for the laminar flow is given by (Bird, Stewart, and Lightfoot, 1960):

$$v_z = \frac{(P_0 - P_L)}{4 \, \mu L} [R^2 - r^2] \tag{D.3}$$

Substituting Equation (D.3) into Equations (D.1) and (D.2) and integrating, the following relation can be obtained:

$$\langle v_z \rangle_p = 1.36 \langle v_z \rangle_g \tag{D.4}$$

Or, as indicated by Equation (D.4), the average particle velocity is about 40% larger than the average main gas velocity.

One of the major drawbacks of the present system is the lack of internal observation ports, which makes the direct measurements of particle velocity difficult. To avoid the problem of attempting to model exact flow fields and velocity distributions in such a complex system, particularly when it is not possible at this time to make experimental checks, Kobayashi's approximation is used to estimate the reaction times of the experiments.

Based on above information, the calculation of reaction times become straightforward. The volumetric flow rate of the main gas at the furnace temperature, Q_F, can be first related to the inlet flow rate, Q_0, by ideal gas law:

$$Q_F = Q_0 \frac{T_F}{T_0} \qquad (D.5)$$

The average main gas velocity is then simply Q_F divided by the cross-sectional area of the muffle tube, A_M. Finally, the reaction time is given by

$$t = \frac{A_M}{1.4 \, Q_F} L \qquad (D.6)$$

where L is the distance between the tip of the char feeder and the mouth of the collector probe.

For Q_0 = 6 l/min and T_0 = 300 K, the results with reaction times reported in milliseconds are summarized on the next page.

Distance, inch Temperature, K	3	4	5	6	7
1250	256	340	427	512	599
1500	213	283	356	426	500
1750	183	243	305	365	428

APPENDIX E

CALCULATION OF BINARY DIFFUSION COEFFICIENTS FOR

OXYGEN/HELIUM AND NITRIC OXIDE/HELIUM SYSTEMS

The Chapman-Enskog formula has been found suitable for evaluating the bulk diffusivity at moderate temperatures and pressures (Hirschfelder, Curtiss and Bird, 1954). The equation is

$$D_{AB,g} = 0.001853 \frac{T^{3/2} (1/M_A + 1/M_B)^{1/2}}{P_t \sigma_{AB}^2 \Omega_{AB}} \qquad (E.1)$$

where

$D_{AB,g}$ = bulk diffusivity, cm^2/sec

T = temperature, K

M_A, M_B = molecular weights of gases A and B

P_t = total pressure of the gas mixture, atm

σ_{AB} = collision diameter or constant in the Lennard-Jones potential energy function for the molecular pair AB, $\overset{o}{A}$

Ω_{AB} = collision internal, function of kT/ε_{AB} for real gases (k = Boltzmann's constant)

The Lennard-Jones constants for the unlike molecular pair AB can be estimated from the constants for like pairs AA and BB:

$$\sigma_{AB} = \frac{1}{2}\left(\sigma_A + \sigma_B\right) \qquad\qquad (E.2)$$

$$\varepsilon_{AB} = k\sqrt{\left(\frac{\varepsilon_A}{k}\right)\cdot\left(\frac{\varepsilon_B}{k}\right)} \qquad\qquad (E.3)$$

The values of Lennard-Jones constants of He, O_2 and NO are given in the literature and are summarized as follows:

	M	σ (Å)	ε/k (K)
He	4	2.576	10.2
O_2	32	3.433	113.0
NO	30	3.470	119.0

Therefore, for O_2/He system:

$$\sigma_{AB} = 3.005$$

$$\varepsilon_{AB}/k = 33.95$$

For NO/He system:

$$\sigma_{AB} = 3.023$$

$$\varepsilon_{AB}/k = 34.84$$

The collision integral Ω_{AB} is given as a function of kT/ε_{AB} in the following table:

$\dfrac{kT}{\varepsilon_{AB}}$	Ω_{AB}
30.0	0.623
40.0	0.596
50.0	0.576
60.0	0.560
70.0	0.546

The bulk diffusivities can therefore be calculated based on the above information. Figure E.1 summarizes the results of the binary diffusion coefficient as a function of the temperature for O_2/He system. Figure E.2 summarizes the results for NO/He system.
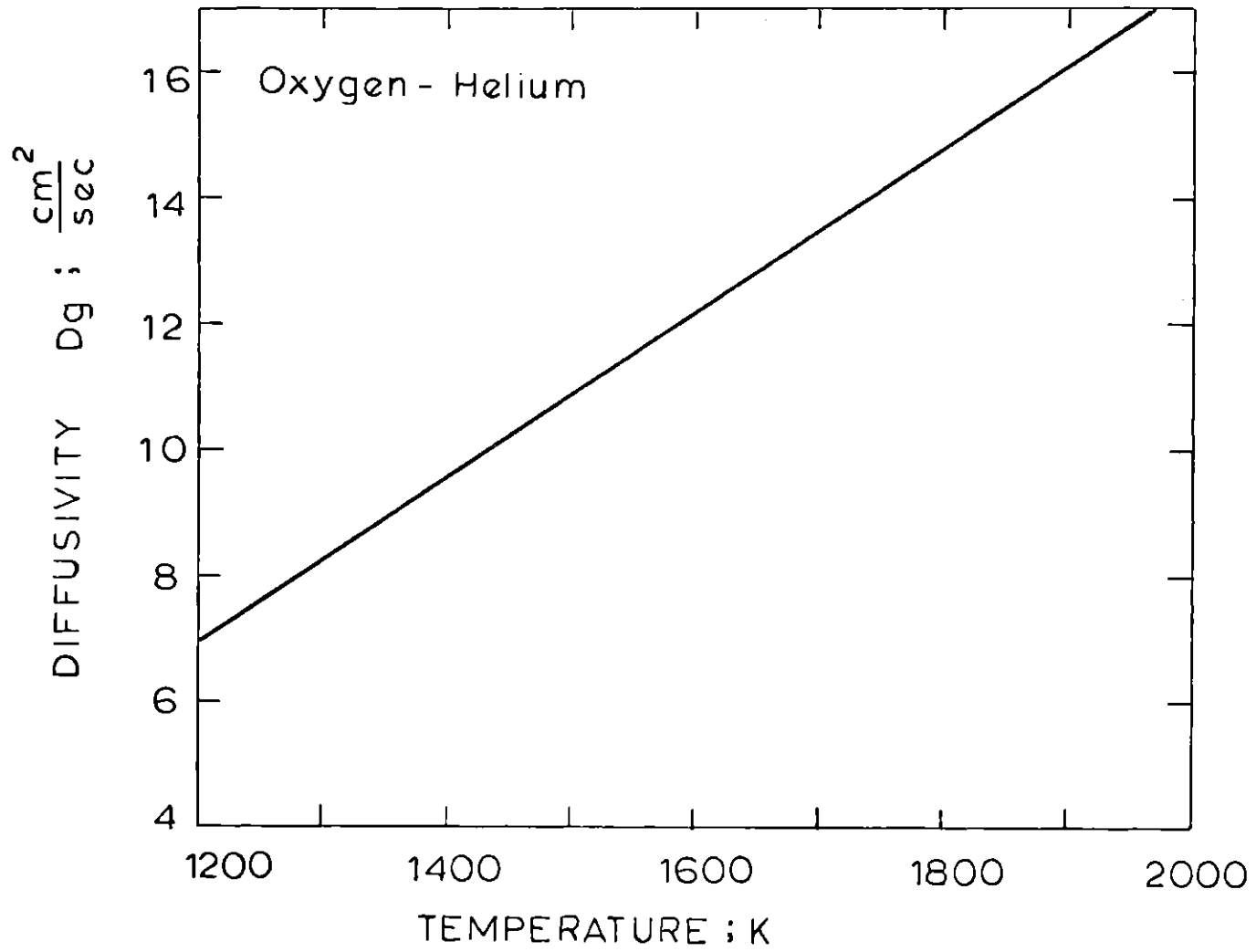
Figure E.1

Binary Diffusion Coefficients for Oxygen-Helium System
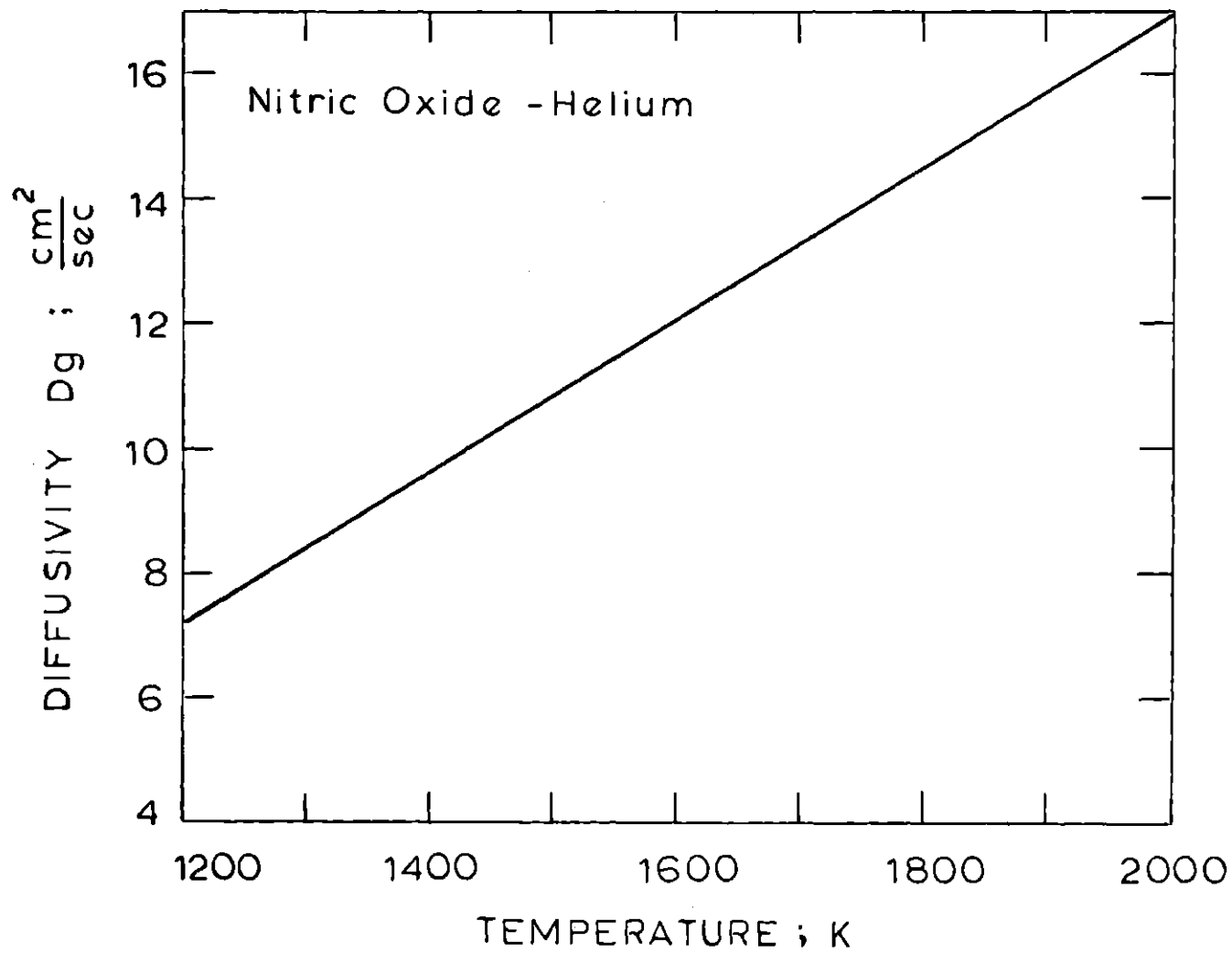
Figure E.2

Binary Diffusion Coefficients for Nitric Oxide-Helium System

APPENDIX F

CALCULATION OF EFFECTIVE PORE
DIFFUSIVITIES FOR OXYGEN AND NITRIC OXIDE

The mass-transport rate within the pore volume for most gaseous diffusions within porous materials is contributed by both bulk and Kundsen diffusion. If the gas density is low, or if the pores are quite small, or both, the molecules collide with the pore wall much more frequently than with each other. Under these conditions, inter-molecular collisions may thus be neglected, and a molecule travels within the pore by a series of random flights interrupted by collisions with the pore wall. More specifically, the Knudsen diffusion becomes dominant, when the magnitude of the pore radius is much smaller as compared to the length of the mean-free-path of molecules between intermolecular collisions.

To specify more closely the conditions under which Knudsen diffusion is operative, we recall that the mean-free-path, λ, of a gas molecule is given by the kinetic theory (Bird, Stewart and Lightfoot, 1960) as

$$\lambda = \frac{1}{\sqrt{2} \pi \sigma^2 n^*} \tag{F.1}$$

where σ is the molecular diameter and is 3.433 $\overset{\circ}{A}$ for O_2 and 3.470 $\overset{\circ}{A}$ for NO (See Appendix E), and n^* is the molecular number density and can

be expressed in terms of T and P as:

$$n^* = 6.023 \times 10^{23} \frac{P}{RT} \tag{F.2}$$

The condition for Knudsen diffusion is that λ must be considerably larger than the pore radius, r_p.

For the char used in the present study, the average radius of the pores is about 20 $\overset{\circ}{A}$ to 30 $\overset{\circ}{A}$. The mean-free-paths, from 1250 K to 1750 K can be calculated by Equation (F.1) to be in the range of 3,000 $\overset{\circ}{A}$ to 5,000 $\overset{\circ}{A}$. Since the mean-free-paths are about two orders of magnitude larger than the average pore radius of the char used, Knudsen diffusion is assumed to be dominant in pore diffusion of the present study.

The kinetic theory provides the following relation for determining the Knudsen diffusivity of gases in a straight round pore (Satterfield, 1970; Smith, 1970):

$$D_K = 9.7 \times 10^3 \ r_p \ \sqrt{T_p/M} \tag{F.3}$$

where D_K is in square centimeters per second, r_p the average pore radius in cm, T_p the temperature in K, and M the molecular weight.

The effective diffusivity based on Knudsen diffusion is given as:

$$D_e = \frac{\theta_p}{\tau} \ D_K \tag{F.4}$$

where θ_p is the porosity and τ the tortuosity. Note that the porosity, θ_p, is obtainable from the density and the void volume of the particle by the expression

$$\theta_p = \frac{\text{void (or pore) volume}}{\text{total particle volume}} \tag{F.5}$$

$$= \frac{v_p}{1/\rho_B} \tag{F.6}$$

where v_p is the pore volume per gram of char and ρ_B is the bulk density of the char. There is no unique relationship between the tortuosity, τ, and the porosity, θ_p, for porous materials. Values of τ of 2 to 7 are readily reconciled with physical reality (Satterfield, 1970). A value of τ equals 2.0 is assumed for the purpose of calculation.

Finally, combining Equations (F.3), (F.4) and (F.6) and the information summarized in Table F.1, working expressions for evaluating effective diffusivities are obtained:

For Char/O_2 experiments

$$D_e = 6.372 \times 10^{-5} \sqrt{T_p} \qquad \frac{cm^2}{sec} \tag{F.7}$$

For Char/NO_x experiments

$$D_e = 5.644 \times 10^{-5} \sqrt{T_p} \qquad \frac{cm^2}{sec} \tag{F.8}$$

TABLE F.1

PERTINENT INFORMATION FOR THE EVALUATIONS

OF THE EFFECTIVE DIFFUSIVITIES

	For Char/O_2 Experiments	For Char/NO_x Experiments
M	32	30
r_p, cm	2.733×10^{-7}	2.110×10^{-7}
ρ_B, g/cm^3	1.71	1.64
v_p, cm^3/g	0.159	0.184
θ_p	0.272	0.302
τ	2	2

APPENDIX G

CALCULATION OF THERMAL CONDUCTIVITIES
FOR OXYGEN AND HELIUM MIXTURES

The thermal conductivities of gaseous helium and oxygen at various temperatures are given in Perry and Chilton (1973). A more detailed table which shows the thermal conductivities of helium can also be found in Weast (1972). The information is used to construct Figure G.1 which shows the thermal conductivities of pure helium and oxygen as functions of temperature.

The thermal conductivities of gas mixtures may be most conveniently calculated from component conductivity values with the equation (Perry and Chilton, 1973):

$$\lambda_g = \frac{\sum y_i \, \lambda_i \, (M_i)^{1/3}}{\sum y_i \, (M_i)^{1/3}} \qquad (G.1)$$

where y_i, λ_i and M_i are the mole fraction, thermal conductivity, and molecular weight respectively of the individual component. Combining Equation (G.1) with the information given in Figure G.1, the thermal conductivities for various mole fractions of He and O_2 mixtures can therefore be obtained as a function of temperature, and are shown in Figure G.2.
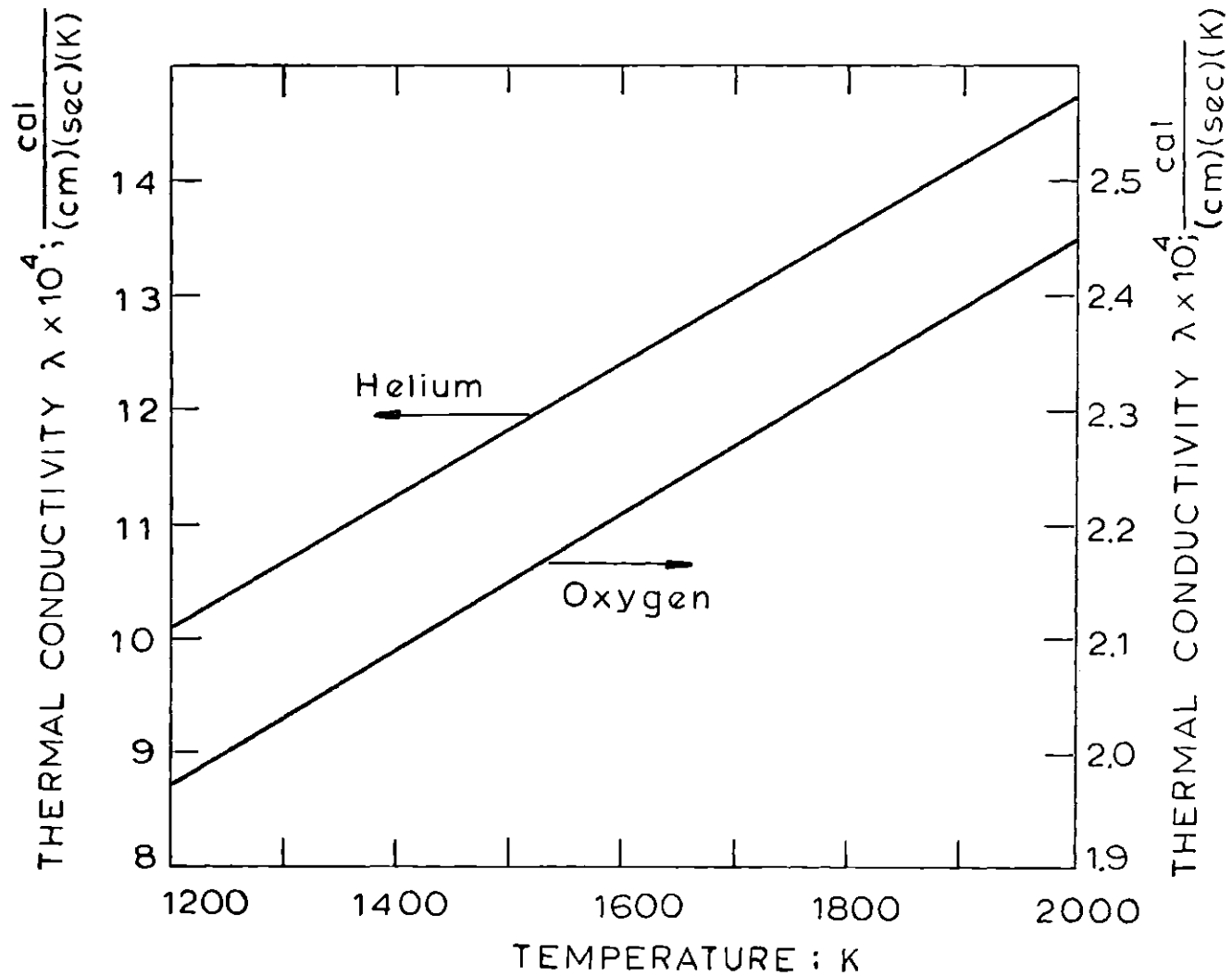
Figure G.1

Thermal Conductivities of Pure Components of Helium and Oxygen
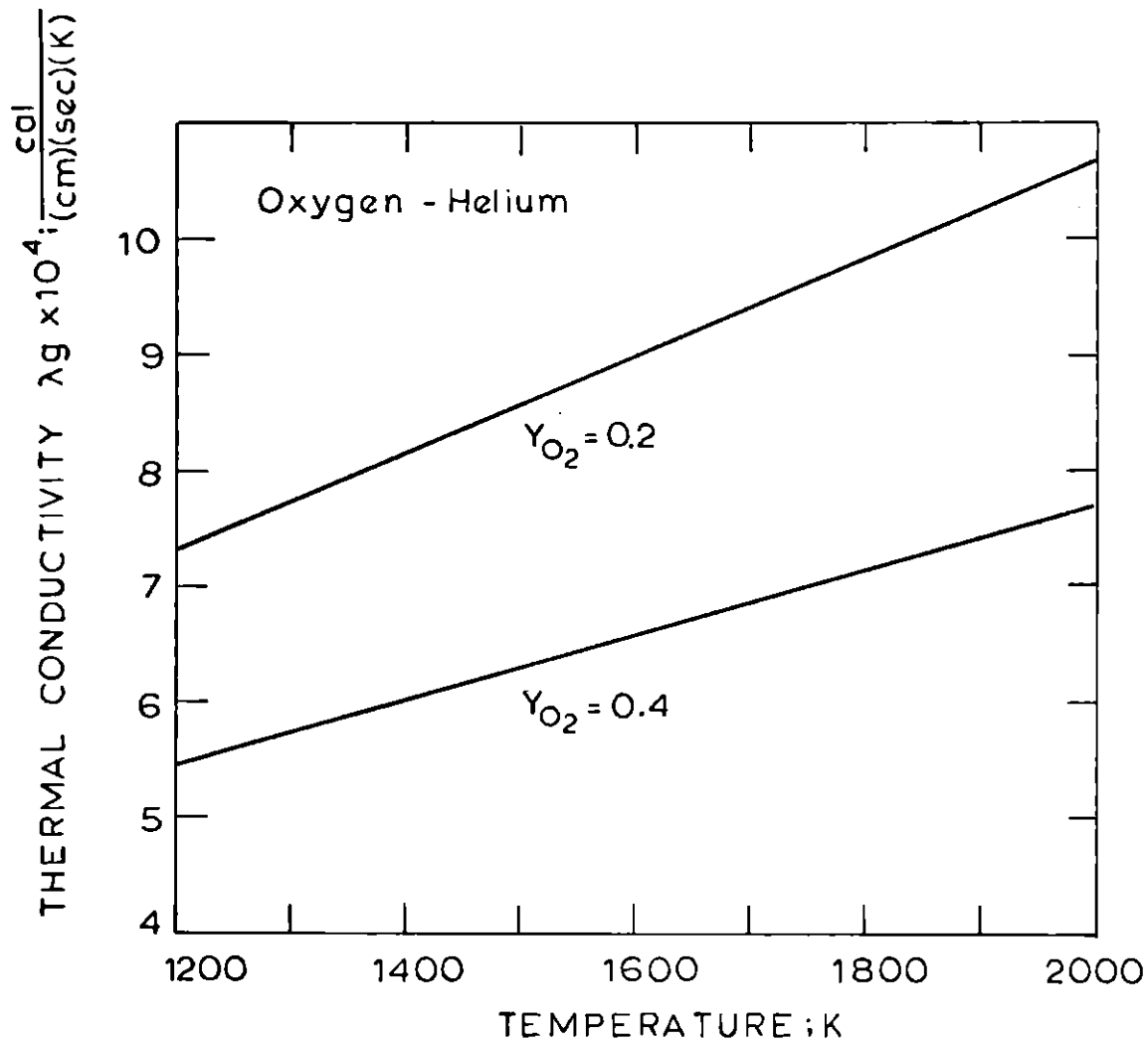
Figure G.2

Thermal Conductivities of Helium and Oxygen Mixtures

APPENDIX H

NITROGEN AND CARBON BALANCES DURING PYROLYSIS OF LIGNITE

H.1 Coal-Nitrogen Distribution During Pyrolysis

Previous research at M.I.T. on the fate of coal-nitrogen during pyrolysis was heavily concentrated on the nitrogen behavior in the solid phase (Pohl, 1976). One area that remained untouched in previous research was the nitrogen distribution in gas phase. Nitrogen distribution during pyrolysis of lignite was obtained in this study to complement previous pyrolysis results. Figure H.1 shows the distribution of coal-nitrogen during pyrolysis at a residence time of one second and temperatures of 1250 K and 1500 K. The data are plotted as percent of the original coal-nitrogen that remains in char, is volatilized and collected as ammonia, hydrogen cyanide and molecular nitrogen. The ammonia, hydrogen cyanide and molecular nitrogen are determined in accordance with the procedures described in Section 5.3. As indicated by Figure H.1, the nitrogen material balances have been closed to an average value of 98% at both 1250 K and 1500 K. There are few words of caution. The muffle tube wall has been known to have some catalytic effect on the decomposition of HCN (see Appendix J) and NH_3. Thus, the HCN and NH_3 observed in the off-gases may not be the primary pyrolysis products. This, in turn, changes the original nitrogen distribution among gaseous components. Nevertheless, the data in Figure H.1 represent the rudimentary information on coal-

PERCENTAGE OF ORIGINAL COAL-NITROGEN
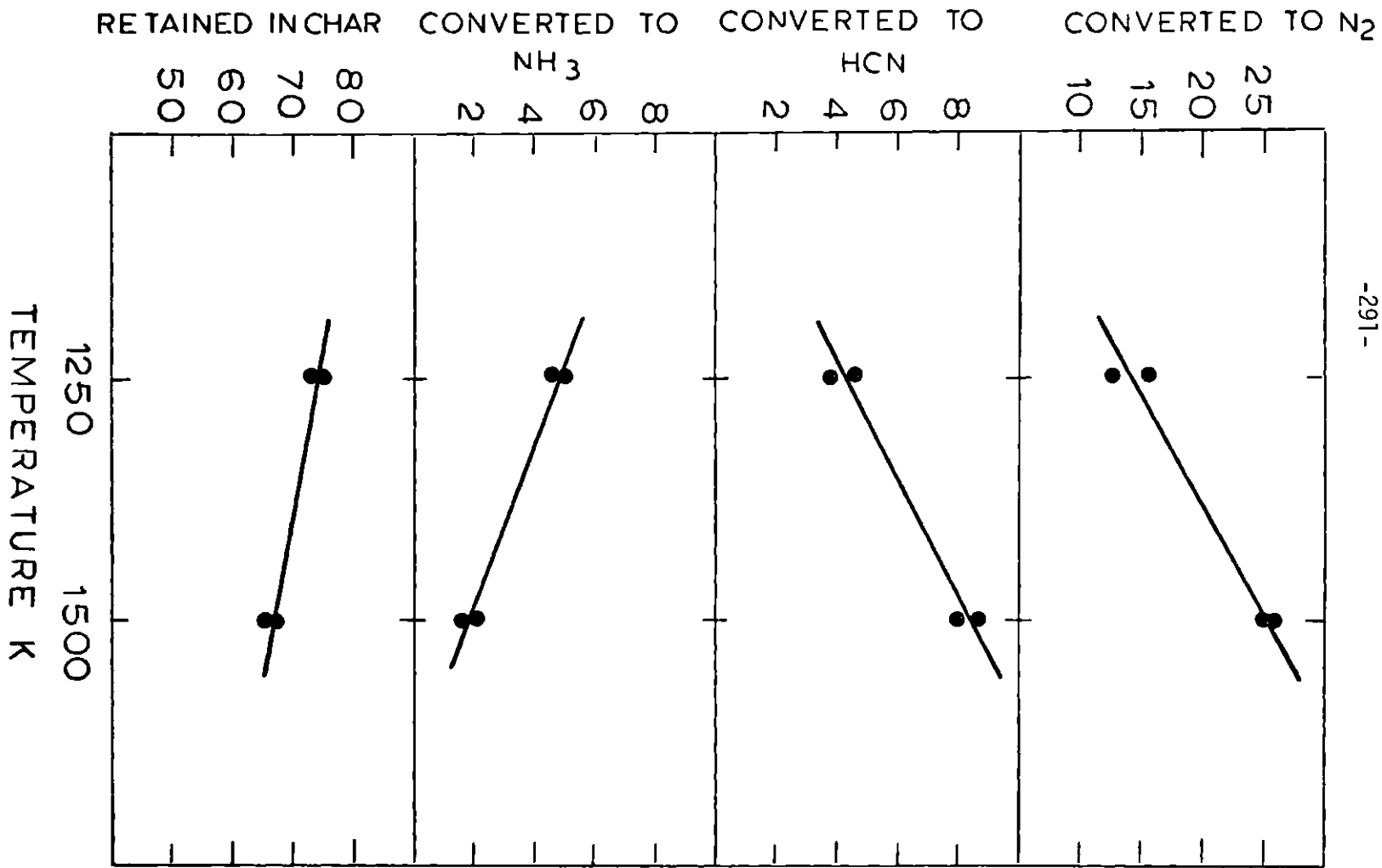
Distribution of Coal Nitrogen During Pyrolysis of Lignite

Figure H.1

nitrogen distribution during pyrolysis. They require careful inter-
pretation and further confirmation.

H.2 Carbone Distribution During Coal Pyrolysis

Carbon distribution during pyrolysis of lignite at a residence time
of one second was determined by measuring carbon conversions to methane,
carbon dioxide and carbon monoxide (according to the procedures described
in Section 5.3) as well as carbon retention in char. Data were obtained
at temperatures of 1250 K and 1500 K are shown in Figure H.2.

Carbon retention in char remains constant at about 72% at both
1250 K and 1500 K. This is because the carbon has reached its asymptotic
value of weight loss and forms stabilized compound in char. Carbon
conversion to CO_2 increases slightly (from 3% to 4%) and carbon
conversion to CO increases significantly (from 5% to 11%) as the
temperature increases from 1250 K to 1500 K. Although CH_4 is the only
hydrocarbon measured in present study, other hydrocarbons are also
believed to exist.

Suuberg (1977) has also investigated the carbon balance for
lignite pyrolysis. His results are summarized in Table H.1. The
present results and Suuberg's results are in general agreement even
though different heating rates are involved. (10^3 C/sec in Suuberg's
study and 10^4 C/sec in present study.)

The carbon material balances are closed up to about an average
of 85%. The undetected carbon exists most likely in tar as well as
hydrocarbons other than CH_4.

PERCENTAGE OF ORIGINAL COAL - CARBON
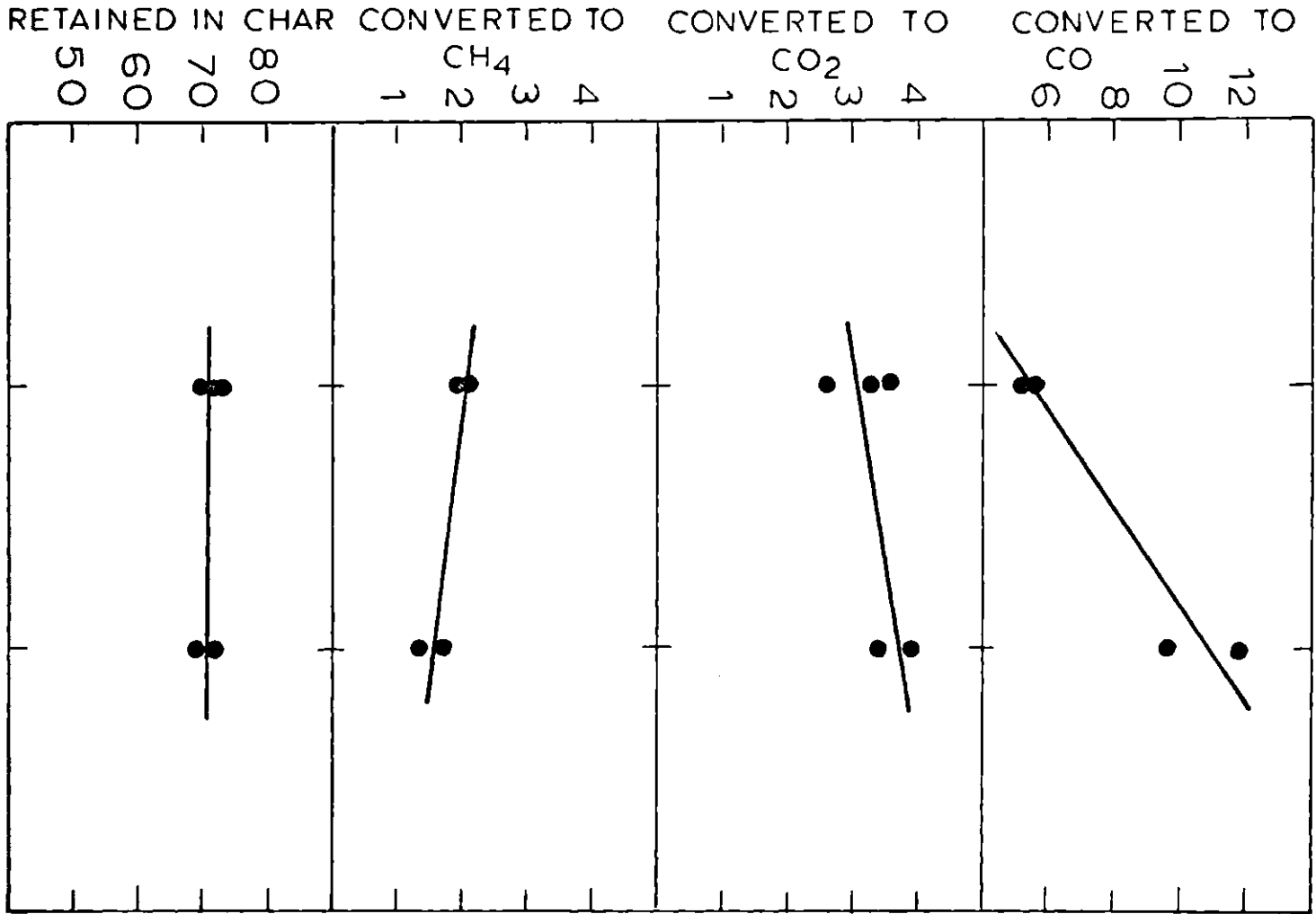
Figure II.2

Distribution of Carbon During Pyrolysis of Lignite

TABLE H.1

CARBON DISTRIBUTION DURING PYROLYSIS OF

LIGNITE AT P = 1 atm AND HEATING RATE = 1000 C/sec

Pyrolysis Products	Weight % of the Original Carbon in Lignite	
	Peak Temperature	
	1183K	1273 K
CO_2	3.88	4.05
CO	5.73	5.40
HC	3.54	4.05
Tar	7.42	7.25
Char	80.10	74.54
Total	100.67	95.29

Source: Suuberg (1977)

APPENDIX I

NITROGEN AND CARBON BALANCES DURING

COMBUSTION OF LIGNITE AT FUEL RICH CONDITION

In Chapter 6, we observed that, during oxidation of lignite at 1750 K, the solid burnout was complete even at fuel/oxygen equivalence ratio of 2 and the solid weight loss was still 95% even at a richer condition when the ratio was 4. It is of interest to study how the carbon and nitrogen are distributed at this high temperature (T = 1750 K) and rich condition (ϕ = 3 to 4).

Table I.1 summarizes the carbon distributions. The carbon material balance has been closed up to an average value of 93%. Only small fraction of the original carbon (about 5%) has been retained in char. Significant portion of the carbon (about 72% to 75%) has been oxidized and converted to CO at this extremely rich condition. This is somewhat expected because that the ultimate analysis has shown that, for Montana lignite, the carbon content is 54.5 Wt% and the oxygen content is 17.4 Wt%. However, the increase in total solid weight loss to 95% (d.a.f.) in this "oxidative" pyrolysis as compared to the total solid weight loss (about 59% d.a.f.) in "pure" pyrolysis implies an important implication. The implication is that the pyrolytic gasification of coal can be significantly improved by a small additive of oxygen to the gasifier.

Table I.2 is the coal-nitrogen distribution during lignite

TABLE I.1

CARBON DISTRIBUTION DURING COMBUSTION OF

LIGNITE AT T=1750 K and ϕ=3~4

Combustion Products	Weight % of the Original Carbon in Lignite
CO	72 ~ 75
CO_2	11 ~ 16
CH_4	1 ~ 2
Other CH	Not Measured
TAR	Not Measured
Char	4 ~ 5
Total	88 ~ 98

TABLE I.2

NITROGEN DISTRIBUTION DURING COMBUSTION OF

LIGNITE AT T=1750 K AND ϕ=3~4

Combustion Products	Weight % of the Original Nitrogen in Lignite
N_2	71 ~ 75
HCN	6 ~ 8
NH_3	Trace
NO_x	1 ~ 3
Char	3 ~ 5
Total	81 ~ 91

combustion at temperature of 1750 K and fuel/oxygen ratio of 3 to 4.
Major fraction of the coal-nitrogen (about 71% to 75%) has been
converted to gaseous nitrogen molecules. Only about 3% to 5% of the
nitrogen has been retained in char. About 6% to 8% and 1% to 3% of
the nitrogen have been detected as HCN and NO_x, respectively. The
overall nitrogen material balance has been closed up to an average of
86%.

APPENDIX J

THERMAL DECOMPOSITION OF HYDROGEN CYANIDE

A certified standard gas containing 116 ppm HCN in He was run through the furnace and checked for HCN recovery. Two different ways were employed to feed the HCN gas into the furnace. First, this 116 ppm HCN gas was used as the main gas and fed to the furnace through the main furnace inlet. In this manner, the whole muffle tube was filled with the HCN gas. This was called a "straight run". The second way to feed the HCN gas was by injecting this 116 ppm HCN gas through the coal feeder (no coal was fed, of course) into the center of the furnace while He gas was fed to the furnace through the main inlet as main gas. The HCN gas would diffuse radially toward the muffle tube wall, even though the centered HCN gas stream was initially surrounded by the main He gas. The time required for HCN to diffuse from the center of the furnace to the muffle tube wall has been estimated by an order-of-magnitude calculation to be about the same as the residence time of the HCN gas in the furnace. The second method was called a "simulated run" (to simulate the HCN generated by coal pyrolysis). In straight run experiments, the HCN flow rate was 3 l/min. In simulated run experiments, 1 l/min HCN gas was injected along with 3 l/min He main gas. The rest of the procedures for both experiments were the same as free-fall experiments described in Chapter 5 except that no coal was fed. The results of the recovery of 116 ppm HCN are shown in Figure J.1.
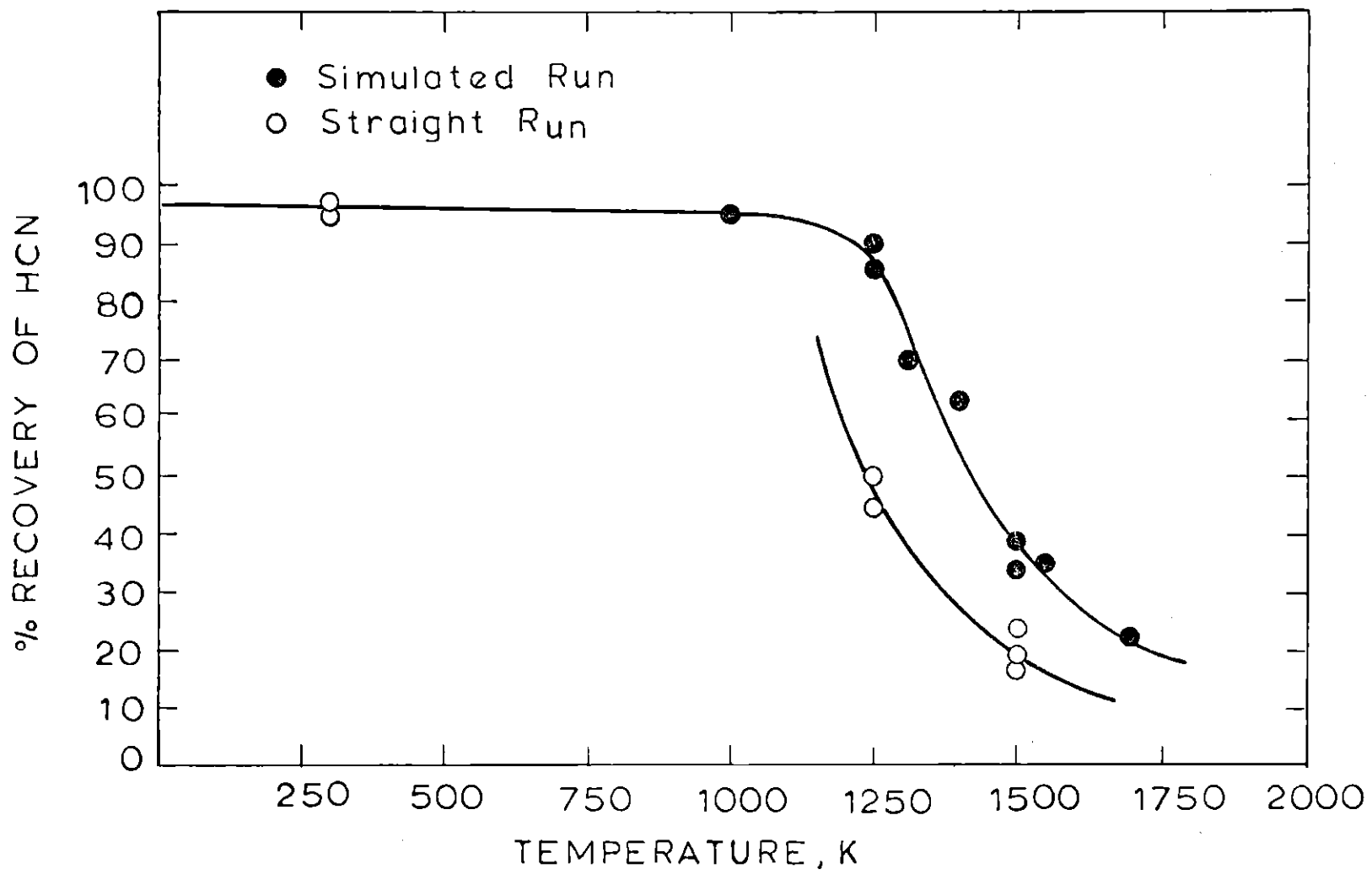
Figure J.1

Recovery of HCN as Function of Temperature

For simulated runs, no significant decomposition of HCN was observed up to a furnace temperature of 1100 K. About 90% of HCN was recovered at 1250 K. The recovery of HCN decreased to about 40% at 1500 K and to about 20% at 1700 K. Less recovery of HCN was found for straight runs. It is conceivable that the muffle tube wall might have some catalytic effect on the decomposition of HCN.

No attempt was made in this study to further investigate the thermal decomposition (both catalytic and non-catalytic) of HCN. The preliminary results were presented here (i.e., Figure J.1), because the author believes that this information might have some importance in the practical implication for HCN reduction.

NOMENCLATURE

A	area
A_B	specific B.E.T. surface area of char
A_E	external surface area of a char particle
b	conversion factor; see Equation (8.19)
C	gas concentration
C	molar concentration of carbon in char
C_r	gas concentration at radius r
C_s	gas concentration at solid surface
D_e	effective pore diffusivity
D_g	bulk diffusivity of fluid system
D_K	Knudsen pore diffusivity
d_p	diameter of pore
d_s	diameter of spherical particle
E	activation energy
E_D	activation energy for diffusion
E_{ob}	observed activation energy
F	ratio of poisoned reaction rate to unpoisoned reaction rate
F_{NO}	molar flow rate of NO
F_f	feed rate of fuel
F_o	feed rate of oxygen
G	normalized specific B.E.T. surface area
H	ash released
ΔH_r	enthalpy change for a reaction

h_t	heat transfer coefficient
K	constant; see Equation (7.63)
k	Boltzmann's constant
k	intrinsic rate constant for Char/NO reaction
k_B	char oxidation rate constant per unit B.E.T. surface area
k_E	char oxidation rate constant per unit external surface area
k_P	char oxidation rate constant per particle
k_g	external mass transfer coefficient
k_{ob}	observed char oxidation rate per unit external area
k_{py}	pyrolysis rate constant of fuel-nitrogen
k_v	intrinsic char oxidation rate constant per unit volume of particle
k'	rate constant; see Section 8.7
$k*$	rate constant; see Section 8.9
L	distance between the tip of char feeder and the mouth of the collector probe
L	length of a pore
M_C	molecular weight of carbon
M_{O_2}	molecular weight of oxygen
M_{NO}	molecular weight of NO
m	intrinsic reaction order
N	molar concentration of nitrogen in char
$\dot{N}_r$	mole flux of gas
Nu	Nusselt number
$[NO]$	NO_x concentration in ppm

n	reaction order
$n*$	molecular number density
P_t	total pressure
P_{O_2}	oxygen partial pressure
Q_F	volumetric flow rate of main gas at furnace temperature
Q_o	inlet volumetric flow rate of main gas
$\dot{Q}_g$	rate of heat generation per particle
$\dot{Q}_l$	rate of heat loss per particle
R	gas constant
R	radius
R	rate
R_B	char oxidation rate per unit B.E.T. surface area
R_E	char oxidation rate per unit external surface area
R_p	char oxidation rate per particle
Re	Reynolds number
R_i	initial rate
R_t	rate at any time t
R_{po}	reaction rate in poisoned pore
R_{un}	reaction rate in unpoisoned pore
$R*$	overall relative reactivity of char
r	radius
r_p	radius of pore
r_s	radius of spherical particle
$-r_{NO}$	consumption rate of NO per unit B.E.T. surface area of char
Sc	Schmidt number

Sh	Sherwood number
T_{Avg}	arithmetic average of T_p and T_F
T_F	main gas temperature or furnace temperature
T_0	room temperature or reference temperature
T_p	particle temperature
t	time
t_g	residence time of gas
u_{in}	inlet volumetric flow rate of NO
V	effective volume of furnace
V_s	total volume of particle
v_p	pore volume of particle
$<v_z>_g$	average main gas velocity
$<v_z>_p$	average particle velocity
W	mass of char
X_{NO}	conversion of NO
x	distance from pore mouth
y	mole fraction
Z	% char retention, d.a.f.
α	fraction of coal-nitrogen that is volatilized
α	fraction of pore surface that is poisoned
α	molar concentration; see Equation (7.15)
β	% char burnout, d.a.f.
β_s	dimensionless volume; see Equation (7.33)
γ	fraction of char-nitrogen that is consumed
γ_s	dimensionless reaction rate; see Equation (7.31)

ε	Lennard-Jones parameter
η	effectiveness factor
η_1	efficiency of conversion to NO_x of volatile-nitrogen
η_2	efficiency of conversion to NO_x of fuel-nitrogen in burned char
η^*	efficiency of conversion to NO_x of coal-nitrogen
θ_p	porosity
λ	mean-free-path of gas molecule
λ_g	thermal conductivity
μ	viscosity
ξ	dimensionless concentration; see Equation 7.24
π	3.1416
ρ_B	bulk density of char
σ	Stefan-Boltzmann constant
σ_{AB}	collision diameter
τ	tortuosity
τ	feeding time of char
ϕ	fuel/oxygen equivalence ratio
ϕ	Thiele modulus (in general)
ϕ_0	Thiele modulus for unpoisoned pore
ϕ_s	Thiele modulus for spherical particle
ψ	dimensionless radius; see Equation (7.24)
Ω_{AB}	collision integral

REFERENCES

Anson, D., Moles, F.D. and Street, P.J., "Structure and Surface Area of Pulverized Coal During Combustion," Combustion & Flame, 16, 265 (1971).

Anthony, D.B., "Rapid Devolatilization and Hydrogasification of Pulverized Coal," Sc.D. Thesis, M.I.T., Cambridge, Massachusetts (1974).

Anthony, D.B., Howard, J.B., Hottel, H.C. and Meissner, H.P., "Rapid Devolatiliation and Hydrogasification of Bituminous Coal," Fuel, 55, 121 (1976).

Anthony, D.B., Howard, J.B., Hottel, H.C. and Meissner, H.P., "Rapid Devolatilization of Pulverized Coal," Fifteenth Symposium (International) on Combustion, p. 1303, The Combustion Institute, Pittsburgh, Pennsylvania (1975).

Armento, W.J. and Sage, W.L., "The Effect of Design and Operation Variables on NO_x Formation in Coal Fired Furnaces," Proceedings, Coal Combustion Seminar. EPA-650/2-73-021, 193 (1973).

Armento, W.J. and Sage, W.L., "Effect of Design and Operation Variables on NO_x Formation in Coal Fired Furnaces: Status Report," AIChE Symp. Ser. No. 148, 71, 63 (1975).

Axworthy, A.E., Jr., "Chemistry and Kinetics of Fuel Nitrogen Conversion to Nitric Oxide," AIChE Symp. Ser. No. 148, 71, 43 (1975).

Axworthy, A.E., Schneider, G.R., Shuman, M.D. and Dayan, V.H., Chemistry of Fuel Nitrogen Conversion to Nitrogen Oxides in Combustion, Final Report EPA-600/2-76-039, Rockwell International, Canoga Park, California, EPA Contract No. 68-02-0635 (1976).

Ayling, A.B. and Smith, I.W., "Measured Temperatures of Burning Pulverized-Fuel Particles, and the Nature of the Primary Reaction Product," Combustion & Flame, 18, 173 (1972).

Bartok, W. and Crawford, A.F. and Piegari, J.J., "Basic Kinetic Studies and Modelling of NO Formation in Combustion Processes," AIChE Symp. Ser. No. 126, 68, 66 (1972).

Baulch, D.L., Drysdale, D.D. and Lloyd, A.C., Critical Evaluation of Rate Data for Homogeneous, Gas-Phase Reactions of Interest in High-Temperatures Systems, Report Numbers 1-5, Dept. of Physical Chemistry, The University, Leeds, England (1968-1970).

Bedjai, G., Orbach, H.K. and Riesenfeld, F.C., "Reaction of Nitric

REFERENCES (cont.)

Oxide with Activated Carbon and Hydrogen," Ind. Eng. Chem., 50, 1165 (1958).

Beet, A.E., "A Further Study of the Kjeldahl Process - Pyridine Caboxylic Acids from Coal," Fuel, 19, 108 (1940).

Bird, R.B., Stewart, W.E. and Lightfoot, E.N., Transport Phenomena, John Wiley & Sons, Inc., New York (1960).

Blair, D.W., Bartok, W. and Wendt, J.O.L., "Devolatilization and Pyrolysis of Fuel Nitrogen from Single Coal Particle Combustion," Sixteenth Symposium (International) on Combustion, p. 475, The Combustion Institute, Pittsburgh, Pennsylvania (1977).

Brown, R.A., Mason, H.B. and Neubauer, P., "Investigation of Staging Parameter for NO_x Control in Both Wall and Tangentially Coal Fired Boilers," Proceedings of the Second Stationary Source Combustion Symp. EPA-600/7-77-073C, 141 (1977).

Chan, L.K., "Nitric Oxide Reduction by Char in a Fixed Bed Reactor," S.M. Thesis, M.I.T., Cambridge, Massachusetts (1977).

Crawford, A.R., Manny, E.H., Bartok, W. and Hall, R.E., "NO_x Emission Control for Coal Fired Utility Boilers," AIChE Symp. Ser. No. 148, 71, 75 (1975).

De Soete, G.G., "Formation and Decomposition of Nitric Oxide in Combustion Products of Hydrocarbon Flames," Paper presented at the AFRC American Flame Days, Chicago, Illinois (1972).

De Soete, G.G., "Overall Reaction Rates of NO and N_2 Formation from Fuel Nitrogen," Fifteenth Symposium (International) on Combustion, p. 1093, The Combustion Institute, Pittsburgh, Pennsylvania (1975).

Edwards, H.W., "Interaction of Nitric Oxide with Graphite," AIChE Symp. Ser. No. 126, 68, 91 (1972).

Federal Energy Administration, National Energy Outlook, Federal Energy Administration, Washington, D.C. (1976).

Fenimore, D.P., "Formation of Nitric Oxide in Premixed Hydrocarbon Flames," Thirteenth Symposium (International) on Combustion, p. 373, The Combustion Institute, Pittsburgh, Pennsylvania (1971).

Fenimore, C.P., "Formation of Nitric Oxide from Fuel Nitrogen in Ethylene Flames," Combustion & Flame, 19, 289 (1972).

REFERENCES (cont.)

Field, M.A., "Measurements of the Effect of Rank on Combustion Rates of Pulverized Coal," Combustion & Flame, 14, 237 (1970).

Field, M.A., "Rate of Combustion of Size-Graded Fractions of Char from a Low-Rank Coal Between 1200 K and 2000 K," Combustion & Flame, 13, 237 (1969).

Field, M.A., Gill, D.W., Morgan, B.B. and Hawksley, P.G.W., Combustion of Pulverized Coal, BCURA Leatherhead, Cherey and Sons, Ltd., Bamberg, England (1967).

Fieldner, A.C. and Davis, J.D., "Gas-, Coke-, and By Product-Making Properties of American Coals and Their Determination," U.S. Bureau of Mines, Monograph 5, (1934).

Fine, D.H., Slater, S.M., Sarofim, A.F. and Williams, G.C., "The Importance of Nitrogen in Coal as a Source of Nitrogen Oxide Emission from Furnaces," Fuel, 53, 120 (1974).

Flagan, R.C. and Appleton, J.P., "A Stochastic Model of Turbulent Mixing with Chemical Reaction: Nitric Oxide Formation in a Plug Flow Burner," Combustion & Flame, 23, 249 (1974).

Flagan, R.C. and Appleton, J.P., "Nitric Oxide Formation from Fuel Bound Nitrogen in an Oil-Fired Burner," AIChE Symp. Ser. No. 148, 71, 62 (1975).

Furursawa, T., Kunii, D., Oguma, A. and Yamada, N., "Kinetic Study of Nitric Oxide Reduction by Carboneceous Materials," paper submitted to Kagaku, Kogaku (Chem. Eng. Japan) (1977).

Gibbs, B.M., Pereira, F.J. and Beér, J.M., "The Influence of Air Staging on the NO Emission from a Fluidized Bed Coal Combustor," Sixteenth Symposium (International) on Combustion, p. 461, The Combustion Institute, Pittsburgh, Pennsylvania (1977).

Gregg, S.J. and Sing, K.S.W., Adsorption, Surface Area and Porosity, Academic, New York (1967).

Habelt, W.W., "The Influence of the Coal Oxygen to Coal Nitrogen Ratio on NO_x Formation," paper presented at 70th Annual AIChE Meeting, New York, New York (1977).

Haynes, B.S. and Kirov, N.Y., "Nitric Oxide Formation During the Combustion of Coal," Combustion & Flame, 23, 277 (1974).

REFERENCES (cont.)

Haynes, B.S., Iverach, D. and Kirov, N.Y., "The Behavior of Nitrogen Species in Fuel Rich Hydrocarbon Flames," Fifteenth Symposium (International) on Combustion, p. 1103, The Combustion Institute, Pittsburgh, Pennsylvania (1975).

Hill, W.H., "Recovery of Ammonia, Cyanogen, Pyridine, and Other Nitrogenous Compounds from Industrial Gases," in Lowry, H.H., ed., Chemistry of Coal Utilization, Vol. II, p. 1008, John Wiley & Sons, Inc., New York (1945).

Hirschfelder, J.O., Curtiss, C.F. and Bird, R.B., Molecular Theory of Gases and Liquids, John Wiley & Sons, Inc., New York (1954).

Hottel, H.C. and Howard, J.B., New Energy Technology, Some Facts and Assessments, M.I.T. Press, Cambridge, Massachusetts (1971).

Howard, J.B. and Essenhigh, R.H., "Pyrolysis of Coal Particles in Pulverized Fuel Flames," Ind. Eng. Chem. Process Design Develop., 6, 74 (1967).

Howard, J.B. and Essenhigh, R.H., "Mechanism of Solid Particle Combustion with Simultaneous Gas-Phase Volatiles Combustion," Eleventh Symposium (International) on Combustion, p. 399, The Combustion Institute, Pittsburgh, Pennsylvania (1967).

Janák, J., "Chromatography of Nonhydrocarbon Gases," in Heftmann, E., ed., Chromatography, A Laboratory Handbook of Chromatographic and Electrophoretic Methods, third ed. p. 882, Van Nostrand, Inc., New York (1975).

Jonke, A.A., Carlis, E.L., Jarry, R.L., Anatasia, L.J., Hass, M., Paulik, J.R., Murphy, W.A., Schoffstau, C.B. and Vargo, G.N., "Reduction of Atmospheric Pollution by Application of Fluidized Bed Combustion," Annual Rept. Anl/ES-CEN-1002, Argonne National Laboratory (1970).

Kirner, W.R., "The Occurrence of Nitrogen in Coal," in Lowry, H.H., ed., Chemistry of Coal Utilization, p. 450, John Wiley & Sons, Inc., New York (1945).

Kobayashi, H., "Devolatilization of Pulverized Coal at High Temperatures," Ph.D. Thesis, M.I.T., Cambridge, Massachusetts (1976).

Kobayashi, H., Howard, J.B. and Sarofim, A.F., "Coal Devolatilization at High Temperatures," Sixteenth Symposium (International) on Combustion, p. 411, The Combustion Institute, Pittsburgh, Pennsylvania (1977).

REFERENCES (cont.)

Levenspiel, O., Chemical Reaction Engineering, Second ed., John Wiley & Sons, Inc., (1972).

Mandel, G., "Gasification of Coal Char in Oxygen and Carbon Dioxide at High Temperature," S.M. Thesis, M.I.T., Cambridge, Massachusetts (1977).

Mason, H.B., Shimizu, A.B., Ferrell, J.E., Poe, G.G., Waterland, L.R. and Evans, R.M., Preliminary Environmental Assessment of Combustion Modification Techniques: Vol. 1 Summary, EPA-600/7-77-119a (1977).

Martin, G.B. and Berkau, E.E., "An Investigation of the Conversion of Various Fuel Nitrogen Compounds to Nitrogen Oxides in Oil Combustion," AIChE Symp. Ser. No. 126, 68, 45 (1972).

McCutchen, G.D., "Air Pollution Control: NO_x Emission Trends and Federal Regulation," Chemical Engineering Progress, Vol. 73, No. 8, 58 (1977).

Morgan, G.B., Golden, C. and Tabor, E.C., "New and Improved Procedures for Gas Sampling and Analysis in the National Air Sampling Network," Journal of the Air Pollution Control Association, 17, 301 (1967).

Mueller, P.K. and Hitchcock, M., "Air Criteria - Toxicological Appraisal for Oxidants, Nitrogen Oxides, and Hydrocarbons," Journal of Air Pollution Control Assoc., 9, 670 (1969).

Mulcahy, M.F.R. and Smith, I.W., "Kinetics of Combustion of Pulverized Fuel: A Review of Theory and Experiment," Rev. Pure and Appl. Chem., 19, 81 (1969).

Ode, W.H., "Coal Analysis and Mineral Matter," in Lowry, H.H., ed., Chemistry of Coal Utilization, Suppl. Vol., p. 202, John Wiley & Sons, Inc., New York, New York (1963).

Patterson, D.J. and Henein, N.A., Emissions from Combustion Engines and Their Control, Ann Arbor Science Publishers, Inc., Ann Arbor, Michigan (1972).

Pereira, F.J., "Nitric Oxide Emissions from Fluidized Coal Combustion," Ph.D. Thesis, Univ. of Sheffield, Sheffield, England (1975).

Pereira, F.J. and Beér, J.M., "NO Formation from Coal Combustion in a Small Experimental Fluidized Bed," presented at Second European Symp. on Combustion, Orleans, France (1975).

Pereira, F.J., Beér, J.M., Gibbs, B. and Hedley, A.B., "NO_x Emissions

REFERENCES (cont.)

from Fluidized-Bed Coal Combustors," Fifteenth Symposium (International) on Combustion, p. 1149, The Combustion Institute, Pittsburgh, Pennsylvania (1975).

Perry, R.H. and Chilton, C.H., Chemical Engineers' Handbook, 5th ed., McGraw-Hill, Inc., New York, New York (1973).

Pershing, D.W., "Nitrogen Oxide Formation in Pulverized Coal Flames," Ph.D. Thesis, Univ. of Arizona, Tucson, Arizona (1976).

Pershing, D.W., Martin, G.B. and Berkau, E.E., "Influence of Design Variables on the Production of Thermal and Fuel NO from Residual Oil and Coal Combustion," AIChE Symp. Ser. No. 148, 71, 19 (1975).

Pershing, D.W. and Wendt, J.O.L., "Effects of Coal Composition on Thermal and Fuel NO_x Production from Pulverized Coal Combustion," paper presented at 1976 Spring Technical Meeting, Central States Section, The Combustion Institute, Columbus, Ohio (1976).

Pershing, D.W. and Wendt, J.O.L., "Pulverized Coal Combustion: The Influence of Flame Temperature and Coal Composition on Thermal and Fuel NO_x," Sixteenth Symposium (International) on Combustion, p. 389, The Combustion Institute, Pittsburgh, Pennsylvania (1977).

Pohl, J.H., "Fate of Fuel Nitrogen," Sc.D. Thesis, M.I.T., Cambridge, Massachusetts (1976).

Pohl, J.H. and Sarofim, A.F., "Fate of Coal Nitrogen During Pyrolysis and Oxidation," paper presented at EPA Symposium on Stationary Source Combustion, Atlanta, Georgia (1975).

Pohl, J.H. and Sarofim, A.F., "Devolatilization and Oxidation of Coal Nitrogen," Sixteenth Symposium (International) on Combustion, p. 491, The Combustion Institute, Pittsburgh, Pennsylvania (1977).

Rosin, P. and Rammler, E., "The Laws Governing the Fineness of Powdered Coal," J. Inst. Fuel, 7, 29 (1933).

Sarofim, A.F., Willimas, G.C., Modell, M. and Slater, S.M., "Conversion of Fuel Nitrogen to Nitric Oxide in Premixed and Diffusion Flames," AIChE Symp. Ser. No. 148, 71, 51 (1975).

Satterfield, C.N., Mass Transfer in Heterogeneous Catalysis, MIT Press, Cambridge, Massachusetts (1975).

REFERENCES (cont.)

Scollon, T.R., "An Assessment of Coal Resources," Chemical Engineering Progress, Vol. 73, No. 6, 25 (1977).

Shaw, J.T. and Thomas, A.C., "Oxides of Nitrogen in Relation to the Combustion of Coal," Proceedings of Seventh International Conference on Coal Science, Prague (1965).

Shelef, M. and Otto, K., "Simultaneous Catalytic Reaction of O_2 and NO with CO and Solid Carbon," Journal of Colloid and Interface Science, 31, 73 (1969).

Smith, J.M., Chemical Engineering Kinetics, McGraw-Hill, Inc., New York (1970).

Smith, I.W., "Kinetics of Combustion of Size-Graded Pulverized Fuels in the Temperature Range 1200-2270 K," Combustion & Flame, 17, 303 (1971).

Smith, I.W., "The Kinetics of Combustion of Pulverized Semi-anthracite in the Temperature Range 1400-2200 K," Combustion & Flame, 17, 421 (1971).

Smith, I.W. and Tyler, R.J., "Internal Burning of Pulverized Semi-anthracite: the Relation Between Particle Structure and Reactivity," Fuel: Lond., 51, 312 (1972).

Smith, I.W. and Tyler, R.J., "The Reactivity of a Porous Brown Coal Char to Oxygen Between 630 and 1812 K," Combustion Sci. & Tech., 9, 87 (1974).

Solomon, P.R., The Evolution of Pollutants During the Rapid Devolatilization of Coal, Report No. R77-952588-3, United Technologies, East Hartford, Connecticut, NSF Grant AER75-17247, Monitored by Fossil Energy Division of ERDA (1977).

Song, Y.H., Beér, J.M. and Sarofim, A.F., "Fate of Fuel Nitrogen During Pyrolysis and Oxidation," Proceedings of the Second Stationary Source Combustion Symp., EPA-600/7-77-073d, 79 (1977).

Sternling, C.V. and Wendt, J.O.L., "Kinetic Mechanisms Governing the Fate of Chemically Bound Sulfur and Nitrogen in Combustion," NTIS Report No. PB-230895, U.S. Department of Commerce, Springfield, Virginia (1972).

Suuberg, E.M., "Rapid Pyrolysis and Hydropyrolysis of Coal," Sc.D. Thesis, M.I.T., Cambridge, Massachusetts (1977).

REFERENCES (cont.)

Suuberg, E.M., Peters, W.A. and Howard, J.B., "Product Composition and Kinetics of Lignite Pyrolysis," paper presented at ACS National Meeting, New Orleans, Louisana (1977).

Thring, M.W. and Essenhigh, R.H., "Thermodynamics and Kinetics of Solid Combustion," in Lowry, H.H., ed., Chemistry of Coal Utilization, Suppl. Vol., p. 754, John Wiley & Sons, Inc., New York, New York (1963).

Turner, D.A., Andrews, R.L. and Siegmund, C.W., "Influence of Combustion Modifications and Fuel Nitrogen Content on Nitrogen Oxides Emissions from Fuel Oil Combustions," AIChE Symp. Ser. No. 126, 68, 55 (1972).

Turner, D.W. and Siegmund, C.W., "Staged Combustion and Flue Gas Recycle: Potential for Minimizing NO_x from Fuel Oil Combustion," American Flame Research Committee Flame Days, Chicago (1972).

Vogt, R.A. and Laurendeau, N.M., Nitric Oxide Formation in Pulverized Coal Flames, Report No. PURDU-CL-76-08, Purdue University, West Lafayette, Indiana, NSF Grant GK-42141 (1976).

Vogt, R.A. and Laurendeau, N.M., "NO_x Formation from Coal Nitrogen: A Review and Model" paper presented at 1976 Spring Technical Meeting, Central States Section, The Combustion Institute, Columbus, Ohio (1976).

Weast, R.C., Handbook of Chemistry and Physics, 53rd ed., The Chemical Rubber Co., Cleveland, Ohio (1972).

Wendt, J.O.L. and Schulze, O.E., "On the Fate of Fuel Nitrogen During Coal Char Combustion," AIChE Journal, 22, 102 (1976).

Wheeler, A., "Reaction Rates and Selectivity in Catalyst Pores," Advance in Catalysis, III, 249 (1951).

Wheeler, A., "Reaction Rates and Selectivity in Catalyst Pores," in Emmett, P.H., ed., Catalysis, Vol. 2, Reinhold, New York, 105 (1955).

Zeldovich, Ya.B., Sadovnikov, P.Ya. and Frank-Kamenetskii, D.A., "Oxidation of Nitrogen in Combustion," Academy of Sciences of USSR, Institute of Chemical Physics, Moscow-Leningrad, translated by M. Shelef (1947).

BIOGRAPHICAL NOTE

The author, Yih Hong Song, the first child of Mr. and Mrs. Chang Tseng Song, was born on September 6, 1948 in a farm near Shuili, Nantou of central Taiwan. He graduated first in his class from Provincial Taichung First High School in 1966. He then enrolled at National Taiwan University and graduated with a degree of B.S. in chemical engineering in 1970. He served in Army ROTC, working at a Military Vehicle Plant as a Chemical Engineering Officer, for one year before he crossed ten thousand miles through the Pacific to the United States for advanced education.

After spending one year as a graduate student in the Chemistry Department of Wesleyan University, Middletown, Connecticut, he transferred to the University of Massachusetts, working in the field of Process Control under the supervision of Professor James M. Douglas of the Chemical Engineering Department. He received a degree of M.S. in chemical engineering in 1974.

He married the former Leila Shia, his classmate at National Taiwan University, on September 6, 1974, just before he joined M.I.T. On the same day when he finished the writing of his doctoral thesis, he was also happy to find out that he is going to be a father for the very first time.

During his stay at M.I.T., he worked in the field of coal combustion science under the supervision of Professors Adel F. Sarofim and Janos M. Beér.

He is the author of four technical publications and is the member of AAAS, AIChE, Combustion Institute and Sigma Xi.

At the present time, he has accepted an appointment as Research Engineer at Exxon Research and Engineering Company, Linden, New Jersey, to begin in May 1978.